Defining Homeostatic and Inflammatory Mononuclear Phagocytes in Human Blood and Tissue and Investigating Their Role in HIV Acquisition

Freja Amaliya Warner Van Dijk
BClinSci BAdvStudies (Hons)

A thesis submitted in fulfilment of the requirements for admission to the degree of Doctor of Philosophy at The University of Sydney

19 November 2025

Faculty of Medicine and Health
School of Medical Science
The University of Sydney

Centre for Virus Research
The Westmead Institute for Medical Research

Declaration

This is to certify that the content of this thesis is my own work. This thesis has not been submitted for any other degree or purpose.

I certify that the intellectual content of this thesis is the product of my own work, and that all assistance received in preparing this thesis and all sources have been acknowledged.

During the preparation of this thesis, OpenAI GPT-4o was minimally used for the purpose of text editing, including as a thesaurus and paraphrasing. Where any text was modified by generative AI, I reviewed the resulting content for any errors, inaccuracies or biases, and modified it as required. I take full responsibility for the submitted thesis and ensure the work is my own and has used generative AI within the parameters of use, see University of Sydney generative AI guide for researchers.

Chapter 1 of this thesis has been published as:

> ***Warner van Dijk, F. A.**, Bertram, K. M., O'Neil, T. R., Li, Y., Buffa, D. J., Harman, A. N., Cunningham, A. L., & Nasr, N. (2025). Recent Advances in Our Understanding of Human Inflammatory Dendritic Cells in Human Immunodeficiency Virus Infection. Viruses, 17(1), 105. https://doi.org/10.3390/v17010105*

I conceptualised and wrote this original manuscript.

Chapter 2 of this thesis has been published as:

> ***Warner van Dijk, F. A.,** Tong, O., O'Neil, T. R., Bertram, K. M., Hu, K., Baharlou, H., Vine, E. E., Jenns, K., Gosselink, M. P., Toh, J. W., Papadopoulos, T., Barnouti, L., Jenkins, G. J., Sandercoe, G., Haniffa, M., Sandgren, K. J., Harman, A. N., Cunningham, A. L., & Nasr, N. (2024). Characterising plasmacytoid and myeloid AXL+ SIGLEC-6+ dendritic cell functions and their interactions with HIV. PLoS pathogens, 20(6), e1012351.* https://doi.org/10.1371/journal.ppat.1012351

I performed all experimental work, along with co-author Tong, O., analysis, along with co-author O'Neil, T. R., and wrote this original manuscript, with contributions from co-author Tong, O and corresponding author Nasr, N.

Material written or published by other persons have been appropriately acknowledged and referenced in this thesis. In addition to the previous statements, in cases where I am not the corresponding author of a manuscript, permission to include the material has been granted by the designated corresponding author.

Freja Amaliya Warner van Dijk
September 2025

As supervisor for the candidature upon which this thesis is based, I can confirm that the authorship attribution statements above are correct.

Associate Professor Najla Nasr
September 2025

Abstract

Tissue mononuclear phagocytes (MNP) are the first line of cellular defence against invading pathogens that breach the physical skin or mucosal barriers of the human genital tract. As potent antigen present cells, MNPs sample and deliver these foreign antigens to CD4 T cells via a vast array of pathogen binding receptors, thereby initiating an immune response. In tissue, MNPs comprise of Langerhans cells, dendritic cells (DC), macrophages and monocytes. In the case of HIV, this system of antigen presentation is exploited, as the virus gains direct access to its primary target, the CD4 T cell. HIV infects, replicates within, and ultimately destroys CD4 T cells. The gradual depletion of these cells leads to the development of acquired immunodeficiency syndrome.

Genital inflammation is a critical risk factor for HIV acquisition. Crucially, the primary preventative HIV intervention, pre-exposure prophylaxis (PrEP), can be ineffective in blocking transmission in genital inflammation. Sexually transmitted infections and genital microbiota dysbiosis are the leading causes of inflammation and is often asymptomatic and undiagnosed. This increased HIV susceptibility in inflamed tissue likely stems from a disrupted epithelial barrier integrity, phenotypic changes in resident MNPs and an influx of inflammatory HIV target cells, including MNPs and CD4 T cells. Gaining insight into how HIV interacts with specific inflammatory MNP subsets could inform the development of new therapeutic strategies to block HIV transmission. However, little is known about the precise role MNPs play in early HIV capture and transmission in inflammatory environments.

In this thesis, using human genital tissues and optimised tissue digestion protocols, we explored the MNP landscape of genital skin and mucosa under conditions of homeostasis and inflammation, delineating cell phenotypes and functions. First, we investigated the known inflammatory plasmacytoid DCs (pDC), $CD123^+$ Axl^+ $Siglec\text{-}6^+$ DCs (ASDC) and $CD11c^+$ ASDCs. pDCs were confirmed the primary type I interferon (IFN-I) producers, whilst ASDCs proved to be potent T cell stimulators and polarisers, and capable of HIV binding and transfer to CD4 T cells. Importantly, we demonstrated for the first time the presence of ASDCs in human genital tissue, the biological site of HIV transmission.

Next, we designed and optimised a 26-parameter flow cytometry panel to interrogate and compare MNP populations residing in human genital tissues across states of homeostasis and inflammation, and to assess their capacity for HIV uptake. Utilising this panel, we demonstrated that the MNP populations present in foreskin, labia, vaginal and cervical tissues are highly heterogenous in their compositions and phenotypes. Notably, in vaginal mucosa we found that: **1)** cDC1s are phenotypically distinct to their counterparts in skin and intestine, **2)** a transitional population of macrophages exists that is a phenotypical intermediate of monocyte-derived macrophages (MDM) and tissue resident macrophages, and **3)** $CD14^+$ MNPs comprise a large fraction of epithelial MNPs – a population not previously quantified. In inflammation, we observed an influx of MDMs into the lamina propria and $langerin^+$ cDC2s in the epithelium, accompanied by many changes in surface marker expression across all MNP populations. Finally, among all the MNP populations identified, macrophage populations demonstrated the most efficient at binding HIV over a two-hour period.

Identifying and defining the inflammatory MNP populations in human genital tissues forms the foundation for developing improved PrEP strategies that are effective in an inflamed mucosa, with the ultimate goal of reducing HIV transmission and contributing to end the global pandemic.

Acknowledgements

What an incredible 3.5-year journey this has been, and so surreal to finally see all this work culminated in a single document. But of course, many of my achievements would not have been possible without the support of some extraordinary people.

To my supervisors, Associate Professor Najla Nasr, Dr Kirstie Bertram and Professor Andrew Harman, thank you for taking me on as your student. Najla, although you joined my supervisory team later, I'm so grateful for the new opportunities you brought, in teaching and achieving my first first-author experimental publication. Your kindness and support, both in and out of the lab, is deeply appreciated. Kirstie, you were the driving force of so much of my research – we encountered many hurdles, but your persistence and flow cytometry knowledge was ultimately what led to our experimental successes. Andrew, five years ago you convinced me to do an honours project with your group, and I suppose the rest is history. I'm extremely grateful for all the conference and international travel opportunities you provided. You truly are a thesis editing wizard and, of course, have an impeccable taste in wine. Thank you all for everything you've done, my time in medical research has been immensely rewarding. And a special mention to Professor Tony Cunnigham – a great inspiration and scholar.

To my lab friends, my sanity assurance, you truly just made every day more enjoyable. Erica, it's fair to say we achieved the near impossible with our flow cytometry panel, it was a pleasure to work and laugh alongside someone of such scientific skill and wisdom. Sam, your friendship has been invaluable, thank you for all the chats and support through the highs and lows. Dan, Tom, Liz, Jason, Jacinta, Katie, Hafsa, Sana, Vicki – we all crossed over at different times through our PhDs, whether as part of the tissue processing team, conference buddies or lunch companions, thank you all for the friendships. Importantly, to all past and present lab and level 6 members who lunched at 12pm sharp, thank you.

To the surgeons, patients and WIMR core services, without your selfless work and contributions this project would not have been possible, thank you.

To my friends and family, it goes without saying, your enduring support is always the root of my motivation, you will forever and always have my love and appreciation.

Publications, Presentations and Scholarships

Peer Reviewed Publications

1. Vine, E. E., Rhodes, J. W., **Warner van Dijk, F. A.**, Byrne, S. N., Bertram, K. M., Cunningham, A. L., & Harman, A. N. (2022). HIV transmitting mononuclear phagocytes; integrating the old and new. *Mucosal immunology*, *15*(4), 542–550. https://doi.org/10.1038/s41385-022-00492-0

2. **Warner van Dijk, F. A**., Tong, O., O'Neil, T. R., Bertram, K. M., Hu, K., Baharlou, H., Vine, E. E., Jenns, K., Gosselink, M. P., Toh, J. W., Papadopoulos, T., Barnouti, L., Jenkins, G. J., Sandercoe, G., Haniffa, M., Sandgren, K. J., Harman, A. N., Cunningham, A. L., & Nasr, N. (2024). Characterising plasmacytoid and myeloid AXL+ SIGLEC-6+ dendritic cell functions and their interactions with HIV. PLoS pathogens, 20(6), e1012351. https://doi.org/10.1371/journal.ppat.1012351

3. **Warner van Dijk, F. A.**, Bertram, K. M., O'Neil, T. R., Li, Y., Buffa, D. J., Harman, A. N., Cunningham, A. L., & Nasr, N. (2025). Recent Advances in Our Understanding of Human Inflammatory Dendritic Cells in Human Immunodeficiency Virus Infection. Viruses, 17(1), 105. https://doi.org/10.3390/v17010105

4. Buffa, D. J., O'Neil, T. R., Vine, E. E., Sarkawt, L., **Warner van Dijk, F. A.**, Dong, O. A., Nasr, N., Cunningham, A. L., Bertram, K. M., & Harman, A. N. (2025). Dendritic cells and HIV transmission: roles and subsets of antigen-presenting cells in the human anogenital tract. *PLoS pathogens*, *21*(9), e1013490. https://doi.org/10.1371/journal.ppat.1013490

Submitted for Publication

1. Erica E. Vine*, **Freja A. Warner van Dijk***, Anthony L Cunningham, Najla Nasr, Andrew N Harman, Kirstie M Bertram. OMIP (unallocated): 26-parameter flow cytometry panel to characterise all homeostatic and inflammatory state mononuclear phagocytes in human skin, type II mucosa and type I mucosa. *Cytometry A* (2025). *In revision after editorial review*

* co-first authors

Presentations

1. Australian Centre for HIV and Hepatitis Virology Research (ACH4) annual meeting, ***oral presentation***, 2022
2. Westmead Hospital Week Research Symposium, ***poster presentation***, 2022
3. Australasian Society for Immunology NSW & ACT branch meeting, ***oral presentation***, 2022
4. International Union of Immunological Societies 16th International Symposium on Dendritic Cells, ***poster presentation***, 2022 (Cairns, Australia)
5. Westmead Hospital Week Research Symposium, ***poster presentation***, 2023
6. Australasian Society for Immunology NSW & ACT branch meeting, ***oral presentation***, 2023
7. Australian Centre for HIV and Hepatitis Virology Research (ACH4) annual meeting, ***oral presentation***, 2023
8. 17th International Workshop on Langerhans Cells – and Related Myeloid Cells of the Skin, ***oral presentation***, 2023 (Paris, France)
9. Westmead Research and Innovation Conference, ***poster presentation***, 2024
10. Society for Mucosal Immunology International Conference, ***oral presentation***, 2024 (Copenhagen, Denmark)
11. The Australasian Cytometry Society conference, ***oral presentation***, 2024 (Hobart, Australia)
12. Australian Society of Immunology conference, ***oral and poster presentation***, 2024
13. Australian Centre for HIV and Hepatitis Virology Research (ACH4) biannual meeting, ***oral presentation***, 2025
14. Australian Society of Immunology Symposium for Mucosal Immunology and Microbiome, ***oral presentation***, 2025

Awards and Scholarships

1. 17th International Workshop on Langerhans Cells – and Related Myeloid Cells of the Skin, ***travel award***, 2023
2. Society for Mucosal Immunology International Conference, ***travel award***, 2024
3. Australian Society of Immunology Symposium for Mucosal Immunology and Microbiome, ***travel award***, 2025

This research reported in this thesis was supported by the award of a Research Training Program scholarship to the PhD Candidate.

Table of Contents

List of Figures

List of Tables

Abbreviations

Acronym	Definition
AF	Autofluorescence
AIDS	Acquired Immunodeficiency Syndrome
APC	Antigen Presenting Cell
ART	Antiretroviral Therapy
ASDC	AXL^+ $SIGLEC\text{-}6^+$ Dendritic Cell
BMP7	Bone Morphogenetic Protein 7
BV	Bacterial Vaginosis
CADM1	Cell Adhesion Molecule 1
cDC	Conventional Dendritic Cell
cDP	Common DC Progenitor
CLEC	C-type Lectin Domain Family
CLR	C-type Lectin Receptors
CSF	Cerebro Spinal Fluid
CXCR	CXC chemokine receptor
DC	Dendritic Cell
DC-SIGN	Dendritic Cell-Specific Intercellular Adhesion Molecule-Grabbing Non-Integrin
DMEM	Dulbecco's Modified Eagle Medium
DNase	Deoxyribonuclease
DPBS	Dulbecco's Phosphate Buffered Saline
DTT	1,4-dithiotreitol
EDTA	Ethylenediaminetetraacetic Acid
FACS	Fluorescence Activated Cell Sorting
FCS	Fetal Calf Serum
FcεR1α	Human Anti-IgE Receptor
FGT	Female Genital Tract
FMO	Fluorescence Minus One
FSC	Forward Scatter
FVS	Fixable Viability Stain
FXIIIA	Factor XIIIA
GFP	Green Fluorescent Protein
GM-CSF	Granulocyte-Macrophage Colony Stimulating Factor
gMFI	Geometric Mean Fluorescence Intensity
GMPD	Granulocyte-Monocyte Progenitor
hAB	Human Type AB
HEPES	4-(2-Hydroxyethyl)-1-piperazineethanesulfonic Acid

Acronym	Definition
HIV	Human Immunodeficiency Virus-1
HSV	Herpes Simplex Virus
HLA-DR	Human Leukocyte Antigen, Antigen D Related Receptor
ICAM-1	Intercellular adhesion molecule 1
IFN	Interferon
IDEC	Inflammatory Dendritic Epidermal Cells
IL	Interleukin
ILC	Innate Lymphoid Cell
IRF	Interferon Regulatory Factor
LC	Langerhans Cell
LP	Lamina Propria
MACS	Magnetic Activated Cell Sorting
MDDC	Monocyte Derived Dendritic Cell
MDM	Monocyte Derived Macrophage
MHC	Major Histocompatibility Complex
MNP	Mononuclear Phagocytes
MOI	Multiplicity of Infection
MR	Mannose Receptor
MS	Multiple Sclerosis
NK	Natural Killer
OMIP	Optimised Multicolour Immunofluorescence Panel
PBMC	Peripheral Blood Mononuclear Cell
PBS	Phosphate Buffered Saline
pDC	Plasmacytoid Dendritic Cell
PFA	Paraformaldehyde
PrEP	Pre-Exposure Prophylaxis
RF10	Roswell Park Memorial Institute supplemented with 10% Fetal Calf Serum
RNA-seq	Ribonucleic Acid Sequencing
rpm	Revolutions per Minute
RPMI	Roswell Park Memorial Institute
RT	Room Temperature
SAMHD1	Sterile Alpha Motif and Histidine/Aspartic Acid Domain-Containing Protein 1
SIGLEC	Sialic Acid-Binding Immunoglobulin-Type Lectins
SSC	Side Scatter
SIRPα	Signal-Regulatory Protein alpha
SIV	Simian Immunodeficiency Virus

Acronym	Definition
STI	Sexually Transmitted Infection
TGF-β	Tumour Growth Factor beta
Th	Helper T cells
TLR	Toll-like Receptor
t-MDM	Transitional Monocyte Derived Macrophage
TNFα	Tumour Necrosis Factor alpha
Treg	Regulatory T cells
t-SNE	t-Distributed Stochastic Neighbour Embedding
opt-SNE	Optimised t-SNE
VCC	Virus Containing Compartment
VEDC	Vaginal Epithelial Dendritic Cell

Chapter 1. Literature Review

Publications incorporated into this chapter

Warner van Dijk, F. A., Bertram, K. M., O'Neil, T. R., Li, Y., Buffa, D. J., Harman, A. N., Cunningham, A. L., & Nasr, N. (2025). Recent Advances in Our Understanding of Human Inflammatory Dendritic Cells in Human Immunodeficiency Virus Infection. *Viruses*, *17*(1), 105. https://doi.org/10.3390/v17010105

The above publication is extensively used throughout the following chapter. Any incorporated sections are indicated by quotation marks. Figures have not been amended but citations and references to figures have been changed for this thesis. To maintain consistency throughout this thesis, references to 'DC1' and 'DC2' from the published text have been changed to 'cDC1' and cDC2'. All text in this chapter was written by this author.

1.1 Introductory Statement

This thesis aims to further elucidate the early events of the sexual transmission of Human immunodeficiency virus (HIV), defining the mononuclear phagocyte (MNP) populations in homeostatic and inflammatory environments within human genital tissues and investigating their role in HIV binding and transmission. This chapter will explore the current tissue MNP landscape, with a particularly focus on known inflammatory populations, discussing their origins, functionality and HIV interactions.

1.2 Introduction

"HIV is predominantly a sexually transmitted virus. Anal intercourse poses the greatest transmission risk in high-income countries (Baggaley et al., 2018, Stannah et al., 2020), whilst vaginal intercourse is the primary transmission route in low- and middle-income nations (Cuadros et al., 2011, Wawer et al., 2005), with women being more vulnerable than men (Yi et al., 2013) – particularly young sub-Saharan African women. In both instances, inflammation is highly associated with transmission (Masson et al., 2015, Esra et al., 2016, Wall et al., 2017, Passmore et al., 2016). This correlation exists regardless of the inflammatory cause, although key drivers include sexual violence trauma (Jewkes et al., 2010), sexually transmitted infections (STI) (Laga et al., 1993, Mlisana et al., 2012), bacterial vaginosis (BV) (Masson et al., 2014, Atashili et al., 2008) and penile anaerobic bacteria, which are common in uncircumcised males

(Liu et al., 2017, Prodger et al., 2021). Crucially, recent investigations have revealed that the primary HIV preventative treatment, pre-exposure prophylaxis (PrEP), can be ineffective in anogenital inflammation (McKinnon et al., 2018, Klatt et al., 2017), which is particularly problematic in sub-Saharan Africa where inflammation is common (Dabee et al., 2019). This highlights the critical need for better PrEP regimens to block transmission in the context of an inflamed mucosa, yet the early HIV transmission events in an inflammatory milieu remain poorly understood.

Factors that promote inflammation at the site of infection were recently summarised by Caputo et al. (2023) and included the ability of different anogenital mucosae (and the pH of the mucus) – whose integrity can be compromised by infections, especially sexually transmitted diseases (including herpes simplex virus), hormonal contraceptives and alterations in microbiome composition – to act as a physical barrier to inflammatory agents. Specifically, microbial vaginal dysbiosis, also referred to as BV, has been identified as a leading cause of the female genital-tract inflammation in sub-Saharan Africa, with the majority of cases being asymptomatic (Koumans et al., 2007, Klebanoff et al., 2004). BV-associated inflammation is characterised by a dominant presence of *Gardnerella vaginalis* or *Prevotella* species and correlates with increases in pro-inflammatory cytokine concentrations, including IL-8, IL-1α, IL-1β, and TNF-α (Anahtar et al., 2015, Masson et al., 2014, Lennard et al., 2018). Contrastingly, those with a 'healthy' vaginal microbiota have an abundant *Lactobacillus* species presence, low levels of inflammation and a lower risk of HIV acquisition (Gosmann et al., 2017, Hearps et al., 2017, Aldunate et al., 2013, Tyssen et al., 2018). While men face a lower risk of heterosexual HIV transmission compared to women, penile microbial dysbiosis can also be a significant contributing factor to HIV acquisition (Nelson and Liu, 2024). This risk is particularly high in uncircumcised males as pro-inflammatory anaerobic species, predominantly *Prevotella*, *Dialister* and *Peptostreptococcus*, colonise the inner foreskin (Prodger et al., 2021, Liu et al., 2017). An inflammatory rectal microbiome signature also plays a major role in HIV acquisition, though its impact is more complex due to the interplay between external environmental factors and the gut microbiome (Fulcher et al., 2022, Chen et al., 2021).

Inflammation rapidly transforms the cellular landscape of a tissue, resulting in an influx of immune cells, changes to resident cells and a complex network of signals from pro-inflammatory cytokines and chemokines. This dynamic and intricate nature of

inflammation poses significant challenges for research, which in part accounts for the incomplete understanding of the relationship between anogenital inflammation and HIV acquisition. The proposed factors contributing to HIV susceptibility in an inflammatory anogenital environment include breached barrier integrity, phenotypic changes in tissue-resident cells and an influx of recruited immune cells. Individuals with an inflammatory profile have an impaired anogenital epithelial barrier, owing to the production of destructive inflammatory proteases (Arnold et al., 2016, Borgdorff et al., 2016, Zevin et al., 2016), exposing the underlying connective tissue, which hosts an array of HIV target cells. Additionally, in an inflamed environment, tissue-resident HIV target cells, including dendritic cells (DCs), macrophages and CD4 T cells, undergo phenotypical and functional changes that make them more susceptible to HIV infection. Under a pro-inflammatory cytokine stimulation, DCs become activated and mature, increasing their likely uptake of HIV and transfer to CD4 T cells (Said and Weindl, 2015, Qin et al., 2012, Turville et al., 2004, Rhodes et al., 2021). Lastly, vulnerability to HIV infection may be due to the recruitment of HIV target cells in response to inflammatory signals. $CCR5^+$ cells are specifically enlisted by the chemo-attractant chemokines CCL3, CCL4 and CCL5 released by the infiltrating inflammatory plasmacytoid DC (pDC) (Li et al., 2009, Shang et al., 2017). As CCR5 is a key HIV entry receptor, specific HIV target cells, including CD4 T cells, monocyte-derived macrophages (MDMs) and DCs, are increased in inflammation. Very little work has been carried out in the genital tract to define DC responses to viruses or other microbial products. Therefore, future investigations into which DCs are responding to sexually transmitted viruses (such as HSV-2 or pathogenic species present in dysbiotic genital tissue, such as *Gardnerella vaginalis*, or *Prevotella)* may identify therapeutic targets to interrupt the ongoing recruitment of immune cells in response to pathogenic microbiomes. This review will provide a comprehensive exploration of the currently defined inflammatory tissue DCs and their known interactions with HIV."

1.3 Human Anogenital Tissue

"Given that sexual transmission occurs within genital and anorectal (anogenital) tissues, understanding the anatomy of these tissues, which HIV penetrates, is important. Anogenital tissue comprises three distinct tissue types: skin, type I mucosa and type II mucosa, which all differ in their structural organisation and composition of

immune cells and hence vary in their susceptibility to HIV infection. Skin comprises two distinct layers – an outer epidermis and an underlying dermis – and covers the most outer anatomical structures of the body, including the labia major, labia minora, outer foreskin, glans penis, and anal verge (**Figure 1.1a**). The epidermis forms an impermeable physical barrier to invading pathogens, consisting of a thick stratified squamous epithelium and a surface layer of dead cornified cells – the stratum corneum. Skin is the most robust barrier against HIV transmission. Type II mucosa includes the vagina, ectocervix, inner foreskin, penile fossa navicularis and anal canal. It consists of a stratified squamous epithelium and underlying connective tissue layer called the lamina propria (LP) (**Figure 1.1b**). However, in contrast to skin, it has no (or a very thin) stratum corneum and is therefore more susceptible to HIV infection. The endocervix, urethra, rectum, and colon are all covered by type I mucosa, which comprises only a single layer of columnar epithelium designed for adsorption and the underlying LP (**Figure 1.1c**). This is the most fragile tissue type and is most vulnerable to HIV penetration and infection."

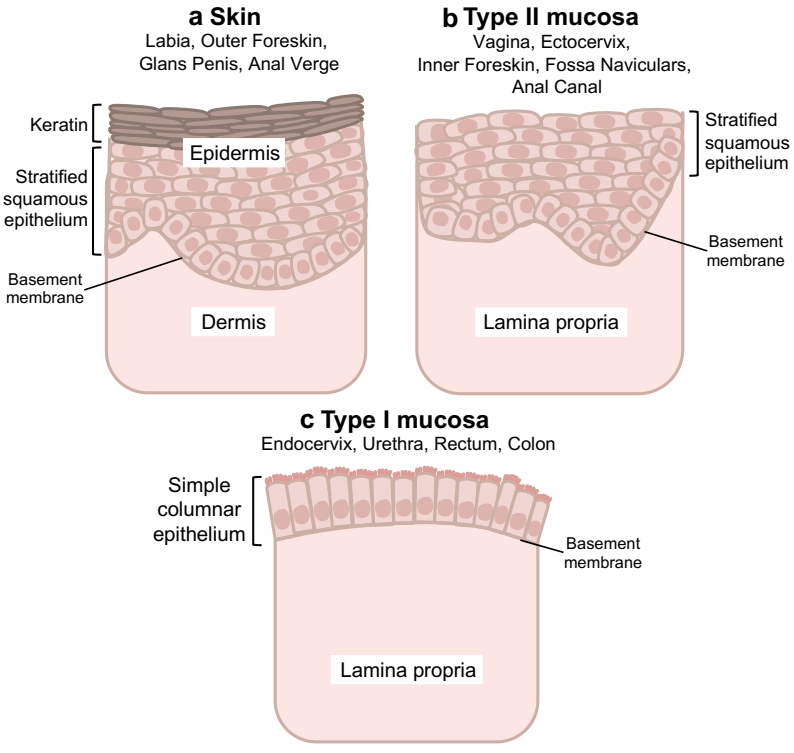

Figure 1.1: Tissue types of the anogenital tract.

a) Skin is comprised of an outer epidermis, containing a stratified squamous epithelium with a top layer of keratinised dead cells, and an underlying dermis. Separating the two is the basement membrane. **b)** Type II mucosa consists of only a stratified squamous epithelium and an underlying Lamina propria. **c)** Type I mucosa has a thin protective layer of simple columnar epithelium overlaying the Lamina propria.

1.4 Dendritic Cells and Macrophages in Human Tissue

“DCs are potent antigen presenting cells (APCs) and form part of the MNP family, which also consists of Langerhans cells (LCs), macrophages and monocytes. They are innate immune cells that form the first line of defence by sampling pathogens via their surface receptors to subsequently trigger an adaptive immune response. Like LCs and macrophages, DCs are also HIV target cells as they express the key HIV entry receptors CD4 and CCR5. They reside in anogenital tissues, and as part of their APC function, they capture HIV at the mucosal entry point and transport the virus to the primary HIV target cell, the CD4 T cell, either within the tissue or nearby lymph nodes.

The development of DCs and macrophages is summarised in **Figure 1.2**. Traditionally, DCs have been classified into two lineages: conventional DCs and inflammatory pDCs. DCs are further divided into cDC1, cDC2 and DC3, with distinct ontology and functions.” cDC1s, cDC2s, LCs and macrophages will be summarised in this following section, whilst pDCs, Axl^{+} Siglec-6^{+} DC (ASDC), monocyte-derived DCs (MDDC) and epithelial CD11c^{+} DCs will be more comprehensively explored throughout this chapter.

1.4.1 cDC1s

cDC1s represent a small population in tissue, especially when compared with cDC2s and macrophages (Rhodes et al., 2021), yet they have a high capacity to activate CD8 T cells (Haniffa et al., 2012). Traditionally, cDC1s were defined by their expression of CD141, but XCR1, CLEC9A and CADM1 are now considered more reliable defining markers in tissue (Botting et al., 2017, Mair and Liechti, 2021). Critically, cDC1s are resistant to HIV infection as they don’t express HIV binding lectin receptors or entry co-receptors CCR5 and CXCR4 and highly express the retroviral restriction factor SAMHD1 (Silvin et al., 2017, Rhodes et al., 2021).

1.4.2 cDC2s

“cDC2s are the most abundant DC population. They are potent naïve T-cell stimulators and highly efficient at transmitting HIV to CD4 T cells (Rhodes et al., 2021, Bertram et al., 2019).” cDC2s are universally characterised by their high expression of CD1c and CD11c, with additional expression of CD1a in skin and SIRPα in intestinal tissue (Rhodes et al., 2021, Botting et al., 2017, Doyle et al., 2021). cDC2s can be further

subdivided into langerin$^+$ and langerin$^-$ subsets. Langerin$^+$ cDC2s are more abundant in mucosal LP and represent preferential HIV target cells, as they efficiently mediate HIV transfer to CD4 T cells via lectin receptor binding and productive infection via CD4/CCR5 entry (Rhodes et al., 2021). Langerin$^-$ cDC2s are also capable of HIV transfer but to a lesser extent.

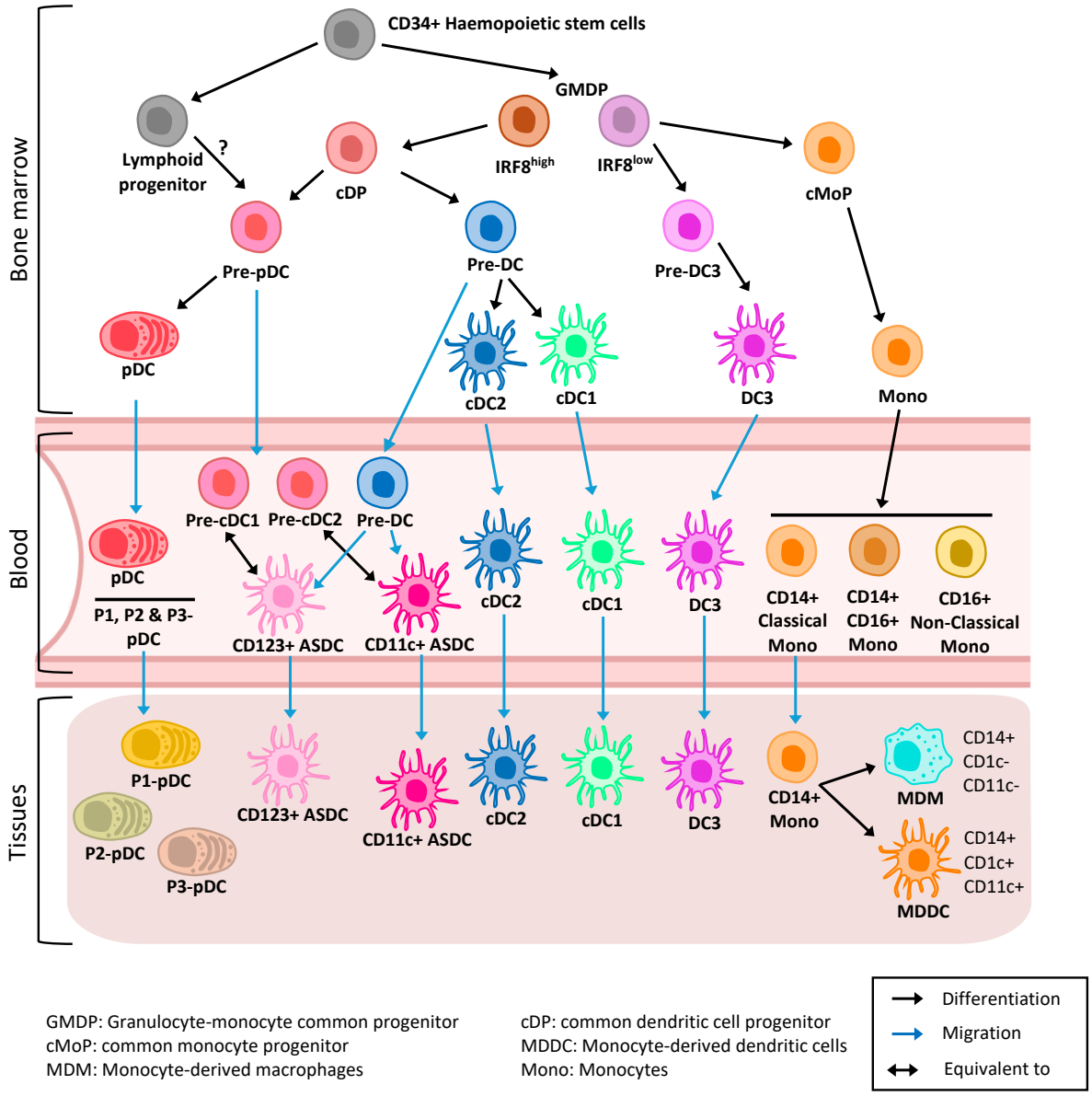

Figure 1.2: Ontogeny of dendritic cells and monocyte-derived macrophages.

"CD34$^+$ hematopoietic stem cells produce granulocyte-monocyte common progenitor (GMDP) and lymphoid progenitors. Based on IRF8 expression, GMDP gives rise to the common DC progenitors (cDP), pre-DC3 and the common monocyte progenitor (cMoP). While cDP generate DCs (pDCs, ASDCs, cDC1, cDC2), pre-DC3 gives rise to DC3 and cMoP gives rise to monocytes. The developmental pathway of ASDCs from pre-pDCs or directly from pre-DCs remains to be fully characterised. PDCs and ASDCs migrate from blood to inflamed tissues. cDC1, DC2 and DC3 are present in healthy and inflamed tissues but become more enriched in inflamed tissues. In inflammation, CD14 monocytes migrate from blood to tissues, and they differentiate into MDM and/or MDDCs."

"DC3s, a recently defined subset, have similar T-cell-activation capacity to cDC2s but are ontologically distinct (Villani et al., 2017, Dutertre et al., 2019, Bourdely et al., 2020, Cytlak et al., 2020)." DC3s will be further discussed in a later section of this chapter.

1.4.3 Langerhans Cells

LCs reside in the tissue epidermis/epithelium and have similar functions to cDC2s yet are considered a distinct class of MNP. They were originally thought to be a DC subset due to their ability migrate from tissue and function as efficient APCs. However, they also display similar ontology and function to macrophages, including a capacity for self-maintenance (Doebel et al., 2017). Bertram et al. (2019) demonstrated LCs are not the sole MNP residing in the epithelium, revealing the presence of an epithelial $CD11c^{+}$ DC and $CD33^{lo}$ MNP. Critically, they showed that LCs are present in lower abundance than DCs in mucosal tissues and possess weaker APC capabilities. LCs are defined as $langerin^{hi}$ $CD1a^{hi}$ $CD11c^{lo}$ and contain Birbeck granules in their cytoplasm – thought to be a key distinguishing feature from $langerin^{+}$ cDC2s (Bigley et al., 2015). LCs are susceptible to HIV infection via CD4/CCR5 and can bind the virus through langerin, however their role in transmission remains debated.

1.4.4 Macrophages

"Macrophages are either tissue-resident autofluorescent macrophages (Haniffa et al., 2009) or monocyte-derived macrophages (MDMs) (McGovern et al., 2014). They phagocytose foreign pathogens and maintain tissue homeostasis. However, they have only a secondary antigen-presenting function." CD14-expressing cells in tissue were traditionally described as macrophages, although this has since been changed to include MDDCs (McGovern et al., 2014) and DC3s (Bourdely et al., 2020). Bujko et al. (2018) defined four distinct macrophage subsets in intestinal tissue, termed Mf1-4, two MDM subsets: Mf1 and Mf2, and two tissue-resident subsets: Mf3 and Mf4. Whether these specific subsets correlate to MDMs and macrophages in genital skin and type II mucosa is yet to be investigated, though as macrophages are highly specialised to their tissue environment, a direct correlation is unlikely. Macrophages express the HIV entry receptor CD4, and though they express the entry co-receptor CCR5 to a lesser degree than DCs, they are susceptible to HIV infection (Rhodes et al., 2021). As macrophages are weak APCs, they were not previously thought to be involved in HIV transmission, however, as lectin receptors Siglec-1 and DC-SIGN, known to be high

affinity HIV-binding receptors, were recently shown to be exclusively expressed by tissue macrophages and not DCs, this suggests macrophages are mediators of HIV transmission (Vine et al., 2022). Additionally, macrophages are known HIV reservoirs in the human intestine and urethral mucosa (Ganor et al., 2019, Zalar et al., 2010).

“Investigations to date characterising MNPs in human tissue have primarily been performed in steady-state conditions. Since anogenital inflammation is now recognised as a key factor in HIV transmission, with epithelial LCs and DCs being the first target cells encountered, investigating and understanding the inflammatory landscape of DCs and their interactions with HIV is urgently needed to reduce the risk of HIV acquisition in the anogenital mucosa. To date, the recognised inflammatory DCs include pDCs, ASDCs, MDDCs and epithelial CD11c$^+$ DCs.” The phenotypes of steady state and inflammatory tissue MNPs are summarised in **Figure 1.3**.

1.5 Mononuclear Phagocyte-T Cell Transmission Mechanisms

“DCs can transfer HIV to CD4 T cells via two distinct mechanisms: first-phase transfer, also referred to as *trans*-infection, and second-phase transfer, or *cis*-infection (McDonald et al., 2003, Turville et al., 2004, Cunningham et al., 2013b, Cunningham et al., 2013a). First-phase transfer is dependent on lectin receptor-mediated uptake into vacuolar virus-containing compartments (VCCs) and occurs independently of DC infection (Turville et al., 2002). These VCCs are continuous with the plasma membrane, connected to the external environment via a narrow canal, at neutral pH and poorly accessed by antibodies. If the virus encounters CD4 T cells within a few hours, a viral synapse forms with contacting CD4 T cells, allowing transfer to and the infection of the T cells. However, within 12–24 hours, the majority of the virus is degraded, but it has not yet been shown how or if the virus leaves these neutral pH compartments for end lysosomal degradation (Turville et al., 2004). Currently, there are five known HIV-binding lectin receptors: langerin/CD207/CLEC4K, Mannose Receptor (MR)/CD206/CLEC13D, DC-SIGN/CD209/CLEC4L, Siglec-1/CD169 and DCIR/CD367/CLEC4A. Langerin has been shown to mediate HIV uptake by epidermal LCs and transfer to CD4 T cells (Nasr et al., 2014), although there is some viral degradation within the Birbeck granules (de Witte et al., 2007). Sub-epithelial langerin$^+$

cDC2s are also very efficient at HIV uptake but they express langerin at 10-fold lower levels than LCs, and it is not known if this langerin expression mediates HIV uptake by these cells. MR is expressed by most tissue DCs as well as macrophages and can mediate HIV uptake (Lai et al., 2009, Turville et al., 2004). However, binding is weak and leads to viral destruction by lysosomes rather than uptake into caves (Turville et al., 2004). DC-SIGN is highly efficient at HIV binding and uptake (Geijtenbeek et al., 2000), and although this was originally thought to be a DC receptor, recent evidence demonstrates that DC-SIGN is expressed by macrophages (Rhodes et al., 2021). Siglec-1 is expressed by most MNPs and inducible by type-I interferon (IFN-I) production (Puryear et al., 2013). Recently, it was induced at the gene level in macrophages by type III interferon (I3), although this remains to be validated at the at the protein level (Wang et al., 2024). It has been shown to directly mediate HIV uptake into intracellular caves in in vitro-generated MDDCs, but only when in a mature state (Pino et al., 2015, Izquierdo-Useros et al., 2012, Yu et al., 2008, Izquierdo-Useros et al., 2009). Siglec-1 can also act to concentrate HIV and transfer it to the CD4/CCR5 entry receptors to facilitate productive infection (Turville et al., 2004, Ruffin et al., 2019). However, like DC-SIGN, Siglec-1 is now known to be expressed predominantly by macrophages, with the notable exception of a subset of inflammatory ASDCs, as discussed below. CLEC4A has also only been explored in in vitro-generated MDDCs, on which it is capable of HIV uptake and transfer (Lambert et al., 2008, Lambert et al., 2013), albeit not as efficiently as DC-SIGN (Jin et al., 2014). CLEC4A is expressed highly by all tissue MNPs; however, it has not yet been shown capable of binding or transmitting HIV in tissue. The varying expression of lectin receptors across MNP subsets not only implicates their roles in first-phase transfer but further serves an additional way to classify MNP subsets.

Second-phase transfer is dependent on productive HIV infection via the entry receptors CD4 and CCR5, which mediate the fusion of the virus envelope with the DC plasma membrane and the release of the viral genome into the cytosol. It occurs 72 h after initial infection as de novo-produced virions bud from the DC plasma membrane and infect CD4 T cells as they interact with DCs via a virological synapse (Jolly et al., 2004, Sourisseau et al., 2007, Aggarwal et al., 2012).”

Inflammatory tissue DCs

Population	Key distinguishing markers
pDC 	HLA-DR^{lo} Axl^{-} CD123^{+} Siglec-6^{-} BDCA2^{+} CD5^{-} BDCA-4^{+} CD11c^{-} CD45RA^{+} CD2$^{+/lo}$
CD11c^{+} ASDC 	HLA-DR^{++} CD45RA^{+} CD2^{+} CD11c^{+} CX3CR1^{-} Axl^{+} Siglec-1$^{+/int}$ Siglec-6^{+} CD1c$^{+/int}$ CD5^{+} CD123^{int} CD33^{+} BDCA-2^{int}
CD123^{+} ASDC 	HLA-DR^{+} CD45RA^{+} CD2^{+} CD123+ CX3CR1^{+} Axl^{+} Siglec-1^{++} Siglec-6^{+} CD1c^{-} CD5^{+} CD11c^{int} CD33^{+} BDCA-2^{+}
DC3 	HLA-DR^{+} S100A8/9^{+} CD11c^{+} BTLA^{-} CD1c^{+} CD88^{-} CD163^{+} CD5^{-} CD14$^{+/-}$ CD1a^{-} CLEC10A^{+}
MDDC 	HLA-DR^{+} S100A8/9^{+} CD11c^{+} CD163^{-} CD1c^{+} CD16^{-} CD14^{+} AF^{-} CD88^{+}
Epi CD11c^{+} cDC2 	HLA-DR^{+} Langerin$^{lo/int}$ CD11c^{+} FcεRIα^{+} CD1c^{+} MR^{+} CD11b^{+} No Birbeck CD1a^{lo} granule

Other tissue MNPs

Population	Key distinguishing markers
Langerhans cell 	HLA-DR^{+} MR^{-} CD1a^{++} Birbeck Langerin^{+} granule CD1c^{+} CD11c^{lo}
cDC1 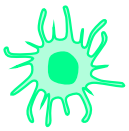	HLA-DR^{+} CD1c$^{lo/-}$ CD141^{++} CD11c^{lo} XCR1^{+} CLEC9A^{+} CADM1^{+}
cDC2 	HLA-DR^{++} CD5$^{+/-}$ CD1c^{+} FcεRIα^{+} CD11c^{+} HLA-DQ^{+} CD11b^{+} CD88^{-} CD1a^{+} CD163^{-} Langerin$^{+/-}$
Macrophage 	HLA-DR^{+} DC-SIGN^{+} CD163^{+} Siglec-1^{+} CD14^{+} AF^{+} CD64^{+} FXIIIA^{+}
MDM 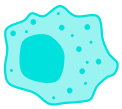	HLA-DR^{+} DC-SIGN^{+} CD14^{+} Siglec-1^{+} CD163^{+} AF^{-} CD11c^{-} CD1c^{-}

DC: Dendritic Cell
MNP: Mononuclear Phagocyte
pDC: Plasmacytoid DC
ASDC: Axl+ Siglec-6+ DC
MDDC: Monocyte-derived DC
Epi: Epithelium
MDM: Monocyte-derived Macrophage
AF: Autofluorescent

Figure 1.3: Human inflammatory and steady state MNP phenotypes.

1.6 Plasmacytoid Dendritic cells

1.6.1 Origins and Discovery

"pDCs were first described in the 1950s in human lymph nodes and were initially thought to be T cells based on their surface protein expression profile (Lennert and Remmele, 1958). Several decades later, upon being cultured, they were found to develop DC-like morphology and express high levels of MHC proteins (O'Doherty et

al., 1994, Rhodes et al., 2019), hence gaining their classification as a DC (although this 'DC' classification remains a topic of debate) (Ziegler-Heitbrock et al., 2023a, Reizis et al., 2023, Ziegler-Heitbrock et al., 2023b). Traditionally defined as $CD123^{+}$ $CD11c^{-}$, pDCs are the primary IFN-I-producing cells in response to viral infection (Cella et al., 1999, Siegal et al., 1999) and crucial mediators of the inflammatory response (Takagi et al., 2011). pDCs are derived directly from the common DC progenitor (cDP), which arises from $IRF8^{high}$ granulocyte monocyte DC progenitors (GMPDs) like cDC1 and cDC2 (Cytlak et al., 2020). Similar to other DCs derived from a myeloid lineage, pDC differentiation can be driven by FLT3/CD135, c-Kit/CD117 and M-CSF/CD115 (Naik et al., 2007), but uniquely, pDCs can also be derived directly from the lymphoid-primed multipotent progenitor regulated by the transcriptional factor TCF4/E2-2 (Cisse et al., 2008, Onai et al., 2013)."

1.6.2 Inflammation and Immunological Functions

"pDCs' high expression of toll-like receptor (TLR) 7, TLR9 and IRF7 enables their potent production of IFN-I (Honda and Taniguchi, 2006, Villani et al., 2017). The production of IFN-I (predominantly IFNα but also IFNβ) is their most fundamental immunological role, which forms one of the first and most important innate immune responses in restricting viral transmission. pDCs are particularly well-recognised in their initial responses to HIV infection (Beignon et al., 2005, Shang et al., 2017, Fonteneau et al., 2004, Tong et al., 2021). They migrate from blood to sites of infection within 1–2 days of exposure, where they mount a strong inflammatory response through the production of pro-inflammatory cytokines, including TNFα and IL-6 (Warner van Dijk et al., 2024, Gilliet et al., 2008, Beignon et al., 2005), and CD4 T-cell-recruiting chemokines CCL3-5 and CXCL8 (Shang et al., 2017, Warner van Dijk et al., 2024, Beignon et al., 2005). Therefore, the role of pDCs during HIV infection is controversial as it is not clear whether these cells exacerbate or limit initial infection. Since the discovery of ASDCs, which were found to be contained within the $CD123^{+}$ pDC population (Villani et al., 2017), pDCs have recently been redefined to have a limited ability in inducing T-cell activation, proliferation and polarisation (See et al., 2017, Warner van Dijk et al., 2024).

After excluding ASDCs, several studies have identified and characterised three subpopulations within the pDC compartment, all with distinct phenotypes and

functionalities that arise upon activation with different stimuli (Alculumbre et al., 2018, Onodi et al., 2021, Sosa Cuevas et al., 2022). In 2018, Alculumbre et al. identified three subsets – P1, P2 and P3 – of activated Axl^- pDCs upon stimulation with TLR7 ligands (influenza and R848), TLR9 ligands (CpG-A, CpG-B and CpG-C), bacteria (S. aureus) or cytokines (IL-3 and GM-CSF). P1-pDCs (PD-$L1^+$ $CD80^-$) maintained a plasmacytoid morphology and high IFN-I production, whereas P3-pDCs (PD-$L1^-$ $CD80^+$) developed a dendritic morphology, had elevated CCR7 expression and were capable of T-cell activation and Th2 polarisation, but they were unable to produce IFN-I. P2-pDCs (PD-$L1^-$ $CD80^+$) displayed a functional continuum of both P1 and P3 and likely are an intermediate cell. TLR7 ligands and CpG-Ca significantly induced all three pDC populations, CpG-A and *S. aureus* primarily induced P1-pDCs, whereas CpG-B, GM-CSF and IL-3 preferentially induced P3-pDCs. Furthermore, they showed that only P1-pDCs were detected in samples (blood or skin) from patients with psoriasis or lupus. Alculumbre et al. also found that the specialisation of these pDCs into P1, P2 or P3 was independent of a pre-existing heterogeneity, a pre-commitment of pDC precursors or IFN feedback but rather a result of cell-to-cell communication from autocrine or paracrine loops of cytokine secretion. Onodi et al. later showed that human pDCs efficiently diversified into functional P1-, P2-and P3-pDC effector subsets in response to SARS-CoV-2, while Sosa Cuevas et al. demonstrated that P3-pDCs accumulated within tumours of melanoma patients and negatively correlated with clinical outcomes. These new discoveries of pDC plasticity and complexity prompt the need to further investigate pDCs' specific functional roles in immunity and inflammation."

1.6.3 HIV Interactions

"pDCs' role in HIV infection serves predominantly as a protective function. Upon infection, pDCs become activated by HIV RNA through the TLR7 signalling pathway which triggers a rapid IFN-I response (Beignon et al., 2005). This defensive viral mechanism was first evidenced through SIV infection in rhesus macaque models (Sandler et al., 2014). Upon blocking the IFN-I receptor preceding an acute rectal SIV infection, there was a rapid depletion of CD4 T cells and expansion of the viral reservoir, resulting in an accelerated onset of AIDS. Indeed, several studies reported IFN resistance to be a major contributor to HIV transmission (Iyer et al., 2017, Foster et al., 2016), emphasising the importance of pDCs' antiviral role.

It was previously believed that pDCs were capable of being productively infected by HIV (Lederle et al., 2014, Fong et al., 2002); however, this has since been attributed to the contaminating $CD123^+$ ASDC population (Ruffin et al., 2019, Warner van Dijk et al., 2024). In fact, the pro-inflammatory chemokines CCL3-5 secreted by pDCs in response to HIV simultaneously recruit CD4 T cells and block HIV infection by binding to the co-receptor CCR5 (Scarlatti et al., 1997). This blockage of the HIV entry receptor and high IFN production both work to inhibit the productive infection of pDCs (Beignon et al., 2005, Tong et al., 2021). One study observed pDCs to be capable of HIV transfer to CD4 T cells at a very limited capacity in first-phase transfer only (Warner van Dijk et al., 2024). This may be explained by their expression of CLEC4A, a C-type lectin that has been shown to bind HIV (Lambert et al., 2008). The diverse roles of pDCs in HIV interactions also raise questions about the functions of activated P1-, P2-, and P3-pDC subsets (Alculumbre et al., 2018). P3-pDCs morphologically resemble DCs and, combined with their high expression of co-stimulatory molecules, migratory capacity and ability to activate and proliferate CD4 T cells, it could be hypothesised that P3-pDCs are able to perform HIV transfer in the first phase. P1-pDCs were the only subset that produced IFN; hence, the rapid IFN response triggered by HIV exposure could be attributed solely to P1-pDCs. Further investigation of these pDC subpopulations' interaction with HIV is needed to fully understand their specific and individual roles in HIV transmission.

The activation of TLR7 to induce HIV expression in latently infected cells through the release of IFNα from pDCs (Tsai et al., 2017) has been explored. However, this approach is limited by the following: **1)** TLR7 polymorphism, which affects the ability of pDCs to activate and secrete IFN (Shi et al., 2020). **2)** A decline in pDC numbers, which occurs in most people living with HIV (PLH). Upon the initiation of antiretroviral therapy (ART), their numbers can increase but are not fully restored. **3)** pDCs are dysfunctional upon ART interruption, thus interfering with TLR signalling. **4)** pDCs predominately produce IFNα2, which is less potent than IFNα8/14 (Sutter et al., 2018). **5)** Only long-term non-progressors and elite controllers of PLH have preserved pDCs counts and functionality (Almeida et al., 2005). Therefore, targeting pDCs for an HIV cure has many limitations, but, potentially, a direct IFNα8/14 treatment may be a better approach to reactivate latent HIV (Tong et al., 2021), especially as IFNα8/14 can reshape the human immune system by activating macrophages, natural killer cells,

DCs, and T cells and secreting a variety of cytokines that modulate B- and T-cell activation (Hervas-Stubbs et al., 2011)."

1.7 Axl$^+$ Siglec-6$^+$ Dendritic Cells

1.7.1 Origins and Discovery

"ASDCs are a newly defined DC population initially identified in human blood, owing to advances in high parameter single-cell technologies; they are distinguished by their unique expression of Axl, Siglec-6 and CD5 (Villani et al., 2017, Alcántara-Hernández et al., 2017, See et al., 2017). ASDCs can be further divided into two discrete subsets by the expression of CD11c or CD123, with each subset having distinctive phenotypical and functional profiles (Villani et al., 2017, Warner van Dijk et al., 2024). The CD123$^+$ and CD11c$^+$ ASDC populations identified by Villani et al. express Axl, Siglec-6, CD2, CX3CR1, CD33, and CD5, similar to the phenotype described for pre-cDC1 and pre-cDC2 (CD33$^+$ CD45RA$^+$ CD123$^+$ CX3CR1$^+$ CD2$^+$ CD5$^+$ Siglec-6$^+$) identified by See et al. Therefore, CD123$^+$ CD11c- ASDCs are pre-cDC1s, while CD123$^-$ CD11c$^+$ ASDCs are pre-DC2s, with CD11c$^+$ ASDCs being a different population from cDC2 (Warner van Dijk et al., 2024). ASDCs infiltrate peripheral tissues during inflammation, while cDC2s are present in both healthy (Rhodes et al., 2021) and inflamed tissues (Reynolds et al., 2021).

The discovery of these new DCs has prompted a rapid reclassification of pDCs' immune function capabilities as many of their previously described roles, including antigen presentation, T-cell activation and also HIV infection (Lederle et al., 2014, Fong et al., 2002), have now been attributed to contaminating ASDCs (Villani et al., 2017, See et al., 2017, Warner van Dijk et al., 2024, Ruffin et al., 2019).

The developmental origins of ASDCs remain contentious; some studies report ASDCs to be an intermediate cell state – a precursor to cDC1 or cDC2 (See et al., 2017), whilst others detail a distinct and functional DC, reminiscent of a bona fide population (Villani et al., 2017). Like pDCs, cDC1s and cDC2s, ASDCs arise from the cDP. See et al. further contends that ASDCs are circulating DC progenitors, transient pre-cDC1s or pre-cDC2s that commit to cDC1/2 differentiation. In contrast, Villani et al. found ASDCs to be a well-defined cell subset, with morphological similarities to cDC2s, high T-cell proliferative capacity and distinct functionalities, including a lack of IFN

production and secretion of IL-12p70 and IL-8. In support of this, Alcántara-Hernández and colleagues further demonstrated that when cultured, ASDCs only transitioned towards a cDC2 phenotype and not cDC1. They also observed that ASDC distribution in inflamed skin and lymphoid organs mirrored pDCs and not DCs, challenging the idea that ASDCs are DC precursors. Importantly, Warner van Dijk et al. showed that ASDCs derived from blood and tissues are a separate population to cDC2s but are mature in phenotypes like cDC2s. Further studies are needed to investigate the developmental origins and differentiation potential of these cells before firm conclusions are made (Rhodes et al., 2019)."

1.7.2 Inflammation and Immunological Functions

"In peripheral tissue and lymphoid organs, ASDCs, like pDCs, are inflammatory cells that infiltrate tissue from the blood in response to stimuli. A recent investigation compared an inflamed rectum from an ulcerative colitis patient to a non-inflamed rectum and found ASDCs to be exclusively present in the inflamed sample (Warner van Dijk et al., 2024). This study further identified ASDCs in the inflamed colon of diverticulitis and colorectal cancer patients and on psoriasis-diseased skin, inflamed mesenteric lymph nodes and inflamed anogenital tissues, including those from the labia and foreskin. ASDCs have also been identified in a range of other inflammatory conditions and locations, including inflamed cerebrospinal fluid (CSF) from multiple sclerosis (MS) patients (Kang et al., 2023), skin from blisters and wounds (Chen et al., 2020), inflamed bronchoalveolar lavage (Jardine et al., 2019), tonsils (Villani et al., 2017, Alcántara-Hernández et al., 2017) and spleens (See et al., 2017, Alcántara-Hernández et al., 2017) (**Table 1.1**).

Many ASDC functional investigations were limited by two main factors: **1)** since ASDCs are infiltrating inflammatory cells, the tissue-derived populations were too small for functional studies (Jardine et al., 2019, Warner van Dijk et al., 2024), so blood-derived ASDCs were used instead, and **2)** few studies separated ASDCs into their discrete $CD11c^+$ and $CD123^+$ subsets (Villani et al., 2017, Warner van Dijk et al., 2024, Jardine et al., 2019, Brouiller et al., 2023, Alcántara-Hernández et al., 2017), meaning that most functional data was derived from a combined ASDC population or only the $CD123^+$ subset. Nonetheless, in blood, ASDCs have higher T-cell-stimulating capacity and a more mature phenotype compared to pDCs, similar to cDC2s (Villani

et al., 2017, See et al., 2017, Warner van Dijk et al., 2024, Alcántara-Hernández et al., 2017, Brouiller et al., 2023). Warner van Dijk et al. further showed that CD11c$^+$ ASDCs expressed higher levels of the costimulatory molecules CD86, ICAM-1 and HLA-DR and hence were more potent inducers of naïve CD4 T-cell activation and proliferation compared to their CD123$^+$ counterpart. pDCs expressed maturation makers at much lower levels and were poor at T-cell stimulation. In the absence of pathogens, naive T cells cultured with ASDCs produced higher levels of IL-4, IL-5, IL-13, IL-9, IL-17, IL-22 and IL-10 than those cultured with pDCs, indicating a polarisation towards Th2, Th9, Th17, Th22, and Treg, which have broad roles in humoral, bacterial and auto-immunity, and less towards Th1, responsible for antiviral responses (O'Neil et al., 2021). This pattern of polarisation was reported to be linked to the ASDCs' high expression of CD5. CD5 is required for cDC2s to stimulate naïve T-cell proliferation and priming towards Th2, Th17, Th22 and Treg cells, while monocyte-like DCs, which express lower CD5, polarise towards Th1 cells (Yin et al., 2017). Warner van Dijk et al. showed that HIV infection downregulated CD5 expression. However, whether this downregulation favours the induction of the antiviral Th1 subset was not investigated due to low isolated ASDC numbers. Unlike pDCs, HIV-exposed ASDCs do not produce IFN-I (Warner van Dijk et al., 2024). This correlates with their lack of TLR7 and IRF7 expression (Villani et al., 2017, Rhodes et al., 2019). Furthermore, their Siglec-1 expression may inhibit IFN production by inducing TBK1 degradation, as reported for macrophages (Zheng et al., 2015).

In the CSF of patients with inflammatory demyelinating diseases, ASDCs were observed to have poly-adhesion functions with the ability to stimulate both CD4 T cells and LAMP3$^+$ DCs (mature/migratory DC) and bind various immune cells, including B and T cells (Kang et al., 2023). The authors concluded that ASDCs significantly contribute to the pathogenesis of conditions like MS by triggering an inflammatory cascade of immune cells. The further investigation of ASDCs in the context of specific inflammatory diseases is needed to uncover condition-specific functionalities."

Table 1.1: Summary of ASDCs in the current literature.

Citation	Source tissue	Defining markers	Separated into CD11c$^+$ and CD123$^+$ subsets?	Immune functions	HIV interactions
Villani et al., 2017	Blood and tonsil	Axl$^+$ Siglec-6$^+$ CD5$^+$ CD11c$^{+/-}$ CD123$^{+/-}$	Yes	• Both subsets are potent stimulators of CD4 and CD8 T cell proliferation	Not investigated
See et al., 2019	Blood and spleen	Siglec-6$^+$ CD123$^+$ CX3CR1$^+$ CD45RA$^+$ CD33$^+$ CD5$^+$ CD2$^+$	No	• Induced proliferation and polarisation of CD4 T cells	Not investigated
Alcántara-Hernández et al., 2017	Blood, tonsil and spleen	Axl$^+$ CD123$^{+/int}$ CD11c$^{+/-}$ CD2$^+$	Yes	• ASDCs have a higher T cell stimulating capacity compared to pDCs	Not investigated
Warner van Dijk et al., 2024	Blood and anogenital tissue	Axl$^+$ Siglec-6$^+$ CD5$^+$ CD11c$^{+/-}$ CD123$^{+/-}$ CX3CR1$^{+/-}$	Yes	• CD11c$^+$ ASDCs are more potent inducers of CD4 T cell activation and proliferation compared to CD123$^+$ ASDCs • Both ASDC subsets polarise T cells towards Th2, Th9, Th17, Th22 and Treg	• CD11c$^+$ ASDCs are more efficient at first-phase transfer to CD4 T cells • CD123$^+$ ASDCs are more efficient at second-phase transfer to CD4 T cells
Kang et al., 2023	Cerebrospinal fluid (demyelinating diseases)	Axl$^+$ Siglec-6$^+$	No	• Stimulate CD4 T cells and mature LAMP3$^+$ DCs • Bind B and T cells	Not investigated
Chen et al., 2020	Skin (blisters and wounds)	Axl$^+$ Siglec-6$^+$ BDCA-2$^+$ CD123^{int}	No	• Identified as an early infiltrator in inflammation	Not investigated
Jardine et al., 2019	Bronchoalveolar lavage	Axl$^+$ Siglec-6$^+$	Yes	• Too few cell numbers for functional investigation	Not investigated
Ruffin et al., 2019	Blood	Axl$^+$ CD123$^+$ CD45RA$^+$ Siglec-1$^+$	No	Not investigated	• CD123$^+$ ASDCs are productively infected with HIV and transfer the virus to CD4 T cells
Brouiller et al., 2023	Blood	Axl$^+$	Yes/No (investigated as both combined and separate)	Not investigated	• Productive HIV Infection of ASDCs was mediated by Vpx which neutralises SAMHD1, a restrictive factor that limits productive infection

1.7.3 HIV Uptake, Infection and Transfer to T Cells by Axl$^+$ Siglec-6$^+$ Dendritic Cells

"Both the CD11c$^+$ and CD123$^+$ ASDC subsets can transmit HIV to T cells via differing mechanisms. Ruffin et al. and Warner van Dijk et al. found that CD123$^+$ ASDCs isolated from blood were productively infected with HIV and transferred the virus to CD4 T cells via second-phase transfer. This correlates with their higher expression of the HIV entry receptors CD4 and CCR5. Warner van Dijk and colleagues further showed in blood-derived ASDCs that the CD11c$^+$ subset was most efficient at mediating first-phase HIV transfer, corresponding with their higher expression of lectin receptor MR (Lai et al., 2009), langerin (Nasr et al., 2014) and DC-SIGN (Bernhard et al., 2004). Mature DCs have a higher capacity to bind HIV compared to immature cells (Harman et al., 2006) but are less capable of supporting productive infection (Ruffin et al., 2019, Turville et al., 2002, Turville et al., 2004). Since CD11c$^+$ ASDCs exhibit a more mature phenotype, characterised by high CD86 and HLA-DR expression (Warner van Dijk et al., 2024), this likely explains their enhanced efficiency in mediating first-phase viral transfer. Additionally, CD11c$^+$ ASDCs expressed higher levels of the HIV restriction factor SAMHD1, which may further explain their lack of productive infection. Brouiller et al. investigated the HIV infection of blood-derived ASDCs and observed high p24 levels within CD11c$^+$ ASDCs, indicating efficient productive infection. However, Warner van Dijk et al. pointed out that this productive infection was mediated by Vpx, which neutralises SAMHD1. This supports their conclusion that SAMHD1 expression in CD11c$^+$ ASDCs limits productive infection.

The HIV infection of skin and mucosal ASDCs has remained unexplored due to low cell numbers. However, a comparison of HIV-binding receptor expression between human-blood and anogenital-tissue ASDCs was performed and revealed both tissue- and blood-derived ASDCs express CD4 and Siglec-1 at similarly high levels (Warner van Dijk et al., 2024). DC-SIGN, MR and langerin were more highly expressed by tissue ASDCs compared to blood, and more so by CD11c$^+$ ASDCs than CD123$^+$ ASDCs, however it is widely recognised that blood and tissue DCs express different levels of the same markers (Rhodes et al., 2021). This purely emphasises the need to investigate HIV interactions with ASDCs at the primary transmission sites and further understand their relative importance in HIV infection compared to other tissue DCs. If tissue-derived ASDCs show similar profiles to blood ASDCs in HIV uptake,

susceptibility to HIV infection, and mode of HIV transfer to T cells, future strategies aiming at inhibiting HIV transmission, namely PrEP regimes, should consider the interactions of ASDCs with HIV to prevent its transfer to CD4 T cells."

1.8 DC3s

1.8.1 Origins and Discovery

"Most recently, DC3s were discovered using scRNA sequencing in human blood by Villani et al. in 2017 (Villani et al., 2017). DC3s are best defined as $CD1c^{+}$-, $CD163^{+}$-, $CD14^{+/-}$-,$CD5^{-}$- and $CD88^{-}$-expressing DCs and for many years were misidentified due to their co-expression of defining markers for cDC2s and monocyte-derived cells (Cytlak et al., 2020, Dutertre et al., 2019, Segura, 2022, Bourdely et al., 2020). They have now been further identified in bone marrow (Cytlak et al., 2020), body skin (Nakamizo et al., 2021, Cytlak et al., 2020), spleens (Cytlak et al., 2020), bronchoalveolar lavage (Jardine et al., 2019), cancerous tumours (Santegoets et al., 2020, Subtil et al., 2024), the synovium, synovial fluid (Qiu et al., 2022), kidneys (Chen et al., 2024), the cervix and the endometrium (Parthasarathy et al., 2024) (**Table 1.2**).

DC3s are a bona fide DC population and develop from a distinctly different lineage to cDC1s and cDC2s. Like monocytes, they arise from an $IRF8^{low}$ GMPD progenitor pathway, which is separate to the $IRF8^{high}$-dependent GMPD pathway of cDC1s, cDC2s and pDCs (Cytlak et al., 2020). Furthermore, Bourdely and colleagues (Bourdely et al., 2020) showed that DC3 differentiation is only driven by a GM-CSF-dependent pathway as opposed to an FLT3L-dependent pathway, the latter of which supports the differentiation of cDP. However, several cancer-specific investigations observed an in vitro tumour microenvironment phenomenon where cDC2s shifted towards a DC3 like-phenotype, acquiring CD14 and CD163 expression, in response to tumour-derived factors including IL-6 and M-CSF (Subtil et al., 2024, Becker et al., 2024). This same shift was not observed in monocytes. It is likely that DC3s are indeed a bona fide population but in specific tumour environments may be capable of arising from highly plastic cDC2s. Whether this cDC2-DC3 shift is possible in other specific inflammatory microenvironments remains to be investigated."

Table 1.2: Summary of DC3s in the current literature.

Citation	Source tissue	Defining markers	Immune functions	HIV interactions
Villani et al., 2017	Blood and tonsil	$CD1c^+$ $CD163^+$	• Stimulates naïve CD4 and CD8 T cells	• High protein expression of HIV co-receptor CXCR4 • RNA expression of HIV lectin receptor Siglec-1
Dutertre et al., 2019	Blood (lupus erythematosus)	$CD1c^+$ $CD163^+$ $CD5^-$ $CD88^-$ $CD14^{+/-}$	• Stimulates naïve CD4 T cells • Induces Th1, Th2 and Th17 polarisation	• RNA expression of HIV lectin receptor Siglec-1 which is increased on inflammatory DC3s
Bourdely et al., 2020	Blood and primary breast tumours	$CD1c^+$ $CD163^+$ $CD88^-$ $CD14^{+/-}$	• Stimulates naïve CD4 and CD8 T cells • Secretes pro-inflammatory cytokines IL-23 and TNFα	Not investigated
Cytlak et al., 2020	Blood, spleen, dermis	$CD1c^+$ $CD163^+$ $CD14^+$ $BTLA^-$	• Secretes pro-inflammatory cytokines IL-8, TNFα and IL-1β	Not investigated
Nakamizo et al., 2021	Blood and body skin (psoriasis)	$CD1c^+$ $CD14^+$ $CD88^-$	• Co-expression of markers IL-6 and IL-23 indicates their potential role in Th17 cell differentiation	Not investigated
Jardine et al., 2019	Bronchoalveolar lavage	$BTLA^-$ $CD5^-$ $CD163^+$ $CD14^+$ $S100A8/9^+$	• Induces Th1 and Th17 polarisation	Not investigated
Chen et al., 2024	Kidney (lupus nephritis)	$CD163^+$ $CD1c^+$ $CD88^-$	• Induces Th1 and Th17 polarisation • High DC3 numbers associated with poor renal prognosis	Not investigated
Subtil et al., 2024	Primary malignant colorectal tumour and liver metastasis	$CD14^+$ $CD1c^+$ $CD163^+$	• Impaired T cell activating and proliferating capacity compared to cDC2s	Not investigated
Santegoets et al., 2020	Oropharyngeal squamous cell carcinoma tumour	$CD1c^+$ $CD163^+$ $CD14^-$	• Secretes cytokines IL-12 and IL-18 • Primes Th1 polarisation	• High protein expression of HIV co-receptor CXCR4
Qiu et al., 2022	Synovium and synovial fluid (osteoarthritis)	$CD1c^+$ $CD163^+$ $CD88^-$	• Secretes pro inflammatory cytokines TNFα, IL-23 and IL12p70 • Primes CD8 T cells	Not investigated
Parthasarathy et al., 2024	Cervix and endometrium	$CD1c^+$ $CD14^+$ (combined with MDDC)	• Upregulation of genes associated with the initiation of inflammation and antiviral roles	• High protein expression of HIV entry receptors CD4, CCR5 and CXCR4

1.8.2 Inflammation and Immunological Functions

“DC3s have been specifically implicated in a number of inflammatory disease settings, with many studies highlighting a strong association between CD14 expression and inflammation. CD14-expressing DC3s are increased in the peripheral blood of patients living with chronic autoimmune diseases and systemic infections, including lupus erythematosus (Dutertre et al., 2019), melanoma (Bakdash et al., 2016) and severe COVID-19 (Winheim et al., 2021). Although the precise immune roles of inflammatory DC3s in these conditions remain unclear, blood DC3s have been shown to stimulate naïve CD4 and CD8 T cells (Bourdely et al., 2020, Villani et al., 2017, Dutertre et al., 2019), secrete pro-inflammatory cytokines such as IL-8, IL-23, TNFα and IL-1β (Bourdely et al., 2020, Cytlak et al., 2020) and induce Th1, Th2 and Th17 polarisation (Dutertre et al., 2019, Bourdely et al., 2020). These immune capabilities are similar to cDC2s. $CD14^{+}$ DC3s were also more abundant in inflamed bronchoalveolar lavage when compared to a non-inflamed control (Jardine et al., 2019). Upon entering the inflammatory airspace, DC3s were functionally altered and capable of inducing IFNγ and IL-17 secretion from CD4 T cells, which stimulates Th1 and Th17 polarisation, respectively, supporting the previous findings of blood-derived DC3s.

In inflamed tissues, DC3s are significantly enriched and frequently associated with poor patient outcomes and treatment unresponsiveness across specific disease contexts (Chen et al., 2024, Subtil et al., 2024, Bakdash et al., 2016). Poor renal prognosis in lupus nephritis patients was directly linked to increased DC3 numbers in the kidney, driven by their potent capacity to prime Th1 and Th17 responses, causing tissue damage and T-cell trafficking (Chen et al., 2024). Within malignant tumour microenvironments (Santegoets et al., 2020) and the synovium of osteoarthritis patients (Qiu et al., 2022), DC3s also demonstrated strong Th1 priming capacity through high production levels of IL-12 and IL-18, and TNFα. Furthermore, synovial DC3s were efficient at activating CD8 T cells. However, in certain malignancies, DC3s exhibited impaired T-cell activation compared to cDC2s, likely influenced by the tumour-specific secretome, which disrupts DC function (Subtil et al., 2024). Inflammatory DC3s identified in lesional body skin of psoriasis and atopic dermatitis patients expressed IL-6 and IL-23, indicating their potential role in Th17 cell differentiation (Nakamizo et al., 2021), although it should be noted that the protein data from this investigation may be contaminated with B cells. Nakamizo et al. identified

DC3s as $CD14^+$ $CD1c^+$ cells; however, CD14, CD3 (T cells) and CD19 (B cells) were all detected with the same fluorophore, which is confounding as a small population of memory B cells have also been reported to express CD1c in blood and lymphoid organs (Delia et al., 1988, Fairhurst et al., 1998, Stewart et al., 2021, Weller et al., 2004, Golinski et al., 2020).

Based on the above, it is likely that many DC3 populations have been misidentified. In fact, a recent review by Odell (2024) found that out of 13 scRNA seq investigations published over the last 5 years investigating inflammatory scleroderma of the skin and lung and liver cirrhosis, only one accurately identified the DC3 population, and the remaining mislabelled DC3s as macrophages or monocytes. Upon re-analysis, Odell reclassified the misidentified populations as DC3s and demonstrated that DC3s were enriched in scleroderma and cirrhosis conditions, and their infiltration often correlated with disease severity. Without this re-analysis, the presence of these inflammatory DC3s would have been missed.

It is evident that DC3s are emerging as a central inflammatory DC with diverse immune functions. Investigations have demonstrated, both in human blood and tissue, that DC3s can stimulate naïve CD4 and CD8 T cells and prime Th1 and Th17 responses, and that they are potent pro-inflammatory cytokine secretors. Research must further elucidate the presence and function of DC3s in human skin and mucosae and their relation to other inflammatory pathologies."

1.8.3 HIV Interactions

"Investigations examining the interactions of DC3s with HIV are limited, and little information exists on their expression of HIV-binding receptors. A very recent study by Parthasarathy and colleagues investigated the changes in the gene and protein signatures of $CD14^+$ DCs, as a combined population of DC3s and $CD14^+$ MDDCs, before and after HIV infection in cervical and endometrial tissue. Upon HIV exposure, they observed an upregulation of genes associated with the initiation of inflammation and antiviral roles; however, they were unable to determine whether these genes were solely attributable to DC3s. Nonetheless, they demonstrated that DC3s had a high protein expression of the HIV entry receptors CD4, CCR5 and CXCR4, indicating the capacity for second-phase transfer and productive infection. A high expression of the HIV co-receptor CXCR4 has also been shown on DC3s in blood (Villani et al., 2017)

and malignant tumours (Santegoets et al., 2020). Villani et al. showed at the RNA level that blood DC3s express Siglec-1 but not as highly as ASDCs. Dutertre et al. confirmed this expression of Siglec-1, further evidencing this increased expression specifically on inflammatory DC3s.

With the striking similarities between the immune functions of DC3 and cDC2, it is tempting to speculate over the potential involvement of DC3 in HIV transmission, given cDC2 can efficiently transfer virus to CD4 T cells (Rhodes et al., 2021, Bertram et al., 2019). However, this remains a critical gap in the HIV-DC literature."

1.9 Other Inflammatory Tissue Dendritic Cells

1.9.1 Monocyte-derived Dendritic Cells

"Traditionally CD14-expressing cells were described as either autofluorescent macrophages or non-autofluorescent $CD14^+$ DCs (Haniffa et al., 2009). McGovern et al. (McGovern et al., 2014) redefined the latter as a transient population of monocyte-derived macrophages (MDMs), which originated from blood-derived $CD14^+$ monocytes. In 2021, Rhodes et al. demonstrated that there are two populations of $CD14^+$-expressing MNPs: a $CD14^+$ $CD1c^-$ $CD11c^-$ MDM population that was non-migratory and transcriptionally and morphologically similar to macrophages, and a $CD14^+$ $CD1c^+$ $CD11c^+$ MDDC population that could spontaneously migrate out of tissue and was transcriptionally and morphologically similar to DCs. This description of a $CD14^+$ MDDC population aligned with previous reports of a $CD14^+$ monocyte-derived cell transcriptionally aligning with DCs rather than blood monocytes (Harman et al., 2013, Watchmaker et al., 2014, Tang-Huau et al., 2018, Richter et al., 2018, Michea et al., 2018) and possessing dendritic morphology (Segura et al., 2013, Michea et al., 2018).

MDDCs are produced at tissue sites during inflammation from infiltrating monocytes or in vivo in the presence of GM-CSF (Sallusto and Lanzavecchia, 1994, Singh et al., 2016, Menezes et al., 2016) and have been identified in a range of inflammatory conditions, including the pleural effusions of tuberculosis patients (Liu et al., 2018), urine of kidney transplant recipients with infection (Salvadé et al., 2024), intestinal LP of Crohn's patients (Martin et al., 2019), psoriatic skin (Singh et al., 2016) and inflamed ascites fluid, synovial fluid and spleens (Segura et al., 2013, Segura, 2022). In human

cervical tissue, inflammation was correlated with an increased $CD14^+$ MDDC infiltrate (Perez-Zsolt et al., 2019). Segura et al. (Segura et al., 2013) characterised a specifically inflammatory DC, termed infDC, distinguished by their expression of CD1c and CD14. These infDCs had a DC-like morphology, were transcriptionally distinct to other known DCs, were monocyte-derived and potently induced the Th17 differentiation of $CD4^+$ memory T cells. Other studies have confirmed this strong Th17 response by MDDCs through IL-23 secretion (Liu et al., 2018), as well as Th1 polarisation through IL-12 secretion (Watchmaker et al., 2014, Tang-Huau et al., 2018, Duluc et al., 2013).

Like cDC2s and DC3s, MDDCs are potent APCs, capable of antigen presentation and migration from tissues to lymph nodes, making them key players in HIV transmission (Perez-Zsolt et al., 2019, Rhodes et al., 2021). Several studies observed a $CD14^+$ $CD11c^{hi}$ MDDC in human cervical tissue that was capable of capturing HIV using lectin receptors without the integration or replication of the virus. Rodriguez-Garcia et al. was the first to demonstrate that tissue-derived MDDCs could capture HIV and showed that this occurred with or without the expression of DC-SIGN, implicating the presence of another lectin receptor mediating uptake. However, it is now known that the $CD14^+$ $CD11c^+$ $DC\text{-}SIGN^+$ cells were in fact MDMs, as MDDCs are $DC\text{-}SIGN^-$ (Rhodes et al., 2021). Trifonova et al. further found MDDCs to be the most efficient mediator of first-phase transfer, particularly when compared to tissue-resident macrophages. MDDCs expressing Siglec-1 were found to efficiently transfer HIV to CD4 T cells by Perez-Zsolt and colleagues, which was partially blocked by Siglec-1 antibodies. These Siglec-1 expressing MDDCs were more abundant in inflammation. The study showed that IFN-α stimulated the production of Siglec-1, thereby promoting HIV uptake and first-phase transfer in inflamed environments. The authors hypothesised that pDC recruitment to inflammation sites, triggering an antiviral IFN-I response, drives the upregulation of Siglec-1. In support of the previous cervical studies, Rhodes et al. showed in human skin and anogenital tissues, MDDCs could preferentially take up, become productively infected by and transfer HIV to CD4 T cells. They further demonstrated that blocking up to 40% of HIV infection in in vivo MDDCs was achieved using a siglec-1 antibody. The investigation concluded that these MDDCs did not express DC-SIGN or langerin, indicating perhaps an unknown lectin receptor was responsible for mediating HIV transfer (Vine et al., 2022). Ex vivo tissue-derived

MDDCs are also highly efficient at HIV transfer to CD4 T cells via the CD4/CCR5 mediated second-phase transfer pathway (Rhodes et al., 2021)."

1.9.2 Epithelial CD11c$^+$ Dendritic Cells

"In addition to LCs, the stratified squamous epithelium of human skin and type II mucosal tissues contains other DCs. Known for being CD11c$^+$ langerin^{lo} and lacking Birbeck granules, this DC has been described in the literature under several different aliases including inflammatory dendritic epithelial cell (IDEC) (Wollenberg et al., 1996), vaginal dendritic epithelial cell (VDEC) (Pena-Cruz et al., 2018), Epidermal CD11c$^+$ DC, and LC2, all probably representing independent identifications of the same cell population (Bertram et al., 2023). In the late 1990's Wollenberg and colleagues were the first to describe an epidermal DC present in inflammatory skin conditions such as atopic eczema and psoriasis. Critically, these cells were not LCs as they differed in expression profile and lacked Birbeck granules, however the functions of IDECs remain largely unexplored and unknown. It was proposed that in vitro generated IDECs are capable of initiating Th1 cell differentiation (Novak et al., 2004), however this has yet to be shown in vivo. Whilst IDECs were never explicitly investigated in relation to HIV, they express high levels of MR. Pena Cruz et al. identified a distinct DC subset within healthy human vaginal epithelium termed VDEC which could become productively infected by HIV using the CD4/CCR5 entry pathway. In 2019 Bertram et al. identified an epidermal HIV transmitting DC, particularly identifiable by their high expression of CD11c and MR and transcriptionally indistinguishable from dermal DCs. They demonstrated in abdominal tissue that epidermal CD11c$^+$ DCs were present in lower proportions than LCs while in genital skin they were present in equal numbers. However, they predominated in type I and II mucosae. Compared to LCs, epidermal CD11c$^+$ DCs were more efficient at HIV uptake and more susceptible to infection and correspondingly efficient at mediating both first- and second-phase transfer to CD4 T cells. The most recent independent identification of an epidermal DC population was described by Liu et al. as LC2s, sharing the same CD11c^{hi} langerin^{lo} profile as all previously mentioned studies and expression of the transcriptional factor IRF4, which is highly associated with cDC2s. LC2s were more abundant in foreskin epidermis and enriched in psoriatic skin inflammation, although they were not investigated in the context of HIV. In 2023 Bertram et al. used high parameter flow cytometry to demonstrate that IDEC, VDEC, epidermal CD11c$^+$ DC

and LC2 as originally identified, all correlated to the same cell type (Bertram et al., 2023). Although Pena-Cruz et al. and Bertram et al. have both showed these are key HIV target cells, their specific immune functions and interactions with HIV in an inflamed environment remain poorly understood."

1.10 Concluding Remarks

"HIV remains a significant global health burden, and as of 2023 there were almost 40 million people living with HIV and 1.3 million new infections (UNAIDS, 2024). Notably, HIV transmission is strongly linked to inflamed anogenital mucosa (Masson et al., 2015, Esra et al., 2016, Wall et al., 2017), a consequence of pre-existing STI's or microbiota dysbiosis (Laga et al., 1993, Mlisana et al., 2012, Masson et al., 2014, Atashili et al., 2008, Liu et al., 2017, Prodger et al., 2021), which frequently presents asymptomatically and hence remains undiagnosed (Koumans et al., 2007, Klebanoff et al., 2004). Despite significant progress over the past 40 years, with reduced incidence owing to revolutionary prophylactic measures and treatments, recent studies have shown that PrEP can be ineffective in the presence of anogenital inflammation (McKinnon et al., 2018, Klatt et al., 2017). Critically, a vaccine or cure for HIV remains elusive.

The early events of HIV transmission in anogenital tissues, particularly in an inflammatory setting, remains relatively unknown. DCs are the first cells to interact with HIV, hence understanding their ontology, immune functions, expression profiles and interactions with HIV forms a crucial step in developing new treatments. However, investigations of in vivo inflammation are challenging to navigate as complex inflammatory signals create a dynamic and unpredictable cellular environment. In inflamed anogenital tissues, increased susceptibility to HIV infection is thought to result from compromised epithelial barrier integrity, which exposes a range of DCs in the underlying tissue (Arnold et al., 2016, Zevin et al., 2016, Borgdorff et al., 2016); changes to resident DCs, which heighten their vulnerability to infection (Said and Weindl, 2015, Qin et al., 2012); and an influx of inflammation-specific HIV target cells (Li et al., 2009, Shang et al., 2017). The infiltrating inflammatory pDCs act as a 'double-edged' sword in their potential as a therapeutic target. pDCs' potent antiviral IFN-I production (Tong et al., 2021) and pro-inflammatory CCL3-5 secretion, which blocks CCR5 (Scarlatti et al., 1997), works as a vital defensive mechanism to prevent viral

transmission. Designing therapeutic interventions to enhance the immunological functions of pDCs may enhance the body's natural anti-HIV immune response (van der Sluis et al., 2020). However, simultaneously, this rapid IFN production induces the expression of Siglec-1 and drives the HIV binding and infection of many other DCs, amongst other limitations. Hence, any treatment targeting pDCs needs careful and innovative design.

ASDCs, $CD14^+$ MDDCs and epidermal $CD11c^+$ DCs are all capable of binding HIV and transmitting the virus to CD4 T cells in first- or second-phase transfer. Thus far, these inflammatory DCs have only been investigated in isolation. Future research should investigate the HIV infectivity of these DCs by comparing them to each other and to other resident DCs, such as cDC2s, to determine a preferential HIV target cell. The ability of DC3s to interact with HIV remains a critical and unresolved question. A comprehensive exploration and profiling of inflammatory DCs, especially in human anogenital tissues, is essential for developing modified PrEP regimens to block DC infection via an inflamed mucosa. Phenotypic characterisation will help identify the specific receptors involved in binding and mediating HIV transmission, exposing the key receptors to target in prophylactic interventions. Closing this knowledge gap hinges on the difficulty of obtaining human anogenital tissue, particularly inflamed samples, and extracting a sufficient yield of viable cells. However, with the need for more effective HIV prevention strategies, this challenge is a necessary scientific pursuit."

A visual summary of the inflammatory DCs found in genital tissues, their immunological functions and interactions with HIV is displayed in **Figure 1.4**.

1.11 Aims

1. To define the phenotype, genotype and immunological functions of blood-derived pDCs, $CD11c^+$ ASDCs and $CD123^+$ ASDCs and to assess their capacity for HIV binding and transfer to CD4 T cells.
2. To design and optimise a high-parameter flow cytometry panel to identify all known MNP subsets in human skin, type II and type I mucosa in states of homeostasis and inflammation.

3. To determine the composition of MNP subsets across different tissues of the human genital tract and to compare their relative proportions and phenotypes between tissue types.
4. To characterise MNP subsets in vaginal tissue, comparing their proportions and phenotypes between homeostatic and inflamed states and to investigate their capacity to bind HIV.

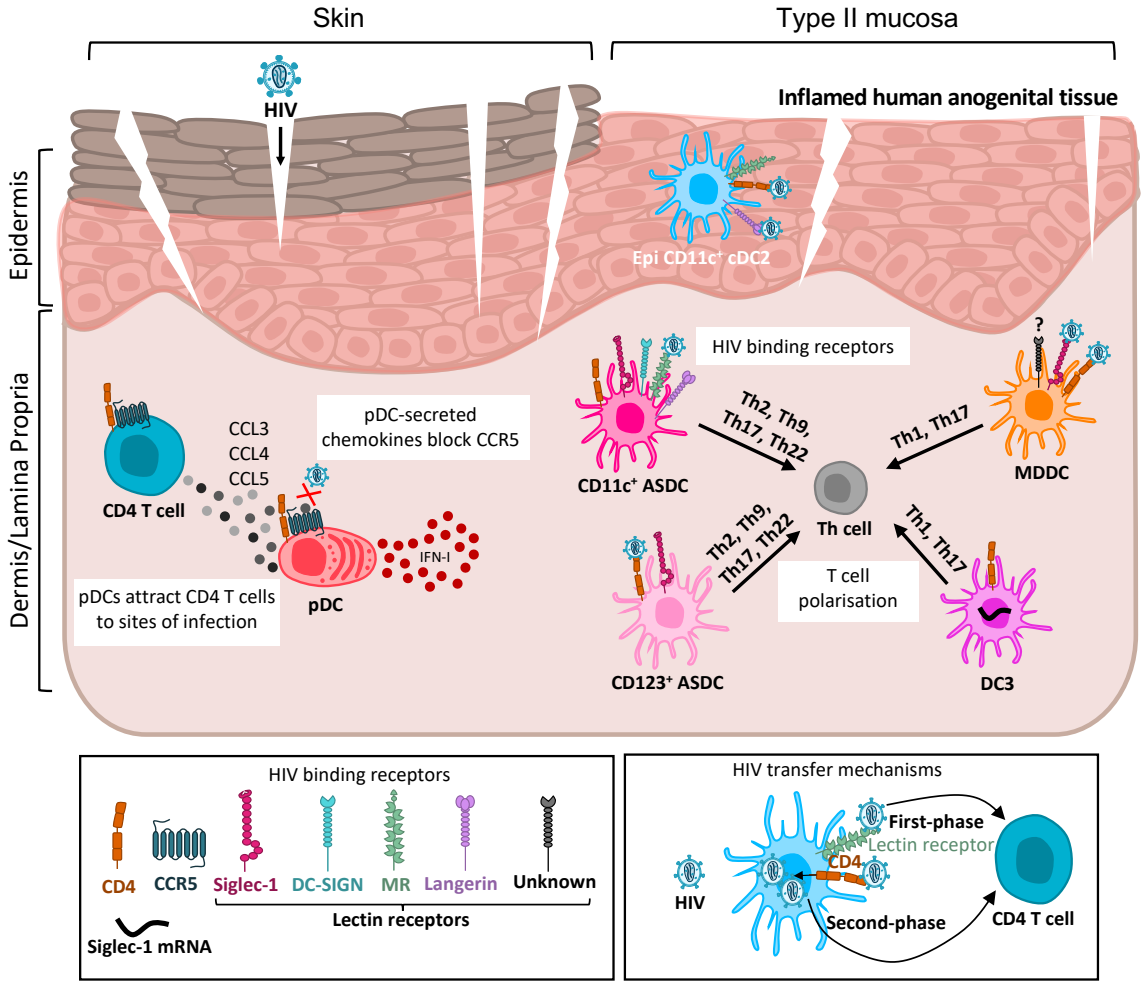

Figure 1.4: Inflammatory DC interactions with HIV in anogenital tissue.

"HIV enters inflamed anogenital tissue through breaches in the epithelium. Upon HIV exposure, pDCs secrete IFN-I to induce an antiviral immune response and chemokines CCL3-5, which recruit CD4 T cells to infection sites and block the binding of HIV to the CCR5 co-receptor. Both ASDC subsets are capable of polarising T cells into Th2, Th9, Th17 or Th22. $CD11c^+$ ASDCs tended to be more efficient at first-phase transfer via HIV binding to lectin receptors (MR, langerin, DC-SIGN and Siglec-1), whilst $CD123^+$ ASDCs tend to be more efficient at second-phase transfer via the entry receptors CD4/CCR5 and productive infection. DC3s can induce Th1 and Th17 polarisation. It has not yet been determined if they are capable of HIV binding and transfer; however, they express the HIV entry receptors CD4/CCR5 and Siglec-1 mRNA. MDDCs can also induce Th1 and Th17 polarisation. They can mediate first-phase transfer via Siglec-1 and likely another unidentified lectin receptor. MDDCs are also highly efficient at CD4/CCR5-mediated second-phase transfer. Epithelial $CD11c^+$ DCs can efficiently bind and transmit HIV through both first- and second-phase transfer."

Chapter 2. Characterising Plasmacytoid and Myeloid Axl^{+} Siglec-6^{+} Dendritic Cell Functions and their Interactions with HIV

Publications incorporated into this chapter

Warner van Dijk, F. A., Tong, O., O'Neil, T. R., Bertram, K. M., Hu, K., Baharlou, H., Vine, E. E., Jenns, K., Gosselink, M. P., Toh, J. W., Papadopoulos, T., Barnouti, L., Jenkins, G. J., Sandercoe, G., Haniffa, M., Sandgren, K. J., Harman, A. N., Cunningham, A. L., & Nasr, N. (2024). Characterising plasmacytoid and myeloid AXL+ SIGLEC-6+ dendritic cell functions and their interactions with HIV. *PLoS pathogens*, *20*(6), e1012351. https://doi.org/10.1371/journal.ppat.1012351

This chapter is being submitted as a published paper which the author of this thesis is first author of. The author of this thesis performed a large proportion of experiments, writing and figure curation, with minor assistance from Tong, O., who conducted initial optimisations, O'Neil, T. R., who processed the publicly available scRNA-seq data and Hu, K., who performed imaging mass cytometry. HIV experiments and manuscript preparation were jointly performed by this author and Nasr, N. Figures have not been amended but citations and references to figures have been changed for this thesis. Some material and reagent manufactures have been amended.

2.1 Abstract

"Axl$^+$ Siglec-6$^+$ dendritic cells (ASDC) are novel myeloid DCs which can be subdivided into CD11c$^+$ and CD123$^+$ expressing subsets. We showed for the first time that these two ASDC subsets are present in inflamed human anogenital tissues where HIV transmission occurs. Their presence in inflamed tissues was supported by single cell RNA analysis of public databases of such tissues including psoriasis diseased skin and colorectal cancer. Almost all previous studies have examined ASDCs as a combined population. Our data revealed that the two ASDC subsets differ markedly in their functions when compared with each other and to pDCs. Relative to their cell functions, both subsets of blood ASDCs but not pDCs expressed co-stimulatory and maturation markers which were more prevalent on CD11c$^+$ ASDCs, thus inducing more T cell proliferation and activation than their CD123$^+$ counterparts. There was also a significant polarisation of naïve T cells by both ASDC subsets toward Th2, Th9, Th22, Th17 and Treg but less toward a Th1 phenotype. Furthermore, we investigated the expression of chemokine receptors that facilitate ASDCs and pDCs migration from blood to inflamed tissues, their HIV binding receptors, and their interactions with HIV

and CD4 T cells. For HIV infection, within 2 hours of HIV exposure, $CD11c^+$ ASDCs showed a trend in more viral transfer to T cells than $CD123^+$ ASDCs and pDCs for first phase transfer. However, for second phase transfer, $CD123^+$ ASDCs showed a trend in transferring more HIV than $CD11c^+$ ASDCs and there was no viral transfer from pDCs. As anogenital inflammation is a prerequisite for HIV transmission, strategies to inhibit ASDC recruitment into inflamed tissues and their ability to transmit HIV to CD4 T cells should be considered."

2.2 Author summary

"This study highlights the significance of AXL^+ Siglec-6^+ dendritic cells (ASDC) in HIV transmission, particularly in inflamed peripheral tissues such as anogenital tissues, where HIV transmission is prevalent. It reveals that ASDCs are present in inflamed human tissues, including psoriasis affected skin, colorectal cancer and anogenital tissues. However, they are absent in uninflamed tissues. Furthermore, we investigated the expression of chemokine receptors that facilitate ASDC migration from blood to inflamed tissues, and their interactions with HIV and CD4 T cells. Notably, different subsets of ASDCs exhibit different expression levels of HIV binding receptors and showed trends of different phases of HIV transmission to T cells. Understanding ASDC involvement in HIV transmission could provide valuable insights for developing strategies to inhibit their recruitment to inflamed tissues and their ability to transmit the virus to CD4 T cells, potentially offering new avenues for HIV prevention and treatment."

2.3 Introduction

"A key event during HIV and SIV transmission is the rapid recruitment of plasmacytoid dendritic cells (pDC) from blood to the mucosal sites of HIV/SIV exposure (Shang et al., 2017) where they produce type I interferons (IFN-I) as one of the first innate immune defences (Beignon et al., 2005). pDCs have been historically associated with antiviral responses mediated by their: **i)** production of IFN-I α and β and subsequent IFN stimulated gene (ISG) expression; **ii)** production of chemokines and cytokines that recruit the primary HIV target CD4 T cells to sites of infection (Li et al., 2009, Shang et al., 2017); and **iii)** antigen presentation and priming of T cells. Therefore, pDCs may act as a 'double-edged sword' in initial HIV infection where production of inflammatory

cytokines and chemokines to recruit CD4 T cells is countered by the antiviral protection provided by IFN-I to limit viral spread.

Recent studies utilising single-cell RNA sequencing (scRNA-seq) have redefined the repertoire of DCs in blood, revealing a novel myeloid DC subset termed AXL^+ $Siglec\text{-}6^+$ (AS) DCs. These ASDCs express classical pDC and DC markers and can be subdivided into CD11c and CD123 expressing subsets (Villani et al., 2017). Therefore, pDCs have now been redefined as IFN-I producing cells with minimal capacity to induce T cell activation, proliferation (Villani et al., 2017, See et al., 2017) and the previously reported pDC responses to HIV might be attributed to ASDCs. Indeed, $CD11c^+$ ASDCs have been shown to produce IL-12 p40 upon toll-like receptor (TLR)7 stimulation whilst pDCs and $CD123^+$ ASDCs did not (Villani et al., 2017). As such, to explore new avenues to block HIV transmission, it is now critical to define the role that pDCs and both ASDC subsets play in initial infection. $CD123^+$ ASDCs in blood have been reported to be permissive to infection (Ruffin et al., 2019) via their expression of the HIV binding receptor CD169/Siglec-1 and they can transfer HIV to T cells. However, it is not known if ASDCs are present in the tissues where HIV transmission occurs or whether $CD11c^+$ ASDCs are also HIV target cells.

Here, we investigated $CD11c^+$ ASDCs, $CD123^+$ ASDCs and pDCs and showed that: **i)** all three cell types are present in inflamed human skin, anogenital tissues and lymph nodes; **ii)** they express the HIV chemokine entry receptors CCR5 and CXCR4; **iii)** both ASDC subsets express costimulatory molecules and stimulate T cell proliferation, activation, and polarisation more toward Th2, Th9, Th17, Th22, Treg and less toward Th1; **iv)** pDCs are the predominant antiviral IFN and pro-inflammatory cytokine (TNF-a and IL-6) producing cells and that they also secrete the CCR5 binding chemokine CCL3-5 which recruit CD4 T cells to sites of infection while inhibiting HIV entry by binding to CCR5 (Scarlatti et al., 1997); and **v)** both ADSC subsets transfer HIV to CD4 T cells in two distinct phases associated with C-type lectin receptor (CLR) mediated uptake and productive infection, while pDCs transferred HIV via CLR-mediated uptake only.”

2.4 Methods and materials

2.4.1 Reagents

Table 2.1: Flow cytometry antibodies

Marker	Clone	Fluorochrome	Company	Volume / 2.5 x 10^6 cells in 100 µL	Applicable methods section
CD45	HI30	BV786	BD Biosciences	1	2.4.3 2.4.5.1
	HI30	BB790	BD Biosciences	0.1	2.4.5.2
HLA-DR	G46-6	BUV395	BD Biosciences	0.5	2.4.3 2.4.5.2 2.4.9
	G46-6	BV605	BD Biosciences	2	2.4.3
	LN3	BUV786	Thermofisher	0.25	2.4.5.1
	L243	APC fire810	BD Biosciences	5	2.4.5.2
	G46-6	BB515	BD Biosciences	0.5	2.4.11
Lineage cocktail (Lin1) containing CD3, CD14, CD16, CD19, CD20, CD56	SK7, MφP9, 3G8, SJ25C1, L27, NCAM16.2	FITC	BD Biosciences	3.5	2.4.3
	OKT3, M5E2, 3G8, HIB19, 2H7, HCD56	BV510	Biolegend	2.4	2.4.3 2.4.9
Axl	DS7HAXL	PE	Thermofisher	1	2.4.3 2.4.5.1
	108724	BV785	BD Biosciences	0.8	2.4.5.2
	108724	BV605	BD Biosciences	1	2.4.9
Siglec-6	REA852	APC	Miltenyi Biotec	1	2.4.3 2.4.5.1
	767329	BV480	BD Biosciences	1	2.4.5.2 2.4.9
CD123	7G3	PE-CF594	BD Biosciences	2.5	2.4.3 2.4.5.1
	7G3	BV421	BD Biosciences	0.5	2.4.3 2.4.9
	6h6	PE-Cy5	Biolegend	0.5	2.4.5.2 2.4.11
CD11c	REA618	PE-Vio770	Miltenyi Biotec	0.5	2.4.3
	B-ly6	BB515	BD Biosciences	1.5	2.4.3 2.4.9
	B-ly6	BV650	BD Biosciences	0.5	2.4.5.1
	B-ly6	BUV395	BD Biosciences	2.5	2.4.5.2
	B-ly6	BUV737	BD Biosciences	0.5	2.4.5.2 2.4.9
	B-ly6	APC	BD Biosciences	5	2.4.11
CX3CR1	2A9-1	BV421	BD Biosciences	*	2.4.3
CD141	1A4	BB700	BD Biosciences	0.75	2.4.3

	1A4	BV711	BD Biosciences	2.5	2.4.9
BDCA2	201A	PE-CY7	Biolegend	1.5	2.4.3 2.4.9
CD3	UCHT1	AF700	BD Biosciences	2.5	2.4.3
	UCHT1	NovaBlue660-120s	Thermofisher	0.5	2.4.5.2
CD14	M5E2	BUV737	BD Biosciences	2.5	2.4.5.1
CD16	3G8	BUV496	BD Biosciences	2.5	2.4.5.1
CD19	SJ25C1	BV605	BD Biosciences	2	2.4.5.1
	HIB19	NovaBlue660-120s	Thermofisher	2.5	2.4.5.2
HLA-DQ	TU169	BUV563	BD Biosciences	2	2.4.5.2 2.4.9
CD103	REA803	PE Vio615	Miltenyi Biotec	2.5	2.4.5.2
CD11b	ICRF44	BV711	BD Biosciences	2	2.4.5.2
CD5	CD5-5D7	PE Cy5.5	Thermofisher	2.5	2.4.5.2
	UCHT2	BUV496	BD Biosciences	2	2.4.9
MR	19.2	BV750	BD Biosciences	1	2.4.5.2
DC-SIGN	DCN46	BV421	BD Biosciences	2.5	2.4.5.2
Siglec-1	7-239	BUV615	BD Biosciences	4	2.4.5.2
	7-239	PE ef610	Thermofisher	2.5	2.4.9
Langerin	MB22-9FS	PE Vio770	Miltenyi Biotec	1.5	2.4.5.2
CD4	OKT4	BV605	Biolegend	4	2.4.5.2
	OKT4	BV785	Biolegend	1	2.4.9 2.4.11
CD83	HB15e	APC	BD Biosciences	2	2.4.9
FcεR1α	AER-37	APC	Biolegend	5	2.4.9
CLEC5A	283834	APC	R&D Systems	2	2.4.9
XCR1	S15046E	APC fire 750	Biolegend	4	2.4.9
CD163	GHI/61	BUV805	BD Biosciences	4	2.4.9
CD80	L307.4	PE	BD Biosciences	2	2.4.9
CXCR4	12G5	PE	BD Biosciences	2.5	2.4.9
CLEC4A	9E8	PE	Biolegend	2.5	2.4.9
CLEC10A	H037G3	APC	Biolegend	1	2.4.9
CCR5	REA245	PE	Miltenyi Biotec	2.5	2.4.9
CD54	84H10	FITC	Beckman Coulter	2	2.4.9
CD1c	F10/21 A3	BV650	BD Biosciences	3	2.4.9
CD86	FUN-1	BV786	BD Biosciences	2	2.4.9
CD8	SK1	BUV737	BD Biosciences	2.5	2.4.11
CD25	M-A251	PE-Cy7	Biolegend	1.5	2.4.11
Tbet	O4-46	BV650	BD Biosciences	7.5	2.4.11
FoxP3	206D	PE Dazzle594	Biolegend	5	2.4.11
RORγT	AFKJS-9	PE	Thermofisher	7.5	2.4.11

*Performed by previous student and no record of concentration.

Table 2.2: Imaging mass cytometry antibodies

Marker	Host	Clone	Conjugate	Company	Concentration (µg/mL)
CD31	Rabbit	EPR3094	155Gd	Abcam	4
CD45	Rabbit	D9M8I	154Sm	Cell Signaling Technology	3
E-cadherin	Mouse	36-E-Cadherin	145Nd	BD Biosciences	8
AXL	Goat	Polyclonal	158Gd	R&D Systems	4
CD11c	Mouse	2F1C10	167Er	Proteintech	4
CD303	Goat	polyclonal	175Lu	R&D Systems	2

2.4.2 Ethics Statement

"This study was approved by the Western Sydney Local Area Health District (WSLHD) Human Research Ethics Committee (HREC) with reference number (4192) AU RED HREC/15 WMEAD/11."

2.4.3 Isolation of Plasmacytoid Dendritic Cells and Axl$^+$ Siglec-6$^+$ Dendritic Cells from Human Blood

"Peripheral blood mononuclear cells (PBMCs) were isolated via Ficoll-Paque (GE Healthcare Life Sciences, Little Chalfont, United Kingdom) density separation from HIV-seronegative blood supplied by the Australian Red Cross Blood Service, Sydney, Australia. pDCs were isolated from PBMCs using either the Human Plasmacytoid Dendritic Cell Isolation Kit II (Miltenyi Biotec) or by enriching for DCs using the Human Pan DC Enrichment Kit (Miltenyi Biotec). This was followed by cell sorting to isolate pDCs and the two populations of ASDCs: CD123$^+$ and CD11c$^+$. Briefly, cells were resuspended in 150 µL of PBS per 20 x 10^6 cells and stained with Live-Dead Near Infra-Red (dilution of 1:1000, LDNIR, Invitrogen) for 10 minutes at room temperature and then washed with a fluorescence activated cell sorting (FACS) wash (1% FCS (v/v), 2 mM EDTA, 0.1% sodium azide (w/v) in PBS). Cells were resuspended in 180 µL of Brilliant Stain Buffer and stained for 30 minutes at 4°C with a combination of different antibodies" detailed in **Table 2.1**.

Cells "were then washed in FACS wash and resuspended in RPMI for either phenotyping or cell sorting. For phenotyping, data was recorded on the BD LSR Fortessa using BD FACSDiva (BD Biosciences) and analysed using FlowJo v10.4 (FlowJo LLC). Cell sorting was carried on the BD Influx Cell Sorter using a 100 µm nozzle. pDCs were sorted as live CD45$^+$ Lin1$^-$ HLA-DR$^+$ CD141$^-$ AXL$^-$ Siglec-6$^-$ BDCA2$^+$

$CD123^+$ cells. ASDCs were sorted as AXL^+ Siglec-6^+ $CD123^+$ or AXL^+ Siglec-6^+ $CD11c^+$ cells. For compensation controls, beads were stained using 1 µL of antibody per 1 drop of beads (4°C for 30 minutes) and washed twice with FACS before acquisition."

2.4.4 Patients' History

"Non-inflamed and inflamed human tissue samples were obtained from patients (**Supplementary table 2.1 and Supplementary table 2.2**) undergoing colorectal surgery at hospitals in the Westmead Health Precinct, and written consent was collected from all donors.The first rectal tissue was obtained from 10-year-old female (with written consent from the parents) with symptoms of rectal pain and pus discharge and medicated with a hydrocortisone colonic enema. The tissue had features of chronic inflammatory bowel disease and mucosal changes of chronic active colitis. No diagnostic features of Crohn's disease or ulcerative colitis were observed in the rectal stump. The second inflamed human rectal tissue was from a patient suffering from chronic ulcerative colitis. The third sample was a lymph node from an inflamed rectum while the tissue used in Imaging mass cytometry was from an inflamed human colon. Tissues from non-inflamed rectal tissues were extracted from patients during the process of removing nearby cancerous tissues. Inflamed human tissues were collected from abdominal skins from abdominoplasties, labia from labiaplasties and foreskin from circumcisions at Westmead Hospital, Westmead Private Hospital and Hunters Hill Private Hospital in Sydney."

2.4.5 Enzymatic Digestion of non-Inflamed and Inflamed Human Tissues to Identify Axl^+ Siglec-6^+ Dendritic Cells and Plasmacytoid Dendritic Cells by Flow Cytometry

2.4.5.1 Colorectal Tissue

"To isolate mucosal immune cells from **colorectal** tissues, the lamina propria (LP) was mechanically separated from other sublayers and cut into pieces of approximately 5 mm across. 25 mm^2 of tissue was incubated in 20 mL of RF10 with 0.30% DTT (w/v) and 2 mM EDTA for 15 minutes at 37°C twice to strip the surface mucus and epithelium. The tissue was washed twice in PBS by passing through a tea strainer and digested in 20 mL of RPMI with 0.35% Type IV Collagenase (Worthington Industries)

for 30 minutes at 37°C twice. The liberated cells were passed through a 100 µm cell strainer twice and washed with Dulbecco's Phosphate Buffered Saline (DPBS, Lonza) twice. The red blood cell fraction was removed by incubating the cells in 5 mL of 1x Red Cell Lysis Buffer (Biolegend) in sterile H_2O for 3 minutes at room temperature prior to staining for flow cytometry to identify pDCs and ASDCS." Isolated cells were stained antibodies listed in **Table 2.1**.

"Data was recorded on the BD LSR Fortessa as above. t-distributed stochastic neighbour embedding (t-SNE) was performed to analyse cell populations using 1000 iterations, a perplexity of 20, a learning rate of 200 and a theta of 0.5, as per the recommended settings."

2.4.5.2 Abdominal and Genital Skin

"To isolate immune cells from **abdominal** skin, samples were cut into triangles, stretched out using large surgical forceps and grafted to 1 mm thickness using a skin graft knife (Zimmer Biomet, USA). The resulting skin was passed through a skin graft mesher (Zimmer Biomet, USA) and evenly distributed in 50 mL Falcon tubes to fill approximately 25% of the tube. Dermis and epidermis were separated by incubation in 30mL of filter sterilised RPMI supplemented with 1 U/mL dispase (Neutral Protease, Worthington Industries) and 0.1% (v/v) gentamicin (Life Technologies) overnight at 4°C on a rotator. Tubes were placed in a 37°C water bath for 15 minutes to initiate enzymatic activity. The skin was washed in PBS to remove dispase and epidermis was mechanically peeled from dermis using fine forceps. Dermis and epidermis were cut into 5 x 5 mm pieces and placed into separate 50 mL falcon tubes up to the 5 mL mark. Cells were liberated from tissue by an incubation in 20 mL of RPMI supplemented with 200 U/mL Type IV collagenase and 100 U/mL DNase (Sigma-Aldrich) for 120 minutes at 37°C on a rotator. Cells were separated from undigested dermal and epidermal tissues by passing supernatants through a tea strainer twice followed by a 100µm cell strainer into a 50mL falcon tube and washing in PBS (300 x*g* for 5 minutes). Cells were washed twice more in PBS, ready for antibody staining.

For the **genital skin** digestion, any excess underlying connective tissue/fat from each sample was removed using a scalpel and surgical scissors and small cuts were made in the epidermal surface to mimic the action of the skin graft mesher. From herein the

tissue was processed similar to abdominal skin, except for the dispase concentration which was increased to 2 U/mL. After isolating cells from both abdominal and genital tissues, they were stained with Fixable Viability Stain 700 (FVS700) (BD) to identify non-viable cells and a combination of the antibodies" detailed in **Table 2.1**.

"Data was acquired on the BD FACSymphony using BD DIVA software and analysed by FlowJo (Treestar V 10.9.0). Compensation controls were prepared as previously described in PBMC staining procedure."

2.4.6 Imaging Mass Cytometry

"Inflamed human colon tissue samples were incubated in 4% PFA in PBS for 18-24 hours prior to paraffin embedding and sectioning at 4 µm thickness. Sections for imaging mass cytometry were baked at 60°C for 1 hour, dewaxed in xylene and rehydrated in decreasing concentrations of ethanol from 100% through to 50%. Slides were then washed twice in TBS (0.1% Tween-20) for 2 min. Antigen retrieval was performed using pH 9 Tris-EDTA buffer (10 mM Tris, 1mM EDTA) in a microwave, first at 100% power for 3 min and next at 30% power for 15 min. Slides were then cooled at room temperature for 45 min before being washed in TBS and DPBS for 10 min each. Sections were blocked with Opal Block (Akoya Biosciences) at 37°C for 45 min and washed twice in PBS for 2 min. Sections were then incubated overnight at 4°C with the primary antibodies diluted in TBS (0.1% Tween-20) with 1% BSA. All primary antibodies had been previously conjugated to metal isotopes using the Maxpar Antibody Labeling Kits (Fluidigm)." Antibodies are detailed in **Table 2.2**. CD303 "was used to replace CD123 as two CD123 clones did not work in our IMC panel. Slides were washed twice, first in PBS 0.1% Triton-X and next in PBS for 8 min each before being counterstained with Cell-ID Intercalator-Ir (Fluidigm) in PBS for 30 min at room temperature. Slides were then washed in Milli-Q water for 5 min and air dried. Images were acquired using the Hyperion Imaging System (Fluidigm) at a laser power of 5 dB and frequency of 200 Hz."

2.4.7 Transcriptomic Profile of Plasmacytoid Dendritic Cells and Axl$^+$ Siglec-6$^+$ Dendritic Cells via Nanostring

"To investigate the gene expression of chemokines, cytokines, markers involved in antigen presentation and HIV infection, the nCounter pre-designed Human Immunology Panel 2 (NanoString Technologies) was used to quantify and assess the

profile of RNA transcripts. Briefly, 10^4 cells of either pDCs, $CD11c^+$ or $CD123^+$ ASDCs were either mock or HIV infected with HIV-1 Bal at an MOI of 1.5 due to the high expression of HIV restriction factors (Bloch et al., 2014). At 18 hours post infection (hpi), supernatants were collected and stored at -80^0C while cells were washed in RNAse free PBS and then lysed in 5 µL of 1/3 RNeasy Lysis (RLT) buffer (Qiagen) that was diluted in molecular grade H_2O. The 5 µL cell lysate of each cell type was then hybridized with the Reporter Code Set and Capture Probe Set for 24 hours at 65°C, loaded onto cartridges via the NanoString Prep Station, and processed using the NanoString nCounter digital analyser. Data was normalised and quality control metrics were calculated using the nSolver software package (NanoString Technologies) according to manufacturer's recommendations. Briefly, the data was normalised to 15 housekeeping genes that were included in the NanoString panel. The normalisation factor for all samples ranged between 0.25 and 4.66 which is within the acceptable range of 0.1-10."

2.4.8 Single Cell RNA Sequencing Analysis

"Publicly available data from E-MTAB-8142 (Reynolds et al., 2021), GSE178341 (Pelka et al., 2021) and GSE94820 (Villani et al., 2017) were downloaded, processed, and analysed in R. Data accessed through E-MTAB-8142 was first sub-setted to only include myeloid cells from non-inflamed and psoriasis lesion tissue. It was then processed using Seurat's reciprocal PCA integration workflow (https://satijalab.org/seurat/). A t-SNE was generated (*RunTSNE*) using dimensions 1:30. Using differential analysis (*FindMarkers*), annotations provided by the authors and known gene signatures, macrophages, cDC1, cDC2, LC, pDC, ASDC, and monocyte clusters were identified. pDCs and ASDCs from data accessed through GSE178341 were identified using annotations provided by the authors (cM07 and cM08, respectively). Additionally, the Seurat function FindTransferAnchors was used to compare data annotations between datasets to assist in verifying annotations (S3 Fig). pDCs and ASDCs were further sub-setted and the processing repeated without integration."

2.4.9 Phenotypic Profiling of Plasmacytoid Dendritic Cells and Axl$^+$ Siglec-6$^+$ Dendritic Cells

"To investigate the surface and intracellular protein expression of pDCs, CD11c$^+$ and CD123$^+$ ASDCs, a high parameter 19-colour flow cytometry panel was designed for acquisition on the BD FACSymphony. Blood PBMCs were isolated from whole blood or buffy coats and enriched using the Human Pan DC Enrichment Kit (Miltenyi Biotec). Enriched cells were resuspended in aliquots of 1 x 10^6 cells per 100 µL of PBS and non-viable cells excluded using Fixable Viability Stain 700 (FVS700) (BD) at a concentration of 1:8000. Cells were stained with a cocktail of surface antibodies and BD Horizon Brilliant Stain Buffer Plus for 30 min at 4℃" as listed in **Table 2.1**.

"For antibodies with identical fluorophore conjugates, drop in panels were used. For SAMHD1, anti-SAMHD1 (I19-18, #MABF933, Merck) was conjugated to APC using the Abcam APC Conjugation Kit (#ab201807, Abcam). For SAMHD1 intracellular staining, cells were first permeabilised with pre-cooled BD Phosflow Perm Buffer II for 2 min at 4℃ in dark. Data was acquired on the BD FACSymphony using BD DIVA software and analysed by FlowJo (Treestar V 10.9.0). Compensation controls were prepared as previously described in PBMC staining procedure." Z

2.4.10 Legend Plex Assay

"Culture supernatants were collected from mock and HIV treated pDCs and ASDCs for 18 hours. They were spun at 3000 rpm to remove debris and were then stored at −80 °C until use. Supernatants were diluted 1:1 in RF10 before the cytokine and chemokine levels were measured according to the manufacturer's instructions as per the Human Proinflammatory Chemokine Panel 1 and Human Inflammation Panel 1 (both from BioLegend). Sample data was acquired with the BD FACSCanto II flow cytometer and analysed using BioLegend LEGENDplex data analysis software. The standard range of detection for the inflammatory cytokine was 2–17000 pg/mL while the range for the chemokines was 2-32000 pg/mL."

2.4.11 T Cell Proliferation, Activation and Polarisation

"Allogeneic T cells isolated from PBMC using the naïve Pan T cell isolation kit (Miltenyi) were stained with Celltrace Violet (Thermofisher) as per the manufacturer's instruction. For T cell proliferation, FACS sorted pDCs and the two ASDC subsets were added to the Celltrace Violet stained naïve T cells at a ratio of 1 DC:10 T cell in

RF10 for 6 days at 37°C. Cells were then surface stained with Fixable Viability Stain 700 (FVS700) (BD) then surface stained for" antibodies listed in **Table 2.1**. "Cells were acquired on the BD LSRFortessa."

"For T cell polarisation, we investigated intracellular transcriptional factors and cytokine production. Unstained naïve T cells were either cultured with pDCs, CD11c+ ASDCs, CD123+ ASDCs, or as T cells alone. Cultures were incubated at 37°C. On day 6, we assessed intracellular transcription factors by incubating the cells with the BD Pharmingen Transcription Factor Buffer Set (BD bioscience) and antibodies to detect" Tbet, FoxP3, and RORγT (**Table 2.1**). "For cytokine production, all conditions were stimulated on day 6 with anti-CD3 and anti-CD28 overnight (5 µg/mL, Sigma-Aldrich). Supernatants were then collected and assessed for cytokine production by the LEGENDplex Human Th Cytokine Panel (Biolegend). As INF-g levels were above the standard range of detection via the LEGENDplex, they were assessed by the ELISA MAX Deluxe Set Human (Biolegend)."

2.4.12 HIV Infection of Plasmacytoid Dendritic Cells and Axl$^+$ Siglec-6$^+$ Dendritic Cells and their Viral Transfer to CD4 T Cells

"pDCs, CD11c$^+$ or CD123$^+$ ASDCs (30,000-60,000 cells) were either mock or HIV infected with HIV-1_{BaL} at an MOI of 1.5 for 2 h at 37℃. They were then washed twice with RPMI and cultured in 200µl of RF10 in 96 U well bottom shaped plates. JLTR T cells were added to pDCs and ASDCs at the ratio of 1 DC: 3 JLTR at 2 and 96 hpi. On day 4 post co-culture, cells were fixed in 4% PFA then HIV transfer to JLTR cells was determined by flow cytometry by measuring GFP expression, as JLTRs express GFP under the control of the HIV-1 promotor. Half the supernatants were collected prior to the addition of JLTR at 96 hpi to assess infectious virus release from pDCs and ASDCs. TZMBL cells (NIH AIDS Research and Reference Reagent Program, contributed by John Kappes and Xiaoyun Wu) were exposed to supernatants and then the LTR β-galactosidase reporter gene expression was measured after a single round of infection. Furthermore, to show that second phase transfer of HIV from ASDCs to CD4 T cells was dependent on their productive infection, we either mock or pre-treated ASDCs with the CCR5 inhibitor, Maraviroc (10µM), for 1 h prior to HIV infection. Cells were cultured for 18 h then washed twice to remove residual virus and Maraviroc. They were cultured for 96 h before the addition of JLTRs. After 5 days of co-culture, GFP

expression in JLTRs was assessed by flow cytometry."

2.4.13 Quantification and Statistical Analysis

"For comparisons between more than two groups, a repeated measure one-way analysis of variance (ANOVA) with Tukey's post-hoc test was conducted. For HIV viral transfer, statistical comparisons between two groups were performed using Wilcoxon signed-rank tests. All statistical analysis was performed in GraphPad Prism 8, and $p < 0.05$ was considered statistically significant for all tests; *$p < 0.05$, **$p < 0.01$, ***$p < 0.001$, ****$p < 0.0001$. Error bars represent standard error mean across all analyses."

2.5 Results

2.5.1 Identification of Axl$^+$ Siglec-6$^+$ Dendritic Cells and Plasmacytoid Dendritic Cells in Human Blood

"We tested the human pDC isolation kit II and a Pan DC enrichment kit to assess which kit can enrich for CD11c$^+$ and CD123$^+$ ASDC subsets from human peripheral blood mononuclear cells (PBMCs) (Villani et al., 2017). Before using any kits, we detected pDCs and ASDCs in very low proportions in PBMCs as of the 96.8% Lin1$^-$HLA-DR$^+$CD141^{lo} cells, 2% were ASDCs and 37% were pDCs (**Figure 2.1a, top row**).

Using the pDC isolation kit, which relies on BDCA2 selection, 98% of the Lin$^-$ HLA-DR$^+$ cells were pDCs, 0.9% were CD123$^+$ ASDCs and no CD11c$^+$ ASDCs were detected (**Figure 2.1a, middle row**). The presence of the CD123$^+$ ASDC population was confirmed by t-stochastic neighbour embedding (t-SNE) analysis of the flow cytometry data, which showed a distinct population from the pDC cluster (**Supplementary figure 2.2a**), and heat map visualisation of the t-SNE plots confirmed the expression of AXL, Siglec-6 and CD123 but not CD11c (**Supplementary figure 2.2b**). Therefore, only CD123$^+$ ASDCs could be isolated using the pDC isolation kit II.

Using the human Pan DC enrichment kit, which negatively selects for CD141$^+$ cDC1, CD11c$^+$ cDC2 and BDCA2$^+$ pDC, we identified pDCs and both subsets of ASDCs (**Figure 2.1a, bottom row**). Of the Lin1$^-$HLA-DR$^+$ cells, 21% were pDCs and less than 2% of each ASDC subset were present (**Figure 2.1b-c**). t-SNE analysis of the flow cytometry data verified that pDCs, CD11c$^+$ and CD123$^+$ ASDCs represented distinct populations of Lin1$^-$HLA-DR$^+$ cells. pDCs were grouped in the bottom right cluster, whilst CD123$^+$ ASDCs were a discrete peninsula of the pDC cluster and CD11c$^+$ ASDCs clustered together but on a separate island (**Figure 2.1d**). Heat map visualisation of the t-SNE analysis also confirmed the phenotype of each population. AXL and Siglec-6 co-expression was only identified on ASDC clusters, whilst BDCA2 and CD123 expression was mainly associated with pDCs and CD123$^+$ ASDCs (**Figure 2.1e**). CD11c expression was limited to the left island containing the CD11c$^+$ ASDCs, which were also clearly separated from the far-right cluster of CD141$^+$ cDC1 based on CD141 expression (**Figure 2.1e**). Back-gating on each population demonstrated that CD11c$^+$ ASDCs had slightly higher SSC, CD45 and HLA-DR expression compared to

other cell types (**Figure 2.1f**). CD11c$^+$ ASDCs also expressed lower levels of AXL, Siglec-6 and BDCA2 than CD123$^+$ ASDCs, as reported by others (Villani et al., 2017). Thus, only the Pan DC enrichment kit successfully isolated pDCs, CD11c$^+$ and CD123$^+$ ASDCs from PBMCs."

2.5.2 Transcriptomic Profiling of Blood-derived Axl$^+$ Siglec-6$^+$ Dendritic Cells and Plasmacytoid Dendritic Cells

"We used NanoString to define the ASDC and pDC genomic signatures on FACS-sorted blood-derived pDCs and both subsets of ASDCs (**Figure 2.2a**). Since our NanoString panel was targeting genes involved in immunology, we were limited in identifying all genes that define pDCs, ASDCs and all those that discriminate between CD123+ and CD11c+ ASDCs as reported by Villani et al. (2017). After normalizing the NanoString data, *TLR7* was detected in pDCs only; *IRF8, IRF7, APP, TCF4* and *LILRA4* were expressed more highly in pDCs and CD123+ ASDCs; *CD5* was exclusively identified in ASDCs. Out of all genes that discriminated between CD123+ and CD11c+ ASDCs, our NanoString panel showed *LILR4* expression only in CD123+ ASDCs. As all the above genes show a similar pattern to that reported by Villani et al. (2017) in differentiating ASDCs and pDCs, this implies that the gene signature for ASDCs did not change upon 18 h of culture prior to NanoString testing. We also noted pDCs were CD45RA+, CD11c+ ASDCs were CD45RO+ while CD123 ASDCs were a mix of CD45RO+ and RA+. A higher expression of the costimulatory molecule *CD86* was detected in CD11c+ ASDCs compared to CD123+ ASDCs. This also correlated with its higher protein expression on CD11c+ ASDCs as previously reported (Villani et al., 2017). Interestingly, we also identified *indoleamine 2,3-dioxygenase (IDO), CLEC5A* and *LAMP-3* as being highly expressed by CD11c$^+$ ASDC, while CLEC4A, *FCER1G* and *FCGR2B* were more expressed in CD123+ ASDCs. Furthermore, our data showed that *ICAM-1* and *HLA-DR* were expressed by pDCs and ASDCs. In summary, we have identified some characteristic genes that identify sorted blood pDCs and the two subsets of ASDCs"

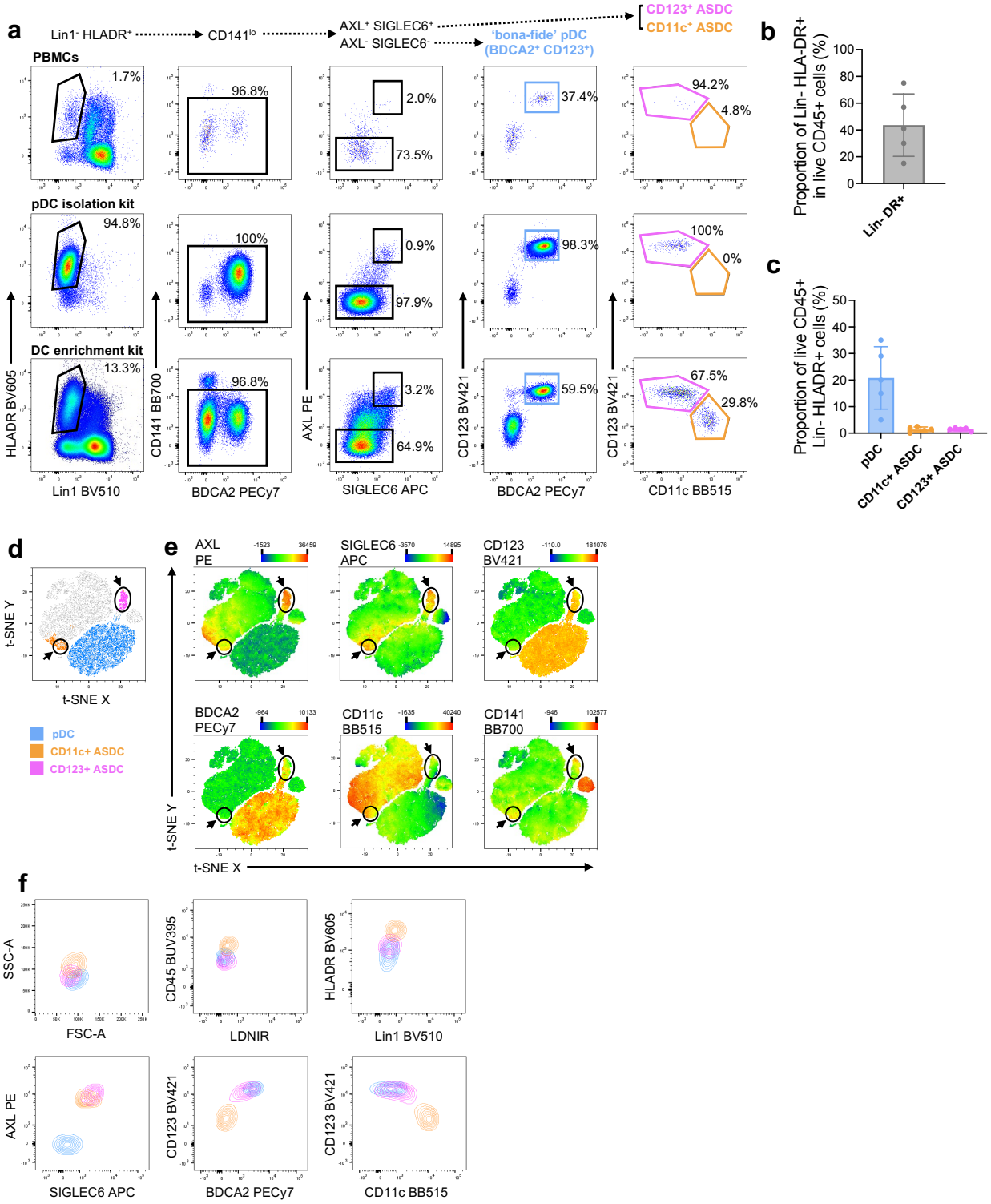

Figure 2.1: Identification of pDCs and ASDCs in PBMCs using pDC Isolation Kit and DC Enrichment Kit

"a) Representative dot plots showing the gating strategy to identify pDCs (AXL$^-$ Siglec-6$^-$ BDCA2$^+$ CD123$^+$), CD123$^+$ ASDCs (AXL$^+$ Siglec-6$^+$ CD123$^+$ CD11c$^{-/lo}$) and CD11c$^+$ ASDCs (AXL$^+$ Siglec-6$^+$ CD11c$^+$ CD123$^{-/lo}$). Top row demonstrates isolation from PBMCs, middle row uses Human pDC Isolation Kit II and bottom row uses Human Pan DC Enrichment Kit. **b)** Mean proportion of Lin1$^-$ HLA-DR$^+$ cells and **c)** mean proportion of pDCs, CD11c$^+$ and CD123$^+$ ASDCs using the Human Pan DC enrichment Kit (±SD, n=5). **d)** A representative distribution of pDCs (blue), CD11c (orange) and CD123 ASDCs (purple) on a t-SNE plot to verify the phenotypes of blood pDCs and ASDCs isolated via the Human Pan DC Enrichment Kit. **e)** Heat map visualisations of the median fluorescence intensity of surface AXL, Siglec-6, CD123, BDCA2, CD11c and CD141 expression for the populations shown on t-SNE plot. **f)** Representative contour plots showing the phenotypic characteristics of pDCs, CD11c$^+$ and CD123$^+$ ASDCs."

2.5.3 Chemokine Receptor Expression that Mediates Axl$^+$ Siglec-6$^+$ Dendritic Cell and Plasmacytoid Dendritic Cell Migration to Peripheral Tissue Sites

"Migration of immune cells into tissues occurs via a number of chemotactic gradients mediated by the expression of the chemokine receptors CCR1-2, CCR5-8, CXCR1-4, CXCR6 or CX3CR1 (Sokol and Luster, 2015). To examine which chemokine receptor(s) may mediate ASDC and pDC migration from blood to inflamed tissues, we interrogated our NanoString data to assess the expression of these receptors (**Figure 2.2c**). The following gene expression profiles were noted: **i)** *CCR2* by pDCs only; **ii)** *CCR6* by both ASDC subsets; **iii)** *CX3CR1* by CD123$^+$ ASDCs only; **iv)** *CCR7* by CD11c$^+$ ASDCs; **v)** *CXCR3* by pDCs and CD123$^+$ ASDCs; **vi)** *CCR5* and *CXCR4* more highly expressed in CD11c$^+$ ASDCs followed by pDCs and CD123$^+$ ASDCs; **vii)** *CCR8* was not detected in any subset. As our NanoString assay did not include *CCR1, CCR3, CCR4, CXCR1-2*, we analysed the scRNA-seq data of blood derived ASDCs from Villani et al. (2017). We found that *CCR1* and *CXCR1-2* were expressed only by pDCs while *CCR3-4* were detected in CD123$^+$ ASDCs only (**Supplementary figure 2.1**). We also confirmed that the chemokine gene expression profiles identified by our NanoString data were similar to this RNAseq dataset. In summary, pDCs and both subsets of ASDCs expressed the genes of many chemokine receptors to allow their migration to inflamed peripheral tissue sites."

2.5.4 Blood-derived Axl$^+$ Siglec-6$^+$ Dendritic Cell and Plasmacytoid Dendritic Cell HIV Binding and Entry Receptor Expression

"To understand HIV interactions with ASDCs and bona-fide pDCs (depleted of CD123$^+$ ASDCs), we examined the gene and surface expression of: **i)** lectin binding receptors that mediate endocytic uptake including those known to bind HIV: CD169/Siglec-1, CD209/DC-SIGN, CD206/MR and CD207/langerin; **ii)** the HIV entry receptors CD4, CCR5, and CXCR4 leading to productive infection; and **iii)** the myeloid cell retroviral restriction nuclear dNTPase SAMHD1. For lectin expression, our NanoString data was limited to *CLEC4A* and *CLEC5A.* Therefore, we again interrogated the publicly available scRNA-seq data of blood derived ASDCs produced by Villani et al. (2017) (**Figure 2.2d**) to investigate the full CLR repertoire. Except for *Sigec-12*, we found that pDCs expressed very low levels of the genes encoding almost all lectin receptors, CD11c$^+$ ASDCs expressed the highest levels of most CLRs, notably the known HIV

binding CLRs *CD207/langerin*, CD206/*MR* as well as *CLEC4A, CLEC5A* and *CLEC10A.* We also noted that CLRs expressed by CD11c$^+$ ASDCs were expressed at much lower levels by CD123$^+$ ASDCs, however the latter expressed other CLRs at high levels including the HIV binding lectins *CD169/Siglec-1* and *CD209/DC-SIGN*. The gene expression of HIV entry receptors *(CD4, CCR5 and CXCR4)* was detected at various levels in all three subsets. Finally, *SAMHD1* was more highly expressed in CD11c$^+$ than CD123$^+$ ASDCs and pDCs.

We then used high parameter flow cytometry to measure surface protein expression levels. In correlation with our gene expression analysis, pDCs did to not express any of the CLRs we measured except CLEC4A. CD169/Siglec-1 was highly expressed by CD123$^+$ASDCs. CD11c$^+$ ASDCs expressed most CLRs including CLEC4A at high levels, while CLEC5A, CD206/MR and CD207/langerin were expressed at low levels (**Figure 2.2e, Supplementary figure 2.3**). Furthermore, despite higher gene expression of DC-CD209/SIGN by CD123$^+$ ASDCs (**Figure 2.2d**), CD11c$^+$ ASDC expressed more DC-SIGN on their surface (**Figure 2.2e, Supplementary figure 2.3**). For HIV entry receptors, pDCs expressed the highest levels of CD4, whereas CXCR4 was expressed at low levels (in contrast to its gene expression) and CCR5 at high levels by all three cell subsets, though CCR5 fluorescent intensity (gMFI) was highest on CD11c ASDCs (**Figure 2.2e**). Finally, SAMHD1 was expressed most highly by CD11c$^+$ ASDCs (**Figure 2.2e**). In summary, CD11c$^+$ ASDCs expressed the highest levels of CD206/MR, CD207/langerin and CD209/DC-SIGN. All subsets expressed the primary HIV entry receptor, CD4, and chemokine co-receptors CCR5 and CXCR4.”

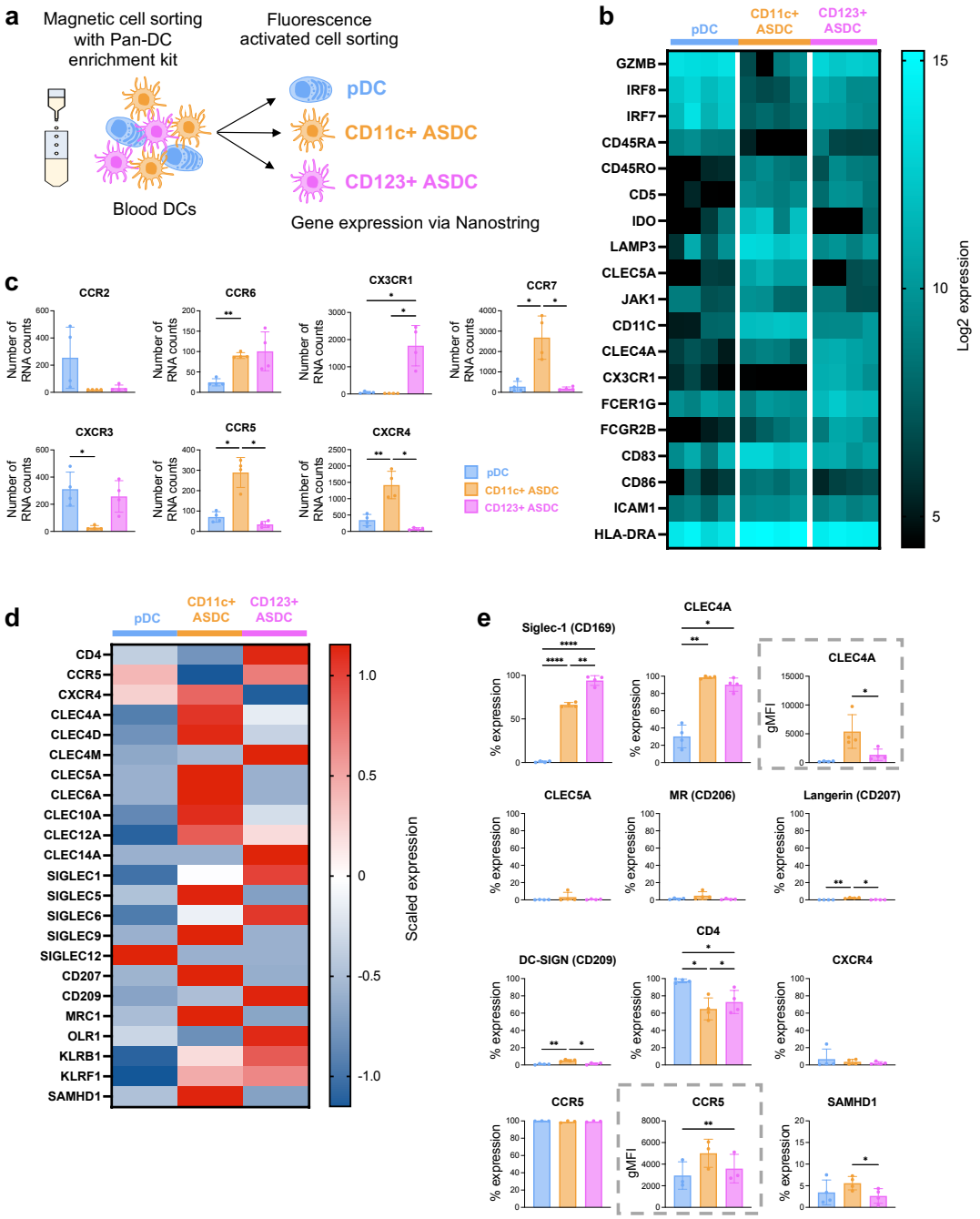

Figure 2.2: Transcriptomic and proteomic profile of pDCs and ASDCs

"a) Workflow for isolating pDCs and ASDCs using the Pan DC enrichment kit followed by FACS cell sorting to separate pDCs, CD123$^+$ ASDCS and CD11c$^+$ ASDCs. RNA was extracted and processed via NanoString. **b)** Heat map for genes delineating pDCs from ASDCs (n=4).**c)** Chemokine gene expression by NanoString in pDCs and ASDCs. Data are presented as ±SD (n=4). Statistical analysis was performed using one-way ANOVA with Tukey's multiple comparisons test, *p< 0.05; **p< 0.01. **d)** Gene expression of HIV binding and uptake receptors on blood derived pDCs and ASDCs. Blood PBMCs (GSE94820) (Villani et al., 2017) were transcriptionally profiled by scRNA-seq. pDC, CD11c$^+$ ASDC and CD123$^+$ ASDC annotations were determined using metadata provided by the authors. All genes pertaining to HIV binding lectin receptors, HIV entry receptors and SAMHD1 were compared between pDCs, CD11c$^+$ ASDCs and CD123$^+$ ASDCs and calculated as a scaled value. The scaled values were plotted on a heat map using Prism. **e)** The expression of Siglec-1 (CD169), CLEC4A, CLEC5A, MR (CD206), Langerin (CD207), DC-SIGN (CD209), CD4, CXC4, CCR5 and SAMHD1 were determined on each cell type immediately after their isolation from blood. The percentage expression of each subset was calculated for each marker, and gMFI (grey dotted box) calculated when percent expression exceeded 80% for multiple subsets (n=3-4). *p < 0.05, **p < 0.01 by one-way ANOVA with Tukey's multiple comparisons test."

2.5.5 Identification of Axl$^+$ Siglec-6$^+$ Dendritic Cells and Plasmacytoid Dendritic Cells in Inflamed Human Tissues

"To date, ASDCs have been described in PBMCs and tonsillar tissue (Villani et al., 2017), spleen (See et al., 2017), inflamed cerebrospinal fluid (Kang et al., 2023), inflamed broncho-alveolar lavage (Jardine et al., 2019) and inflamed skin (Chen et al., 2020). To determine if they are present in tissues affected by other inflammatory diseases, we used our blood ASDC-specific gene of Fig 2b to cross reference several publicly available human tissue scRNA-seq datasets of cells derived from ulcerative colitis (Luoma et al., 2020, Smillie et al., 2019), atopic dermatitis (He et al., 2020), psoriasis (Reynolds et al., 2021), colorectal cancer (Pelka et al., 2021) and vagina (Li et al., 2021). The sub-setting steps of the scRNA-seq analysis are shown in **Supplementary figure 2.4**. We detected two pDC and two ASDC clusters in psoriasis affected skin (**Figure 2.3a-b**) and colorectal cancer (**Figure 2.3c-d**). One pDC cluster appeared to be more mature (*CD83*$^+$), with decreased expression of *GZMB, IRF8* and *IRF7*. CD11c$^+$ ASDCs expressed *IDO1*, *LAMP3*, and *JAK1* while the CD123$^+$ ASDCs expressed *CLEC4A, FCER1G* and *FCGR2B*. We found equal proportions of CD123$^+$ and CD11c$^+$ ASDCs in psoriasis (**Figure 2.3a**) while in colorectal cancer there were more CD123$^+$ than CD11c$^+$ ASDCs (**Figure 2.3c**). In colorectal cancer, there were more immature than mature pDCs and vice versa for psoriasis. Immune cell enrichment was performed on both the psoriasis and colorectal cancer data sets, but not the others. As ASDCs are present in very low numbers, this lack of enrichment may account for our inability to identify ASDCs in ulcerative colitis, atopic dermatitis, and vagina via RNAseq. As such, further studies are required to confirm the presence of ASDCs in these tissues and disease settings.

With ASDCs presence in inflamed tissue confirmed via transcriptomics, we set out to determine if ASDCs were also present in fresh human tissue by flow cytometry. Initially, we obtained inflamed rectal tissue from patients undergoing surgery for a range of inflammatory intestinal conditions (**Supplementary table 2.1**). Immune cells were isolated using our optimised enzymatic digestion protocols for intestinal tissues (Doyle et al., 2021) where samples are processed within 15 minutes of their removal from the body. ASDCs and pDCs were identified using high parameter flow cytometry an inflamed rectums affected by active ulcerative colitis. Similar to blood, tissue pDCs were in greater proportion than ASDCs (**Figure 2.4a-c**). Back gating was performed

to show that pDCs, and both CD11c^{+} and CD123^{+} ASDCs were present (**Figure 2.4b)**. We also detected pDCs and ASDCs in inflamed mesenteric lymph nodes (**Figure 2.4d**), but neither cell type was present in non-inflamed rectum (**Figure 2.4e**). This was confirmed *in situ* in one inflamed colon affected by diverticulitis using imaging mass cytometry where pDCs and both ASDC subsets were detected and were mostly present in submucosal lymphoid follicles (**Figure 2.4f**). Furthermore, we identified both ASDC subsets in very low numbers in the epidermis and underlying dermis of inflamed human tissues including abdominal skin, labia, and outer foreskin and in the epithelium and LP of inner foreskin (**Supplementary table 2.2, Figure 2.4g**). cDC2s were additionally identified in these samples as a separate population to ASDCs and in much higher numbers. Functional assays on tissues derived ASDCs were impossible due to the low number of isolated cells. In summary, we have shown that ASDCs are present in inflamed human anogenital tissues."

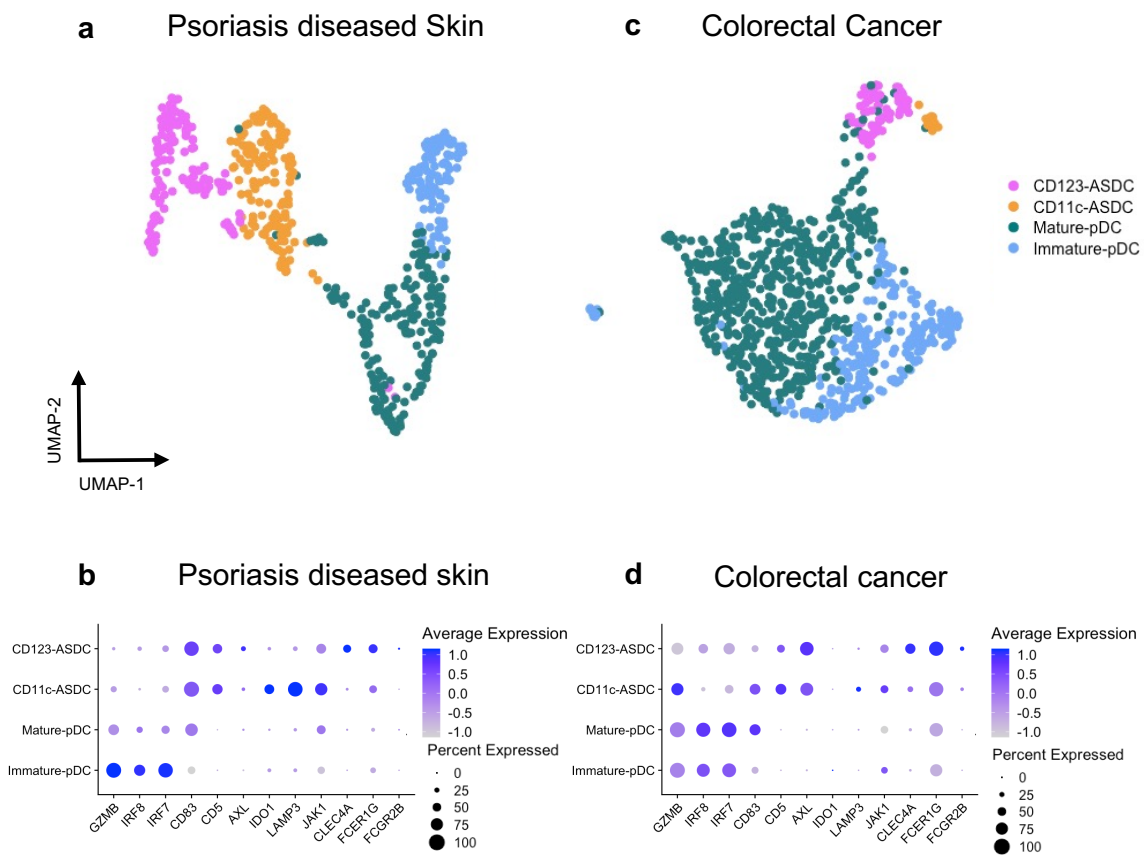

Figure 2.3: Transcriptomic profile of pDCs and ASDCs via scRNA-seq

"UMAP plots and expression of genes delineating pDCs from ASDCs in data sets of cells derived from inflamed tissues of psoriasis diseased skin (E-MTAB-8142(Reynolds et al., 2021)) is shown in **a-b** and from colorectal cancer (GSE178341(Pelka et al., 2021)) in **c-d."**

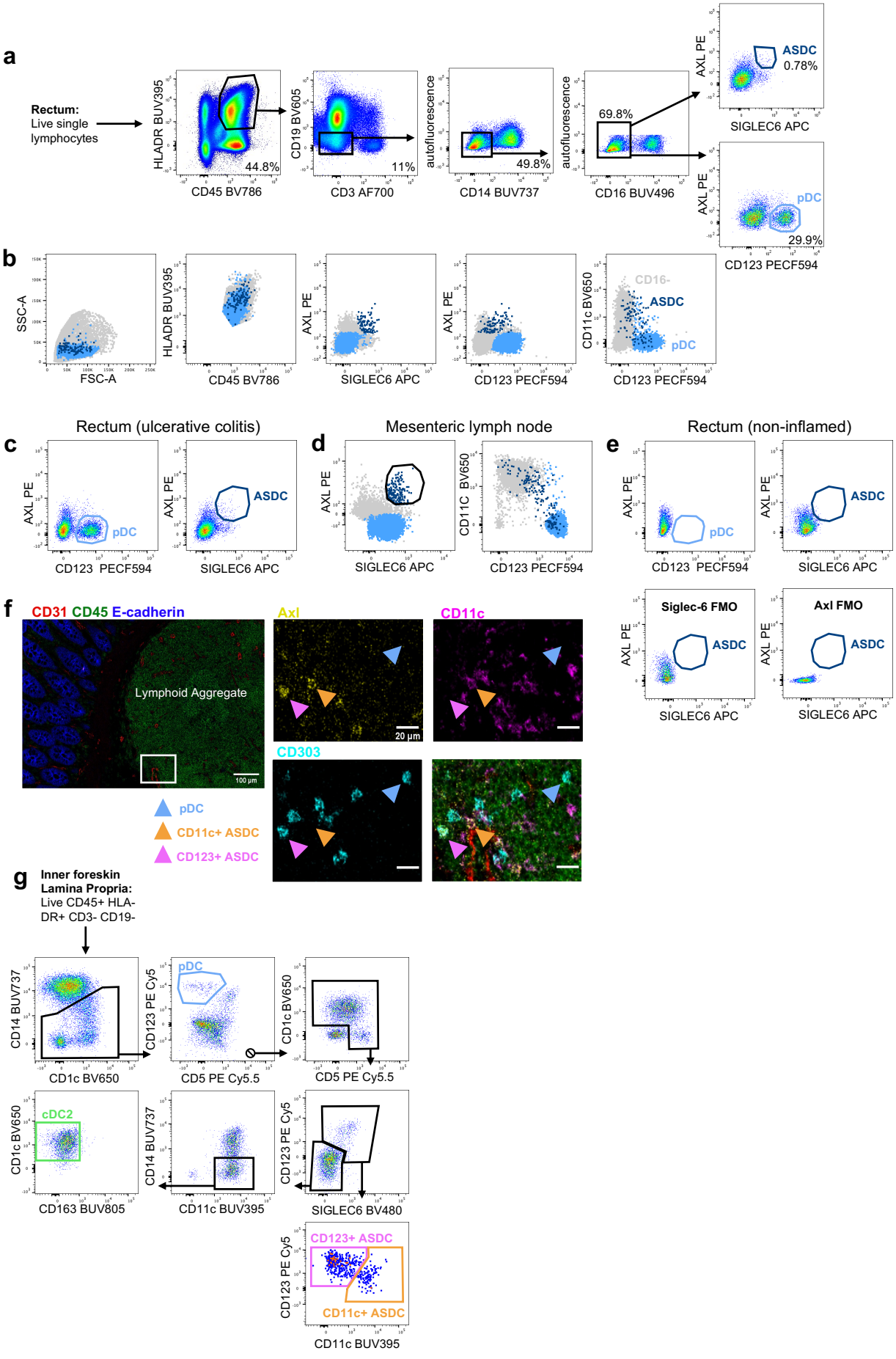
a
Rectum:
Live single
lymphocytes
HLADR BUV395
CD45 BV786
44.8%
CD19 BV605
CD3 AF700
11%
autofluorescence
CD14 BUV737
49.8%
autofluorescence
CD16 BUV496
69.8%
AXL PE
SIGLEC6 APC
ASDC
0.78%
AXL PE
CD123 PECF594
pDC
29.9%
b
SSC-A
FSC-A
HLADR BUV395
CD45 BV786
AXL PE
SIGLEC6 APC
AXL PE
CD123 PECF594
CD11c BV650
CD123 PECF594
CD16-
ASDC
pDC
c
Rectum (ulcerative colitis)
AXL PE
CD123 PECF594
pDC
AXL PE
SIGLEC6 APC
ASDC
d
Mesenteric lymph node
AXL PE
SIGLEC6 APC
CD11C BV650
CD123 PECF594
e
Rectum (non-inflamed)
AXL PE
CD123 PECF594
pDC
AXL PE
SIGLEC6 APC
ASDC
f
CD31 CD45 E-cadherin
Lymphoid Aggregate
100 µm
Axl
20 µm
CD11c
CD303
pDC
CD11c+ ASDC
CD123+ ASDC
Siglec-6 FMO
AXL PE
SIGLEC6 APC
ASDC
Axl FMO
AXL PE
SIGLEC6 APC
ASDC
g
Inner foreskin
Lamina Propria:
Live CD45+ HLA-
DR+ CD3- CD19-
CD14 BUV737
CD1c BV650
CD123 PE Cy5
pDC
CD5 PE Cy5.5
CD1c BV650
CD5 PE Cy5.5
CD1c BV650
cDC2
CD163 BUV805
CD14 BUV737
CD11c BUV395
CD123 PE Cy5
SIGLEC6 BV480
CD123 PE Cy5
CD123+ ASDC
CD11c+ ASDC
CD11c BUV395

Figure 2.4: Identification of pDCs and ASDCs in human tissues

"a) Representative dot plots identifying pDCs (AXL^- $CD123^+$) and ASDCs (AXL^+ $Siglec\text{-}6^+$) in a rectum of a patient with ulcerative colitis. **b)** Back gating to show the surface expression of pDCs and ASDC and to confirm the phenotype detected in a. **c-d)** Representative data showing pDCs and ASDCs in the rectum of patient with chronic ulcerative colitis in c and in mesenteric lymph nodes of inflamed rectum in d. All cells were first gated as live $HLA\text{-}DR^+$ $CD45^+$ $CD19^-$ $CD3^-$ $Autofluorescent^-$ $CD14^-$ $CD16^-$ cells. **e)** Absence of pDCs and ASDCs in non-inflamed rectal tissue (top) after adopting the gating strategy listed in a. Siglec-6 FMO and Axl FMO (bottom) confirmed real expression. **f)** ASDCs Axl^+ $CD303^+$ (pink arrows), ASDCs Axl^+ $CD11c^+$ (orange arrows) and pDCs (blue arrows) were identified by microscopy at the periphery of a submucosal lymphoid aggregate in an inflamed human colon. ASDCs were located proximal to a blood vessel based on CD31 expression. **g)** Representative gating strategy as demonstrated by inner foreskin lamina propria to identify pDCs, ASDCs and cDC2s. All cells were first gated as live $CD45^+$ $HLA\text{-}DR^+$ $CD3^-$ $CD19^-$; pDCs (blue) were defined as $CD14^{lo}$ $CD5^-$ $CD123^+$, $CD123^+$ ASDCs (pink) as $CD14^{lo}$ $CD5^+$ $CD1c^+$ $Siglec\text{-}6^+$ $CD123^+$, $CD11c^+$ ASDC (orange) as $CD14^{lo}$ $CD5^+$ $CD1c^+$ $Siglec\text{-}6^+$ $CD11c^+$ and cDC2 (green) as $CD14^-$ $CD5^+$ $CD1c^+$ $CD11c^+$ $CD163^-$. This gating strategy differed to the gating in a-e as a different panel design was used to allow for identification of cDC2s."

2.5.6 Expression of HIV Binding and Entry Receptors on Axl^+ $Siglec\text{-}6^+$ Dendritic Cells and Plasmacytoid Dendritic Cells Isolated from Inflamed Human Tissues

"CLR surface expression was assessed by flow cytometry on the pDCs and ASDCs isolated from epithelium and dermis/LP of inflamed human abdominal skin, labia, and inner/outer foreskin (**Figure 2.5a**). Higher expression of CD169/Siglec-1 was detected on $CD123^+$ rather than $CD11c^+$ ASDCs while pDCs had very low to no expression. CD209/DC-SIGN, CD206/MR and CD207/langerin were expressed more highly on $CD11c^+$ than $CD123^+$ ASDCs and pDCs. CD4 was expressed at high levels in all three cell subsets. This preliminary data indicates that blood (**Figure 2.5b**) and tissue ASDCs express similar levels of Siglec-1 and CD4. However, expression of the CLRs CD206/MR, CD207/langerin and CD209/DC-SIGN trended higher on tissue ASDCs compared to blood. We have also identified cDC2 in tissues (**Figure 2.4g**) and blood (**Supplementary figure 2.5**). In tissues, cDC2 differed in CLR expression compared to $CD11c^+$ ASDCs (**Figure 2.5**) as they had low Siglec-1 and no DC-SIGN expression."

2.5.7 Functional Phenotyping and Polarisation of T Cells by Blood-derived Axl^+ $Siglec\text{-}6^+$ Dendritic Cells and Plasmacytoid Dendritic Cells

"DCs are highly efficient antigen presenting cells (APC) and deliver antigens to activate naïve T cells driving them to be polarised into various CD4 T helper (Th) subsets or effector CD8 T cells. Therefore, we next assessed the surface expression of costimulatory markers on blood derived pDCs and ASDCs that are required for DCs to perform these functions. pDCs did not express CD80, CD83 or CD86 on their

surface. Compared to ASDCs, they expressed low levels of HLA-DR and the T cell adhesion marker CD54/ICAM-1 **(Figure 2.6a)**. Similar to blood cDC1 and cDC2 (Botting et al., 2017), both ASDC subsets did not express CD80 or CD83. However, 80% of both subsets expressed CD86 and CD54/ICAM-1 with CD11c$^+$ ASDCs expressing higher levels of HLA-DR than CD123$^+$ ASDCs. It is worth noting that low mRNA levels can negatively correlate to high level of protein expression and vice versa. This was the case for CD83 and CD86. CD83 was expressed by all cells at the RNA level in Fig 2b but was not detected at the cell surface in Fig 6a. However, CD86 which had lower mRNA counts than CD83 in all subsets was expressed at the cell surface as per the RNA counts i.e. higher gMFI on CD11c$^+$ ASDCs, followed by CD123$^+$ ASDCs, then pDCs."

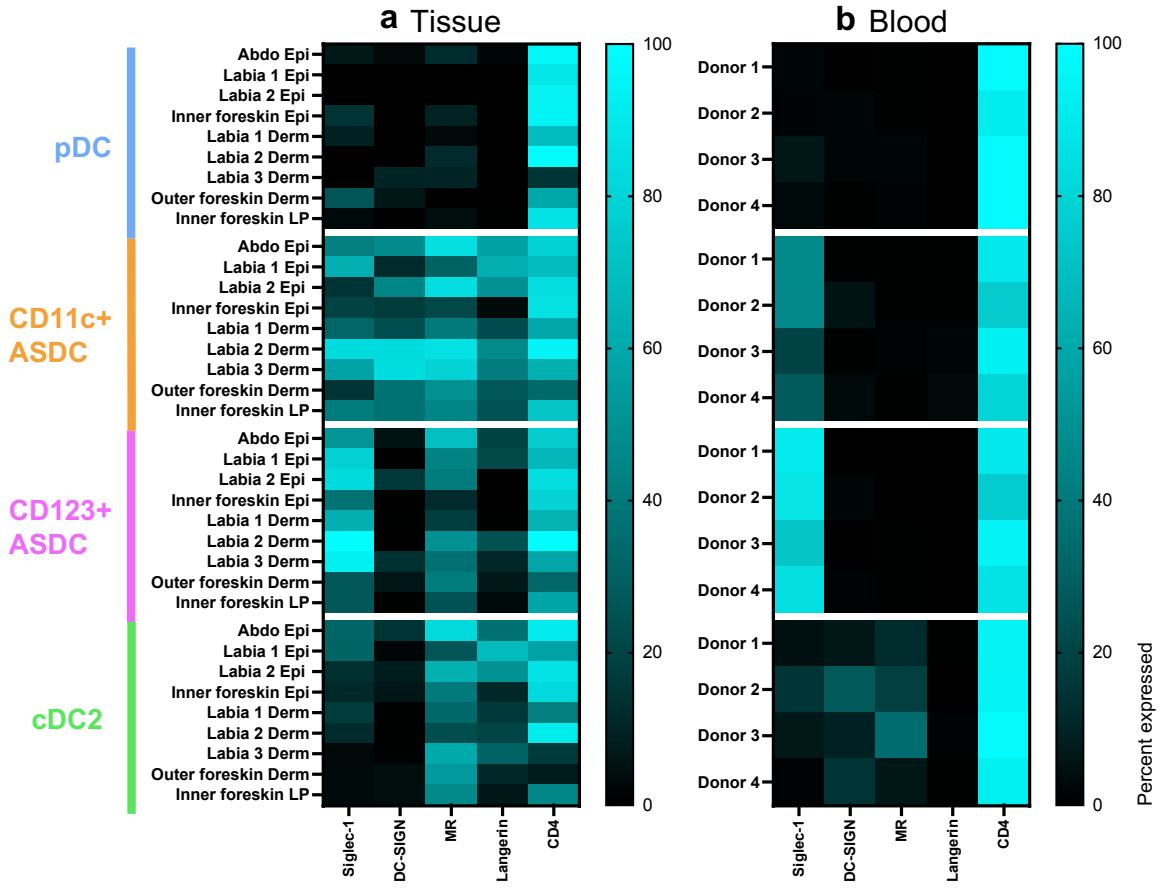

Figure 2.5: Expression of key HIV binding receptors on ASDCs, pDCs and cDC2s from human tissues and blood

"a) Immune cells liberated from abdominal epidermis (abdo epi) (n=1), labia epidermis (n=2), inner foreskin epithelium (n=1), labia dermis (derm) (n=3), outer foreskin dermis (n=1) and inner foreskin LP (n=1) were stained for flow cytometry. The percentage expression of Siglec-1, DC-SIGN, MR, Langerin, and CD4 on pDCs, CD11c$^+$ ASDCs, CD123$^+$ ASDCs and cDC2s for each tissue was plotted on a heat map and compared to blood-derived pDCs, ASDCs and cDC2s in **b)."**

"We next assessed the capacity of pDCs and ASDC to stimulate allogeneic naïve T cell proliferation, activation, and Th polarisation (**Figure 2.6b**). Corresponding with their surface expression profiles, pDCs were very poor inducers of CD4 (**Fig 2.6c**) and CD8 T cell activation and proliferation **(Supplementary figure 2.6a-b)**, whereas both ASDC subsets could perform these functions, with $CD11c^+$ ASDCs inducing more CD4 and CD8 T cell activation and proliferation than $CD123^+$ ASDCs, aligning with a previous report by Alcántara-Hernández et al. (2017). We also examined T cell cytokine production and possible subset polarisation by pDCs and ASDCs (**Figure 2.6d**). pDCs induced low levels of all Th cell cytokines. Compared to T cells that were not polarised with any APCs, ASDCs stimulated low levels of Th1 (TNF-a, IL-2) cytokines and higher levels of Th2 (IL-4, IL-5 and IL-13), Th9 (IL-9) and Th22 (IL-22) cytokines. IL-17 secretion from Th17 and IL-10 from Treg was low but higher than non-polarised T cells. IFN-g secretion was high but similar to non-polarised T cells. Selected expression of transcription factors Tbet, FoxP3, RORγt, which identify Th1, Treg, and Th17, respectively, was examined. ASDCs induced the highest proportion of T cells expressing RORγt followed by FoxP3 and low T bet expression (**Supplementary figure 2.6c**).

In summary, both subsets of ASDCs, expressed the co-stimulatory molecules CD86, ICAM-1 and HLA-DR at higher levels than pDCs, with $CD11c^+$ having the highest expression. pDCs stimulated very low levels of naïve T cell allo-proliferation whereas ASDCs induced a much higher level of proliferation. Both ASDC subsets polarised naïve T cells more toward Th2, Th9, Th22, Th17 and Treg but less toward Th1."

2.5.8 Chemokine and Cytokine Production in Blood-derived Axl^+ $Siglec\text{-}6^+$ Dendritic Cells and Plasmacytoid Dendritic Cells in Response to HIV

"As anogenital inflammation is now thought to be a pre-requisite to HIV transmission (Nasr et al., 2014), and ASDCs are only found in inflamed tissues, we next investigated ASDCs in the context of HIV infection. To this end, we either mock or HIV treated pDCs and ASDCs for 18 hours to define any HIV induced transcriptional changes using NanoString. Firstly, we compared HIV to mock treated cells and found that all characteristic genes for blood pDCs and ASDCs identified in the heat map of **Figure 2.2b** were downregulated upon HIV exposure, except for *CD86* and *ICAM-1*, which

were upregulated in HIV treated CD11c^{+} and CD123^{+} ASDCs, respectively (**Supplementary figure 2.7a**)."

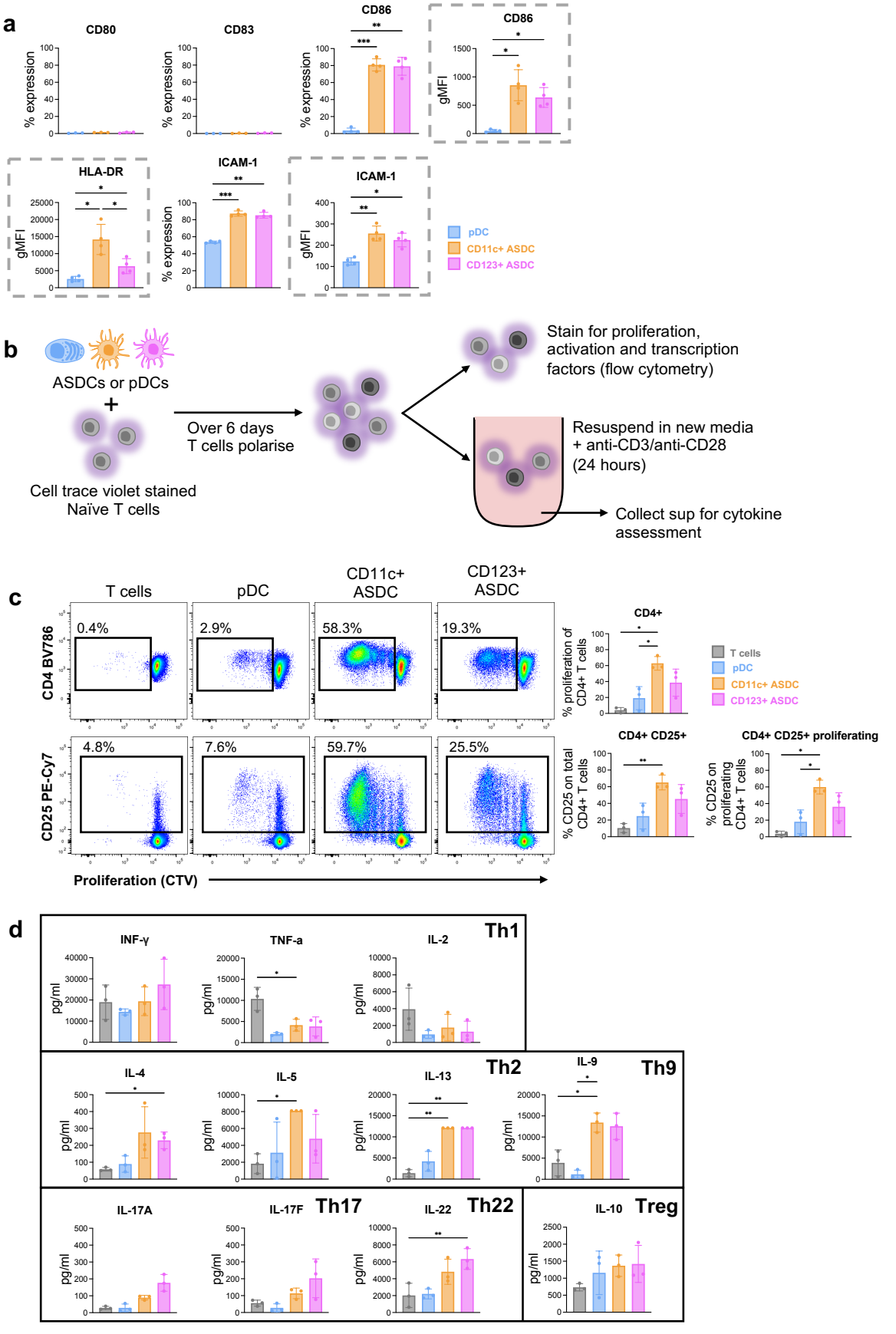

Figure 2.6: Functional phenotyping of blood-derived pDCs and ASDCs

"a) Cell surface expression of CD80, CD83, CD86, HLA-DR and ICAM-1 was determined on each cell type immediately after their isolation from blood. The percentage of expression and gMFI (when % of expression was above 80%, outlined in grey dotted box) of each subset was calculated. **b)** Workflow for functional phenotyping. **c-d)** FACS sorted pDCs, CD123 and CD11c ASDC were cultured at 37 °C with Cell trace Violet-stained naïve T cells at a ratio of 1 ASDC or pDC: 10 T cells. On day 6, cultures were analysed by flow cytometry to assess CD4 T cell **c)** proliferation via CTV stain and activation via CD25 expression. **d)** on day 6, all conditions were treated with anti-CD3/CD28 for 24 hours. Supernatants were collected to assess cytokine production. Data is presented as ±SD (n=3-4). Statistical analysis was performed using one-way ANOVA with Tukey's multiple comparisons test. *p < 0.05; **p < 0.01; ***p < 0.001."

"We then investigated the expression of chemokines and cytokines and measured their secretion into the culture supernatant using a LEGEND plex bead array. In response to HIV treatment, pDCs increased their gene expression and secreted more of the CCR5 binding chemokines CCL3 (MIP1a), CCL4 (MIP1b), CCL5 (RANTES) and CXCL10 compared to ASDCs. CXCL8/IL-8 known to be produced in response to viruses was expressed and secreted at significantly greater levels by $CD11c^+$ ASDCs when compared to pDCs and $CD123^+$ ASDCs (**Figure 2.7 and Supplementary figure 2.7b**). The pro-inflammatory cytokines TNF-a and IL-6 were secreted at high levels by HIV exposed pDCs but not from ASDCs, even though ASDCs expressed the TNF-a gene (**Supplementary figure 2.7c**). The proinflammatory cytokine IL-1b was detected at very low levels in mock and HIV treated pDCs and ASDCs at the protein level, and only in mock $CD11c^+$ ASDCs at gene level (**Supplementary figure 2.7c and Supplementary figure 2.7**). There was no gene or protein detection of IL-10, IL-12A, IL-13, IL-17, IL-18, or IL-33. pDCs expressed *IFN-a, b* and *I1* in response to HIV (**Supplementary figure 2.7d**) and IFN-a2 was secreted at high levels. However, ASDCs did not produce any interferons in response to HIV (**Figure 2.7**). Finally, IFN-stimulated genes (ISG) including *IFTM1, IFIT2, MX1* and *IFI35* were upregulated in HIV exposed pDCs and both ASDC subsets (**Supplementary figure 2.7e**), despite the lack of IFN production in the latter. This was similar to HIV induction of ISGs in DCs and macrophages in the absence of IFN as we have previously reported (Nasr et al., 2012, Harman et al., 2011).

In summary, pDCs were the main producers of CCR5 binding chemokines, interferons and proinflammatory cytokines in response to HIV, while $CD11c^+$ ASDCs produced only high levels of CXCL8."

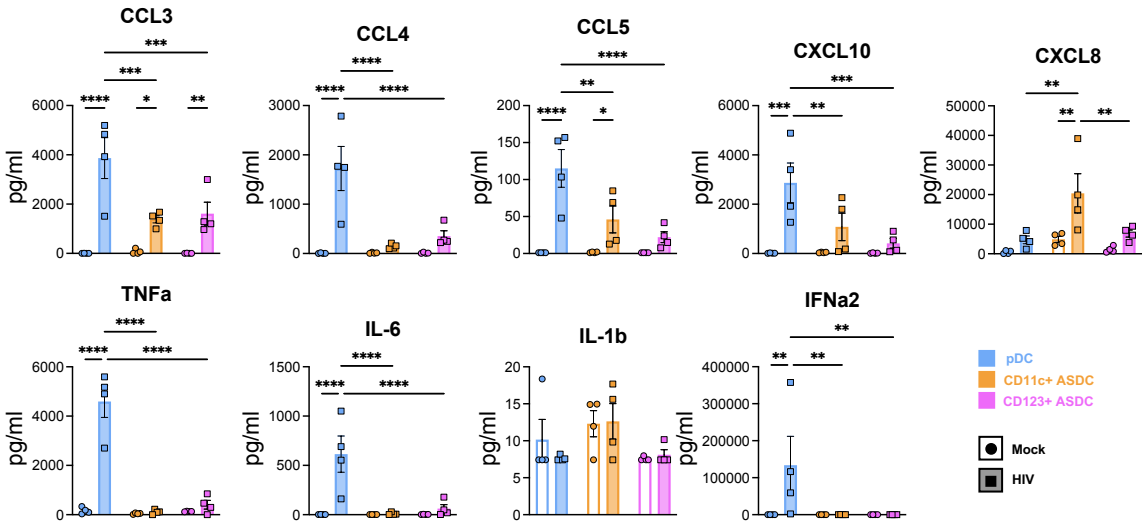

Figure 2.7: Chemokine and cytokine production after HIV interaction with pDCs and ASDCs

"LEGENDplex assay was carried out to determine the concentration of cytokines in the supernatants of mock and HIV-1 BaL treated pDCs and ASDCs at 18 hours post HIV treatment. Data are presented as ±SD (n=4). Statistical analysis was performed using one-way ANOVA with Tukey's multiple comparisons test. *p< 0.05; **p< 0.01; ***p< 0.001; ****p< 0.0001."

2.5.9 HIV Viral Transfer from Blood-derived Axl$^+$ Siglec-6$^+$ Dendritic Cells and Plasmacytoid Dendritic Cells to CD4 T Cells

"We have shown in several key studies that human tissue DCs and Langerhans cells function to capture HIV and then transfer the virus to CD4 T cells in two phases, an early first phase which is dependent on CLR-mediated endocytic uptake (and not infection) followed by a later second phase which is dependent on CD4/CCR5 mediated entry and infection. As ASDCs are present in extremely low numbers in human tissue, it was impossible to carry out uptake and infection assays using tissue derived ASDCs. Therefore, we next assessed the ability of blood-derived pDCs and each ASDC subset to mediate first phase (2 hours post HIV exposure) and second phase (96 hours post HIV exposure) transfer of HIV to CD4 T cells.

We observed two successive phases of HIV viral transfer to T cells from ASDCs. Both pDCs and ASDCs mediated first phase transfer but interestingly, CD11c$^+$ ASDCs showed a trend of higher capacity for binding HIV (**Figure 2.8a**). Contrastingly in second phase, CD123$^+$ ASDCs showed a trend of more virus transfer to T cells than CD11c$^+$ ASDC while pDCs did not, suggesting that CD123$^+$ ASDCs support the highest levels of productive infection. This was confirmed by inoculating the CD4 T cell line TZMBL1 (which express *lacZ* under control of the HIV-1 promoter) with

supernatants collected from infected cells after 96 hours post infection (hpi) (**Figure 2.8b**). No TZMBL infection occurred when inoculated with supernatant derived from HIV-exposed pDCs. Low TZMBL infection was detected from CD11c^{+} ASDCs supernatants but as expected, CD123^{+} ASDC supernatants gave rise to the highest levels of infected TZMBL cells, although this did not reach a statistical difference. Furthermore, to confirm productive infection of ASDCs via CD4/CCR5, we demonstrated that the CCR5 inhibitor maraviroc was able to completely block the ability of ASDCs to mediate second phase transfer (**Figure 2.8c**).”

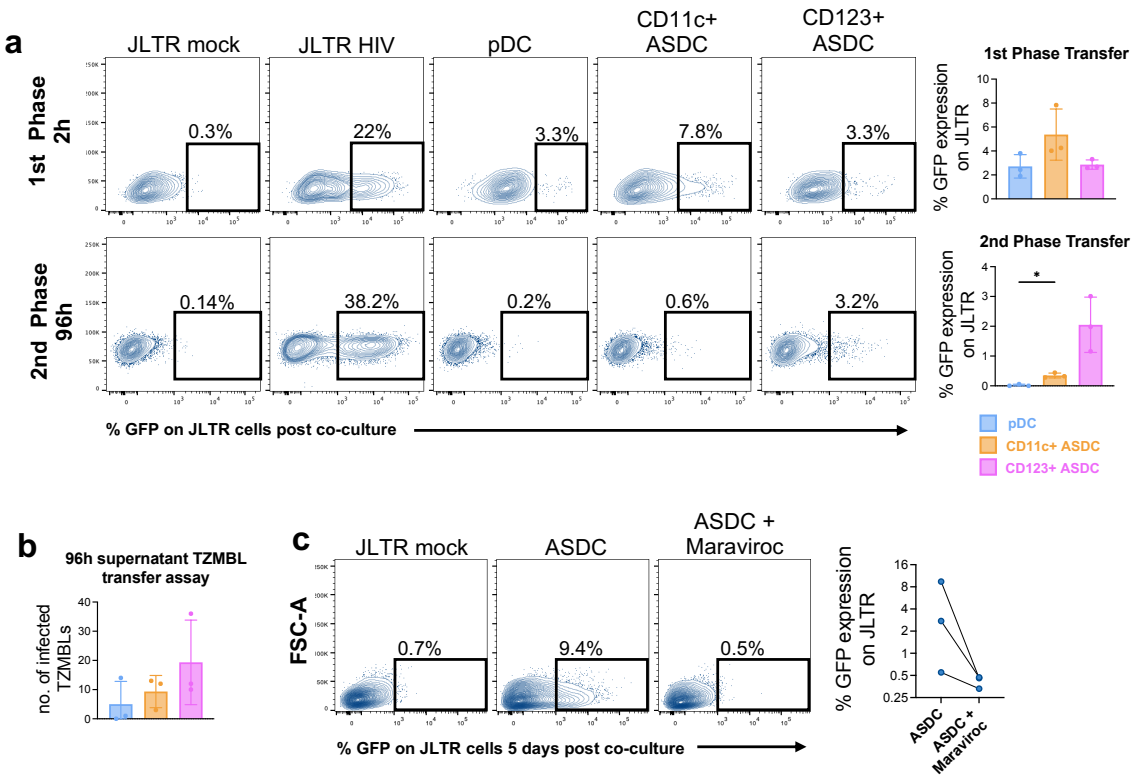

Figure 2.8: HIV interactions with blood-derived pDCs and ASDCs and viral transfer to T cells

“a) HIV transfer to JLTR cells was determined by measuring JLTR GFP fluorescence intensity by flow cytometry 2h and 96h post co-culture for first phase and second phase transfer respectively. Representative flow data and graph (data presented as ±SD, n=3) show transfer of HIV from HIV-treated cells to JLTR (GFP^{+} JLTR). **b)** Number of infected TZMBL cells after inoculation with supernatants collected at 96 hpi of pDCs, CD123^{+} and CD11c^{+} ASDCs. Data presented as ±SD (n=3). **c)** HIV transfer to JLTR cells in the presence and absence of Maraviroc. Data presented as ±SD (n=3). Statistical analysis was performed using Wilcoxon Rank Sum Test.”

2.6 Discussion

2.6.1 Definition of Axl^{+} Siglec-6^{+} Dendritic Cells in Human Blood and Tissue

"The CD123^{+} and CD11c^{+} ASDC populations described in this manuscript correspond to DC5 identified by Villani et al. (2017) which express AXL, Siglec-6, CD2, CX3CR1, CD33, and CD5, similar to the phenotype described for pre-DC1 and pre-DC2 (CD33^{+} CD45RA^{+} CD123^{+} CX3CR1^{+} CD2^{+} CD5^{+} Siglec-6^{+}) identified by (See et al., 2017). Based on our data of **Figure 2.1f** showing CD11c^{+} ASDCs express lower levels of AXL and Siglec-6 than CD123^{+} ASDCs and as reported by Villani et al., we believe that pre-DC1 are the CD123^{+high} CD11c- ASDCs while pre-DC2 are the CD123$^{-/l0}$ CD11c^{+} ASDCs. Therefore, ASDCs investigated in this study are the equivalent of the previously described pre-DCs and ASDCs. Furthermore, our findings shows that ASDCs are a different population than cDC2 and that they are mature in phenotype like cDC2.

We first confirmed the presence of pDCs, CD11c^{+} and CD123^{+} ASDCs by flow cytometry (**Figure 2.1**) and transcriptomic profiling (**Figure 2.2**) in human blood. We then showed that these cell populations were present in a range of inflamed human cutaneous and mucosal tissues including lymph nodes, colorectal mucosa affected by inflammatory bowel disease and cancer, genital and trunk skin affected by psoriasis (**Figure 2.3, Figure 2.4**). We did not observe pDCs or ASDCs in non-inflamed tissues. Importantly, we showed that CD11c^{+} ASDCs are a distinct population from bona fide CD1c^{+} cDC2 in tissues (**Figure 2.4g**) and blood (**Supplementary figure 2.5**), they are detected at a much lower frequency than cDC2 (**Supplementary table 2.2**). Thus, we propose that like pDCs, ASDCs infiltrate peripheral tissues during inflammation while cDC2 are present in both healthy (Rhodes et al., 2021) and inflamed tissues (Reynolds et al., 2021).

Our preliminary investigation into the cell surface expression of HIV binding receptors revealed that both tissue and blood derived ASDCs have similar high expression of CD4 and CD169/Siglec-1. However, tissue ASDCs expressed more CD209/DC-SIGN, CD206/MR and CD207/langerin compared to blood ASDCs (**Figure 2.5**). It is well known that blood and tissue DC expression profiles can differ extensively, for instance

CD206/MR is highly expressed by most tissue DCs and macrophages, but is variable in blood (Rhodes et al., 2021). Furthermore, tissue derived cDC2 expressed more MR compared to their blood counterparts. They also did not express DC-SIGN and had low Siglec-1 compared to tissue derived CD11c$^+$ ASDCs (**Figure 2.5**). Unfortunately, the very low cell numbers of pDCs and ASDCs in inflamed human tissue explants restricted us from performing any functional assays."

2.6.2 Functional Profiling of Axl$^+$ Siglec-6$^+$ Dendritic Cell Subsets and Plasmacytoid Dendritic Cells

"Our data showed that CD11c$^+$ ASDCs stimulated naïve T cell proliferation and activation more strongly than CD123$^+$ ASDCs, while a marginal stimulation of T cells by pDCs was observed (**Figure 2.6**)**.** This is due to CD11c$^+$ ASDCs expressing more CD86, CD54/ICAM-1 and HLA-DR than CD123$^+$ ASDCs (**Figure 2.6a**), while pDCs did not express these markers or expressed them at very low levels. Our findings that ASDCs, and not pDCs, are potent inducers of T cell proliferation and activation, and that ASDCs are mature in phenotype similar to cDC2s, are in agreement with See et al. (2017) and Villani et al. (2017). However, the former study did not separate the two ASDC subsets and the latter did not also detect a significant difference in bulk T cell proliferation and activation between the two ASDC subsets using TLR agonists for activation. In addition, we showed here that ASDCs polarise naïve T cells more towards Th2, Th9, Th17, Th22, Treg, and less toward Th1. As T-bet regulates the differentiation of Th1 cells and represses Th2 lineage commitment (Matsui et al., 2005, Neurath et al., 2002), the low level of T bet expression supports a reduced polarising toward Th1. Our high proportion of T cells expressing RORγt which does not correlate with the relatively low levels of IL-17 production is similar to Segura et al. (2013) when naïve T cells were co-cultured with inflammatory DCs. This may be explained by Th17 cells evolving into Th1, Treg or they can co-express either RORγT/Tbet or RORγT/FoxP3 (McAleer and Kolls, 2011) to reduce IL-17 secretion. Furthermore, the pattern of polarisation may be also linked to ASDC high expression of CD5 (**Figure 2.2b and Supplementary figure 2.7a**), which has been reported to be required for cDC2 to stimulate high naïve T-cell proliferation and preferential priming of Th2, Th17, Th22 and Treg cells while monocyte-like cDCs, which express lower CD5, polarise mainly Th1 cells (Yin et al., 2017). Here we showed that HIV infection downregulated *CD5* (**Supplementary figure 2.7**) and this may favor the induction of the anti-viral Th1

subset. We attempted to test this hypothesis several times, but the low ASDC numbers we could isolate made the experiment impossible to perform."

2.6.3 Cytokine Production in HIV Exposed Axl$^+$ Siglec-6$^+$ Dendritic Cells and Plasmacytoid Dendritic Cells

"Upon HIV infection, the pro-inflammatory chemokines (CCL3-5 and CXCL10) were mainly produced by pDCs followed by ASDCs except CXCL8, which was highly produced from CD11c$^+$ ASDCs. Similar to our data, CCL3, CXCL10 and CXCL8 were also detected by Brouiller et al. (2023) upon infection of AXL$^+$ ASDCs by NL-AD8. The pro-inflammatory cytokines (TNF-a and IL-6) and IFN were only produced by pDCs (**Figure 2.7**). Siglec-1 has been shown to inhibit IFN production via degradation of TBK1 (Zheng et al., 2015). As ASDC subsets expressed variable level of Siglec-1 (**Figure 2.2e**), this may explain the lack of IFN production by HIV exposed ASDCs due to their Siglec-1 expression (**Figure 2.2e**). While pDCs attract CD4 T cells to the site of infection via their pro-inflammatory chemokines (CCL3-5) (Li et al., 2009, Shang et al., 2017), they also inhibit HIV entry as these chemokines bind to CCR5 (Scarlatti et al., 1997) and with their IFN production, they inhibit viral spread. CXCL10 induces latency (Wang et al., 2021) by dephosphorylating cofilin to promote HIV integration (Cameron et al., 2010) while CXCL8 can stimulate HIV replication in CD4 T cells (Lane et al., 2001). Based on the cytokine and chemokine profiles upon HIV infection and our data that the direct activation of CD4 T cells is attributed to ASDCs and not pDCs, strategies to inhibit ASDC recruitment and functions in inflamed mucosa should be considered."

2.6.4 Axl$^+$ Siglec-6$^+$ Dendritic Cells and HIV Transmission

"pDCs have been previously shown to be productively infected by HIV (Lederle et al., 2014, Fong et al., 2002), but these studies were carried out prior to the discovery of ADSCs and were therefore examining a combination of pDCs and ASDCs. Our data showed in first phase transfer that CD11c$^+$ ASDCs had a trend of transferring more HIV to CD4 T cells than CD123$^+$ ASDCs and pDCs. Importantly, we showed that this corresponded with CD11c$^+$ ASDC higher expression of CLRs **(Figure 2.2e and Supplementary figure 2.3**), which we have previously shown to bind HIV and mediate its uptake via CD206/MR (Lai et al., 2009), CD207/langerin (Nasr et al., 2014) and CD209/DC-SIGN (Bernhard et al., 2004). We then showed that CD123+ ASDCs had

a trend of transferring more HIV to CD4 T cells in the second phase (**Figure 2.8**). We attempted to directly assess the productive infection of $CD123^+$ ASDCs and $CD11c^+$ ASDCs via p24 expression. However, due to low numbers of blood derived ASDCs, we had insufficient cells for accurate measurement. The higher Siglec-1 expression on $CD123^+$ ASDCs compared to their $CD11c^+$ counterparts confirmed the role of Siglec-1 in binding HIV to facilitate productive infection as shown previously for DCs (Zou et al., 2011), macrophages (Turville et al., 2004) and ASDCs (Ruffin et al., 2019). Furthermore, we found that $CD11c^+$ ASDCs expressed higher levels of the HIV restriction factor SAMHD1 than $CD123^+$ ASDCs, explaining their reduced capacity in mediating second phase transfer. Additionally, $CD11c^+$ ASDCs had a higher gMFI for CD86 and HLA-DR than $CD123^+$ ASDCs, indicating a more mature phenotype. It is known that mature DCs bind more HIV than immature cells (Harman et al., 2006) and that they are less susceptible to productive infection (Ruffin et al., 2019). This also explains why $CD11c^+$ ASDCs are efficient at mediating first phase and not second phase transfer and perhaps an increase in the maturation of the $CD123^+$ ASDC subset would increase their rate of first phase HIV transfer as previously reported (Ruffin et al., 2019). Finally, pDCs transferred HIV to T cells at low efficiency in first phase only. This could be explained by their expression of CLEC4A, known to bind HIV (Lambert et al., 2008) for transmission in first phase, while their IFN production acts to inhibit viral replication and spread (Tong et al., 2021, Beignon et al., 2005) in second phase transfer.

Ruffin et al. (2019) investigated the interactions of blood derived pre-DCs with HIV but their study encompassed the combined $CD123^{+high}$ $CD11c^-$ and $CD123^{-/lo}$ $CD11c^{+/high}$ ASDCs as their pre-DCs were defined as $HLA\text{-}DR^+$ Lin^- $CD33^{int}$ $CD45RA^+$ $CD123^+$ Axl^+. They showed that the combined ASDC subsets took HIV via CD169/Siglec-1, become infected and transfer HIV to CD4 T cells, similar to our data of HIV infection of $CD123^{+/high}$ $CD11c^-$ ASDCs. Brouiller et al (2023) also investigated the interactions of blood derived ASDCs with HIV either as combined ASDC subsets (when sorted on Axl^+ $CD123^+$) or separated subsets (when sorted on CD11c+ and $CD11c^-$). The high p24 detected in their $CD11c^+$ Axl^+ DCs was due to infection by HIV-1 (NL-AD8) in the presence of Vpx, thus neutralising SAMHD1. This correlates with our reasoning of high SAMHD1 expression in $CD11c^+$ ASDCs which reduces their productive infection compared to $CD123^+$ ASDCs expressing lower SAMHD1."

2.6.5 Concluding Remarks

“In summary, we have shown for the first time that inflammatory ASDCs are present in inflamed tissues where HIV transmission occurs. This is extremely important as the body of evidence that anogenital inflammation is a causative factor in HIV transmission is now undeniable, especially in sub-Saharan Africa (Masson et al., 2015, Passmore et al., 2016). Although a dysregulated vaginal microbiome is clearly a contributing factor (Masson et al., 2016, Anahtar et al., 2015), the key inflammatory HIV target cells have not yet been identified. Our findings here that both ASDC subsets can mediate HIV transmission to CD4 T cells has important implications for better PrEP design. For example, current PrEP drugs that block the HIV replication cycle (e.g. Tenofovir) will likely be effective at blocking the ability of $CD123^+$ ASDCs from becoming infected and transmitting HIV to T cells. However, drugs that block HIV binding to CLRs will likely be required to block $CD11c^+$ ASDCs from performing this function as they transmit the virus independent of infection and replication.

In future, we will use our expertise in high parameter imaging of human tissues (Baharlou et al., 2022, Baharlou et al., 2021) to carry out imaging mass cytometry and spatial transcriptomics to: **i)** define ASDCs in all human anogenital tissues (Li et al., 2009) and whether they reside in lymphoid aggregates; **ii)** assess whether they interact or cluster with specific immune cells present in the mucosa and; **iii)** investigate their relative importance in taking up HIV and transferring it to CD4 T cells in inflamed anogenital mucosae compared to other infiltrating or resident DCs (cDC1, cDC2, DC3 and monocyte derived DCs). This will determine their relative importance in therapeutic strategies that aim at preventing HIV uptake in anogenital mucosae. Given the difference in the biology of pDCs and ASDC subsets and particularly their interactions with HIV, it will be essential to study all three subsets in the pathogenesis of other viruses and diseases. As knowledge progresses, specific interventions related to any of these subsets in other diseases may be become apparent.”

2.7 Supplementary Material

2.7.1 Figures

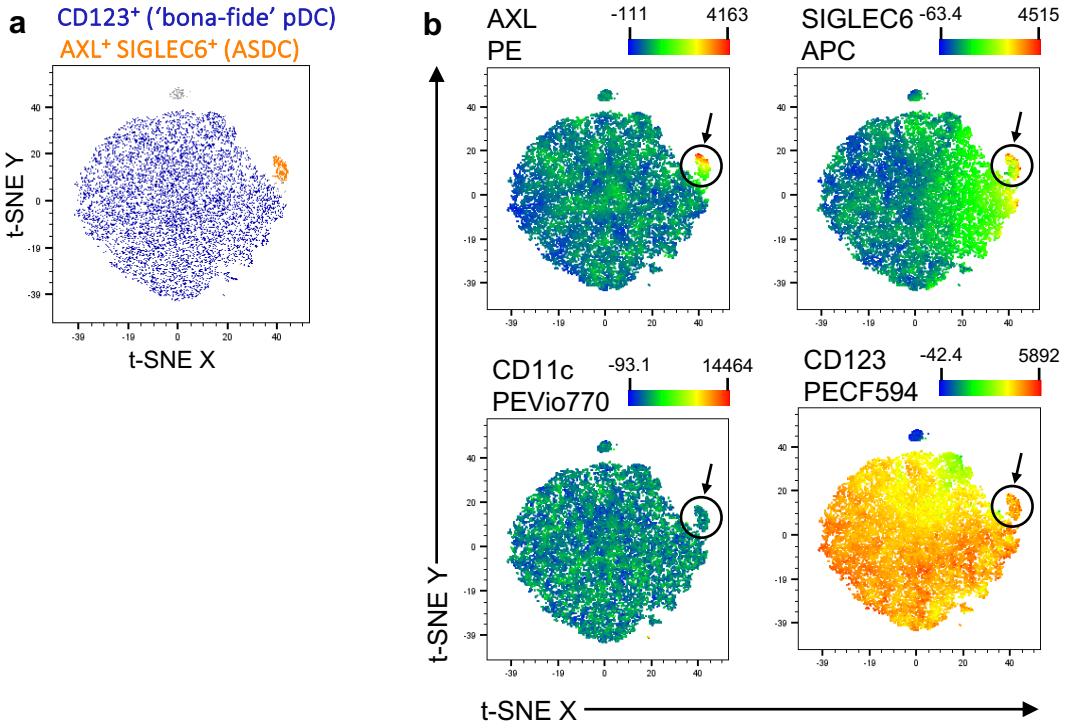

Supplementary figure 2.1: Transcriptional profiling of pDCs and ASDCs for gene expression of chemokine receptors from publicly available scRNA-seq dataset

"Sorted blood PBMCs were transcriptionally profiled by scRNA-seq (GSE94820)(Villani et al., 2017). pDC, CD11c$^+$ ASDC and CD123$^+$ ASDC annotations were determined using metadata provided by the authors. Chemokine receptors gene expression is shown in pDCs, CD123$^+$ and CD11c$^+$ ASDCs."

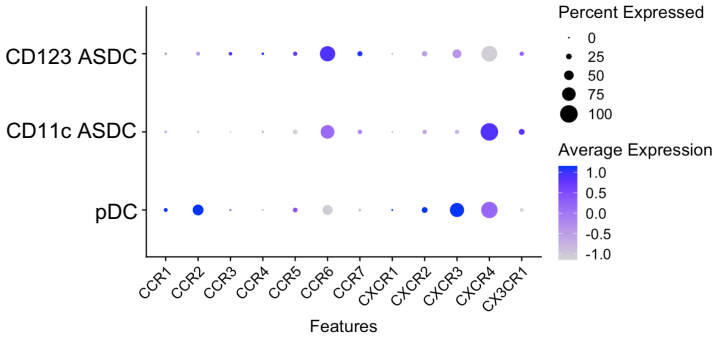

Supplementary figure 2.2: Identification of ASDCs and pDCs isolated using the Human Plasmacytoid Dendritic Cell Isolation Kit II

"t-stochastic distributed neighbour embedding (t-SNE) analysis performed on live single Lin1-HLA-DR$^+$ cells based on AXL, Siglec-6, CD123, and CD11c. **a)** Representative t-SNE dot plot shows the distribution of AXL$^+$ Siglec-6$^+$ DCs (orange) and AXL$^-$ Siglec-6$^-$ CD123$^+$ pDCs (blue) on t-SNE plot. **b)** Heat map visualisations of the median fluorescence intensity of surface AXL, Siglec-6, CD123, and CD11c expression for populations on t-SNE plot."

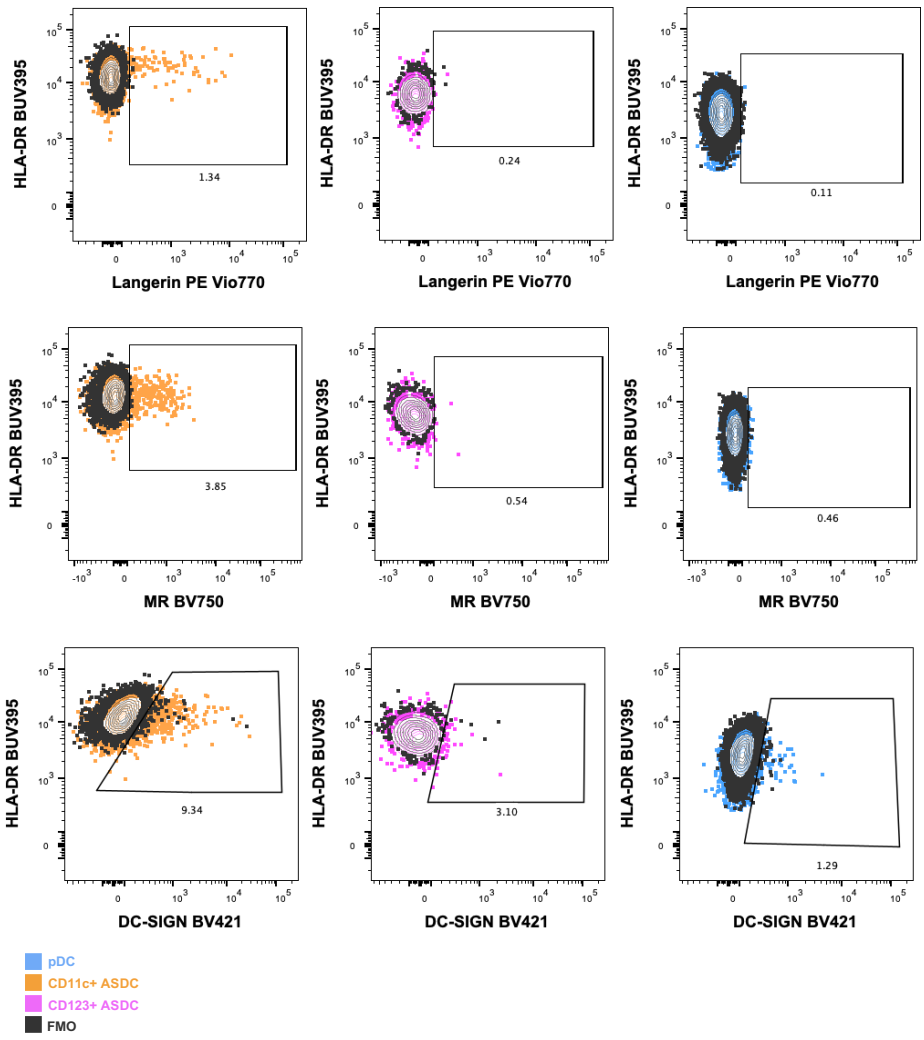

Supplementary figure 2.3: Protein expression of lectin receptors on blood ASDCs and pDCs

"Pan DCs were FACS sorted into CD11c^{+} ASDCs, CD123^{+} ASDCs and pDCs and surface stained for flow cytometry. Representative plots show the percentage expression of Langerin, MR and DC-SIGN displayed as an FMO (grey) overlayed with true expression for each population. As the percent of positive population was small, expression was displayed as a percentage rather than gMFI."

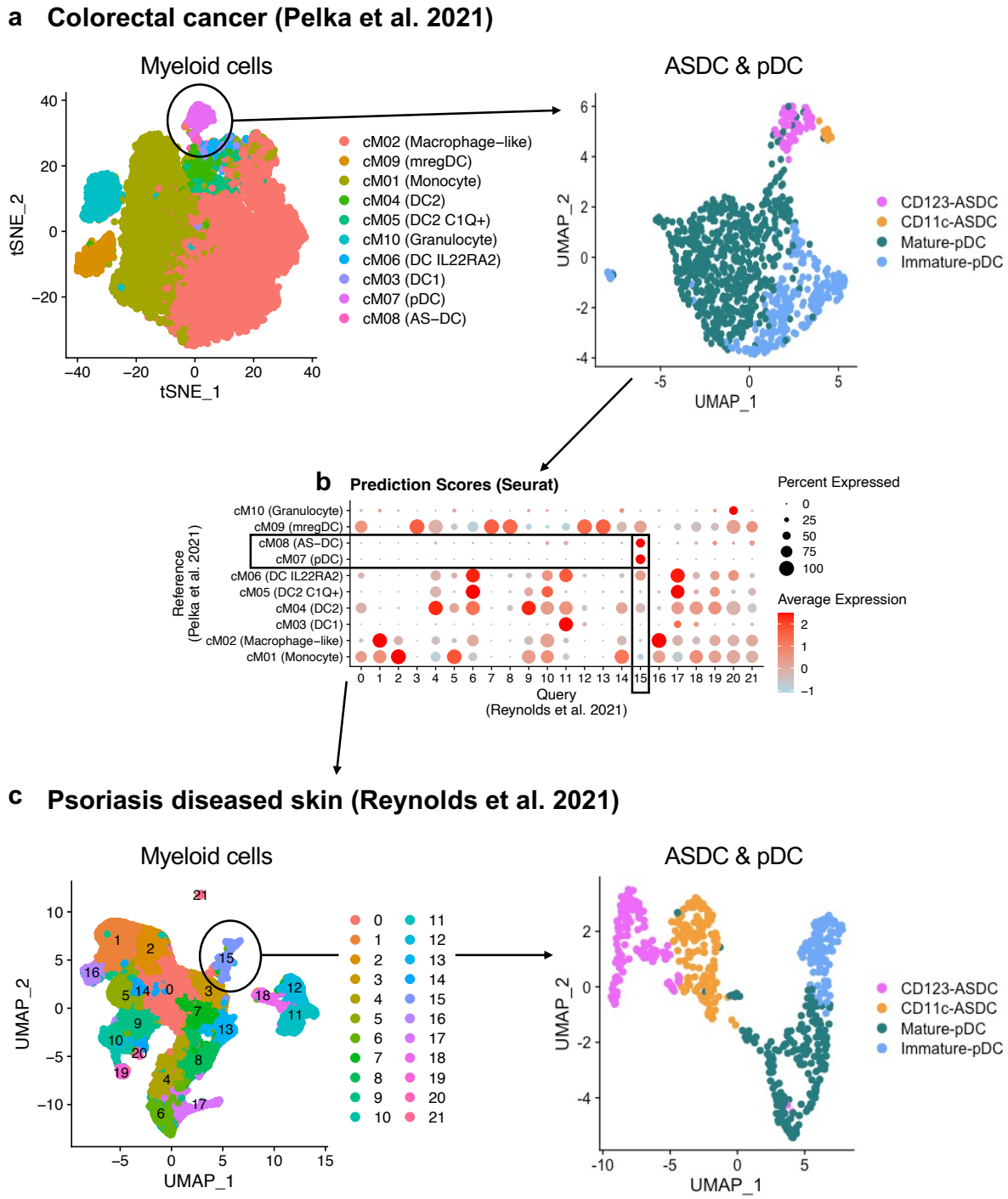

Supplementary figure 2.4: scRNA-seq data analysis

"a) Pelka et al. 2021 data was downloaded from the GEO (GSE178341). Myeloid clusters (cM01-10) were isolated and analysed separately. The tSNE coordinates used by the authors were downloaded from the Broad Institute's Single Cell Portal (SCP1162). ASDCs and pDCs described by the authors were isolated and reclustered for analysis. **b-c)** Reynolds et al. 2021 data was downloaded from Developmental Human Cell Atlas (E-MTAB-8142). Myeloid cells, as annotated by the authors, were isolated and analysed separately. Data was batch corrected using Seurat's RPCA method, and clustered using a resolution of 0.6, resulting in 22 clusters. Seurat's *FindTransferAnchors* and *TransferData* functions were used to determine predicted annotations, with GSE178341 (or colorectal cancer) acting as the reference data to E-MTAB-8142 (or psoriasis skin) as the query. A DotPlot was used to demonstrate the prediction scores generated by the functions. ASDCs and pDCs, identified as cluster 15, were isolated and reclustered for analysis."

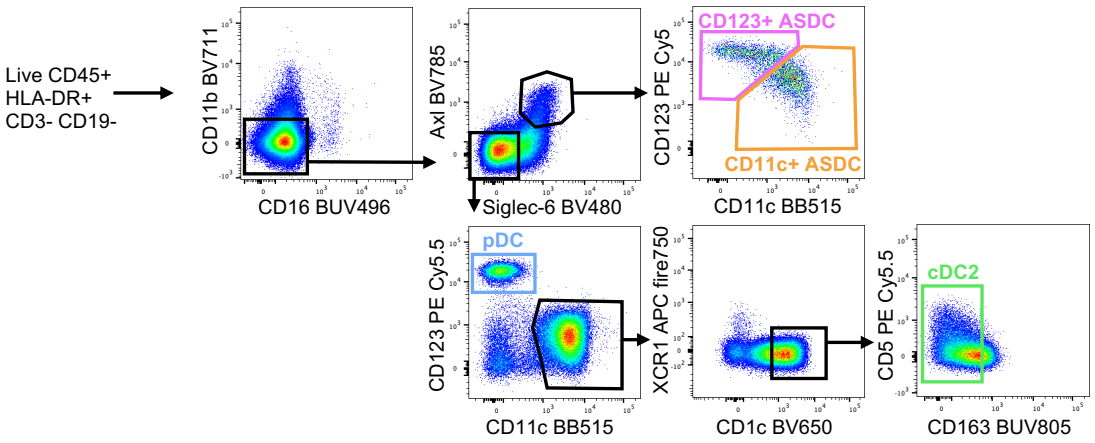

Supplementary figure 2.5: Flow cytometry gating strategy identifying pDCs, ASDCs and cDC2s in blood

"Blood pan DCs were isolated and stained for flow cytometry using a modified panel to allow for the identification of cDC2s. All cells were first gated as Live CD45$^+$ HLA-DR$^+$ CD3$^-$ CD19$^-$. Subsequent cell populations were identified as CD123$^+$ ASDCS (CD11b$^-$CD16$^-$AXL$^+$Siglec-6$^+$CD123$^+$), CD11c$^+$ ASDCs (CD11b$^-$CD16$^-$AXL$^+$Siglec-6$^+$CD11c$^+$), pDCs (CD11b$^-$CD16$^-$AXL$^-$Siglec-6$^-$CD11c$^-$CD123$^+$) and cDC2s (CD11b$^-$CD16$^-$AXL$^-$Siglec-6$^-$CD123$^-$CD11c$^+$CD1c$^+$XCR1$^-$CD163$^-$)."

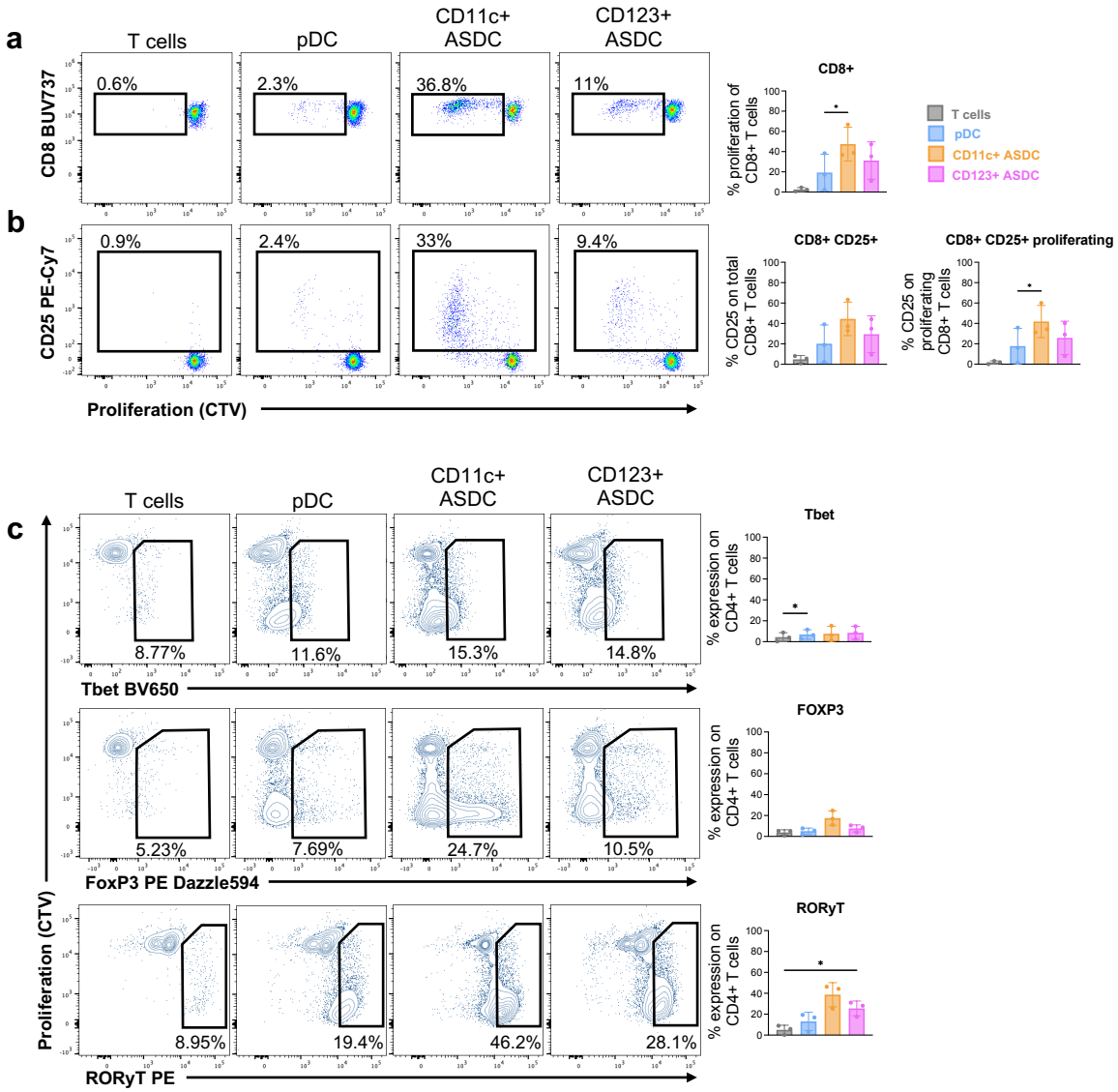

Supplementary figure 2.6: T cell proliferation, activation and polarisation after co-cultured with pDCs and ASDCs

"FACS sorted pDCs, CD123$^+$ and CD11c$^+$ ASDC were cultured for 7 days at 37 °C with Cell trace Violet-stained naïve T cells at a ratio of 1 ASDC or pDC: 10 T cells. Cultures were analysed by flow cytometry to assess **a)** CD8+ T cell proliferation, **b)** CD8+ T cell activation via CD25 expression, **c)** CD4+ T cells percentage expression of transcription factors Tbet, FoxP3 and RORγT. Data presented as mean of ±SD. For all data, *p < 0.05 using one-way ANOVA with Tukey's multiple comparisons test."

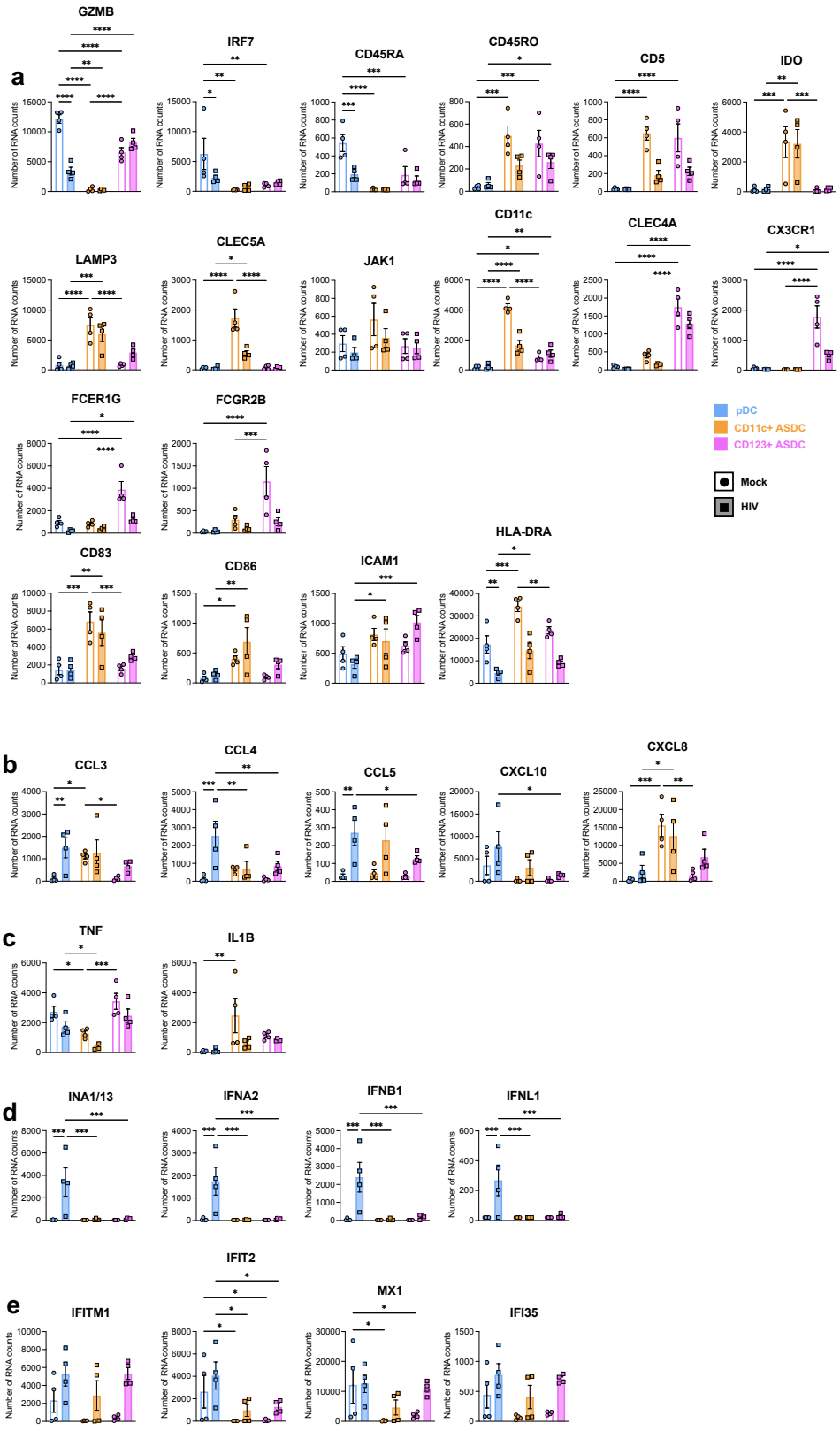

Supplementary figure 2.7: Gene profiling of pDCs and ASDCs in mock and HIV conditions

"pDCs and ASDCs were profiled using NanoString as either mock or after 18 hours of HIV exposure. **a)** Markers defining pDCs, CD11c^{+} and CD123^{+} ASDCs; **b)** Chemokines (CCL3, 4, 5; CXCL10 and 8), **c)** cytokines (TNFα, IL-1B), **d)** IFN, **e)** ISGs in mock and HIV exposed pDCs and ASDCs. Data presented as mean of ±SD. For all data, *p < 0.05, **p < 0.01, ***p < 0.001, ****p < 0.0001 using one-way ANOVA with Tukey's multiple comparisons test."

2.7.2 Tables

Supplementary table 2.1: Patient information from inflamed tissue samples in Figure 2.4

Samples	Gender & age of donor	Reason for removal
Inflamed rectum (Fig 4a-c)	Female, 10 Not disclosed	Ulcerative colitis (active colitis)
Inflamed Mesenteric lymph node (Fig 4d)	Not disclosed	Tumour resection
Uninflamed rectum (Fig 4e)	Not disclosed (n=3)	Tumour resection (uninflamed adjacent tissue)
Inflamed colon (Fig 4f)	Not disclosed	Diverticulitis
Inflamed foreskin (fig 4g)	Male, 70	Circumcision

Supplementary table 2.2: Patient information from inflamed tissue samples in Figure 2.5 and relative proportions of pDCs, ASDCs and cDC2

Samples	Gender & age of donor	Reason for removal	pDC	CD11c+ ASDC	CD123+ ASDC	cDC2
Inflamed Abdominal Epidermis	Female, 60	Abdominoplasty	0.37%	0.13%	0.16%	1.9%
Inflamed Labia 1 Epidermis	Female, not disclosed	Labiaplasty	0.15%	0.13%	0.08%	4.87%
Inflamed Labia 2 Epidermis	Female, 26	Labiaplasty	0.39%	0.44%	0.26%	2.89%
Inflamed Inner Foreskin Epithelium	Male, 70	Circumcision	0.62%	0.53%	0.75%	9.74%
Inflamed Labia 1 Dermis	Female, not disclosed	Labiaplasty	0.09%	0.12%	0.76%	19%
Inflamed Labia 2 Dermis	Female, 26	Labiaplasty	0.12%	0.65%	0.3%	3.69%
Inflamed Labia 3 Dermis	Female, not disclosed	Labiaplasty	0.099%	0.099%	0.14%	3.12%
Inflamed Outer Foreskin Dermis	Male, 70	Circumcision	0.14%	0.28%	1.22%	6.88%
Inflamed Inner Foreskin LP	Male, 70	Circumcision	1.21%	0.33%	1.71%	7.35%

Chapter 3. 26-parameter Flow Cytometry Panel to Characterise all Homeostatic and Inflammatory State Mononuclear Phagocytes in Human Skin, Type II Mucosa and Type I Mucosa

This chapter is formatted as a manuscript for *Cytometry Part A*. At the time of this thesis submission the manuscript was being finalised for re-submission in response to editorial review.

Erica E. Vine*, **Freja A. Warner van Dijk***, Tony L. Cunningham, Najla Nasr, Andrew N. Harman, Kirstie M. Bertram. 26-parameter flow cytometry panel to characterise all homeostatic and inflammatory state mononuclear phagocytes in human skin, type II mucosa and type I mucosa. *Cytometry A* (2025) *in revision after editorial review*

*Co-first Authors

This chapter is presented in the format of a Cytometry Part A Optimised Multicolour Immunofluorescence Panel (OMIP) manuscript and details the design and optimisation of a 26-parameter conventional flow cytometry panel for the BD FACSymphony A5. All experiments, analysis and writing were equally contributed to by this author and Erica Vine, a previous PhD student.

For this chapter, several lectin receptors are referred to throughout by their 'CD' classification: MR/CD206, DC-SIGN/CD209, Siglec-1/CD169, langerin/CD207.

3.1 Abstract

We developed a 26-colour flow cytometry panel to comprehensively characterise mononuclear phagocytes (MNP) in steady and inflammatory states for human skin, type II and type I mucosal tissues. The capacity to isolate and define Langerhans cells, dendritic cells, macrophages and monocytes from fresh human tissue is critical to understanding their roles as antigen presenting cells. Liberating MNPs from tissue via enzymatic digestion requires careful consideration to prevent cleavage of surface proteins, particularly those markers necessary for identification. Additionally, tissue-resident cells emit unique and varied autofluorescent signatures that further complicate design and analysis. Furthermore, the expression levels of key surface receptors vary across different tissues, ranging from low to extremely high, making fluorophore selection and cytometer setup crucial. Here we present an optimised multicolour immunofluorescence flow cytometry panel capable of defining Langerhans cells (LC), conventional dendritic cell (cDC) -1, cDC2, DC3, plasmacytoid DC (pDC),

Axl^{+} Siglec-6^{+} (AS)DC, monocytes and a variety of macrophages across a range of human peripheral tissues including skin, type II mucosae and intestine.

3.2 Introduction

The first cellular line of defence in the human immune system is dependent on the action of antigen presenting cells (APCs), which distinguish between antigens of pathogenic or commensal microbes. Mononuclear phagocytes (MNP) are a phagocytic subgroup of professional APCs responsible for detecting and binding exogenous antigens via surface receptors and presenting them to naïve T cells. In human tissue, MNPs comprise of Langerhan cells (LC), macrophages, dendritic cells (DC) and monocytes. These cells are the sentinels of the innate immune response and are crucial for triggering adaptive immunity, including against the sexually transmitted viruses HIV and HSV.

MNP subsets and definitions, particularly in blood, are continuously evolving. When MNPs migrate into peripheral tissues, their phenotype and function can be altered by the micro-environment. Homeostatic human tissue-derived MNPs have been relatively well investigated, however, across different tissue types, MNP subsets have been defined using an inconsistent variety of markers. Furthermore, tissue MNPs from an inflammatory milieu remain poorly understood (Segura et al., 2013, Mair and Liechti, 2021, Rhodes et al., 2021, Villani et al., 2017), specifically those that reside in anal and genital (anogenital), and, colon and rectal (colorectal) tissues. Crucially, anogenital inflammation is highly associated with increased HIV and HSV transmission (Hearps et al., 2017, De La Cruz et al., 2021, Rana et al., 2024, Masson et al., 2015, Lemos et al., 2014). This highlights the need to identify and characterise the MNPs residing not only in steady state but also in inflamed human anogenital tissues. Utilising a flow cytometry panel that can consistently identify MNP subsets across different mucosal tissues will allow for a direct comparison of populations. This thorough characterisation will aid the development of improved mucosal vaccines and immunotherapy that target inflammatory MNPs (Vine et al., 2024). Therefore, we have designed a 26-colour phenotyping panel to comprehensively phenotype all MNP subsets in both steady state and inflamed human tissues and skin from both male and female genital tracts and the intestinal tract (**Table 3.1**, **Table 3.2**) Additionally, it should be emphasised that this phenotyping of MNP subsets across different tissue

types, particularly the inflammatory subsets, is both novel and highly exploratory. This represents the first investigation of these cells in these tissues. While some populations were not detected during optimisation, the limited number of samples analysed limits any definitive conclusions about their presence or absence.

Human sexual transmission sites are either skin, type II mucosa or type I mucosa. All three tissues consist of a surface epithelium and an underlying layer of connective tissue referred to as dermis for skin and lamina propria (LP) for type I and II mucosa. Skin (trunk skin, often used as a model, outer foreskin, labia, glans penis and the anal verge) is relatively impermeable to pathogens as it contains a stratified squamous epithelium and a surface layer of keratinized dead cells (stratum corneum). Type II mucosa (vagina, ectocervix, inner foreskin, fossa naviculars and anal canal) similarly comprises a stratified squamous epithelium but either lacks or possesses a thin stratum corneum (Rana et al., 2024). Type I mucosa (endocervix, penile urethra, rectum and all intestinal tissues) comprises a single layer of fragile columnar epithelium and is most vulnerable to pathogen invasion. Importantly, the tissue barrier integrity of inflamed skin and mucosa is often disrupted (Arnold et al., 2016, Borgdorff et al., 2016, Zevin et al., 2016). This results in pathogens having direct access to the underlying tissue layers and the complement of MNPs found therein, including inflammation specific MNP subsets.

Access to all human anogenital and colorectal tissues in this study was facilitated by extensive collaborations with surgeons across the Western Sydney Local Health district. Using our previously optimised tissue digestion protocols (Botting et al., 2017, Doyle et al., 2021), MNPs were liberated from these tissues in a functionally intact state (**Figure 3.1**). To ensure the accurate assessment of the MNP compartment, lymphocyte markers CD3 and CD19 were included to omit T cells and B cells respectively. HLA-DR, the marker of all APCs was also an essential inclusion.

LCs reside in the stratified squamous epithelium of skin and are defined by high expression of HLA-DR, CD207 (langerin) and CD1a, and low expression of CD11c (Bertram et al., 2019, Vine et al., 2022). They are found in smaller proportions in type II mucosa and are absent from type I mucosa. Previously, it was thought that LCs were the only MNP residing in epithelium, however Bertram et al. revealed a previously overlooked steady-state MNP subset, the epithelial $CD11c^+$ DC ($HLA\text{-}DR^+$ $CD11c^{hi}$

CD207$^{+/-}$ CD1a^{+}), which shared similarities with an epidermal DC previously identified in inflamed tissues (Wollenberg et al., 1996, Pena-Cruz et al., 2018). These epithelial CD11c^{+} DCs predominate over LCs in type II mucosal tissue (Bertram et al., 2019) and are enriched in inflammation (Wollenberg et al., 1996, Pena-Cruz et al., 2018). With CD11c being the key distinguishing marker between these epithelial LCs and DCs, its inclusion in this panel was crucial.

DCs predominantly reside in deeper dermal/LP layers of human tissues. They are HLA-DR^{hi} expressing cells and can be divided into subgroups of conventional DCs (cDC), cDC1 and cDC2, as well as the recently defined DC3 (Villani et al., 2017, Bourdely et al., 2020, Cytlak et al., 2020, Dutertre et al., 2019). cDC1s are functionally and phenotypically quite distinct from other DCs, as they are resistant to HIV infection (Silvin et al., 2017). They are clearly distinguishable by their expression of XCR1 (Mair and Liechti, 2021, Silvin et al., 2017). In skin and type II mucosa, cDC2 identification has become increasingly difficult. They share a distinctive phenotypic similarity with DC3s and *in vivo* monocyte-derived DCs (MDDC), all of which are CD11c^{+} and CD1c^{+}, markers which were previously used to exclusively identify cDC2s. Therefore, historical cDC2 classifications need re-evaluation to ensure their accurate isolation from other MNPs (Bourdely et al., 2020, Cytlak et al., 2020, Bertram et al., 2023, Vine et al., 2022, Villani et al., 2017, Dutertre et al., 2019). Adding further complexity, MDDC and DC3 populations both express CD14 (Rhodes et al., 2021, Villani et al., 2017, McGovern et al., 2014), while DC3s and MDMs both express CD163 (Villani et al., 2017). However, when comparing between these three CD11c^{+} CD1c^{+} DC subsets, precise identification of cDC2s is achieved by first isolating DC3s based on their CD163 expression (CD163^{+} CD14$^{+/-}$), before dividing the remaining cells according to their CD14 expression: MDDC (CD14^{+}) and cDC2 (CD14^{-} CD207$^{+/-}$). In type I mucosa, cDC2s are distinguishable from DC3s and MDM subsets (CD14^{+}) by these markers, in addition to CD172a (Richter et al., 2018, Watchmaker et al., 2014, Doyle et al., 2021).

In human skin and type II mucosa, CD14^{+} macrophages are divided broadly into tissue resident macrophages (Macrophage) identified by their high autofluorescence, and non-autofluorescent monocyte-derived macrophages (MDM), derived from migrated monocytes. In type I mucosal tissues, based on intestinal macrophage subsets defined by Bujko et al (Bujko et al., 2018), macrophages were divided into MDMs (CD11c^{+}

HLA-DR^{lo}), MDMs transitioning to a tissue-resident phenotype: transitional-MDMs (t-MDM) (CD11c^{+} HLA-DR^{+}), and tissue-resident macrophages (Macrophage) (CD11c^{-} HLA-DR^{+}). Calprotectin (S100A8/S100A9), in addition to CD88 and CD16, were included to identify and characterise infiltrating monocytes and monocyte-derived cells (Bourdely et al., 2020, Bujko et al., 2018, Ziegler-Heitbrock et al., 2010). To further assist in macrophage subset differentiation, lectin receptors CD169 (Siglec-1), CD206 (MR) and CD209 (DC-SIGN) were included as they are associated with a tissue-resident phenotype. Previously, CD169 and CD209 were thought to be markers specific to DCs (Perez-Zsolt et al., 2019, Gurney et al., 2005, Bernhard et al., 2004), however, Rhodes et al. revealed that they are important phenotypic markers for tissue macrophages.

One of the central aims of this panel was to more comprehensively identify and phenotype inflammatory MNPs present in inflamed anogenital tissues (Warner van Dijk et al., 2025). CD123^{+} pDCs are a known MNP that infiltrate into inflamed tissues. However, owing to the advances of scRNA-seq technologies a novel population of cells was distinguished from the pDC lineage, identifiable by their expression of Axl and Siglec-6 (CD327), termed ASDCs (Villani et al., 2017)/pre-pDCs (See et al., 2017, Ruffin et al., 2019). These ASDCs can be further divided into CD123^{hi} and CD11c^{lo} populations. Importantly, a recent study demonstrated that ASDCs reside in human anogenital tissues exclusively in the context of inflammation, revealing their presence in inflamed rectums of ulcerative colitis and diverticulitis patients, and their absence in healthy rectum (Warner van Dijk et al., 2024). In inflammation, MDDCs are recruited to affected tissue sites and have been previously reported in skin (Zaba et al., 2009), nasal mucosa (Eguíluz-Gracia et al., 2016) and anogenital tissues (Rhodes et al., 2021). As detailed earlier, these cells are CD14^{+} CD1c^{+} cells, but in an inflammatory context they have also been described to express CD1a, CD206 and CD11b (Segura et al., 2013, Tang-Huau et al., 2018). CD14 expression has also been linked to inflammatory DC3s (CD5^{-}CD163^{+}CD14^{+}) which have been shown to accumulate in the blood and kidneys of lupus patients when compared to healthy donors (Chen et al., 2024, Dutertre et al., 2019), and they increased in numbers in psoriatic skin (Nakamizo et al., 2021) and inflamed broncho-alveolar lavage (Jardine et al., 2019). Another key feature of tissue inflammation is cell cycling and division, and migration out of tissue. To evaluate DC proliferation and migration, we included the intracellular

marker KI67 to assess cellular proliferation (Reynolds et al., 2021) and the chemokine receptor CCR7 required for DC maturation and migration to lymph nodes (Ohl et al., 2004).

This panel utilises the most recent definitions of MNPs to comprehensively identify all known subsets of DCs, macrophages, LCs and monocytes across skin, type I and type II mucosal tissues – settings where the MNP landscape remain largely unexplored. Designed to operate in both homeostatic and inflammatory environments, this panel enables the identification of specific inflammatory MNP populations and offers valuable insight into tissue-specific and disease-specific immune dynamics. In the evolving sphere of MNP classifications, this panel provides a comprehensive and current reference point. Given the central role of MNPs as professional APCs and key mediators of the innate immune response, their accurate definition in tissue is a critical component to elucidating their broader functional roles and interactions within the immune system. With minor optimisations to compensate for tissue-specific expression of markers of interest, this panel could be applied to other tissue and mucosal settings, such as oral or respiratory mucosa and peripheral lymphoid organs, facilitating further investigation and understanding of the roles of tissue-specific MNPs in diverse inflammatory disease contexts.

3.2.1 Similarity to Other OMIPs

Several previously published OMIPs have focused on broadly characterising the immune cell composition of human PBMCs, in which some DC subsets and monocytes were identified (OMIP-024, OMIP-042, OMIP-051, OMIP-069, OMIP-078, OMIP-102, OMIP-104). OMIP-044 is the only other OMIP which comprehensively phenotypes APCs, and was demonstrated in PBMCs, fresh human blood and fresh human non-lymphoid tissues. OMIP-102 only included PBMC samples, however, the marker CD45, a human tissue-derived leukocyte marker, was included for future tissue use. The only other three previous OMIPs specifically designed for and assessed in human tissue are, OMIP-070, identifying NK cells in human tumours, OMIP-082, identifying lymphoid cells in human intestinal tissue and OMIP-096, identifying T cells in human skin, intestine and type II mucosa. This OMIP is the first to characterise human tissue APCs and MNPs, across a range of human tissues (skin, type II and type I mucosa), specifically in the context of inflammation – making it broadly

applicable to many human disease settings.

Table 3.1: Summary table for application of OMIP

Purpose	Characterisation of human mononuclear phagocytes isolated from skin, type I and Type II mucosa
Species	Human
Cell types	Colon, rectum, foreskin, vagina
Cross reference	OMIP-044, OMIP-070, OMIP-082, OMIP-096

Table 3.2: Reagents used for OMIP

Specificity	Fluorochrome	Clone	Purpose
HLA-DR	BUV395	G46-6	MNP
CD16	BUV496	3GB	Monocyte
Siglec-1	BUV615	7-239	Macrophage
CCR7	BUV661	2-L1-A	Lymph node homing
CD14	BUV737	B-ly6	Macrophage, monocyte, MDM, MDDC
CD163	BUV805	GHI/61	DC3, macrophage
CD209	BV421	DCN46	Macrophage
Siglec-6	BV480	767329	ASDC
CD1a	BV510	HI149	Epidermal DC and LC
CD4	BV605	OKT4	Conventional $CD4^+$ T cells
CD1c	BV650	F10/21A3	DC
CD11b	BV711	ICRF44	Macrophage, DC
Axl	BV785	108724	ASDC
CD11c	BB515	B-ly6	DC
CD3	NovaFluor Blue 660-120S	UCHT1	T cell dump
CD19	NovaFluor Blue 660-120S	HIB19	B cell dump
CD88	PerCP eFluor710	20/70	MDDC
CD206	RB780	19.2	DC, macrophage
Calprotectin	PE	MAC387	Monocyte, MDM
CD103	PE Vio615	REA803	Colorectal DC
CD123	PE-Cy5	6H6	pDC and ASDC
CD5	PE-Cy5.5	CD5-5D7	ASDC
CD207	PE Vio770	REA770	LC and $CD207^+$ cDC2
XCR1	APC	S15046E	cDC1
Viability	FVS700	N/A	Live cells
KI67 biotin	Streptavidin Dylight800	MKI67/2465	Proliferating cells

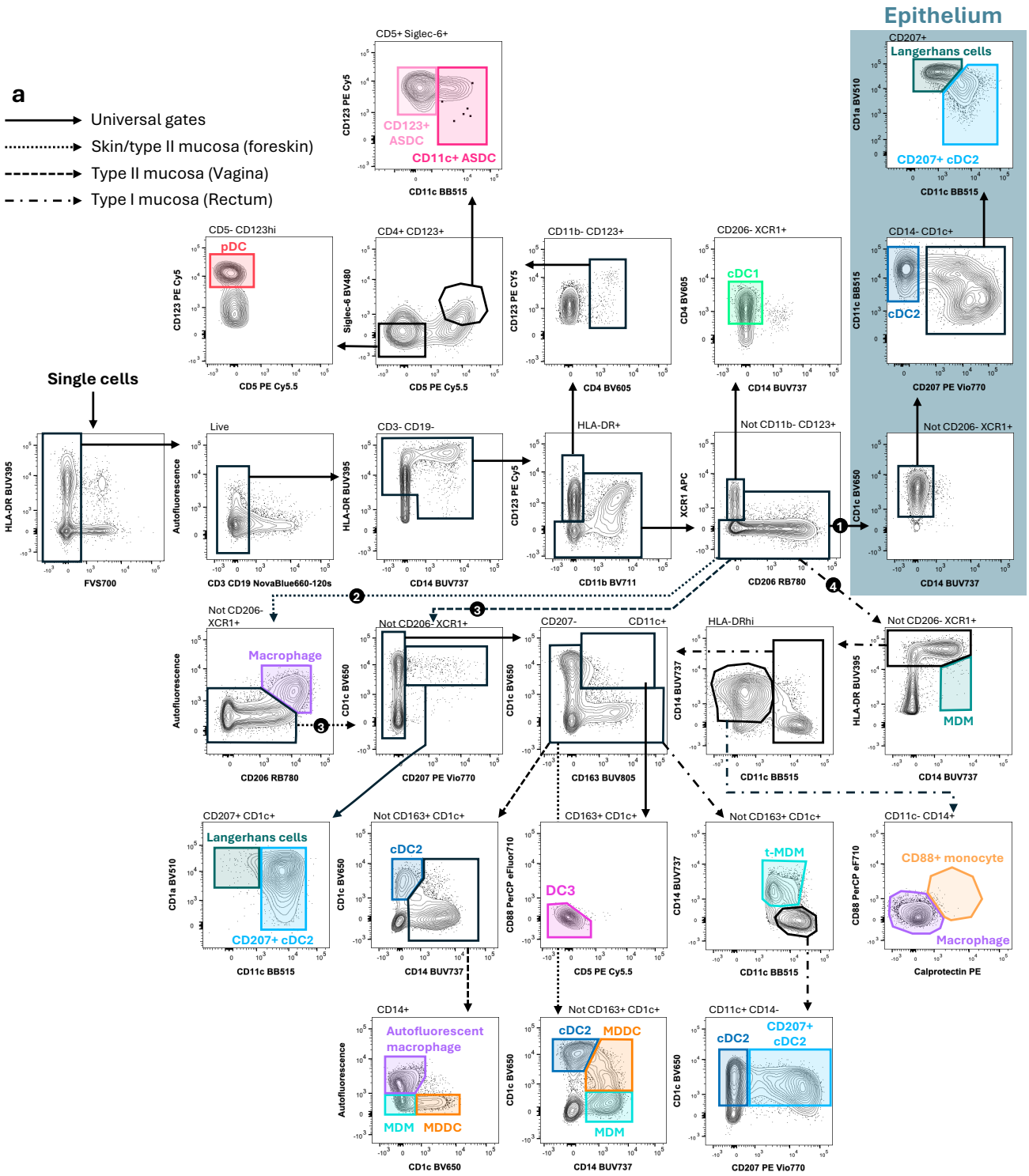

Continued over page

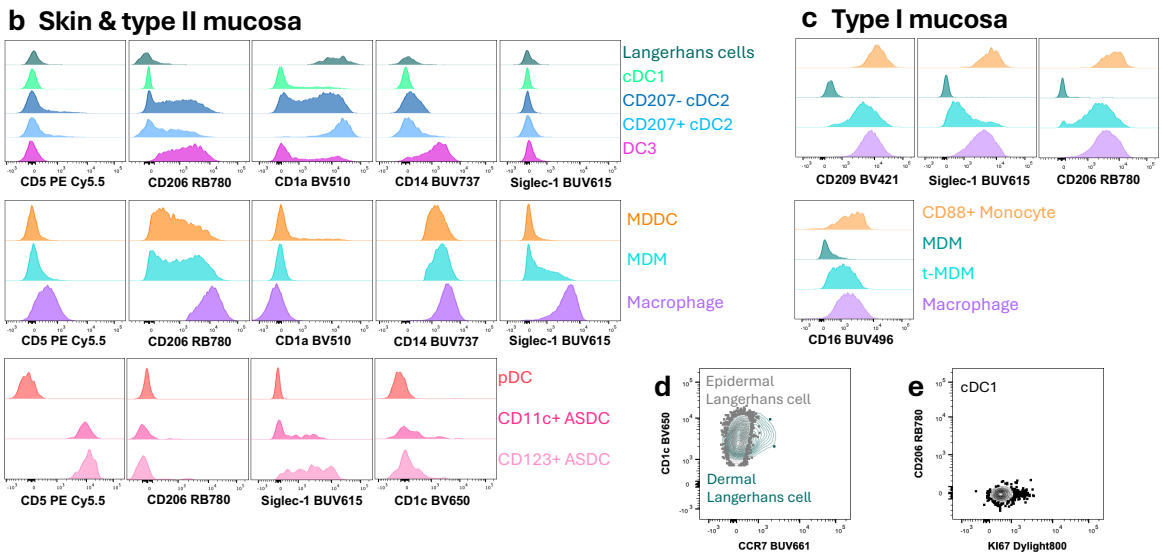

Figure 3.1: Gating strategy to identify MNPs in human skin, type II and type I mucosal tissues

a) Cells were isolated from fresh colorectal and anogenital tissues, stained and acquired on a BD FACSymphony A5 instrument. Cells were gated on single cells (FSC-H vs FSC-A and SSC-W vs SSC-A), live cells (FVS700$^-$) and HLA-DR$^+$ cells. T and B cells were excluded using a CD3/CD19 dump gate against autofluorescence to account for any autofluorescent MNPs spreading into the CD3/CD19 channel. The infiltrating inflammatory cells are identified as CD123$^{+/int}$ CD11b$^-$ CD4$^+$. **pDC** are defined as Siglec-6$^-$ CD5$^-$ CD123$^+$, whilst **ASDC** are Siglec-6$^+$ CD5$^+$ and further divided by expression of CD11c. **cDC1** are gated as a population of XCR1$^+$ CD206$^-$ cells and defined as CD4$^+$ CD14$^-$. The XCR1$^-$ vs CD206 gate is divided into 4 different pathways. 1) Following the unbroken line is the gating strategy for the epithelium (highlighted in blue). After gating on CD1c$^+$ CD14$^-$ cells the **epithelial cDC2** are identified as CD11c$^+$ CD207$^-$, the **epithelial CD207$^+$ cDC2** as CD207$^+$ CD11c$^+$ CD1a^{lo} and **Langerhans cells** as CD207$^+$ CD11c^{lo} CD1a$^+$. 2) Following the dotted line for skin and type II mucosal tissues of the foreskin identifies the **macrophage** as autofluorescent$^+$ CD206$^+$, the autofluorescent$^-$ gate flows onto pathway number 3. 3) Following the dashed line for type II vaginal mucosa and dotted line for foreskin leads to the identification of CD207$^+$ CD1c$^+$ CD11c$^+$ **cDC2s** and migrated epithelial **Langerhans cells** as CD207$^+$ CD1c$^+$ CD11c^{lo} CD1a$^+$. 4) Following the dot-dash line of type I mucosa leads to the identification of HLA-DR^{lo} CD14$^+$ MDMs and the remaining HLA-DR$^+$ population flows onto a CD14 vs CD11c plot. The CD11c$^-$ CD14$^+$ cells leads to the identification of Calprotectin$^+$ CD88$^+$ **monocytes** and Calprotectin$^-$ CD88$^-$ **Macrophages**. The CD11c$^+$ portion of the CD14 vs CD11c plot along with pathways 2 and 3 all lead to the CD1c vs CD163 plot. **DC3** are defined as CD1c$^+$ CD163$^+$ CD88$^-$ CD5$^-$. The dashed line of type II vaginal mucosa identifies **cDC2** as CD1c$^+$ CD14$^-$, **MDDC** as CD14$^+$ CD1c$^+$ autofluorescent$^-$, **MDM** as CD14$^+$ CD1c$^-$ autofluorescent$^-$ and **autofluorescent macrophages** as CD14$^+$ CD1c$^-$ autofluorescent$^+$. The dotted line of foreskin skin and type II mucosa identifies **cDC2s** as CD1c$^+$ CD14$^-$, **MDDC** as CD14$^+$ CD1c$^+$ and **MDM** as CD14$^+$ CD1c$^-$. The dot-dashed line of type I mucosa identifies t-MDM CD14$^+$ CD11c$^+$, whilst the CD14$^-$ cells define the CD1c$^+$ **cDC2**, further split by their expression of CD207. **b)** Histograms of markers expressed by MNPs in skin and type II mucosa divided into dendritic cell subsets, monocytes and macrophages and inflammatory cells. **c)** Histograms of markers expressed by monocytes and macrophages in type I mucosa. **d)** Representative outer foreskin plot of the expression of migratory marker CCR7 on Langerhans cells in the epidermis compared to the Langerhans cells that migrate into the dermis. **e)** Representative inner foreskin LP plot of cellular proliferation marker KI67 on a cDC1 population.

3.3 Supplemental: Development Plan

We developed a 26-parameter human tissue MNP panel for a BD FACSymphony A5 cytometer, equipped with 8 lasers and 48 detectors. The configuration of this cytometer can be found in **Supplementary table 3.1**. All reagents for the final panel are listed in **Supplementary table 3.2**. All iterations of the panel are summarised in **Supplementary table 3.3**. All reagents tested but not present in the final panel are listed in **Supplementary table 3.4**. All compensation controls are listed in **Supplementary table 3.5**. All titration staining panels are listed in **Supplementary table 3.6**. All reagents were titrated on fresh human abdomen, labia, colon, small bowel, lymph node, or Pan-DC selected PBMC as outlined in **Supplementary figure 3.1**.

3.3.1 Considerations for Flow Cytometry on Mononuclear Phagocytes Isolated from Human Tissues

The main objective of this panel was to define all known MNPs in all tissues associated with sexual transmission of disease. This consists of three tissue types: skin (labia, outer foreskin, glans penis and anal verge), type II mucosa (vagina, ectocervix, inner foreskin, fossa navicularis and anal canal) and mucosa type I (endocervix, penile urethra, colon and rectum). Markers were included that would be able to isolate specific inflammatory MNPs found exclusively in inflamed tissue, as well as markers known to have variable expression across different tissues and disease states to ensure that this panel could be used not only on homeostatic or steady-state samples, but also in a variety of different inflammatory and disease settings. Importantly, this panel was designed to work with specific tissue digestion protocols. Utilising a low-tryptic activity digestive enzyme, namely collagenase type IV (Worthington) and neutral protease (Dispase, Worthington), limits the cleavage of surface protein markers for accurate characterisation, while short digestive incubations enables the isolated cells to be preserved in their *in situ* state (Botting et al., 2017, Doyle et al., 2021, Doyle et al., 2022, O'Neil et al., 2023). These digestion protocols, optimised for each unique tissue, are specified in this document.

3.3.2 Marker Selection and Expression on Tissue Mononuclear Phagocytes

The challenges for designing a comprehensive DC and macrophage fluorescent flow cytometry panel that works across a range of human tissues, including skin, type II mucosa and type I mucosa is three-fold:

1. Understanding the biological expression patterns of all markers across each cell population in such varied tissue settings.
2. Designing a panel that accounts for the variation in antigen expression across tissue-types and tissue donors, ranging from extremely high, to very low or no expression.
3. Accounting for the high autofluorescent of some MNPs, particularly macrophages.

Our lab has spent 30 years isolating and researching DCs and macrophages from a vast range of human tissues, and through experience working with these cells, have accumulated an extensive knowledge of biological expression patterns. However, as the panel included a novel combination of markers and fluorophores, some marker expressions across different cell populations and tissues were initially uncertain. Specifically, several newly defined MNP populations in human blood or skin had not yet been characterised in mucosal tissues. It was unclear whether these populations were **1)** present in mucosal tissues, and **2)** whether their defining markers displayed the same expression patterns in mucosa. To address this, we relied on known expression patterns and conducted iterative testing to clarify the expression of each marker on specific cell types across various tissues to accurately identify the similar MNP subsets in different tissues. Optimisations for this panel were performed on both non-inflamed and inflamed samples at each iteration to ensure that all marker expression differences were considered.

3.3.3 Iteration 1

To start, utilising our experience and knowledge, and references from the literature, we investigated the marker expression across all our target cell populations (**Supplementary table 3.7**). After identifying which markers were expressed by each cell type, together with the preliminary stain index run on our BD Symphony A5 (**Supplementary table 3.8**), we first assigned the markers HLA-DR (as it is high on all cell types), all markers that were exclusive to only 1-2 cell types, or those of limited

fluorophore availability. Additionally, as we have experience with autofluorescent macrophages, and understood that while autofluorescence can be excited by all lasers and emits over a broad range of wavelengths, the 700-800 emission detectors captured less autofluorescence across all the tissues (**Supplementary figure 3.2**). Therefore, the important macrophage markers were allocated to the 700-800nm emission range. As we had previously designed panels for the Symphony to identify MNPs in various tissues, we already had optimised fluorophore/marker combinations for the backbone of MNP defining markers, which we utilised where possible.

HLA-DR BUV395 (U379) – HLA-DR is highly expressed by all MNPs. BUV395 was considered the best place for this marker as it has minimal spectral spillover into other channels and has been successfully used in our lab previously across multiple MNP panels.

CD123 PE-Cy5 (Y670) – CD123 is highly expressed by pDCs and ASDCs (and basophils). PE-Cy5 is a very bright fluorophore that can cause problematic spread. As pDCs and ASDCs represent a very small proportion of MNPs in inflamed tissue and have mutually exclusive defining markers to other DCs and macrophages, CD123 was assigned to PE-Cy5.

XCR1 APC Fire 750 (R780) – XCR1 is the only marker we found to consistently work in identifying human tissue conventional cDC1s, having previously tested and found CLEC9A and CADM1 to be poor DC markers when isolated from human skin (Botting et al., 2017). Whilst CD141 (BDCA3) works well in human body skin, we found it does not work well in human intestine (Doyle et al., 2021). Additionally, CD141 is problematic as its expression can be induced on maturing cDC2 (Botting et al., 2017). The XCR1 clone S15046E is the only clone we have found to work successfully in tissue isolated DCs and has limited fluorophore availability. We assigned XCR1 to APC Fire 750 with the objective that XCR1 positive cDC1s would not be impacted by the mutually exclusive cDC2 and macrophage markers assigned to the 750 – 800 emission detectors.

CD207 (langerin) PE Vio770 (Y780) – CD207 is highly expressed by LCs, with a spread of low to high expression on some cDC2s. As CD207 is a C-type lectin binding receptor capable of antigen capture, we wanted to capture all $CD207^{+}$ cDC2s, even at

low expression levels. Both the Beckman Coulter clone DCGM4 (Cohen et al., 2022) and the Miltenyi clone MB22-9F5 (Botting et al., 2017, Doyle et al., 2021) are effective in human tissue. With limited fluorophore availability and previous success using PE Vio770 to detect low expression, we assigned CD207 to PE Vio770.

Since there are multiple highly expressed markers on MNPs from human tissue, we minimised spread into lowly expressed markers by saturating one wavelength range with the highest expressed markers. We chose to detect these markers on a higher wavelength (around 750-800nm) due to significant spectral spillover in this range. Since CD207 and XCR1 were already within this range, we chose markers that would either be higher in the gating strategy or not expressed on LCs, cDC2s and cDC1s, ensuring optimal resolution for these markers.

Axl BV786 (V820) – Axl was needed to define ASDCs. As there is considerable spread into the BV786 channel from other fluorophores, and it was initially thought ASDCs did not express many macrophage markers we intended to allocate to the 780-800 emission detectors, we assigned Axl to BV786. However, Axl is also expressed by macrophages, and since it was allocated to a saturated wavelength, the resolution of Axl on macrophages was somewhat sacrificed.

CD14 APC Fire 810 (R820) – CD14 is a critical macrophage marker with variable expression and hence it was important to choose a fluorophore that was moderately bright and not greatly affected by autofluorescence. Additionally, very few markers were available on APC Fire 810 when this panel was initially designed. As CD14 is not expressed by cDC1s (with XCR1 APC Fire 750 assigned on R780), and there is limited expression of CD207 (assigned to PE Vio770 on Y780) on $CD14^+$ cells, CD14 APC Fire 810 was chosen.

CD11c BUV737 (U740) – CD11c is predominantly a marker for DCs, although it has variable expression on some macrophages. This made high resolution and accurate identification of $CD11c^+$ cells crucial. BUV737 is a bright fluorophore and has little spillover into other channels, hence, CD11c was placed on BUV737.

CD163 BUV805 (U820) – CD163 is traditionally recognised as being highly expressed by macrophages. However, recently CD163 has been determined a key identifying marker for DC3s, though it's expression on these cells is dimmer. As BUV805 is a

relatively bright fluorophore, has little autofluorescent signal, and minimal spillover into other channels, it was chosen for CD163.

Viability stain (FVS700, R730) – As this panel is designed for enzymatically digested tissue, there is generally a higher proportion of cell death, so definitively identifying live cells is crucial. FVS700 has consistent and accurate staining and importantly, has limited macrophage autofluorescence interference, which we experienced with other viability stains such as FVS UV440. Additionally, the fluorophores available on the Red 730/45 detector are relatively dim or suboptimal, making FVS700 a suitable choice.

CD11b BV711 (V710) – CD11b is a useful marker for gating macrophage populations and is occasionally expressed by cDC2s and DC3s. BV711 is not impacted by our main macrophage marker CD14 on APC Fire 810, so CD11b BV711 was objectively a good choice.

CD209 (DC-SIGN) BV421 (V427) – CD209 is a C-type lectin receptor important for antigen capture (particularly HIV). Importantly, we have previously found this marker to be sensitive to cleavage and difficult to detect when on a dull fluorophore. Therefore, we assigned CD209 to BV421, as it is a very bright fluorophore with limited spillover.

CD1a BV510 (V525) – CD1a is an antigen presentation marker extremely highly expressed by LCs and highly expressed by cDC2s. While BV510 can be a challenging fluorophore due to its dullness, our decade long experience using CD1a on BV510 has consistently yielded excellent detection of LCs and cDC2 from skin. Therefore, we opted to keep this reliable marker/fluorophore pair.

Siglec-6 (CD327) BV480 (V474) – Siglec-6 is exclusive to ASDCs (also expressed on some granulocytes and B cells) and an important marker to delineate these cells. ASDCs had not been identified in human tissues when this panel was first designed so biological expression patterns had only been identified from blood-derived ASDCs. We assumed these cells did not express CD209 or CD1a, which were already assigned to V427 and V525 either side of BV480 and would cause some spillover into this channel. Therefore, we assigned Siglec-6 to BV480.

Slan (M-DC8) PE (Y586) – Slan/ M-DC8 is exclusive to Slan$^+$ inflammatory monocytes and when this panel was designed, PE was the only fluorophore conjugate available for this marker.

FcεR1α AF488 (B515) - FcεR1α was identified by Duterte et al (Dutertre et al., 2019) as an important marker for defining tissue cDC2s, later confirmed in blood by Mair & Liechti et al (Mair and Liechti, 2021). We had previously shown that the clone 9E1 worked well in human intestine and was vastly superior to the clone AER-37 (Doyle et al., 2021). Clone 9E1 had limited availability so was assigned to AF488, which received minimal spillover from other channels.

CD103 PE Vio615 (Y610) – CD103 is an important marker previously used to identify cDC1s and a subset of cDC2s in human intestine (Doyle et al., 2021, Richter et al., 2018). It is also present on lymphocytes including intraepithelial ILC1-like cells (Doyle et al., 2022) and T cells as a marker of residency (O'Neil et al., 2023). We had previously identified the REA803 clone to be more resistant to enzymatic cleavage and more reliable in detecting CD103$^+$ cells isolated from tissue compared to the Ber-ACT8 clone (O'Neil et al., 2023). The REA803 clone had limited availability, therefore we assigned it to PE Vio615. Importantly, it was thought that CD103$^+$ DCs would not express Slan (PE fluorophore).

CD1c BV650 (V677) – CD1c is an essential marker for defining cDC2s and DC3s. The primary sources of spillover into this channel were markers expressed on other cell types or at low levels. Additionally, our previous experience with this antibody-fluorophore combination demonstrated reliable resolution.

CD16 BV570 (V586) – CD16 is predominantly expressed by certain macrophage populations (and useful for distinguishing neutrophils in inflamed tissues). Although dull, we had previously used BV570 in another panel to detect CD16$^+$ macrophages in human lymph nodes.

CD3/CD19 NovaBlue660/120S (B670) (dump) – The predominant immune cell populations from digested tissue are T cells and B cells. As these cells express markers that are co-expressed by MNPs, their identification and exclusion was necessary. The Blue 670/30 channel has limited fluorochrome availability and presents challenges with other channels, particularly autofluorescence, making it a

suitable place for a dump channel. CD3 and CD19 were both available on NovaBlue660/120S and were assigned accordingly.

CD89 BB700 (B710) – CD89 was included to aid in identifying monocytes, as CD88 and CD89 have recently been described as monocyte markers (Dutertre et al., 2019, Mair and Liechti, 2021). Since the expression of CD89 was low, a bright fluorophore was chosen. BB700 spills into multiple channels, however, since CD89 is only expressed on newly emigrated monocytes, spillover from this channel is expected to have minimal impact.

CD169 (Siglec-1) BUV615 (U610) – CD169 is a pattern binding receptor, important in binding pathogens such as HIV (Vine et al., 2024, Warner van Dijk et al., 2025), with moderate to high expression on tissue macrophages. Since $CD103^+$ populations (assigned to PE Vio615 on Y610) exhibit little to no CD169 expression, BUV615 was deemed a suitable option for this marker.

Calprotectin (S100A8/9) AF594 (O616) – Calprotectin, traditionally an intracellular marker, was included to gate newly emigrated blood monocytes, though it is also highly expressed by intestinal monocyte-derived macrophages (MDM) (Bujko et al., 2018, Doyle et al., 2021) . Calprotectin can also be upregulated in DCs in inflammation (Shimizu et al., 2011).

CD45 BB790-P (B820) – CD45, present on all immune cells, had previously performed well on BB790-P when the antibody titre was kept low to limit spread into other channels (Doyle et al., 2022). At the time of initial panel design, fluorophore availability on this channel was limited. Therefore, we maintained a low antibody concentration to just sufficiently resolve $CD45^+$ cells while minimising impact on other detectors.

CD5 PerCP Cy5.5 (Y710) – CD5 is a key defining marker for ASDCs and used to identify a subpopulation of cDC2s. This CD5 PerCP Cy5.5 antibody was successfully used on a blood myeloid panel by Mair and Liechti (2021), making it a strong choice for our panel.

CD4 BV605 (V610) – CD4 is widely expressed on tissue MNP populations, including DCs and macrophages, and has long been used to identify antigen presenting cells in

peripheral tissues (Jardine et al., 2013). While CD4 is ubiquitous, it is relatively dim on MNPs, hence BV605 was selected as a bright fluorophore to resolve MNP populations without interfering with gating on other cell populations.

CD206 (MR) BV750 (V750) – CD206 is a key C-type lectin receptor often used to distinguish macrophage and DC subsets in tissue. It is not expressed in blood-derived cells but has variable expression in tissue. As BV750 was one few remaining spots available in the 700-800 emission range and we wanted to saturate this wavelength with macrophage markers, it was a suitable fluorophore for CD206.

CD86 APC (R670) and CCR7 BUV661 (U670) – The Red 670/30 detectors and UV 670/30 detectors were chosen to measure functional markers relating to DC maturation and activation. BUV661, a bright fluorophore, has spillover into the Red 670/30 detector; however, CCR7 expression is relatively low compared to many other markers on MNPs, making this a suitable assignment. Based on our experience, CD86 is the most differential of the three maturation markers (CD80, CD83 and CD86) and commonly used to assess DC maturation status. Therefore, we placed CD86 on APC with the potential to swap for other markers of interest.

HLA-DQ BUV563 (U586) – HLA-DQ was included based on findings from Duterte et al (2019), which demonstrated that FcεR1α and HLA-DQ could effectively delineate cDC2s. While BUV563 posed a problematic interference risk with Slan PE, the impact was minimised by the fact Slan^{+} monocytes were the only subset expressing Slan, reducing the likelihood of significant spillover from the highly expressed HLA-DQ.

Autofluorescence Blue 610/20 – Once all the other fluorophores were allocated, we evaluated the remaining channels for their autofluorescence detection. B610 was a good candidate as autofluorescence has a strong peak around 600nm and this channel has limited fluorophore availability.

One detector was left intentionally open in this first iteration design. U515, most often used with BUV496, was chosen as this fluorophore is dim and has minimal spillover. Keeping this spot open provided flexibility to relocate any highly expressed markers that proved problematic in subsequent iterations. We also optimised blocking reagents to reduce non-specific antibody binding to Fc receptors on MNPs (**Supplementary figure 3.3**). Following the recommendations of Kristensen et al. (2021), we utilised a

dual-blocking approach by titrating Human Antibody serum and Oligo-block to suit our tissue samples.

3.3.4 Iteration 2

Once the markers were titrated and the panel run on samples, it became apparent that our objective to restrict the most severe spillover to the 700-800 wavelengths was more problematic than expected. We encountered extreme spillover and difficulty achieving good resolution on CD14 APC Fire 810 and CD45 BB790, despite extensive optimisation of acquisition voltages and attempts to maintain a low antibody concentration, as per our previous successful experiments on lymphocytes (**Supplementary figure 3.4a**). Additionally, excessive spillover in the red detectors prevented the resolution of viability on FVS700 (R710) (**Supplementary figure 3.4b**). To address this, we repositioned several markers to attempt to improve gating and resolution. HLA-DR was moved to APC Fire 810 (R820) to shift the spillover from this fluorophore higher in the gating strategy. CD14 was moved to BUV737 (U740), a well-established position used in our previous panels, and CD11c, originally on BUV737, was moved to BUV395 (U379) – the spot previously held by HLA-DR.

Additionally, markers assigned to the 600-670nm wavelength were challenging to resolve. The markers causing spillover were CCR7 BUV661 (U670), CD103 PE Vio615 (Y610), CD169 BUV615 (U610) and Calprotectin AF594 (O616) (**Supplementary figure 3.5**). Of these markers, Calprotectin had the brightest signal, significantly brighter than originally anticipated for such a relatively dull fluorophore. We endeavoured to minimise this signal by switching from intracellular staining to surface staining, which we had performed successfully in previous panels to decrease calprotectin signal. As we preferred to keep CD103 and CD169 on their assigned detectors, we opted to removed CCR7 from this iteration. This allowed a more accurate assessment of how the calprotectin staining change impacted the two markers. We additionally included Ki67 to the panel assigned to DyLight 800 (N820), using a biotinylated anti-Ki67 to accommodate for this very dim detector.

We observed that the CD16 signal was not bright enough on tissue cells to resolve with BV570. Accordingly, we moved CD16 to BUV496, the fluorophore we had left unallocated for necessary changes, which is a slightly brighter fluorophore. Furthermore, we replaced CD89 with CD88 as our designated monocyte marker as

data published after the initial panel design showed CD88 as a more reliable marker for monocytes (Mair and Liechti, 2021), which we confirmed by dual staining (**Supplementary figure 3.6**). While we kept it in the same detector (Y710), we could only source it on PerCP-efluor710.

3.3.5 Iteration 3

Despite the changes made in the previous iteration, spillover issues persisted, particularly for markers allocated to the ~600 and ~800nm wavelengths. APC Fire 810 exhibited the most troublesome spillover at its wavelength, leading us to exclude it from the panel. As a result, HLA-DR was moved back to BUV935 (U379), displacing CD11c, which we moved to BB515 (B515), removing FcεR1α from the panel. We further found HLA-DQ BUV563 to be highly expressed by most tissue antigen presenting cells and not exclusively cDC2s. Given its brightness, this caused greater spectral spillover errors than anticipated. Since HLA-DQ contributed little phenotypic information whilst introducing significant compensation and spreading errors, it was removed from the panel. We also decided to move CD45 from the ~800 wavelength as we were unable to maintain a consisting low staining across highly varied tissues. Due to its high expression and limited alternative placement options that would not cause spreading errors, we posited it could be effectively resolved on AF350, utilising a previously unused dim detector (U450).

Additionally, we observed that the three macrophage markers on adjacent violet detectors: CD11b BV711 (BV711), CD206 BV750 (V750) and Axl BV756 (V820), were spilling into each other and compromising their resolution. To introduce more space into this wavelength we removed the middle marker and reassigned CD206 to RB780 (B820), which became available after moving CD45 from BB790. Additionally, RB780 had a tighter spectral footprint than BB790, further reducing panel interactions.

Despite reducing the calprotectin signal by utilising surface staining, the interactions between AF594 and CD103 PE Vio615 and CD169 BUV615 still posed a problem as spillover persisted at the voltages required for optimal marker resolution. Given our previous success using Calprotectin on PE (Y586) (Doyle et al., 2021), we reassigned it to this fluorophore. Slan was subsequently relinquished to accommodate this change, meaning Slan^{+} monocytes could no longer be specifically identified. However, as Calprotectin no longer occupied the ~600 wavelength, we reintroduced CCR7

BUV661 to this iteration, as we anticipated the overall changes would now accommodate its inclusion.

3.3.6 Iteration 4

For CD45 AF350, we found two available pre-conjugated clones (I430I and I430u). After testing and titrating, we found clone I430u to most effectively resolved $CD45^+$ cells and selected a high concentration to provide the best resolution to account for donor variability (**Supplementary figure 3.7a**).

However, from the first run of the previous iteration, it became clear that CD45 could not be reliably resolved on AF350 with the current panel, even after multiple titrations attempts across different tissue donors. We conducted FMO comparisons and examined $CD45^+$ selected cells (but not stained for CD45 AF350) and were still unable to resolve the $CD45^+$ cells.

With no other suitable alternative for CD45 in the panel, we decided to remove it. We were confident we could use HLA-DR in combination with FSC and SSC for gating strategies and determined CD45 was not essential for identifying our target populations (**Supplementary figure 3.7b**).

Moving Calprotectin from AF594 to PE corrected the resolution issues with Siglec-1 BUV615 and CD103 PE Vio615 (**Supplementary figure 3.8**). However, this correction revealed another previously masked problem – XCR1 was not being properly resolved on APC Fire 750. Among the only three available fluorophores for our selected clone; PE, BV421 and APC, we determined APC (R670) to be the most suitable option. This meant sacrificing CD86 from the panel as we were hesitant to disrupt other successfully working markers. These final adjustments allowed for the resolution of all markers and creation of gating strategies across all tissue types. The final spillover matrix is provided in **Supplementary table 3.9**.

Minor adjustments were made to several markers post-titration throughout iterations after several samples were run with the panel. The affected markers – HLA-DR BUV395, CD4 BV605, CD11c BB515 and XCR1 APC – can be identified by their final optimal titres, which sit between two tested dilutions (**Supplementary figure 3.1**). The initial titrations performed on these antibodies were performed on a specific tissue; however, this tissue served only a guideline and may not be representative for all

tissue types. Adjustments to antibody volumes were made to ensure optimal concentrations across a broader range of tissues.

Separate gating strategies identifying all known MNPs have been created for skin (**Supplementary figure 3.9**), type II mucosa (**Supplementary figure 3.10**) and type I mucosa (**Supplementary figure 3.11**).

3.3.7 Correction of Autofluorescence post-Acquisition

While spectral flow cytometry enables background signal correction in the acquisition software, conventional flow cytometry lacks this capability. As such, an unstained donor and tissue matched sample is necessary to be acquired with all samples. This sample serves as an exogenous single-colour control and, when added to the bead controls to create a new compensation matrix, reduces spilled autofluorescence signal while allowing it to be quantified in its allocated detector (Doyle et al., 2021). All gating strategies presented in this OMIP have been designed on autofluorescence corrected samples. As gut tissue has the highest autofluorescence of all the tissues contained herein, an example gating strategy without autofluorescence correction has been included in **Supplementary figure 3.11b**.

3.3.8 Tissue Digestion and Flow Cytometry Staining Protocol

3.3.8.1 Materials

- Roswell Park Memorial Institute (RPMI) 1640 (Lonza, Switzerland)
- Neutral Protease (Dispase) (Worthington, USA)
- Gentamicin (Life Technologies, USA)
- Dulbecco's Phosphate-Buffered Saline (PBS) without $Ca2^{+}$ and $Mg2^{+}$ (Lonza, Switzerland)
- Collagenase Type IV (Worthington, USA)
- DNase I (Sigma-Aldrich, USA)
- Ficoll-Paque Plus (GE Healthcare, USA)
- Human AB serum (Sigma Aldrich, USA)
- Phosphorothioate-oligodeoxynucleotides (Oligoblock) (Sigma-Aldrich, USA)
- Brilliant Stain Buffer PLUS (BD Bioscience, USA)
- EDTA (Sigma-Aldrich, USA)
- Sodium azide (Sigma-Aldrich, USA)

- Cytofix (BD Biosciences, USA)
- Cytofix/Cytoperm (BD Biosciences, USA)
- Foetal Bovine Serum (FBS) (Sigma-Aldrich, Missouri, USA)
- Dithiothreitol (DTT) (Sigma-Aldrich)
- Derma Carriers Skin Graft Carriers, (Zimmer, USA)
- Zimmer Skin Graft Mesher, (Zimmer, USA)
- MACSmix Tube Rotators, (Miltenyi Biotec, Germany)
- Easy Strainer 100 µm, (Greiner Bio-One, Austria)

3.3.8.2 Solutions

- **FACS wash:** PBS supplemented with 0.1% w/v sodium azide + 2 mM EDTA + 1% v/v human AB serum (filter sterilised)
- **Perm Wash:** PBS supplemented with 1% w/v BSA + 0.1% w/v saponin + 0.1% w/v sodium azide + 1% v/v FCS
- **RF10:** 10% FBS in RPMI 1640
- **Epithelial Strip Solution:** 0.3% DTT and 2 mM EDTA in RF10
- **Collagenase Solution 1:** 525 U/mL Collagenase IV with 750 U/mL DNase I in RPMI
- **Collagenase Solution 2:** 640 U/mL Collagenase IV with 750 U/mL DNase I in RPMI
- **Dispase Solution 1:** 0.8 mU/mL Dispase in RPMI with 50 ug/mL Gentamicin and filter sterilised with 0.22 µm filter
- **Dispase Solution 2:** 1.6 mU/mL Dispase in RPMI with 50 ug/mL Gentamicin and filter sterilised with 0.22 µm filter

3.3.8.3 Intestinal Tissue Digestion (Type I Mucosa)

4. Using curved surgical scissors and forceps, remove any staples, open intestinal tube, and clean with PBS if necessary.
5. With the luminal surface on a PBS-dampened cutting board, remove any fat or mesentery.
6. Remove the muscle layer in small strips with surgical scissors and forceps, keeping the tissue section whole, and leaving the entire submucosal thickness.

7. Use a scalpel to cut the tissue into 5 mm x 5 mm square pieces and place in 50 mL Falcon tube, no higher than the 5 mL mark.
8. Add 20 mL of Epithelial Strip Solution into the tube containing the tissue.
9. Vortex for 10 seconds and incubate for 15 mins in 37°C water bath.
10. Using tea strainer, strain tissue into a waste container to remove epithelial components and place tissue back in the tube, a P1000 pipette tip can be used to manoeuvre the tissue.
11. Repeat steps 5-7 once more.
12. After second epithelial strip solution is removed, wash tissue briefly in PBS and strain again, placing the tissue into a clean 50 mL Falcon tube.
13. To the tissue, add 20 mL Collagenase Solution 1.
14. Vortex for 10 seconds, seal tube with Parafilm, and incubate for 30 mins at 37°C (incubator) in a rotator, placing the tubes askew to maximise movement in the tube.
15. Strain tissue with tea strainer, collecting the cell suspension in a new 50 mL Falcon tube, placing the tissue back into its original tube.
16. Repeat steps 6-8 with the tissue tube.
17. Dilute the collected cell solution to 50 mL and pass over a 100 µm cell strainer, before a 5 minutes 300 x g spin.
18. Wash cells again in 50 mL PBS. Resuspend cell pellet in 5 mL RPMI and store on ice until second collection.
19. For second collections, strain tissue with tea strainer, collecting the cell suspension in a new 50 mL Falcon tube, placing the tissue back into its original tube.
20. Add 20 mL PBS to tissue and gently vortex to collect all liberated cells from the tissue. Strain tissue again into the same collection tube and discard tissue.
21. Repeat steps 14-15, combining the resuspended pellet with the pellet from the first collection for target cell enrichment.
22. Dilute the combined cells in 35 mL of RPMI, underlay with 15 mL of Ficoll-Paque, and centrifuge at 400 x g for 20 mins without breaks. Collect the cells from the RPMI:Ficoll interface using a transfer pipette and wash twice in PBS, first at 400 x g, then at 300 × g for 5 mins. Count the cells for staining on a haemocytometer.

3.3.8.4 Abdomen Skin Tissue Digestion

1. Stretch skin samples until taut using large surgical forceps and graft to a 1mm thickness using a skin grafting knife.
2. Pass grafted skin through a skin graft mesher to increase the surface area and distributed evenly the resultant meshed skin across 50 mL Falcon tubes.
3. Fill each tube with 30 mL of **Dispase Solution 1** and incubate at 4°C on a rotator. Dispase cleaves the bonds between the epidermis and dermis. The following morning, place tubes in a 37°C water bath for 15 mins to initiate enzymatic activity.
4. Wash skin by dunking in 40 mL of PBS and using surgical tweezers peel the epidermis from the dermis. Keep the epidermis moist in a 50mL Falcon tube of PBS on ice. On peeling completion, centrifuge the epidermis (300 x g for 5 mins), tip off supernatant and cut epidermis into small pieces using long surgical scissors. Cut dermis into 5 x 5 mm pieces using a scalpel and collect in separate tubes, filled up to the 5 mL mark.
5. Fill each tube with 20 mL of warmed **Collagenase Solution 2** and incubate for 120 mins at 37°C on a MACSmix Tube Rotator. Collagenase liberates the cells from the connective tissue.
6. Collect the supernatants of each tube by pouring through a tea strainer. Wash the undigested tissue with 10 mL PBS and strain again. Filter the strained supernatants using a 100 µm cell strainer and centrifuge at 300 x g for 5 mins.
7. Wash the cells twice more using PBS (300 x g for 5 mins).
8. Count the dermal cells and resuspend in 100 µL PBS, ready for antibody staining.
9. Enrich the epidermal cells further using Ficoll-Paque. Resuspend the cells in 35 mL of RPMI, underlay with 15 mL of Ficoll-Paque, and centrifuge at 400 x g for 20 mins without breaks. Collect the cells from the RPMI:Ficoll interface using a transfer pipette and wash twice in PBS, first at 400 x g, then at 300 x g for 5 mins. Count the epidermal cells and prepare for staining.

3.3.8.5 Genital Tissue Digestion (Skin and Type II Mucosa)

Genital skin and Type II mucosa samples cannot be grafted or passed through the skin graft mesher due to their small size.

1. Remove the underlying connective tissue and fatty layers using surgical scissors, thinning the sample to no more than 3 mm thick.
2. Make small cuts using a scalpel to mimic the action of a mesher.
3. Place the tissue in either a 50 mL or 15 mL Falcon tube, depending on sample size, and fill with **Dispase Solution 2** to a volume of either 30 mL or 10 mL accordingly.
4. From herein, process the tissue identically to abdominal skin from steps 3–8. Adjust all volumes to 10 mL if using a 15 mL tube.

Note: The epidermal cell yield from these samples is often low, and Ficoll-Paque enrichment in step 9 is only performed on a large pellet. In this case, resuspend the cells in 10 mL RPMI and underlay with 5 mL Ficoll-Paque.

3.3.8.6 Staining Protocol

1. Place isolated cells in a 5 mL FACS tube in 100 µL PBS.
2. Stain cells with Fixable Viability Stain FVS700 for 30 mins at 4˚C.

Note*:* Set aside a small number of cells for an unstained control tube for each sample.

3. Wash cells with 2 mL FACS wash (300 x g for 5 mins) and resuspend in 100 µL.
4. Incubate cells with 10 µL human AB serum and 3.2 µL Oligoblock for 10 mins at 4°C in the dark.
5. Add the antibody cocktail containing all surface stain antibodies (outlined in **Supplementary table 3.2**) and 10 µL Brilliant Buffer PLUS per test (one test = 2.5 x 10^6 cells) without washing. Incubate for 30 mins at 4°C in the dark.
6. Wash cells twice with FACS wash.
7. Add 100 µL of Cytofix/Cytoperm to cells and incubate for 20 mins at 4˚C in the dark.
8. Wash cells once with Perm wash and repeat step 4.
9. Add biotin KI67 as per **Supplementary table 3.2** and incubate for 30 mins at 4˚C.
10. Repeat step 8 with two washes.

11. Add streptavidin DyLight800 as per **Supplementary table 3.2** and incubate for 30 mins at 4˚C.
12. Wash cells twice with Perm wash.
13. Repeat step 7 with 100 µL of Cytofix.
14. Wash cells with FACS wash and resuspend in 100 µL, ready for acquisition on FACSymphony A5.
15. Pass cells through a 100 µm cell strainer immediately before acquisition on the flow cytometer.

3.4 Supplementary Tables

Supplementary table 3.1: Instrument Configuration - BD FACSymphony A5

Laser	Wavelength [nm]	Laser Type	Laser Power [mW]	Dichroic mirror	Notch filter [nm]	Bandpass Filter [nm]	Spectral Range	Detector	Assigned Fluorochrome
Red	637	Solid State, OBIS 637 LX	140	800 LP		820/60 BP	800-850	R820	
				750 LP	785	780/60 BP	750-800	R780	
				685 LP		710/40 BP	690-730	R710	FVS700
				665 LP		670/30 BP	665-685	R670	APC
UV	355	Solid State, Genesis CX-355	100	800 LP	785	820/60 BP	800-850	U820	BUV805
				770 LP		780/60 BP	770-800	U780	
				710 LP		740/35 BP	722.5-757.5	U740	BUV737
				685 LP		695/40 BP	685-710	U695	
				635 LP		670/30 BP	655-685	U670	BUV661
				600 LP		610/20 BP	600-620	U610	BUV615
				570 LP	594	586/15 BP	578.5-593.5	U586	
				450 LP		515/30 BP	500-530	U515	BUV496
				410 LP		450/50 BP	425-450	U450	
						379/28 BP	365-393	U379	BUV395
Yellow	561	Solid State, OBIS 561 LS	150	800 LP		820/60 BP	800-850	Y820	
				750 LP	785	780/60 BP	750-800	Y780	PE Vio770
				685 LP		710/50 BP	685-735	Y710	PE Cy5.5
				635 LP		670/30 BP	655-685	Y670	PE Cy5
				600 LP		610/20 BP	600-620	Y610	PE Vio615
				570 LP	594	586/15 BP	578.5-593.5	Y586	PE
Blue	488	Solid State, Sapphire 488 LP	200	800 LP		820/60 BP	800-850	B820	RB780
				770 LP	785	780/60 BP	770-800	B780	
				735 LP		750/30 BP	735-765	B750	
				685 LP		710/50 BP	685-735	B710	PerCP eF710
				635 LP		670/30 BP	655-685	B670	NovaBlue 660-120s
				600 LP	594	610/20 BP	600-620	B610	
				505 LP		515/30 BP	505-530	B515	BB515
						488/10 BP	483-493	SSC	
Orange	594	Solid State OBIS 594 LS	100	635 LP		660/20 BP	650-670	O660	
				610 LP		616/23 BP	610-627.5	O616	
Violet	406	Solid State,	200	800 LP		820/60 BP	800-850	V820	BV786
				770 LP	785	780/60 BP	770-800	V780	

Laser	Wavelength [nm]	Laser Type	Laser Power [mW]	Dichroic mirror	Notch filter [nm]	Bandpass Filter [nm]	Spectral Range	Detector	Assigned Fluorochrome
		OBIS 405 LX		735 LP		750/30 BP	735-765	V750	
				685 LP		710/50 BP	685-735	V710	BV711
				635 LP		677/20 BP	667-685	V677	BV650
				600 LP		610/20 BP	600-620	V610	BV605
				550 LP	594	586/15 BP	578.5-593.5	V586	
				505 LP		525/50 BP	505-550	V525	BV510
				450 LP		474/25 BP	462.5-485.5	V474	BV480
				410 LP		427/25 BP	415.5-438.5	V427	BV421
						405/10 BP	400-410	V405	Violet SSC
Indigo/ NIR Collinear	446/779	Solid State, OBIS 785 LX	75/100	800 LP		820/60 BP	800-850	N820	DyLight 800
				635 LP		660/20 BP	650-670	I660	
				600 LP		605/40 BP	600-625	I605	
				500 LP		515/30 BP	500-530	I515	
				450 LP		470/15 BP	462.5-477.5	I470	

Supplementary table 3.2: Commercial reagents used in OMIP - all dilutions

Specificity	Fluorochrome	Clone	Catalogue #	Manufacturer	Dilution (µL) (antibody volume in µL/100µL of stain buffer per 2.5 x 10^6 cells)
HLA-DR	BUV395	G46-6	564040	BD Biosciences	1.5
CD16	BUV496	3GB	564653	BD Biosciences	2.5
Siglec-1	BUV615	7-239	751124	BD Biosciences	2
CCR7	BUV661	2-L1-A	749824	BD Biosciences	5
CD14	BUV737	B-ly6	612763	BD Biosciences	1
CD163	BUV805	GHI/61	749201	BD Biosciences	2
CD209	BV421	DCN46	564127	BD Biosciences	2.5
Siglec-6	BV480	767329	767329	BD Biosciences	1
CD1a	BV510	HI149	563481	BD Biosciences	1
CD4	BV605	OKT4	317436	Biolegend	4
CD1c	BV650	F10/21A3	742749	BD Biosciences	3
CD11b	BV711	ICRF44	301344	Biolegend	2
Axl	BV785	108724	747857	BD Biosciences	2.5
CD11c	BB515	B-ly6	564490	BD Biosciences	1.5
CD3	NovaFluor Blue 660-120S	UCHT1	H002T03B08-A	ThermoFisher scientific	0.5
CD19	NovaFluor Blue 660-120S	HIB19	H004T03B08-A	ThermoFisher scientific	2.5
CD88	PerCP eFluor710	20/70	46-0882-82	ThermoFisher scientific	2.5
CD206	RB780	19.2	755605	BD Biosciences	0.5
Calprotectin	PE	MAC387	MA5-28130	ThermoFisher scientific	4
CD103	PE Vio615	REA803	130-111-837	Miltenyi Biotec	2.5
CD123	PE-Cy5	6H6	306008	Biolegend	0.5
CD5	PE-Cy5.5	CD5-5D7	MHCD0518	ThermoFisher scientific	0.5
CD207	PE Vio770	REA770	130-100-586	Miltenyi Biotec	1
XCR1	APC	S15046E	372606	Biolegend	4
Viability	FVS700	N/A	564997	BD Biosciences	0.01
KI67 biotin (Intracellular)	Streptavidin DyLight800	MKI67/2465	ab21811	AbCam	2.5 (KI67) 0.5 (Streptavidin)

Supplementary table 3.3: Experiment iterations of panel development.

Reagents that were removed after an individual iteration are highlighted in **blue**. Reagents that remained constant across all four iterations are highlighted in green.

		Iterations			
Detector	**Fluorochrome**	**1**	**2**	**3**	**4**
R670	APC	CD86	CD86	CD86	XCR1
R730	FVS700	LiveDead	LiveDead	LiveDead	LiveDead
R780	APC Fire 750	XCR1	XCR1	XCR1	
R820	APC Fire 810	CD14	HLA-DR		
U379	BUV395	HLA-DR	CD11c	HLA-DR	HLA-DR
U450	AF350			CD45	
U515	BUV496		CD16	CD16	CD16
U586	BUV563	HLA-DQ	HLA-DQ		
U610	BUV615	CD169	CD169	CD169	CD169
U670	BUV661	CCR7		CCR7	CCR7
U740	BUV737	CD11c	CD14	CD14	CD14
U820	BUV803	CD163	CD163	CD163	CD163
Y586	PE	Slan/ MDC8	Slan/ MDC8	Calprotectin	Calprotectin
Y610	PE Vio615	CD103	CD103	CD103	CD103
Y670	PE Cy5	CD123	CD123	CD123	CD123
Y710	PE Cy5.5	CD5	CD5	CD5	CD5
Y780	PE Vio770	CD207	CD207	CD207	CD207
B515	BB515	FcER1a AF488	FcER1a AF488	CD11c	CD11c
B610	Autofluorescence	Autofluorescence	Autofluorescence	Autofluorescence	Autofluorescence
B670	NovaBlue660 / 120S	CD3 CD19	CD3 CD19	CD3 CD19	CD3 CD19
B710	PerCP eF710	CD89 BB700	CD88	CD88	CD88
B820	RB780	CD45 BB790	CD45 BB790	CD206	CD206
O616	AF594	Calprotectin	Calprotectin		
V427	BV421	CD209	CD209	CD209	CD209
V474	BV480	Siglec-6	Siglec-6	Siglec-6	Siglec-6
V525	BV510	CD1a	CD1a	CD1a	CD1a
V586	BV570	CD16			
V610	BV605	CD4	CD4	CD4	CD4
V677	BV650	CD1c	CD1c	CD1c	CD1c
V710	BV711	CD11b	CD11b	CD11b	CD11b
V750	BV750	CD206	CD206		
V820	BV785	Axl	Axl	Axl	Axl
N820	Dylight 800		Ki67 biotin	Ki67 biotin	Ki67 biotin

Supplementary table 3.4: Antibodies tested but not included

Specificity	Fluorochrome	Clone	Reason for inclusion	Reason for removal
CD89	BB700	A59	MDDC	CD88 was shown to be more reliable than CD89 in identifying tissue monocytes
CD45	BB790	HI30	All immune cells	The bright CD45 signal spilled over into too many detectors of a similar wavelength. Moved to AF350
CD45	AF350	I430u	All immune cells	The signal from AF350 was not bright enough to be able to get clean separation, even at high titre
HLA-DR	APC Fire 810	L243	All MNPs	HLA-DR was moved to BUV395 after the bright signal spilled over into other detectors of a similar wavelength
CD14	APC Fire 810	63D3	Macrophage, monocyte, MDM, MDDC	CD14 was moved to BUV737 after the bright signal spilled over into other detectors of a similar wavelength
XCR1	APC Fire 750	S15046E	cDC1	XCR1 was moved to APC to reduce spillover in the red detectors
CD83	APC	HB15e	Mature DC	CD86 was removed from the panel to make space for XCR1 after it was removed from APCFire750
CD11c	BUV737	B-ly6	DC	CD11c was moved to BUV395 to make space for CD14 after it was removed from APCFire810
CD11c	BUV395	B-ly6	DC	CD11c was moved to BB515 to make space for HLA-DR after it was removed from APCFire810
FcER1A	AF488	9E1	cDC2	FcER1A was removed to free up the B515 detector for CD11c, after it was removed from BUV395
HLA-DQ	BUV563	Tu169	cDC2	HLA-DQ was removed with FcER1A as they were to be used in conjunction to isolate a subset of DC
Calprotectin	AF594	MAC387	Monocyte, MDM	Calprotectin was moved to PE as there was too much spillover with PEVio615 and BUV615
SLAN	PE	S15046E	Slan DC	SLAN was removed to free up the Y586 detector for Calprotectin, after it was removed from AF594
CD206	BV750	19.2	DC, macrophage	CD206 was moved to RB780 to reduce the spillover in the higher violet wavelength, allowing for better resolution of CD11b and Axl on BV711 and BV786 respectively

Supplementary table 3.5: Compensation reagents

For each compensation control, 50 µL of positive and 5 0µL of negative beads were combined in a 5 mL FACS tube and washed (350 x *g* for 5 mins) in FACS wash (1% FBS (v/v), 2 mM EDTA, 0.1% sodium azide (w/v) in PBS). The beads were resuspended in 100 µl of FACs wash and stained for 15 mins at 25°C. Beads were then washed twice using FACS wash. Dilution is shown as antibody volume in µL/100 µL.

Specificity	Fluorochrome	Compensation bead	Dilution (µL)
HLA-DR	BUV395	BD CompBeads Plus Anti-Mouse Ig (P)	1
CD16	BUV496	P	1
Siglec-1	BUV615	P	1
CD163	BUV805	P	1
Calprotectin	PE	P	0.5
CD5	PE Cy5.5	P	0.5
CD207	PE Vio770	P	1
CD3	NovaFluor Blue 660-120S	P	0.8
CD19	NovaFluor Blue 660-120S	CD3 antibody used for compensation	-
CD88	PerCP eFluor710	P	1
CD206	RB780	P	0.4
Siglec-6	BV480	P	0.5
CD1a	BV510	P	1.3
CD4	BV605	P	0.8
CD1c	BV650	P	1
Axl	BV785	P	0.5
CCR7	BUV661	BD CompBeads Normal Anti-Mouse Ig (N)	1
CD14	BUV737	N	1
CD209	BV421	N	1
CD11b	BV711	N	1
CD11c	BB515	N	1
CD123	PE Cy5	N	0.5
CD103	PE Vio615	MACS Comp Bead Kit, anti-REA	1
XCR1	APC	Slingshot SpectraComp	1.3
Viability	FVS700	Arc Amine Reactive Compensation Bead Kit	1
KI67	Streptavidin DyLight800	Cells (HEKS293 cell line)	As per Supplementary table 3.2

Supplementary table 3.6: Summary of titration panels including reagents and fluorochromes used

Antibody titrated	Titration panel	Gated population
HLA-DR BUV395	CD45 AF350, CD45 BB790, FVS700, HLA-DR BUV395	Cells, live, FSC-H high
CD16 BUV496	FVS700, CD16 BUV496, CD45 PE	Cells, live, CD45$^+$
Siglec-1 BUV615	HLA-DR BUV395, Siglec-1 BUV615, CD163 BUV805, CD14 BV421, LiveDead Aqua, MR BV750	Cells, live, HLA-DR$^+$, autofluorescence$^-$
CD163 BUV805	HLA-DR BUV395, Siglec-1 BUV615, CD163 BUV805, CD14 BV421, LiveDead Aqua, MR BV750	Cells, live, HLA-DR$^+$, autofluorescence$^-$
Calprotectin PE	Calprotectin PE, CD14 BUV737, CD16 BUV496, FVS700, HLAD-DR BUV395, XCR1 APC	Cells, live, autofluorescent$^-$
CD5 PE Cy5.5	CD3 NovaFluor Blue 660-120S, CD5 PE Cy5.5, FVS700, HLA-DR BUV395	Cells, live, HLA-DR$^+$, autofluorescent$^-$, CD1a$^-$
CD207 PE Vio770	CD1c BV650, CD11b BV711, CD16 BV570, CD19 NovaFluor Blue 660-120S, CD45 BB790, DC-SIGN BV421, FVS700, Langerin PE Vio770	Cells, live, HLA-DR$^+$
CD3 NovaFluor Blue 660-120S	CD3 NovaFluor Blue 660-120S, CD5 PE Cy5.5, FVS700, HLA-DR BUV395	Cells, live, CD14$^-$
CD19 NovaFluor Blue 660-120S	CD1c BV650, CD11b BV711, CD16 BV570, CD19 NovaFluor Blue 660-120S, CD45 BB790, DC-SIGN BV421, FVS700, Langerin PE Vio770	Cells, live, autofluorescent$^-$
CD88 PerCP eFluor710	CD11c BUV395, CD14 BUV737, CD45 PE, CD88 PerCP-eFluor710, HLA-DR APC fire810, HLA-DER BB515, NIR R780	Cells, live, HLA-DR$^+$, CD45$^+$
CD206 RB780	HLA-DR BUV395, MR RB780, UV440	Cells, live, HLA-DR$^+$, autofluorescent$^-$
Siglec-6 BV480	Axl BV785, CD11c BUV661, CD123 PE Cy5, FVS700, HLA-DR BUV395, Siglec-6 BV480	Cells, live, HLA-DR$^+$, CD11c$^+$
CD1a BV510	CD1a BV510, Langerin PE Vio770, FVS700, HLA-DR BUV395	Cells, live, HLA-DR$^+$
CD4 BV605	FVS700, HLA-DR BUV395, CD14 APC Fire810, CD89 BB700, CD4 BV605, CCR5 VioBright B515, Calprotectin AF594	Cells, live, HLA-DR$^-$, autofluorescent$^-$
CD1c BV650	CD1c BV650, CD11b BV711, CD16 BV570, CD19 NovaFluor Blue 660-120S, CD45 BB790, DC-SIGN BV421, FVS700, Langerin PE Vio770	Cells, live, HLA-DR$^+$, autofluorescent$^-$
Axl BV785	FVS700, HLA-DR BUV395, CD11c BUV661, Siglec-6 BV480, Axl BV785	Cells, live, HLA-DR$^+$, CD11c$^+$
CCR7 BUV661	UV440, NIR R780, HLA-DR BUV395, CD83 APC, CD45 BB790, CD11c BB515, CCR7 BUV661	Cells, live, HLA-DR$^+$, CD11c$^+$
CD14 BUV737	CD11c BUV395, CD14 BUV737, CD45 PE, CD88 PerCP-eFluor710, HLA-DR APC fire810, HLA-DER BB515, NIR R780	Cells, live, CD45$^+$, autofluorescence$^-$
CD209 BV421	CD1c BV650, CD11b BV711, CD16 BV570, CD19 NovaFluor Blue 660-120S, CD45 BB790, DC-SIGN BV421, FVS700, Langerin PE Vio770	Cells, live, HLA-DR$^+$, AF$^-$
CD11b BV711	CD1c BV650, CD11b BV711, CD16 BV570, CD19 NovaFluor Blue 660-120S, CD45 BB790, DC-SIGN BV421, FVS700, Langerin PE Vio770	Cells, live, HLA-DR$^+$, autofluorescent$^-$
CD11c BB515	FVS700, HLA-DR BUV395, CD3 BUV486, CD14 BUV737, CD45 PE Cy7, CD11c BB515, CD19 BV750	Cells, live, HLA-DR$^+$, CD45$^+$, CD3$^-$, CD19$^-$, autofluorescent$^-$
CD123 PE-Cy5	CD11c BV421, CD14 BUV737, CD45 BB790, CD123 PE Cy5, FVS700, HLA-DR BUV395	Cells, live, HLA-DR$^+$
CD103 PE Vio615	CD3 BUV496, CD103 PE Vio615, HLA-DR BUV395, LiveDead Violet, XCR1 APC Fire750	Cells, live, HLA-DR$^-$, CD3$^+$
XCR1 APC	CD1a BV510, CD1c PE Vio770, CD11c PE-CF594, CD14 BUV737, CD45 BV786, CD141 BV711, HLA-DR BUV395, Langerin Vioblue, LiveDead NIR, XCR1 APC	Cells, live, CD45$^+$, HLA-DR$^+$, Autofluorescent-, CD141$^+$, CD14$^-$
Viability FVS700	FCER1a APC, FVS700, HLA-DR BUV395, CD3 BUV496, CD11c BUV661, CD14 BUV737, CD123 PE-Cy5, XCR1 BV421, CD16 BV570, CD1c BV650, CD19 BV750	Cells, live
1' KI67-biotin 2' streptavidin Dylight800	Streptavidin AF647, LiveDead Violet, KI67 Biotin	Cells, live

Supplementary table 3.7: Summary of antigen expression across all MNP subsets in human skin and mucosa

	cDC1	cDC2	DC3	pDC	ASDC	LC	Monocyte	MDDC	MDM (skin & type II mucosa)	MDM (type I mucosa)	t-MDM (type I mucosa)	Autofluorescent macrophage
HLA-DR												
XCR1												
CD11c	+/-				+/-				+/-		+/-	
CD1c					+/-							
CD1a	+/-	+/-	+/-		+/-			+/-				
CD5		+/-										
CD14			+/-									
CD163									+/-			
CD123		+/-	+/-		+/-			+/-	+/-			
Axl												
Siglec-6												
Siglec-1					+/-							
CD88												
CD11b		+/-										
CD16												
CD206		+/-	+/-		+/-			+/-	+/-			
CD207	+/-	+/-			+/-							
CD209			+/-									
CD103	+/-	+/-										
Calprotectin		+/-	+/-									
CD4												
CCR7	+/-	+/-	+/-	+/-	+/-	+/-	+/-	+/-				
FcεR1α												
CD89												
HLA-DQ												

Very high	High	Moderate	Low	None	**+/-** can be expressed or not expressed

Supplementary table 3.8: Preliminary stain index for BD Symphony A5

All fluorophores were conjugated to CD4 and stained on PBMCs, except DyLight800 and AF350 which were stained on beads.

JAN-2021-V2 SYMPHONY-SSM		BB515	BB630	BB660	BB700	BB755	BB790	DYLIGHT800	AF594	APC	APCR700	APCH7	APCFIRE810	BUV395	AF350	BUV496	BUV563	BUV615	BUV661	BUV737	BUV805	BV421	BV480	BV510	BV570	BV605	BV650	BV711	BV750	BV786	BYG584	PECF594	PECY5	PECY7
		B515_30-A	B610_20-A	B670_30-A	B710_50-A	B750_30-A	B820_60-A	N820_60-A	O616_23-A	R670_30-A	R710_40-A	R780_60-A	R820_60-A	U379_28-A	U450_50-A	U515_30-A	U586_15-A	U610_20-A	U670_30-A	U740_35-A	U820_60-A	V427_25-A	V474_25-A	V525_50-A	V586_15-A	V610_20-A	V677_20-A	V710_50-A	V750_30-A	V820_60-A	Y586_15-A	Y610_20-A	Y670_30-A	Y820_60-A
BB515	B515_30-A	0.00	0.60	0.40	0.26	0.30	0.14	0.00	0.28	0.35	0.05	0.02	0.00	0.10	0.00	0.08	0.31	0.17	0.13	0.04	0.00	0.00	0.05	0.11	0.13	0.25	0.16	0.09	0.06	0.00	0.31	0.00	0.02	0.00
BB630	B610_20-A	0.06	0.00	1.99	1.19	1.74	0.75	0.00	1.92	1.67	0.79	0.06	0.01	0.18	0.00	0.00	0.34	0.90	1.14	0.51	0.29	0.00	0.00	0.00	0.34	2.28	2.05	1.06	0.96	0.59	0.62	2.76	0.78	0.35
BB660	B670_30-A	0.03	0.41	0.00	1.85	2.81	1.37	0.16	0.32	4.82	2.58	0.54	0.47	0.11	0.00	0.00	0.18	0.17	1.48	0.85	0.44	0.02	0.00	0.00	0.22	0.38	3.27	1.50	1.48	0.87	0.29	0.17	1.62	0.61
BB700	B710_50-A	0.07	0.37	2.54	0.00	4.87	2.36	0.39	0.26	2.65	4.04	0.75	0.68	0.20	0.00	0.00	0.21	0.21	1.42	1.52	0.83	0.22	0.00	0.06	0.23	0.39	2.86	2.74	2.73	1.66	0.29	0.10	0.88	0.75
BB755	B750_30-A	0.06	0.36	0.65	0.99	0.00	2.85	0.48	0.27	0.48	0.72	0.41	0.42	0.19	0.00	0.00	0.16	0.19	0.25	1.10	0.99	0.10	0.00	0.03	0.16	0.36	0.52	0.64	2.83	1.93	0.29	0.00	0.00	0.72
BB790	B820_60-A	0.19	0.87	0.98	1.01	16.1	0.00	1.21	0.39	0.67	0.73	0.52	0.47	0.22	0.00	0.00	0.24	0.26	0.38	1.25	1.61	0.20	0.00	0.06	0.28	0.45	0.74	0.60	3.39	3.01	0.37	0.12	0.18	0.85
DYLIGHT800	N820_60-A	0.00	0.00	0.00	0.01	0.52	0.51	0.00	0.01	0.00	0.02	0.28	0.41	0.00	0.00	0.00	0.00	0.05	0.00	0.13	0.84	0.00	0.00	0.00	0.05	0.04	0.00	0.03	0.78	0.89	0.05	0.05	0.00	1.11
AF594	O616_23-A	0.00	0.76	0.70	0.29	0.33	0.05	0.00	0.00	0.68	0.32	0.03	0.05	0.00	0.00	0.00	0.24	0.65	0.70	0.32	0.22	0.00	0.00	0.00	0.00	0.48	0.63	0.42	0.42	0.26	0.38	2.76	0.82	0.54
APC	R670_30-A	0.00	0.04	1.04	0.24	0.40	0.28	0.00	0.28	0.00	2.31	0.62	0.56	0.15	0.00	0.00	0.05	0.16	1.52	0.71	0.38	0.00	0.00	0.00	0.00	0.07	1.28	0.61	0.69	0.52	0.10	0.24	1.74	0.89
APCR700	R710_40-A	0.00	0.01	0.30	0.31	0.63	0.42	0.00	0.05	0.86	0.00	0.75	0.65	0.12	0.00	0.02	0.04	0.08	0.36	0.82	0.41	0.00	0.00	0.00	0.00	0.02	0.36	0.54	0.75	0.54	0.00	0.00	0.37	0.98
APCH7	R780_60-A	0.00	0.00	0.00	0.02	1.44	1.59	2.56	0.06	0.40	0.48	0.00	2.03	0.40	0.00	0.00	0.13	0.31	0.28	0.70	2.04	0.00	0.00	0.00	0.14	0.09	0.00	0.08	2.18	2.16	0.36	0.00	0.12	4.27
APCFIRE810	R820_60-A	0.00	0.00	0.23	0.08	1.61	1.75	3.57	0.03	0.92	0.87	0.65	0.00	0.35	0.07	0.00	0.15	0.22	0.33	0.39	2.44	0.00	0.00	0.07	0.01	0.03	0.02	0.18	2.52	2.77	0.11	0.00	0.41	5.20
BUV395	U379_28-A	0.00	0.00	0.00	0.00	0.00	0.00	0.00	0.12	0.00	0.00	0.01	0.00	0.00	0.32	0.10	0.14	0.08	0.06	0.01	0.00	0.00	0.00	0.00	0.00	0.00	0.00	0.01	0.01	0.00	0.13	0.00	0.01	0.00
AF350	U450_50-A	0.05	0.01	0.02	0.05	0.09	0.00	0.00	0.62	0.23	0.00	0.03	0.00	0.00	0.00	0.65	0.95	0.69	0.52	0.23	0.07	0.00	0.00	0.43	0.47	0.29	0.22	0.22	0.14	0.11	0.86	0.00	0.00	0.00
BUV496	U515_30-A	0.28	0.10	0.07	0.00	0.00	0.00	0.00	1.50	0.52	0.14	0.02	0.00	1.49	0.28	0.00	1.66	1.04	1.11	0.40	0.14	0.00	0.39	0.42	0.69	0.56	0.46	0.23	0.00	0.16	1.73	0.10	0.00	0.00
BUV563	U586_15-A	0.00	0.78	0.59	0.33	0.27	0.16	0.00	2.33	1.19	0.20	0.00	0.02	1.20	0.15	0.12	0.00	1.83	1.61	0.52	0.25	0.00	0.00	0.00	0.48	0.51	0.38	0.20	0.05	0.01	3.36	1.75	0.47	0.16
BUV615	U610_20-A	0.00	0.96	0.75	0.33	0.42	0.22	0.00	3.92	1.91	0.60	0.06	0.02	0.79	0.11	0.03	0.78	0.00	2.71	1.18	0.57	0.00	0.00	0.00	0.15	0.71	0.88	0.49	0.42	0.29	0.83	3.20	0.99	0.63
BUV661	U670_30-A	0.00	0.06	0.82	0.23	0.37	0.22	0.15	0.42	3.95	2.31	0.54	0.46	0.51	0.08	0.00	0.11	0.32	0.00	1.26	0.65	0.00	0.00	0.00	0.00	0.09	0.97	0.47	0.53	0.39	0.09	0.25	1.23	0.62
BUV737	U740_35-A	0.00	0.00	0.20	0.37	1.66	0.71	0.28	0.01	0.20	0.90	0.52	0.46	0.43	0.10	0.01	0.07	0.06	0.20	0.00	1.12	0.00	0.00	0.00	0.00	0.02	0.05	0.27	0.78	0.56	0.13	0.00	0.02	0.43
BUV805	U820_60-A	0.00	0.00	0.00	0.00	0.40	0.39	1.71	0.11	0.07	0.00	0.22	0.30	0.73	0.10	0.00	0.07	0.12	0.09	0.27	0.00	0.00	0.03	0.00	0.00	0.00	0.00	0.00	0.58	0.68	0.05	0.00	0.02	0.64
BV421	V427_25-A	0.00	0.00	0.00	0.00	0.00	0.00	0.00	0.11	0.04	0.00	0.00	0.00	0.06	0.48	0.05	0.15	0.14	0.07	0.01	0.00	0.00	1.08	0.75	0.27	0.14	0.12	0.04	0.11	0.04	0.39	0.00	0.00	0.00
BV480	V474_25-A	0.23	0.12	0.06	0.02	0.06	0.00	0.00	0.55	0.14	0.18	0.00	0.03	0.28	0.04	0.47	0.58	0.46	0.43	0.19	0.04	0.11	0.00	1.46	0.92	0.79	0.72	0.34	0.34	0.16	1.08	0.32	0.01	0.00
BV510	V525_50-A	0.00	0.16	0.03	0.00	0.08	0.00	0.00	1.24	0.56	0.55	0.03	0.00	0.48	0.09	0.40	1.35	0.96	1.04	0.59	0.40	0.31	1.43	0.00	1.50	1.43	1.78	0.86	0.94	0.80	1.91	0.62	0.00	0.10
BV570	V586_15-A	0.00	0.83	0.72	0.39	0.38	0.16	0.00	1.46	0.77	0.66	0.00	0.00	0.45	0.12	0.03	1.87	1.11	1.19	0.53	0.37	0.67	0.32	0.43	0.00	1.93	2.28	1.05	1.10	0.72	3.30	2.24	0.60	0.11
BV605	V610_20-A	0.00	0.79	0.76	0.42	0.57	0.40	0.00	1.85	1.16	1.02	0.04	0.00	0.20	0.06	0.00	0.64	1.31	1.79	0.92	0.55	0.32	0.12	0.13	0.70	0.00	3.09	1.56	1.66	1.07	1.00	2.66	0.86	0.70
BV650	V677_20-A	0.00	0.14	0.47	0.20	0.26	0.13	0.00	0.50	1.54	1.53	0.29	0.26	0.19	0.03	0.00	0.06	0.33	1.77	0.97	0.48	0.33	0.16	0.12	0.10	0.62	0.00	1.71	1.58	0.96	0.15	0.53	0.66	0.46
BV711	V710_50-A	0.00	0.00	0.35	0.54	1.14	0.59	0.16	0.07	0.66	2.89	0.73	0.60	0.18	0.08	0.00	0.03	0.07	0.60	2.10	1.14	0.43	0.11	0.08	0.09	0.07	1.33	0.00	3.17	2.11	0.05	0.00	0.19	0.71
BV750	V750_30-A	0.00	0.00	0.03	0.25	1.34	0.71	0.18	0.05	0.05	0.58	0.40	0.44	0.22	0.06	0.00	0.00	0.12	0.13	1.84	1.31	0.43	0.29	0.11	0.16	0.08	0.16	0.65	0.00	2.78	0.16	0.00	0.00	0.59
BV786	V820_60-A	0.00	0.00	0.04	0.06	1.05	0.75	0.71	0.07	0.09	0.51	0.45	0.48	0.24	0.08	0.00	0.11	0.13	0.19	1.48	2.17	1.28	0.22	0.22	0.13	0.08	0.36	0.59	7.37	0.00	0.14	0.00	0.00	0.83
BYG584	Y586_15-A	0.00	0.56	0.39	0.15	0.23	0.15	0.00	0.30	0.23	0.11	0.01	0.02	0.09	0.00	0.00	0.27	0.20	0.18	0.09	0.03	0.02	0.00	0.00	0.30	0.28	0.29	0.14	0.13	0.09	0.00	1.84	0.51	0.34
PECF594	Y610_20-A	0.00	1.50	1.17	0.76	1.09	0.49	0.00	1.23	0.94	0.41	0.05	0.00	0.10	0.00	0.00	0.16	0.52	0.64	0.28	0.16	0.00	0.00	0.00	0.09	0.76	0.79	0.46	0.43	0.25	0.66	0.00	0.81	0.61
PECY5	Y670_30-A	0.00	0.16	2.69	1.53	2.43	1.20	0.06	0.10	3.63	1.64	0.37	0.32	0.10	0.00	0.00	0.08	0.07	1.36	0.59	0.28	0.04	0.01	0.00	0.04	0.16	1.84	0.91	0.88	0.51	0.35	0.29	0.00	1.38
PECY7	Y820_60-A	0.00	0.12	0.17	0.25	2.81	2.14	0.49	0.04	0.04	0.12	0.22	0.24	0.05	0.00	0.00	0.03	0.08	0.06	0.33	0.61	0.05	0.00	0.00	0.01	0.02	0.04	0.08	1.05	1.01	0.31	0.21	0.07	0.00

Supplementary table 3.9: Spill-over spreading error (SSE) matrix (SSM)

Obtained with compensation beads and cells in the case of DyLight 800. The reagents from the final panel (**Supplementary table 3.3**, **iteration 4**) were used.

	B515_30	B670_30	B710_50	B820_60	N820_60	R670_30	R710_40	U379_28	U515_30	U610_20	U670_30	U740_35	U820_60	V427_25	V474_25	V525_50	V610_20	V677_20	V710_50	V820_60	Y586_15	Y610_20	Y670_30	Y710_50	Y780_60
B515_30	1.00	0.01	0.00	0.00	0.00	0.00	0.00	0.00	0.02	0.00	0.00	0.00	0.00	0.00	0.00	0.00	0.00	0.00	0.00	0.00	0.00	0.00	0.00	0.00	0.00
B670_30	0.16	1.00	0.31	0.03	0.00	0.72	0.49	0.00	0.00	0.00	0.01	0.01	0.00	0.00	0.00	0.00	0.00	0.07	0.02	0.01	0.00	0.00	0.07	0.02	0.01
B710_50	0.00	0.19	1.00	0.18	0.11	0.06	0.94	0.00	0.00	0.00	0.05	0.46	0.12	0.00	0.00	0.00	0.00	0.19	0.79	0.33	0.00	0.00	0.10	0.48	0.19
B820_60	0.10	0.01	0.02	1.00	0.29	0.00	0.00	0.00	0.00	0.00	0.00	0.08	0.36	0.00	0.00	0.00	0.00	0.00	0.00	0.21	0.00	0.00	0.00	0.00	0.02
N820_60	0.05	0.01	0.01	0.01	1.00	0.00	0.01	0.04	0.04	0.01	0.01	0.02	0.07	0.04	0.06	0.06	0.04	0.02	0.02	0.08	-0.11	0.00	0.01	0.01	0.01
R670_30	0.00	0.02	0.00	0.00	0.00	1.00	0.66	0.00	0.00	0.00	0.14	0.10	0.02	0.00	0.01	0.01	0.00	0.12	0.05	0.02	0.00	0.01	0.49	0.13	0.05
R710_40	0.00	0.01	0.01	0.00	0.00	0.22	1.00	0.00	0.00	0.00	0.02	0.08	0.02	0.00	0.00	0.00	0.00	0.02	0.05	0.02	0.00	0.00	0.03	0.07	0.03
U379_28	0.00	0.00	0.00	0.00	0.00	0.00	0.00	1.00	0.08	0.00	0.00	0.00	0.00	0.01	0.00	0.00	0.00	0.00	0.00	0.00	0.00	0.00	0.00	0.00	0.00
U515_30	0.07	0.00	0.00	0.00	0.00	0.00	0.00	0.27	1.00	0.11	0.03	0.02	0.01	0.01	0.08	0.15	0.03	0.01	0.00	0.00	0.00	0.00	0.00	0.00	0.00
U610_20	0.00	0.02	0.01	0.00	0.00	0.00	0.00	0.05	0.01	1.00	0.43	0.24	0.04	0.00	0.00	0.00	0.16	0.06	0.02	0.01	0.19	0.70	0.31	0.12	0.04
U670_30	0.00	0.02	0.01	0.00	0.00	0.77	0.72	0.03	0.01	0.03	1.00	0.66	0.12	0.00	0.00	0.00	0.00	0.08	0.04	0.01	0.00	0.01	0.25	0.09	0.03
U740_35	0.00	0.00	0.02	0.01	0.00	0.00	0.11	0.02	0.00	0.00	0.00	1.00	0.26	0.00	0.00	0.00	0.00	0.00	0.02	0.02	0.00	0.00	0.00	0.01	0.01
U820_60	0.00	0.00	0.00	0.01	0.53	0.00	0.00	0.07	0.02	0.00	0.00	0.06	1.00	0.00	0.00	0.00	0.00	0.00	0.00	0.06	0.00	0.00	0.00	0.00	0.00
V427_25	0.00	0.00	0.00	0.00	0.00	0.00	0.00	0.00	0.01	0.00	0.00	0.00	0.00	1.00	0.13	0.02	0.00	0.00	0.00	0.00	0.00	0.00	0.00	0.00	0.00
V474_25	0.07	0.00	0.00	0.00	0.00	0.00	0.00	0.00	0.23	0.03	0.01	0.00	0.00	0.00	1.00	0.80	0.17	0.03	0.01	0.00	0.00	0.00	0.00	0.00	0.00
V525_50	0.02	0.00	0.00	0.00	0.00	0.00	0.00	0.00	0.36	0.15	0.06	0.05	0.01	0.01	0.37	1.00	0.54	0.17	0.08	0.03	0.00	0.00	0.00	0.00	0.00
V610_20	0.00	0.03	0.01	0.00	0.00	0.00	0.00	0.00	0.00	0.24	0.13	0.09	0.02	0.14	0.02	0.00	1.00	0.39	0.18	0.06	0.17	0.35	0.19	0.07	0.02
V677_20	0.00	0.02	0.01	0.00	0.00	0.20	0.20	0.00	0.00	0.05	0.33	0.21	0.04	0.25	0.04	0.01	0.17	1.00	0.49	0.11	0.00	0.03	0.19	0.08	0.02
V710_50	0.00	0.01	0.08	0.02	0.00	0.05	0.94	0.00	0.00	0.00	0.04	0.77	0.19	0.23	0.03	0.01	0.00	0.13	1.00	0.41	0.00	0.00	0.01	0.05	0.02
V820_60	0.00	0.00	0.00	0.01	0.09	0.00	0.00	0.00	0.00	0.00	0.00	0.14	0.36	0.21	0.03	0.01	0.00	0.00	0.02	1.00	0.00	0.00	0.00	0.00	0.01
Y586_15	0.00	0.02	0.01	0.00	0.00	0.00	0.00	0.00	0.00	0.01	0.00	0.00	0.00	0.00	0.00	0.00	0.02	0.00	0.00	0.00	1.00	0.11	0.03	0.01	0.00
Y610_20	0.00	0.36	0.16	0.01	0.01	0.01	0.01	0.00	0.00	0.10	0.06	0.04	0.01	0.00	0.00	0.00	0.14	0.07	0.04	0.01	0.42	1.00	0.64	0.28	0.08
Y670_30	0.00	0.57	0.21	0.02	0.00	0.26	0.21	0.00	0.00	0.00	0.08	0.06	0.01	0.00	0.00	0.00	0.00	0.08	0.03	0.01	0.07	0.01	1.00	0.36	0.13
Y710_50	0.00	0.17	0.48	0.06	0.00	0.07	0.34	0.00	0.00	0.00	0.03	0.13	0.04	0.00	0.00	0.00	0.00	0.05	0.11	0.03	0.23	0.03	0.35	1.00	0.37
Y780_60	0.00	0.00	0.01	0.30	0.12	0.00	0.00	0.00	0.00	0.00	0.00	0.06	0.16	0.00	0.00	0.00	0.00	0.00	0.00	0.16	0.12	0.02	0.01	0.01	1.00

3.5 Supplementary Figures

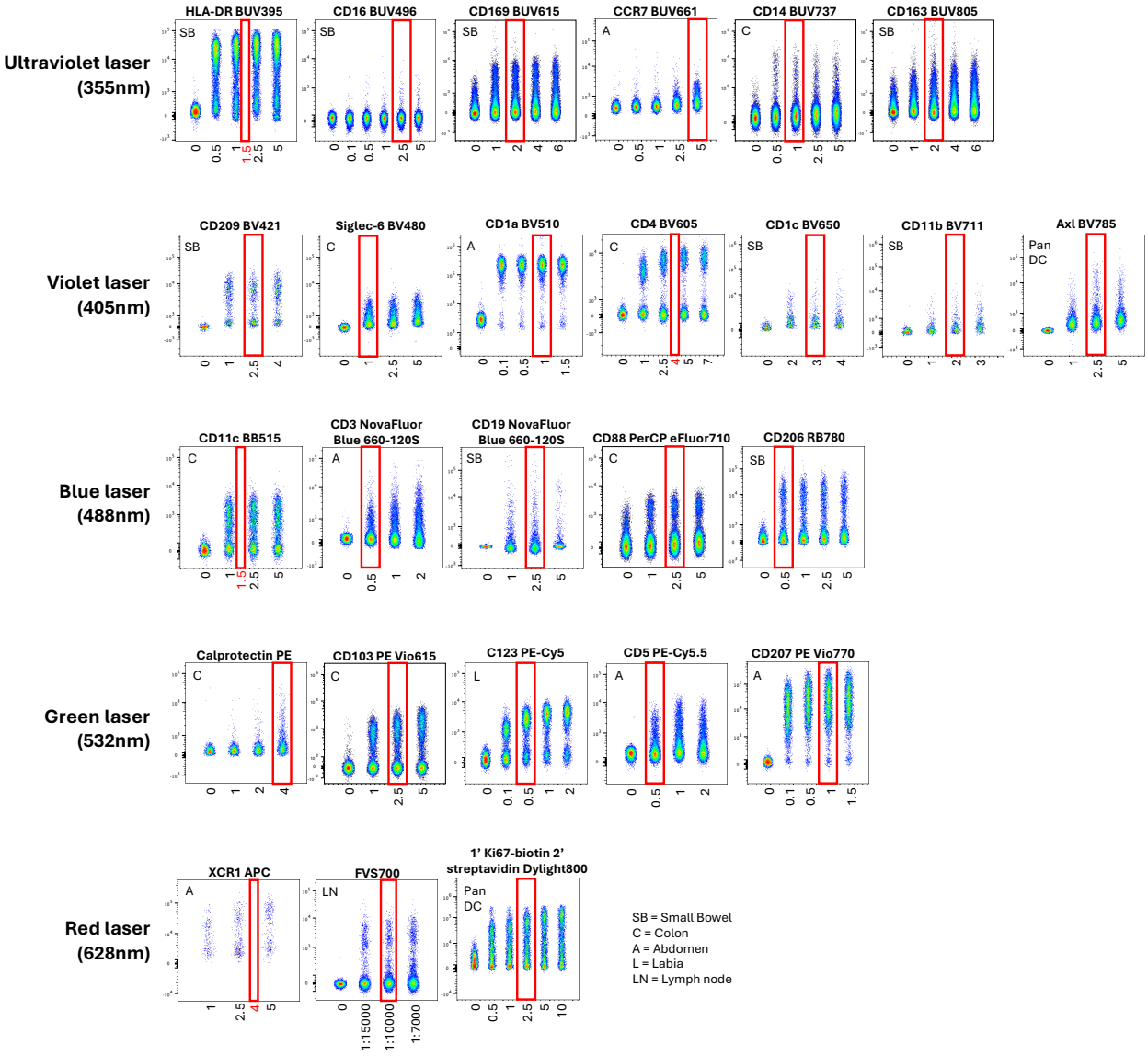

Supplementary figure 3.1: Titration experiments of the antibodies used in the optimised 26 parameter panel

All titrations were performed on a human tissue, including small bowel (SB), colon (C), abdomen (A), labia (L) or lymph nodes (LN), or on isolated blood derived Pan DCs, indicated in the top left corner of each plot. The specific titre selected for the OMIP is highlighted by the red box and volume indicated below. Optimal concentrations were chosen based on maximal separation between positive and negative populations and minimal shifting of the negative population. The percent of positive set against an FMO was used to determine the optimum volume. All titrations were optimised for 2.5 x 10^6 cells with a final staining volume of x µL/100 µL, except for FVS700 which is displayed as a dilution.

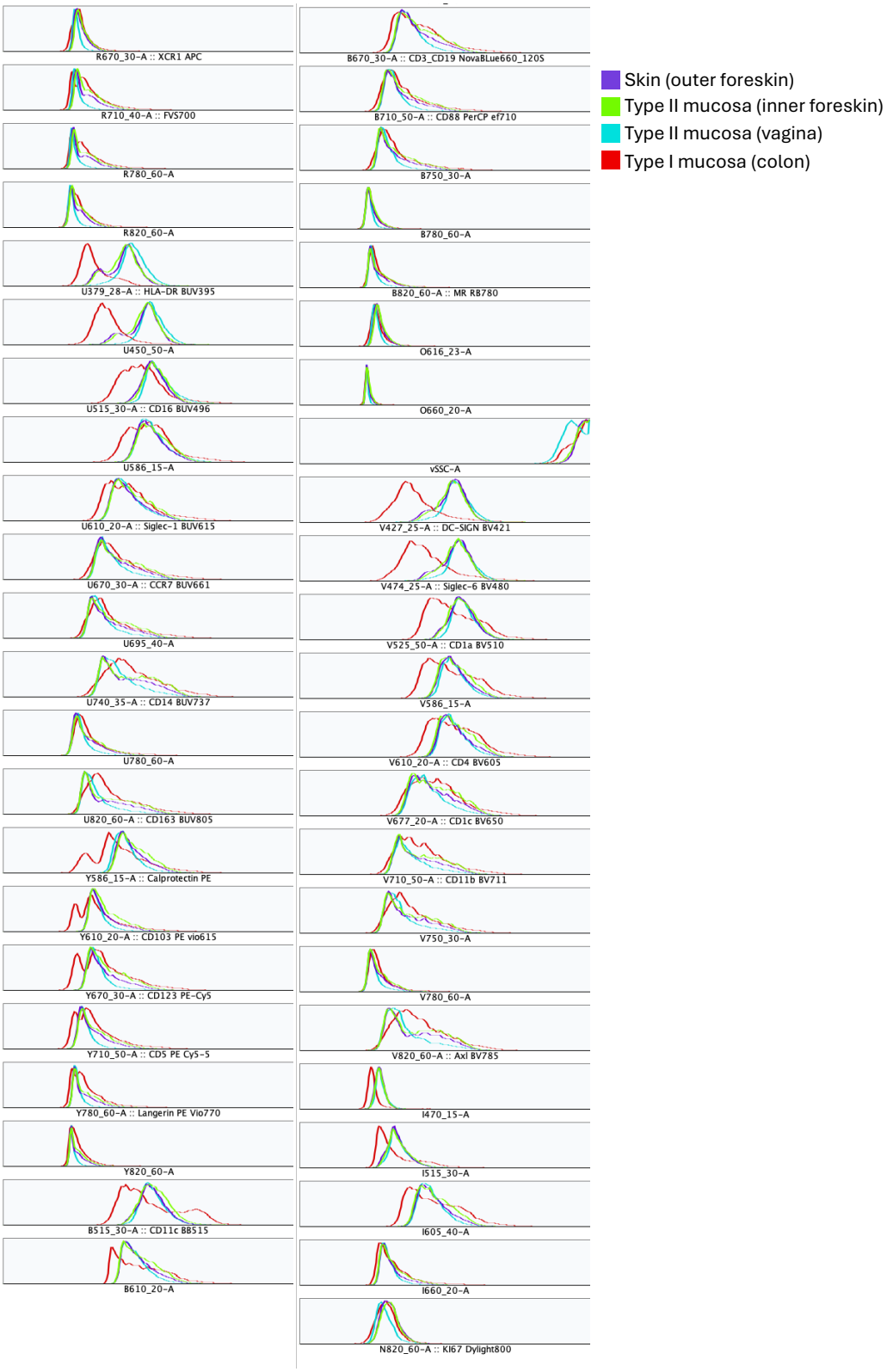

Supplementary figure 3.2: Autofluorescent signal across all FACSymphony A5 detectors in tissues of the skin, type II and type I mucosa

All cells were isolated from fresh samples and not stained with any antibodies (unstained samples). The autofluorescent positive population was gated using detectors B610 and Y586, and histograms generated.

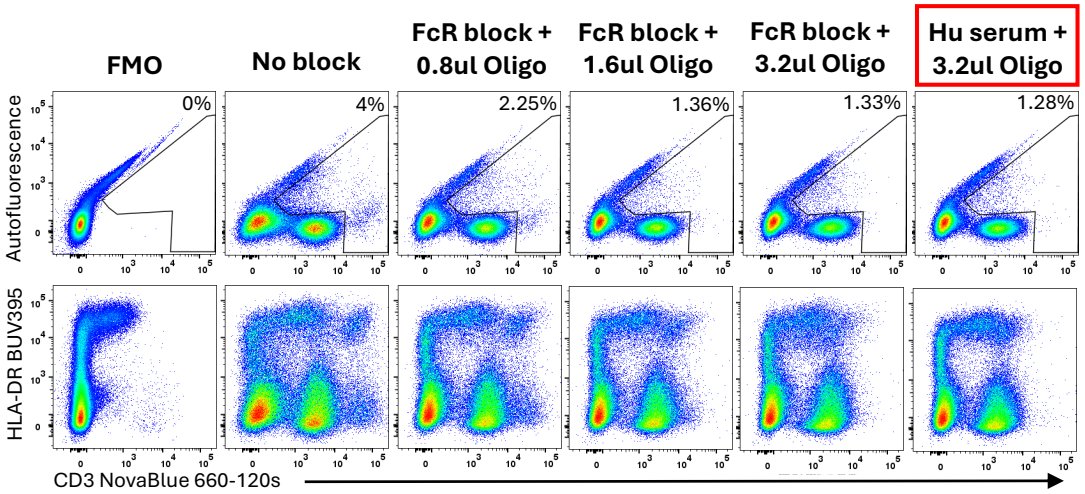

Supplementary figure 3.3: Optimisation of blocking reagents in human tissue

Demonstrated by cells isolated from colon LP. The testing assessed the non-specific binding (background staining) picked up by CD3 NovaBlue 660-120s and the sample was divided into a CD3 NovaBlue 660-120s FMO, and differing dual combinations of FcR block (5 uL), Human antibody serum (10 uL) and Oligo-block. Cells were gated as live (FVS700$^-$), single (FSC-A vs FSC-H and SSC-A vs SSC-W), CD45$^+$ cells. The most optimal blocking combination was 10ul human antibody serum and 3.2 uL Oligo-block (boxed in red).

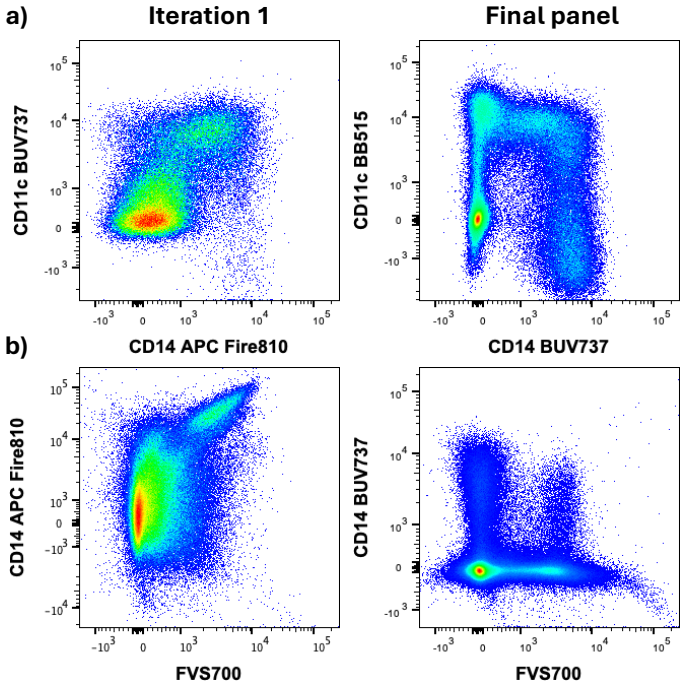

Supplementary figure 3.4: Resolution of CD14 and FVS700

Unresolved staining of **a)** CD14 APC Fire810 and **b)** FVS700 in iteration 1 compared to resolved CD14 and live cell populations in the final panel as demonstrated by human skin dermis (left: labia, right: outer foreskin). Cells in iteration 1 were gated as live (FVS700$^-$), single (FSC-A vs FSC-H and SSC-A vs SSC-W), CD3$^-$ CD19$^-$ and cells in final panel as single cells (FSC-A vs FSC-H and SSC-A vs SSC-W). Data is shown with compensation matrix generated at acquisition.

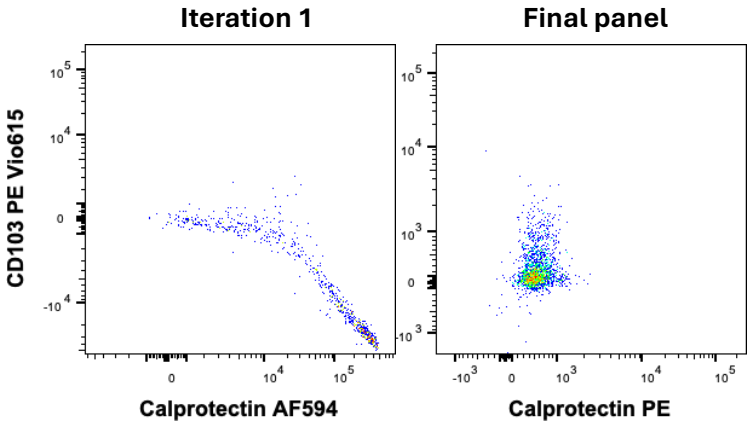

Supplementary figure 3.5: Resolution of CD103 and calprotectin

CD103 PE Vio615 interaction with calprotectin AF594 in iteration 1 compared to resolved expression of CD103 PE Vio615 and calprotectin PE in the final panel. Cells were isolated from colon LP and gated as live ($FVS700^-$), single (FSC-A vs FSC-H and SSC-A vs SSC-W), $CD3^-$ $CD19^-$ $XCR1^+$ cDC1s.

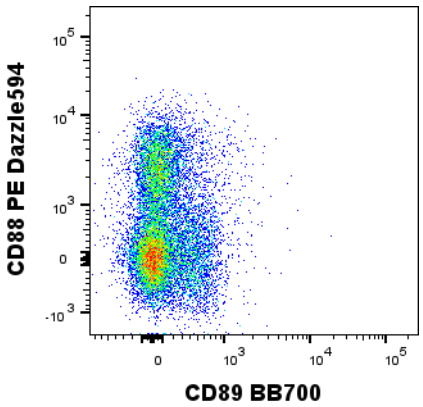

Supplementary figure 3.6: comparison of CD88 and CD89

Marker comparison of CD88 and CD89 to identify monocytes in human tissue (demonstrated in colon LP). Cells were gated as live ($FVS700^-$), single (FSC-A vs FSC-H and SSC-A vs SSC-W), $CD3^-$ $CD19^-$ $XCR1^-$. CD88 was selected for the final panel due to its superior staining.

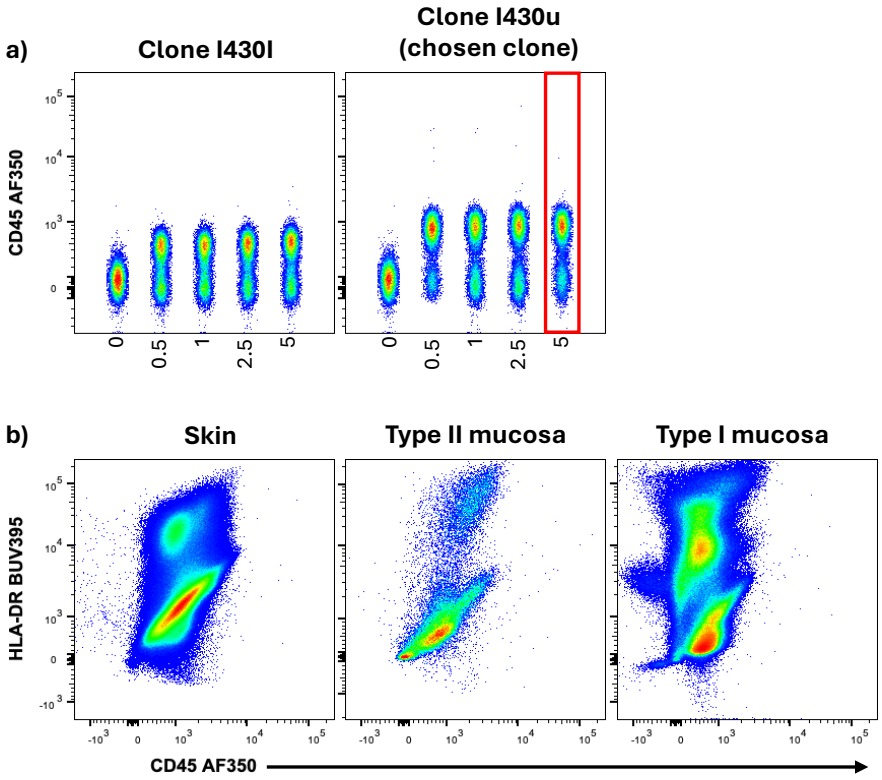

Supplementary figure 3.7: Optimisation of CD45 AF350

a) Two clones of CD45 AF350, I430I and I430u, were titrated on human colon cells. The clone I430u was selected for its higher staining with a volume of 5ul (boxed in red). All titrations were performed on 2.5 x 10^6 cells with a final staining volume of x µL/100 µL. **b)** Unresolved CD45 AF350 staining across skin dermis (labia), type II LP (vagina) and type I mucosa LP (colon) despite using the favourable clone and optimised volume. Cells were gated as live (FVS700$^-$), single (FSC-A vs FSC-H and SSC-A vs SSC-W). Data is shown with compensation matrix generated at acquisition.

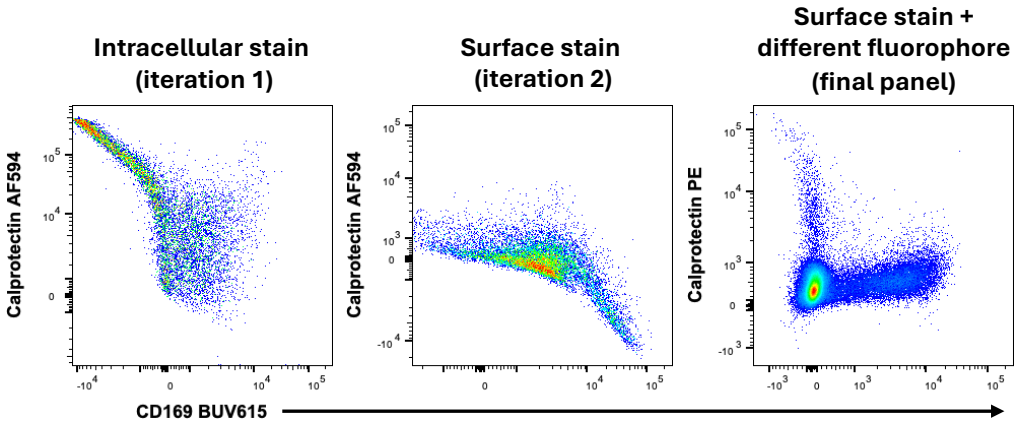

Supplementary figure 3.8: Resolution of calprotectin and CD169

Calprotectin resolution and interaction with CD169 BUV615 across multiple panel iterations as demonstrated by colon LP. Cells were gated as live (FVS700$^-$), single (FSC-A vs FSC-H and SSC-A vs SSC-W), CD3$^-$ CD19$^-$. Data is shown with compensation matrix generated at acquisition.

Skin

a) Outer foreskin epidermis

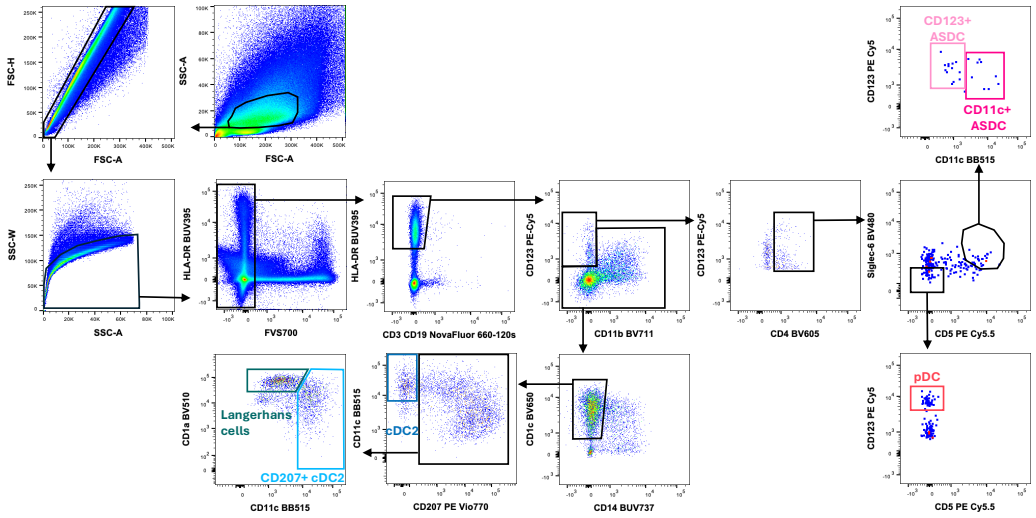

b) Outer foreskin dermis

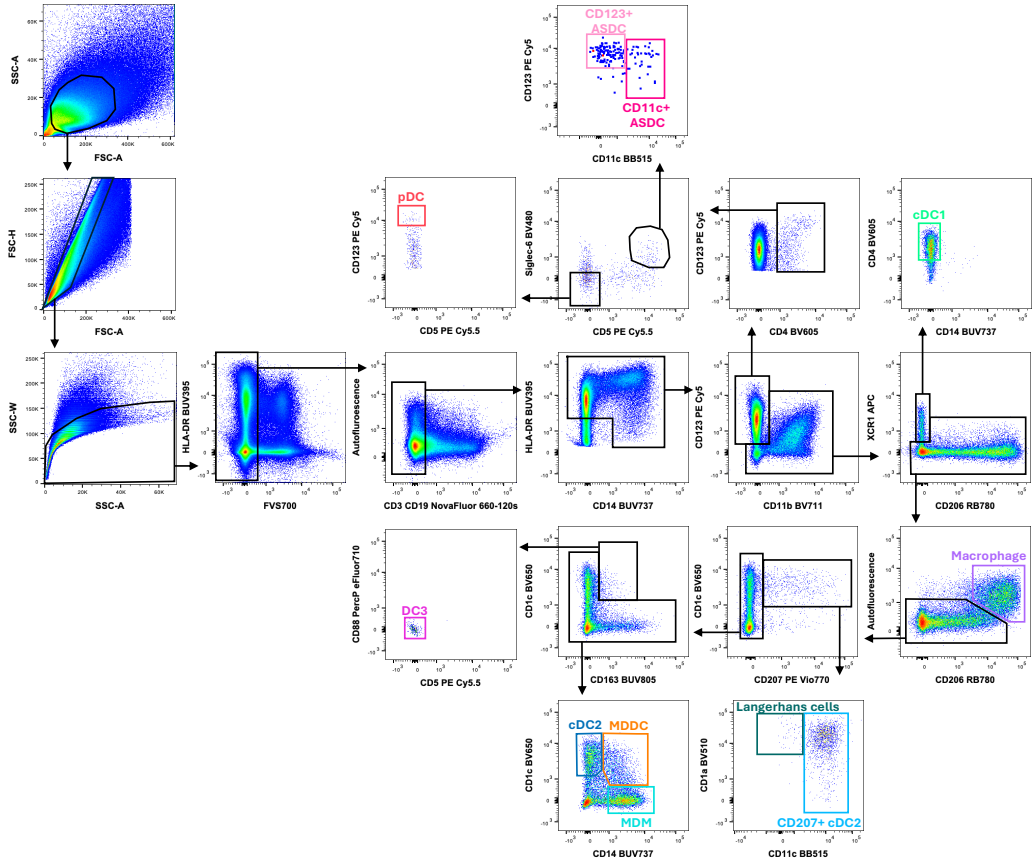

Supplementary figure 3.9: Complete gating strategy of the 26-colour optimised panel identifying all known MNPs in skin

Demonstrated by outer foreskin in the **a)** epidermis and **b)** dermis. The representative gating is a combination of different donors to showcase the highest cell yield and presence of inflammatory populations. Cells were freshly processed and isolated from the tissue, stained and acquired on a BD FACSymphony A5. A comprehensive description of gating can be found in **Figure 3.1**.

Type II mucosa

a) Inner foreskin epithelium

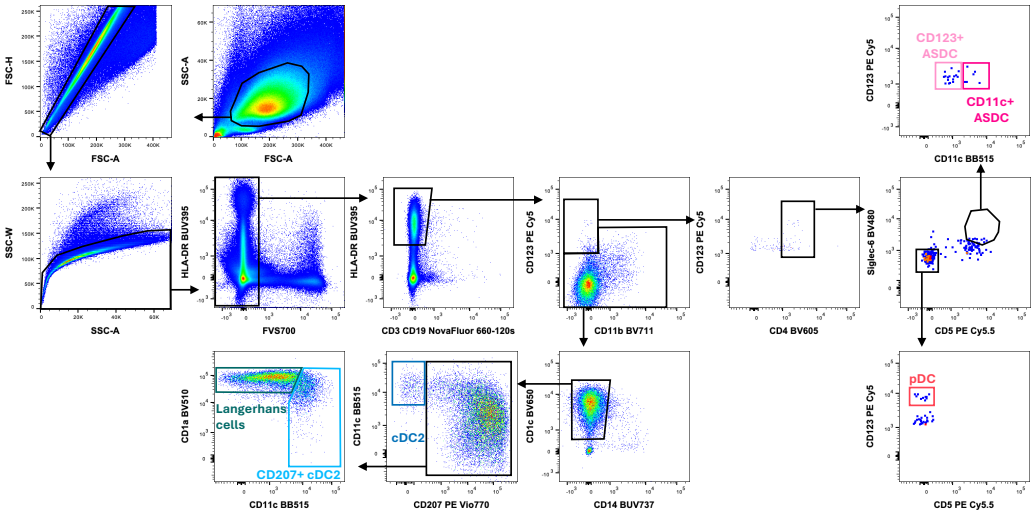

b) Inner foreskin lamina propria

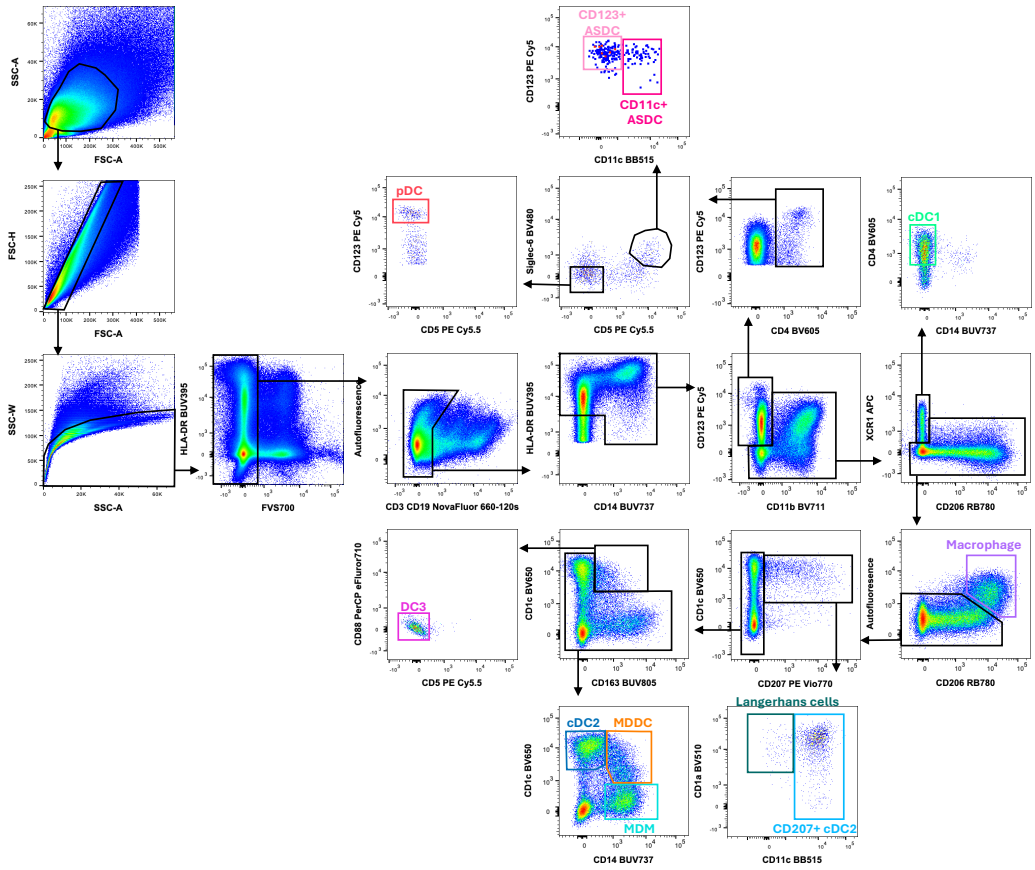

Continued over page

c) Vagina epithelium

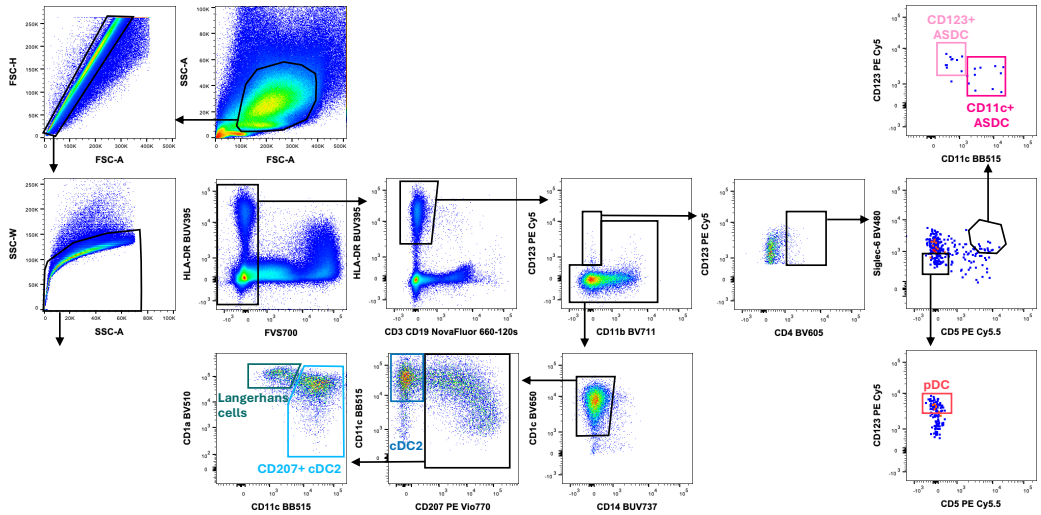

d) Vagina lamina propria

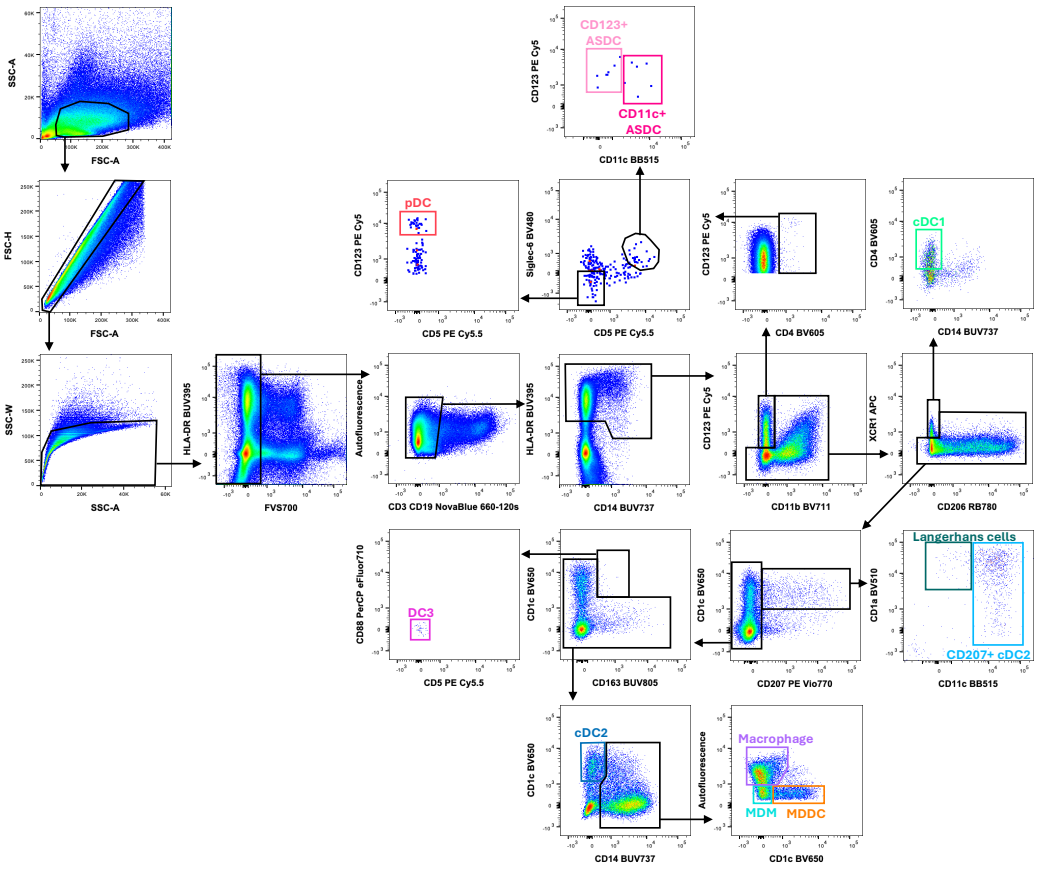

Supplementary figure 3.10: Complete gating strategy of the 26-colour optimised panel identifying all known MNPs in type II mucosa

Demonstrated by inner foreskin **a)** epithelium and **b)** LP and vagina **c)** epithelium and **d)** LP. Whilst the epithelial gating strategy remains identical across both type II mucosal tissue types, the LP strategy differs due to the strong autofluorescent macrophage signal in inner foreskin. The representative gating is a combination of different donors to showcase the highest cell yield and presence of inflammatory populations. Cells were freshly processed and isolated from the tissue, stained and acquired on a BD FACSymphony A5. A comprehensive description of gating can be found in **Figure 3.1**.

Type I mucosa

a) Colon lamina propria acquisition compensation

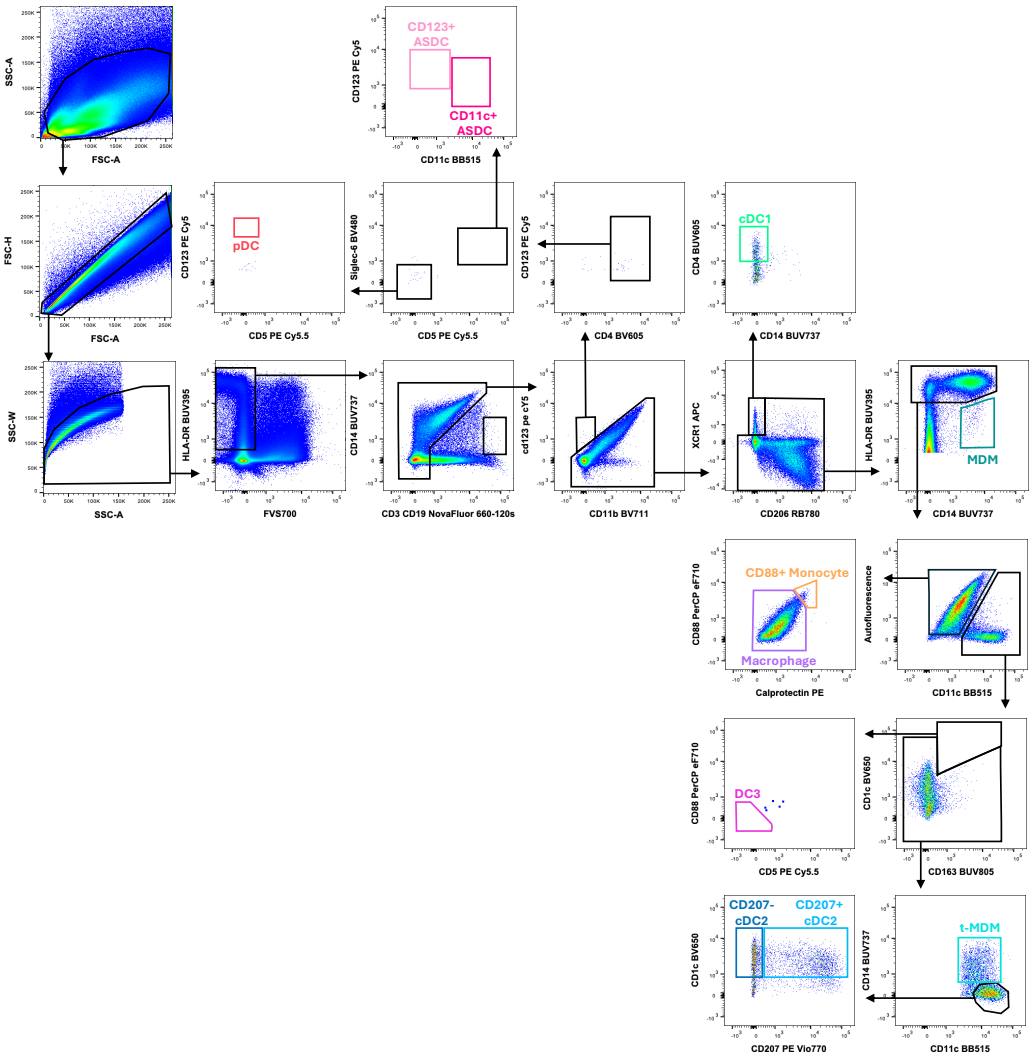

Continued over page

b) Colon lamina propria autofluorescent corrected compensation

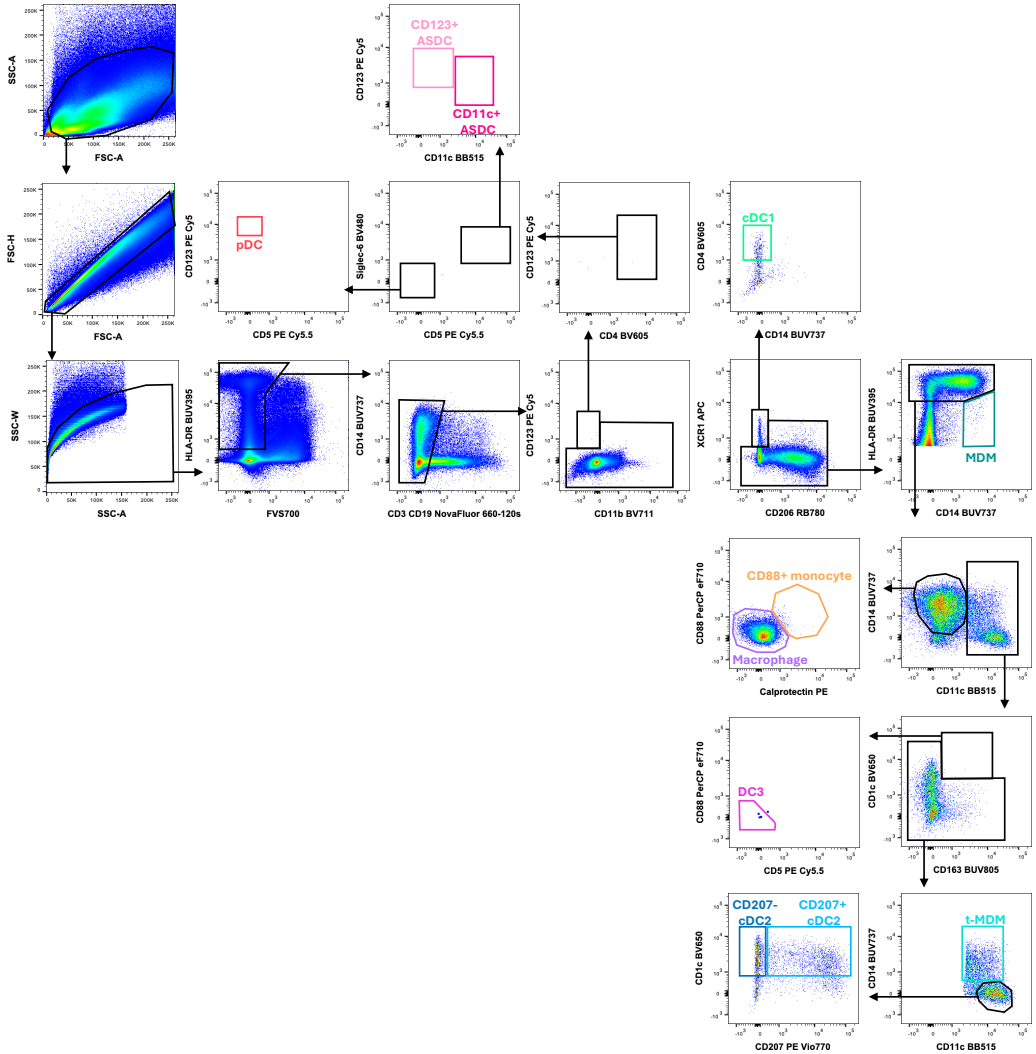

Supplementary figure 3.11: Complete gating strategy of the 26-colour optimised panel identifying all known MNPs in type I mucosa

Demonstrated by colon LP using either **a)** acquisition compensation or **b)** autofluorescent corrected compensation. All gates downstream of cDC1 identification differ to those of skin and type II mucosa due to the presence of different cell populations, particularly monocyte and macrophage populations. Cells were freshly processed and isolated from the tissue, stained and acquired on a BD FACSymphony A5. A comprehensive description of gating can be found in **Figure 3.1.**

Chapter 4. Defining Homeostatic and Inflammatory Mononuclear Phagocytes in Human Genital Skin and Mucosa and Investigating their Early Interactions with HIV

This chapter investigates the expression profiles of mononuclear phagocytes (MNP) that reside in human genital tissue, utilising the flow cytometry panel described in **Chapter 3**. The proportion of specific MNP subsets present as well as their differential surface marker profiles were determined between tissue type (skin vs mucosa) and inflammatory status (uninflamed vs inflamed). Vaginal MNPs were assessed for their expression of HIV binding receptors (CD4, MR, Siglec-1, DC-SIGN, langerin) and HIV uptake ability. Fundamentally, this research aims to contextualise the current definitions of MNPs in human genital tissue. All experiments, analysis and writing for this chapter were completed by this author with minor help from Oscar Dong for initial processing of IMC images generated and Daniel Buffa for H&E staining.

4.1 Introduction

Adolescent girls and young women, particularly in sub-Saharan Africa, have a disproportionate risk of acquiring HIV via sexual transmission. In 2024, 63% of new HIV infections in sub-Saharan Africa were borne by women, with the infection prevalence in young women three times higher than their male counterparts (UNAIDS, 2025, UNICEF, 2024). A number of socioeconomic circumstances contribute to this high incidence, such as poor education (De Neve et al., 2015), sexual violence (Kuchukhidze et al., 2023) and lack of access to health services (Gutiérrez and Trossero, 2021). Biological factors further compound this vulnerability including specific anatomical features of the female genital tract (FGT) (Chersich and Rees, 2008), and specific cervicovaginal immune cell compositions and microbiota (Atashili et al., 2008). However, there remains a limited scientific understanding of the early events of HIV transmission across genital mucosa. The precise immunological mechanisms and immune cell populations that first interact with HIV is incompletely defined and complicated by the ever-evolving cell classifications, especially mononuclear phagocytes (MNP). Access to human tissue also remains a significant barrier to this field of research.

Critically, the transmission of HIV across an inflamed mucosa significantly increases the risk of acquisition in both male and female genital tracts (Masson et al., 2015, Esra et al., 2016). Sexually transmitted infections (STI), bacterial vaginosis (BV) and penile anaerobic bacteria are prominent drivers of mucosal inflammation (Laga et al., 1993, Masson et al., 2014, Liu et al., 2017) and highly prevalent in sub-Saharan African

communities (Michalow et al., 2025, Bukusi et al., 2006). A host of HIV target cells reside within the genital tissue. Inflammation is thought to: **1)** disrupt the epithelial barrier, allowing greater access to underlying target cells (Arnold et al., 2016); **2)** induce phenotypical changes that increase susceptibility of resident cells to HIV (Said and Weindl, 2015, Qin et al., 2012); **3)** promote an influx of additional target cells (Li et al., 2009, Shang et al., 2017). However, inflammation is a highly complex, multi-faceted process making research challenging, meaning the innate immune cell landscape in inflamed tissues remain poorly defined. Thus, the mechanisms driving heightened HIV acquisition in inflamed tissues is still poorly understood. Perhaps most alarming are the recent findings that pre-exposure prophylaxis (PrEP), the principal HIV preventative treatment, can be ineffective in an inflamed cervicovaginal mucosa (McKinnon et al., 2018, Klatt et al., 2017). These observations highlight the urgent need to investigate HIV target cells in both steady-state and inflamed genital mucosa, particularly within the FGT, to advance understandings of the early events of HIV capture and inform the development of improved PrEP regimes.

The HIV target cells that occupy genital mucosa include MNPs, comprising of dendritic cells (DC), Langerhans cells (LC), macrophages and monocytes. These classes of MNPs can be further categorised into an ever-increasing array of subsets, that can be defined by their unique transcriptional and protein surface expression profiles and well as their functions. According to the most recent literature, MNPs comprise a single LC subset, cDC1, cDC2, DC3, monocyte-derived DC (MDDC), tissue resident macrophage and monocyte-derived macrophage (MDM) (Villani et al., 2017, Dutertre et al., 2019, Rhodes et al., 2021, Bujko et al., 2018). Several inflammatory populations have also been identified including plasmacytoid DCs (pDC) and two subsets of Axl^+ Siglec-6^+ DCs (ASDC) (Villani et al., 2017, Warner van Dijk et al., 2024). All MNPs are antigen presenting cells (APC), responsible for sampling invading pathogens and interacting with T cells to trigger an adaptive immune response. As CD4 T cells are the primary HIV target cells, MNPs play a significant role in HIV transmission by capturing the virus and then transferring it to CD4 T cells which can occur via two different mechanisms. **1)** First-phase transfer involves HIV binding to lectin receptors on the MNP surface triggering rapid internalisation into virus-containing compartments which occurs independent of MNP infection (Turville et al., 2002). The HIV virion is then passed to a CD4 T cell via a virological synapse. **2)** Second-phase transfer occurs

when HIV infects the MNP, mediated by binding to the HIV entry receptor CD4 and co-receptor CCR5. This leads to fusion of the viral envelope with the host cell membrane to release the viral capsid (containing the HIV genome) into the host cell resulting in productive HIV infection and *de novo* synthesis of virions (Jolly et al., 2004).

Known HIV binding lectin receptors include Manose Receptor (MR) (CD206), DC-SIGN (CD209), Siglec-1 (CD169) and langerin (CD207). Each MNP population has a unique profile of lectin receptor expression, which underlies their differential HIV uptake capability. However, studies that have explored HIV uptake within the FGT remain limited. Furthermore, there is a notable gap in the comprehensive characterisation of MNPs in genital tissues in line with the most recent high parameter single cell analyses, such as those of Villani et al., (2017). Utilising our privileged access to human genital tissues, this study sought to expand knowledge on this interplay between genital MNPs, HIV and inflammation.

Using high parameter flow cytometry, we conducted an extensive exploration and characterisation of MNPs across human tissues that HIV encounters during sexual transmission, namely foreskin, labia, vagina and cervix. Of particular clinical relevance to the HIV epidemic in young women in sub-Saharan Africa, we focused on profiling vaginal MNPs in homeostasis and inflammation and examined their role in HIV uptake. This investigation comprised three stages: **1)** unbiased clustering and phenotyping of MNPs across all genital tissues; **2)** characterisation of inflammatory vaginal MNPs; **3)** assessment of vaginal MNP HIV binding capacity. We identified 15 MNP populations that were highly heterogenous across genital tissues, differing in frequency and surface protein expression profiles. Some fit within the current MNP subset definitions and some were novel. Within the vagina, four macrophage populations were distinguished by maturation status, including monocytic, transitionary and tissue resident, and $CD14^+$ MNPs were defined within the epithelium. In inflammation, ASDCs, pDCs and $CD123^+$ $CD1a^+$ Inflammatory DCs emerged, accompanied by an influx of MDMs and epithelial $langerin^+$ cDC2s. Macrophage populations expressed the greatest amount of Siglec-1, DC-SIGN and MR and were consequently the most efficient HIV binders after 2 hours of exposure. Notably, MDMs may represent a key inflammatory HIV binding population, given their increased abundance in inflammation and high capacity to capture HIV.

4.2 Methods and Materials

4.2.1 Reagents

Table 4.1: Flow cytometry antibodies

Marker	Fluorochrome	Clone	Company	Volume / 2.5 x 10^6 cells in 100 µL
HLA-DR	BUV395	G46-6	BD Biosciences	1.5
CD16	BUV496	3GB	BD Biosciences	2.5
Siglec-1	BUV615	7-239	BD Biosciences	2
CCR7	BUV661	2-L1-A	BD Biosciences	5
CD14	BUV737	B-ly6	BD Biosciences	1
CD163	BUV805	GHI/61	BD Biosciences	2
DC-SIGN	BV421	DCN46	BD Biosciences	2.5
Siglec-6	BV480	767329	BD Biosciences	1
CD1a	BV510	HI149	BD Biosciences	1
CD4	BV605	OKT4	Biolegend	4
CD1c	BV650	F10/21A3	BD Biosciences	3
CD11b	BV711	ICRF44	Biolegend	2
CD141	BV711	1A4	BD Biosciences	2.5
Axl	BV785	108724	BD Biosciences	2.5
CD11c	BB515	B-ly6	BD Biosciences	1.5
	PE CF594	B-ly6	BD Biosciences	2.5
CD3	NovaFluor Blue 660-120S	UCHT1	ThermoFisher scientific	0.5
CD19	NovaFluor Blue 660-120S	HIB19	ThermoFisher scientific	2.5
CD88	PerCP eFluor710	20/70	ThermoFisher scientific	2.5
MR	RB780	19.2	BD Biosciences	0.5
Calprotectin	PE	MAC387	ThermoFisher scientific	4
CLEC9A	PE	8F9	Miltenyi Biotec	5
CD103	PE Vio615	REA803	Miltenyi Biotec	2.5
	APC	REA803	Miltenyi Biotec	2.5
CADM1	FITC	3E1	MBL International Corporation	5
CD54	FITC	84H10	Beckman Coulter	2
CD123	PE-Cy5	6H6	Biolegend	0.5
CD5	PE-Cy5.5	CD5-5D7	ThermoFisher scientific	0.5
Langerin	PE Vio770	REA770	Miltenyi Biotec	1
XCR1	APC	S15046E	Biolegend	4
	BV421	S15046E	Biolegend	4
	PE Dazzle594	ZET	Biolegend	6
Viability	FVS700	N/A	BD Biosciences	0.01
SIRPα	APC Fire750	SE5A5	Biolegend	3
Intracellular stain				
p24	APC	2B87	MediMabs	1
	PE	KC57	Beckman Coulter	1

Table 4.2: Imaging mass cytometry antibodies

Marker	Conjugate	Clone	Company	Concentration (µg/mL)
Non-metal tagged antibodies for indirect detection				
FOXP3	Biotin	263A/E7	Invitrogen	20
Langerin	Cy3	Polyclonal	R&D Systems	10
CD69	Cy5	EPR21814	Abcam	5
Metal tagged antibodies				
α-SMA	89Y	1A4	R&D Systems	1
CD20	141Pr	H1	BD Biosciences	4
CD45RO	142Nd	UCHL1	BD Biosciences	2
CD45RA	143Nd	HI100	BioLegend	2
FITC	144Nd	FIT-22	BioLegend	8
E-cadherin	145Nd	36/E-Cadherin	BD Biosciences	8
CD8	146Nd	D8A8Y	CST	2
Podoplanin	147Sm	Polyclonal	R&D Systems	0.5
CD38	148Nd	240726	R&D Systems	2
IL-17	149Sm	Polyclonal	R&D Systems	4
CD163	150Nd	Polyclonal	Proteintech	4
Cy3	152Sm	A-6	SCBT	10
MPO	153Eu	E1E7I	CST	8
CD45	154Sm	D9M8I	CST	3
CD31	155Gd	EPR3094	Abcam	4
CXCR3	156Gd	49801	Abcam	0.1
Axl	158Gd	Polyclonal	R&D Systems	4
CCR7	159Tb	EPR23192-57	Abcam	4
CD14	160Gd	EPR3653	Abcam	0.5
FXIIIa	161Dy	Polyclonal	Affinity Biologicals	0.2
CCR6	162Dy	EPR22259	Abcam	2
CD11b	163Dy	EPR1344	Abcam	2
Biotin	164Dy	1D4-C5	BioLegend	10
Na^+/K^+-ATPase	165Ho	EP1845Y	Abcam	8
CD11c	167Er	2F1C10	Proteintech	4
Ki-67	168Er	Polyclonal	R&D Systems	1
Cy5	169Tm	CY5-15	Sigma-Aldrich	10
CD3	170Er	Polyclonal	Agilent Dako	6
CD1c	171Yb	OTI2F4	Novus Biologicals	4
Siglec-1	172Yb	5F1.1	Sigma-Aldrich	4
CD4	173Yb	EPR6855	Abcam	4
HLA-DR	174Yb	EPR3692	Abcam	0.2
CD303	175Lu	Polyclonal	R&D Systems	2
CXCR5	176Yb	EPR23463-30	Abcam	2

4.2.2 Identification of Human Genital Mononuclear Phagocyte Subsets

4.2.2.1 Human Genital Tissue

This study was approved by the Western Sydney Local Area Health District (WSLHD) Human Research Ethics Committee (HREC) with reference number (4192) AU RED HREC/15 WMEAD/11. Human genital tissues were collected from gynaecology, urology and plastic surgeons from hospitals across Sydney, including Westmead Public Hospital, Westmead Private hospital, Sydney Adventist Hospital and Nepean Private Hospital in Sydney. Sample processing began immediately after collection, which was within one hour of their surgical removal.

4.2.2.2 Genital Tissue Processing, Enzymatic Digestion, and Flow Cytometry Staining and Acquisition

All genital tissues were processed as described in both **Chapter 2 and 3**, **sections 2.4.5.2** and **3.3.8.5**. Ficoll-Paque enrichment was only performed on epidermal cells of outer foreskin and labia.

Unless otherwise stated all samples and compensation controls were stained according to the panel in **Chapter 3**, **Supplementary table 3.2** and **Supplementary table 3.5**, excluding the marker KI67 DyLight800. The staining protocol was performed as described in **section 3.3.8.6**. All follow cytometry data in this chapter was acquired on the BD FACSymphony with BD FACSDiva software and analysed using Flow Jo v10.10.0 (BD Biosciences).

For the comparison of cDC1 defining markers in vaginal tissue, cells were stained using the panel described in **Table 4.3.**

Table 4.3: cDC1 phenotype panel

Marker	Fluorochrome	Volume / 2.5 x 10^6 cells in 100 µL	Compensation beads	Optimal volume on beads (µL / 50µL)
HLA-DR	BUV395	1.5	BD CompBeads Plus Anti-Mouse Ig (P)	1
CD16	BUV496	2.5	P	1
Siglec-1	BUV615	2	P	1
CD163	BUV805	5	P	1
CLEC9A	PE	5	Used Calprotectin PE P	0.5
CD5	PE Cy5.5	2	P	0.5

Langerin	PE Vio770	2.5	P	1
CADM1	FITC	5	Used CD54 FITC P	1
CD3	NovaFluor Blue 660-120S	1	P	0.8
CD19	NovaFluor Blue 660-120S	1	CD3 antibody used for compensation	N/A
CD88	PerCP eFluor710	4	P	1
MR	RB780	3	P	0.4
Siglec-6	BV480	2	P	0.5
XCR1	BV421	4	Slingshot SpectraComp	1.3
CD1a	BV510	2.5	P	1.3
CD4	BV605	1.5	P	0.8
CD1c	BV650	0.5	P	1
CD141	BV711	2.5	Used CD11b BV711 P	0.5
Axl	BV785	2.5	P	0.5
CCR7	BUV661	2.5	BD CompBeads Normal Anti-Mouse Ig (N)	1
CD14	BUV737	0.5	N	1
CD123	PE Cy5	0.5	N	0.5
CD11c	PE CF594	2.5	N	1
CD103	APC	2.5	Used XCR1 APC SpectraComp	1.3
Viability	FVS700	0.01	Arc Amine Reactive Compensation Bead Kit	1
SIRPα	APC Fire750	3	P	1

4.2.3 Unbiased Clustering Analysis of Human Genital Mononuclear Phagocyte Subsets

The OMIQ (Domatics, www.omiq.ai, www.dotmatics.com) online analysis platform was used to perform unbiased clustering analysis of flow cytometry data. All samples were first compensated for autofluorescent correction using Flow Jo, as described in **section 3.3.7**. Samples and modified compensation matrices were then imported into OMIQ. Following OMIQ's in-built workflow, all samples underwent *scaling*, *gating* and *subsampling* to gate and isolate the cells of interest. *CyCombine* was used for normalisation (Pedersen et al., 2022), *opt-SNE* for dimensionality reduction (Belkina et al., 2019) and *PhenoGraph* for clustering (Levine et al., 2015). All further visualisation and heatmap functions used were embedded features of OMIQ.

4.2.4 Imaging Mass Cytometry Staining, Imaging and Analysis

Imaging Mass Cytometry (IMC) staining and imaging were performed as described in **section 2.4.6**. Vaginal samples were stained using the panel outlined in **Table 4.2** – this panel has since been published as an OMIP in Cytometry A (Hu et al., 2024). Image analysis was performed using ImageJ (Fiji - 2.16.0/1.54p).

4.2.5 Haematoxylin and Eosin Staining and Analysis

Haematoxylin and Eosin (H&E) stationing was used to inform the inflammatory status of vaginal samples. Samples were fixed in 4% paraformaldehyde (Electron Microscopy Science), embedded in paraffin wax, sectioned to 7 µm thickness and slide mounted. Slides were placed under running water for 2 minutes, then dipped 10 times and placed in Haematoxylin for 15 minutes. The slides were blotted dry, washed for another two minutes in running water, dipped in alcohol 3 times, and washed again for 2 minutes. The slides were next stained in Scott's blue for 2 minutes then washed in running water for 2 minutes. Uniformity of staining was checked under a light microscope. Slides were then submerged in 70% alcohol for 1 minute and immediately dipped in eosin 10 times. Following this, slides were serially dipped in three trays containing 70% ethanol to stop the eosin stain. This was performed 6-12 times depending on the staining intensity. The slides were air dried then dipped in Xylene 3 times, each for 5 minutes, then mounted and cover-slipped using Ultra Mount No.4 Permanent Mounting (Thermo Scientific). Once dried, slides were imaged at 40x magnification on the Olympus VS200 Slide scanner.

The images were then processed using ImageJ to create a 60 µm region of interest (ROI) band in the most distal regions of the lamina propria (LP) (bordering the epithelium). The images and ROI were then further analysed using QuPath (0.6.0-arm64). The cells within the ROI (60 µm band) were counted and totalled per sample using QuPath's automated cell detection software for H&E staining. The area of the ROI was calculated via converting pixels to µm at a conversion rate of 6.1418 pixels/µm - the microscope's standard conversion for 40x magnification. Thus, the cells per μm^2 was calculated by dividing the total cells within the ROI by the total area of the ROI.

4.2.6 Generation of HIV_{BaL} Stocks

Stocks of the HIV-1_{BaL} virus was prepared as described in the Bertram et al. (2019) study. In brief, HEK293T cells, seeded at 16 x 10^6 cells/20 mL per T150 flask (Becton Dickinson, Franklin Lakes, NJ, USA), were cultured in Dulbecco's Modified Eagle Medium (DMEM; Lonza) supplemented with 10% fetal bovine serum (FBS; Lonza). The following day, cells were transfected with 80 µg of plasmid DNA encoding the laboratory-adapted HIV-1_{BaL} strain (pWT/BaL, contributed by Dr. Bryan R. Cullen, NIH AIDS Research and Reference Reagent Program), and suspended in a solution of 15 mL DMEM with 10% FBS, 128 µL 2 M $CaCl_2$, 1 mL (1 mMTris,0.1 mM EDTA, pH8.0), 1 mL Hepes-buffered saline (280 mM NaCl, 50 mM HEPES, pH7.1), 10 µL 0.15 M Na_2HPO_4 (pH 7.1) – all from Sigma-Aldrich. Cells were incubated for 18 h, after which the transfection medium was replaced with DMEM + 10% FBS and cultures were maintained for a further 48 hours. The media was collected into 50 mL falcon tubes and centrifuged at 1600g for 20 minutes. The supernatant was concentrated using 300,000 molecular weight cut-off Vivaspin 20 filters (Sartorius, Göttingen, Germany), centrifuged at 3000g until reduced to 1 mL/filter. To deplete contaminating $CD45^+$ microvesicles, HIV-1_{BaL} supernatant was incubated with CD45 magnetic microbeads (Miltenyi Biotech) at a 9:1 ratio (supernatant:beads) for 2 hours at room temperature, then filtered through LS separation columns (Miltenyi Biotech) to collect the CD45-depleted HIV-1_{BaL}. The CD45-depleted virus was further concentrated by ultracentrifugation. Samples were resuspended in PBS and underlaid with 1 mL of 20% sucrose prior to centrifugation at 100,000g for 90 minutes at 4°C (Beckman Optima XL-100 K Ultracentrifuge with 70Ti rotor). Viral pellets were resuspended in PBS, aliquoted into cryovials, and stored at −80 °C. Viral infectivity was assessed using TZMBL cells (NIH AIDS Research and Reference Reagent Program, contributed by John Kappes and Xiaoyun Wu). The 50% tissue culture infectious dose ($TCID_{50}$) was calculated from LTR β-galactosidase reporter gene expression following a single round of infection, with titres consistently in the range of 10^7 – 10^8 $TCID_{50}$/mL.

4.2.7 HIV Uptake Assay

Liberated vaginal cells with a yield > 5 x 10^6 cells underwent CD45 positive magnetic selection on LS columns to reduce the virus quantities required. For smaller samples (2-5 x 10^6 cells), $CD45^+$ selection was omitted to preserve cell numbers. 5 x 10^5 $CD45^+$ cells or 1-2 x 10^6 unselected cells were then resuspended in DC Culture media,

exposed to HIV-1_{BaL} at an MOI of 5 and incubated at 37°C for 2 hours. Cells were then washed 3 times with DPBS and stained with the FACSymphony uptake panel (**Table 4.4**). Intracellular p24 staining was performed the following day. Samples were permeabilised with 100 µL of BD Cytofix/Cytoperm for 15 minutes at room temperature, then washed with Perm Wash. Cells were then blocked with 10% human AB serum and 3.4 µL oligoblock for 10 minutes, followed by dual staining of HIV p24 clones KC57 and 28B7 and incubation for 30 minutes at room temperature. Cells were washed twice with Perm wash, fixed with BD Cytofix and washed once with FACS wash.

Table 4.4: MNP phenotype and HIV uptake panel

Marker	Conjugation	Volume / 2.5 x 10^6 cells in 100 µL	Compensation beads	Optimal volume on beads (µL / 50µL)
HLA-DR	BUV395	1.5	BD CompBeads Plus Anti-Mouse Ig (P)	1
CD16	BUV496	2.5	P	1
Siglec-1	BUV615	2	P	1
CD163	BUV805	5	P	1
p24	PE	1	Used Calprotectin PE P	0.5
CD5	PE Cy5.5	2	P	0.5
Langerin	PE Vio770	2.5	P	1
CD3	NovaFluor Blue 660-120S	1	P	0.8
CD19	NovaFluor Blue 660-120S	1	CD3 antibody used for compensation	N/A
CD88	PerCP eFluor710	4	P	1
MR	RB780	3	P	0.4
Siglec-6	BV480	2	P	0.5
CD1a	BV510	2.5	P	1.3
CD4	BV605	1.5	P	0.8
CD1c	BV650	0.5	P	1
Axl	BV785	2.5	P	0.5
CCR7	BUV661	2.5	BD CompBeads Normal Anti-Mouse Ig (N)	1
CD14	BUV737	0.5	N	1
DC-SIGN	BV421	4	N	1
CD11b	BV711	2.5	N	1
CD11c	BB515	0.5	N	1
CD123	PE Cy5	0.5	N	0.5
XCR1	PE Dazzle594	6	Slingshot SpectraComp	1.3
P24	APC	1	Used XCR1 APC SpectraComp	1.3
Viability	FVS700	0.01	Arc Amine Reactive Compensation Bead Kit	1

4.2.8 Statistical Analysis

GraphPad Prism 10 was used to create graphs and perform statistical analysis. When normalised distribution could not be assumed, due to donor variability, statistics were calculated using un-paired, non-parametric Mann-Whitney t tests. For grouped data, a repeated measure one-way analysis of variance (ANOVA) or mixed-effects analysis with Tukey's Multiple Comparisons was conducted. Results were considered statistically significant when $p \leq 0.05$. for all tests; *$p < 0.05$, **$p < 0.01$, ***$p < 0.001$.

4.3 Results

4.3.1 Obtaining and Processing Human Genital Skin and Mucosa for Immunophenotyping of Tissue Immune Cells using Flow Cytometry

Investigating the MNPs in human genital tissues is crucial to understanding the early events of sexual transmission of HIV and is much more biologically relevant than MNPs derived from blood, which many previous studies have focussed on. For this study we obtained tissues from the male and female genital tracts: foreskin; labia; vagina; cervix. Foreskins were acquired from circumcisions, labia tissue from labiaplasty procedures, vaginal tissue from vaginal prolapse surgeries and cervical tissue from hysterectomy procedures. All human tissues processed and analysed for this study are summarised in **Table 4.5**, including donor number and age.

A significant challenge when immunophenotyping tissue immune cells using flow cytometry is extracting the cells from tissue and maintaining their immature, tissue resident state and maximise cell yield. This hinges on several key factors: **1)** timing of the collection and processing of the tissue; **2)** sufficient tissue thinning and meshing; **3)** choice of digestion enzymes. To reduce cell hypoxia and minimise activation and maturation of the cells, it was vital the tissue was collected and processed soon after removal from the body, typically within 15 minutes – 2 hours. Removing excess connective tissue by thinning the tissue to approximately 3 mm thick and 'meshing' the sample with scalpel cuts was critical to ensure the digestion enzyme dispase completely permeated the sample. This was particularly important for more fibromuscular tissues like the cervix. Lastly, different brands and lots of digestion enzymes can cause surface marker cleavage and poor cell yields. We have previously demonstrated Worthington's Neutral Protease NPRO2 (partially purified dispase) to most successfully preserve the surface expression of HIV entry receptors CD4, CCR5 and CXCR4 on immune cells (**Supplementary figure 4.1**) (Jake Rhodes PhD Thesis, 2020) and that type IV collagenase best preserves the majority of relevant surface marker expression and yields high cell numbers in skin (Botting et al., 2017).

Table 4.5: Overview of tissue donors

Tissue	Donor number	Age	Reason for surgery
Foreskin	1	6	Circumcision
	2	11	
	3	19	
	4	12	
Labia	1	N/A	Labiaplasty
	2	N/A	
	3	31	
Vagina	1	72	Vaginal prolapse
	2	88	
	3	N/A	
	4	78	
	6	83	
	7	63	
	8	69	
	9	45	
	10	70	
	11	61	
	12	62	
	13	71	
	14	66	
	15	72	
	16	N/A	
	17	56	
	18	71	
Cervix	1	47	Hysterectomy
	2	49	
	3	35	

Figure 4.1 illustrates our optimal tissue processing workflow for isolating cells from fresh human genital tissue, including thinning and meshing the tissue to increase surface area for enzymatic absorption, an overnight dispase digestion and 120-minute collagenase type IV digestion.

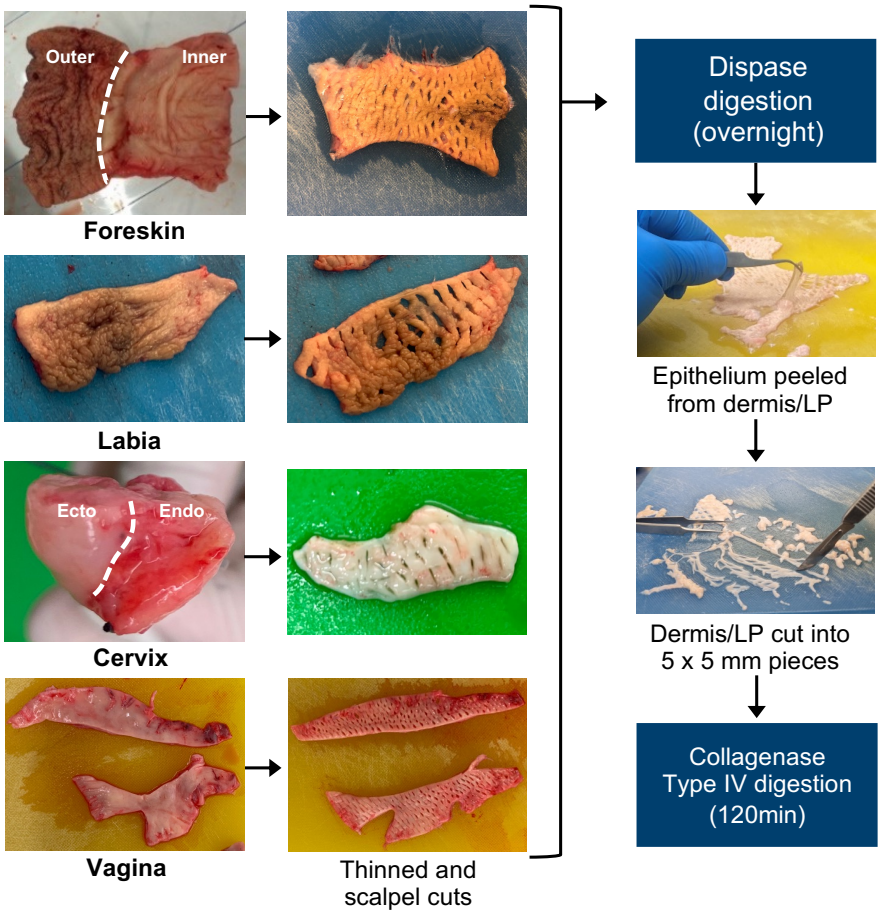

Figure 4.1: Processing human genital tissue

Human genital tissues were obtained from surgeries and processed with 15 minutes – 2 hours of their removal from the body. Excess connective tissue was removed, and scalpel cuts were used to 'mesh' the sample. The sample was then incubated overnight at 4°C in a dispase solution. The next day, the epithelium was mechanically separated from the underlying dermis/LP, then incubated with type IV collagenase at 37°C for 2 hours, liberating the immune cells from the tissue.

4.3.2 Unbiased High Dimensionality Clustering of Mononuclear Phagocytes from Human Genital Tissue

4.3.2.1 Data Selection and Cleaning

To investigate the MNP populations in genital skin and mucosa, samples were stained with the FACSymphony panel detailed in **Chapter 3**, **Supplementary table 3.2**, omitting the marker KI67 biotin Streptavidin DyLight800 as it was a more complex two-step intracellular staining procedure and had contributed little phenotypic information in previous trial panel runs. From the samples listed in **Table 4.5**, the epithelium and underlying dermis/LP from four foreskins, four vaginas, two labias and three cervixes were selected to perform an unbiased high dimensionality reduction and clustering analysis. These samples were chosen for clustering owing to their high cell numbers

and clean compensation. MNPs were gated as live (FVS700$^-$), single, CD3$^-$ CD19$^-$ HLA-DR$^+$ cells, excluding CD11b$^-$ CD123^{int} CD4$^-$ cells using the Boolean OR gate (**Figure 4.2**) to ensure the inclusion of the CD123$^+$ CD4$^+$ pDCs and ASDCs. This 'clean' population of cells underwent dimensionality reduction which was performed and visualised using optimised t-Distributed Stochastic Neighbour Embedding (opt-SNE) (Belkina et al., 2019).

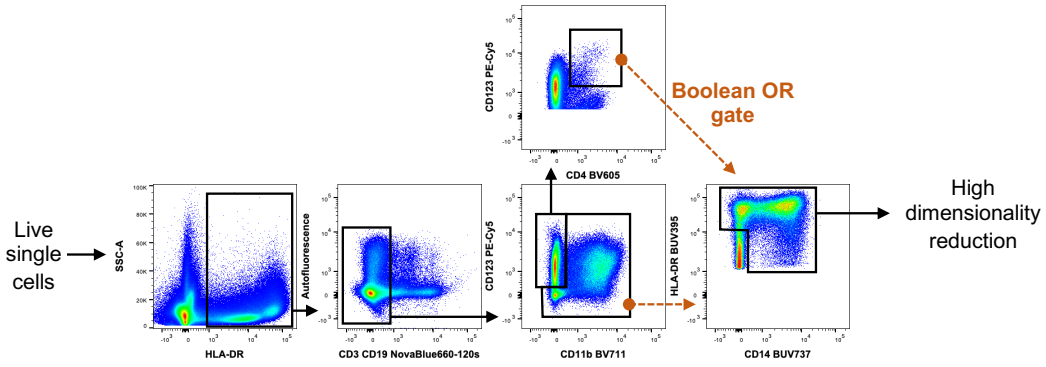

Figure 4.2: Gating strategy to isolate population of interest for dimensionality reduction

Cells were isolated from genital tissue using techniques described in **section 4.2.2.2** and stained with the flow cytometry panel outlined in **Supplementary table 3.2**. A population of interest was gated for each foreskin, labia, vagina and cervix sample included in the dimensionality reduction and clustering analysis. Representative gating on a vaginal sample demonstrates isolation of T and B cells, HLA-DR$^-$ cells and other non-MNPs. The resultant population was comprised of live, single, HLA-DR^{hi}, CD3$^-$, CD19$^-$ cells. A Boolean OR gate was used to ensure the inclusion of CD123$^+$ CD4$^+$ pDCs and ASDCs and exclusion of CD11b$^-$ CD123^{int} CD4$^-$ non-MNPs.

4.3.2.2 Batch Normalisation

CyCombine (Pedersen et al., 2022), the most current single-cell batch normalisation method for cytometry datasets, was utilised to correct for any non-biological variations between samples. This step was particularly crucial for ensuring the different donors and tissue types integrated and clustered based on differential marker expression and not biological similarities. Although some individual donors remained distinct, the contrast between no correction and batch correction is evident (**Figure 4.3a**). The distribution of the different tissue types (outer foreskin, labia, inner foreskin, vagina, ectocervix and endocervix) and different tissue compartments (skin epidermis and dermis, and mucosa epithelium and LP) were also visualised (**Figure 4.3b&c**) to confirm integration of datasets.

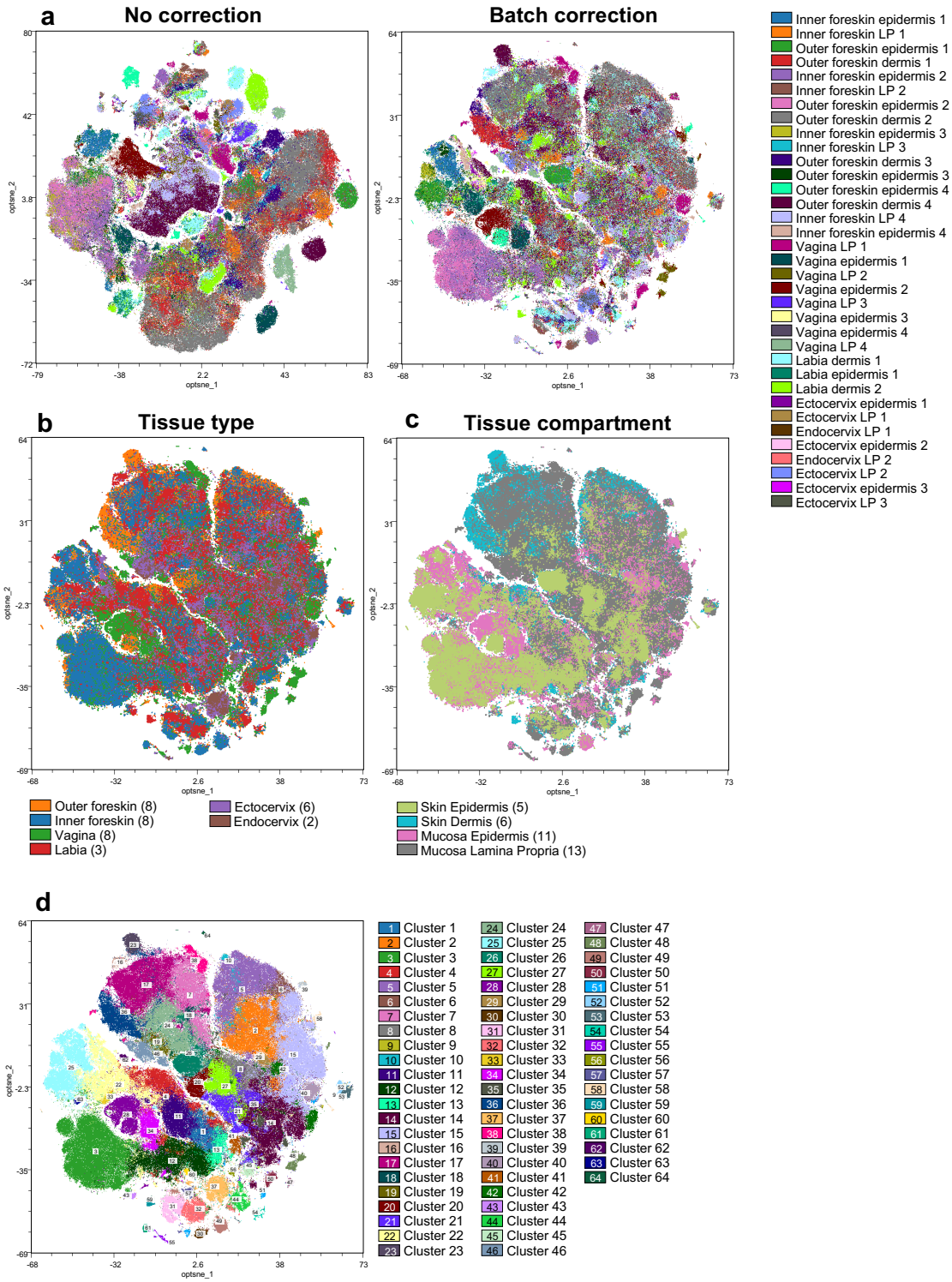

Figure 4.3: High dimensionality reduction of human genital tissues

The gated populations of interest from outer foreskin (n=4) epidermis and dermis, inner foreskin (n=4) epithelium and LP, vagina (n=4) epithelium and LP, labia epidermis (n=1), labia dermis (n=2), ectocervix (n=3) epithelium and LP, and endocervix (n=2) LP underwent high dimensionality reduction and visualised using opt-SNE. **a)** The normalisation algorithm CyCombine was used to correct for batch discrepancies between donors and tissues. The poor integration of donors before normalisation (left) is distinct to the more even dispersal of donors after correction (right). To confirm this even distribution, samples were visualised according to their **b)** tissue types (outer foreskin, labia, inner foreskin, vagina, ectocervix and endocervix) and **c)** tissue compartments (skin epidermis and dermis, and mucosa epithelium and LP). **d)** 64 distinct cell clusters were identified after using the clustering algorithm PhenoGraph and manual sub-clustering (see **Supplementary figure 4.5**).

4.3.2.3 Unsupervised Clustering

PhenoGraph (Levine et al., 2015) was used to perform unsupervised clustering analysis for its capacity to produce precise, coherent and robust clustering results (Liu et al., 2019). PhenoGraph was selected over the alternative high performing unsupervised tool, FlowSOM (Van Gassen et al., 2015), owing to its superior ability to identify and group cell diversity, and hence able to identify small, rare cell populations. FlowSOM requires an arbitrary number of predetermined clusters which limits exploratory population investigation – a central node of this research. Exclusion markers FVS700, to gate out dead cells, and CD3 CD19 NovaBlue660-120s, to gate out T and B cells, were not included in the clustering analysis.

PhenoGraph initially identified 34 distinct clusters (**Supplementary figure 4.2a**). 21 of those clusters were further subclustered either based on an obvious separation in dispersal of cells across the opt-SNE (**Supplementary figure 4.2b**) or a distinct divide in marker expression (one half of the cluster expressed a marker whilst the other half did not) (**Supplementary figure 4.2c**). The new clustering resolved 64 discrete clusters (**Figure 4.3d**). A summary of the initial PhenoGraph clusters split, number of resulting clusters, reason for split and new cluster numbers are detailed in **Supplementary table 4.1**. It should be noted that the 64 identified clusters do not correlate to 64 discrete MNP subsets, it refers to 64 different groups of cells based on their unique expression profiles.

A clustered heatmap of marker expression across all 64 clusters was generated (**Supplementary figure 4.2d**) and any clusters with similar expression profiles, no distinctive distinguishing markers and in close proximity on the opt-SNE were merged (**Supplementary table 4.2**). The final resulting PhenoGraph comprised 38 unique clusters (**Figure 4.4a**).

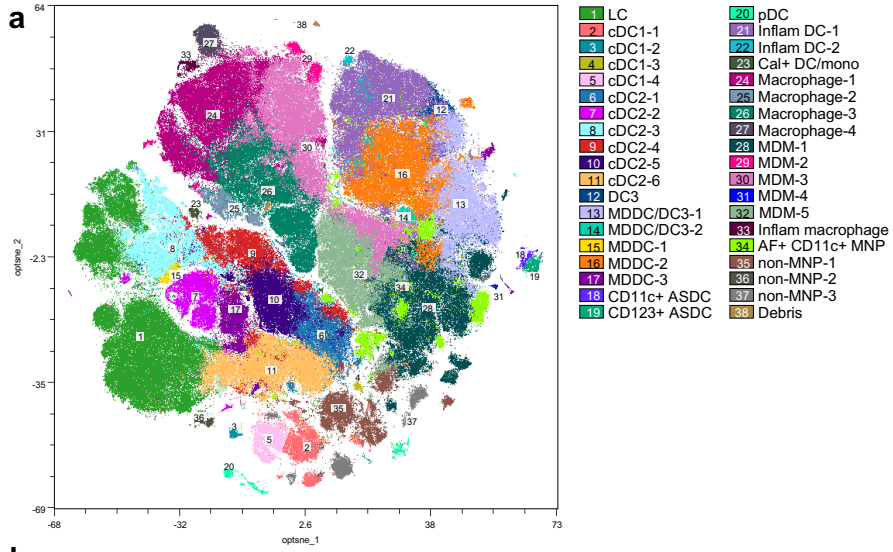
a
optsne_1
optsne_2
1 LC
2 cDC1-1
3 cDC1-2
4 cDC1-3
5 cDC1-4
6 cDC2-1
7 cDC2-2
8 cDC2-3
9 cDC2-4
10 cDC2-5
11 cDC2-6
12 DC3
13 MDDC/DC3-1
14 MDDC/DC3-2
15 MDDC-1
16 MDDC-2
17 MDDC-3
18 CD11c+ ASDC
19 CD123+ ASDC
20 pDC
21 Inflam DC-1
22 Inflam DC-2
23 Cal+ DC/mono
24 Macrophage-1
25 Macrophage-2
26 Macrophage-3
27 Macrophage-4
28 MDM-1
29 MDM-2
30 MDM-3
31 MDM-4
32 MDM-5
33 Inflam macrophage
34 AF+ CD11c+ MNP
35 non-MNP-1
36 non-MNP-2
37 non-MNP-3
38 Debris

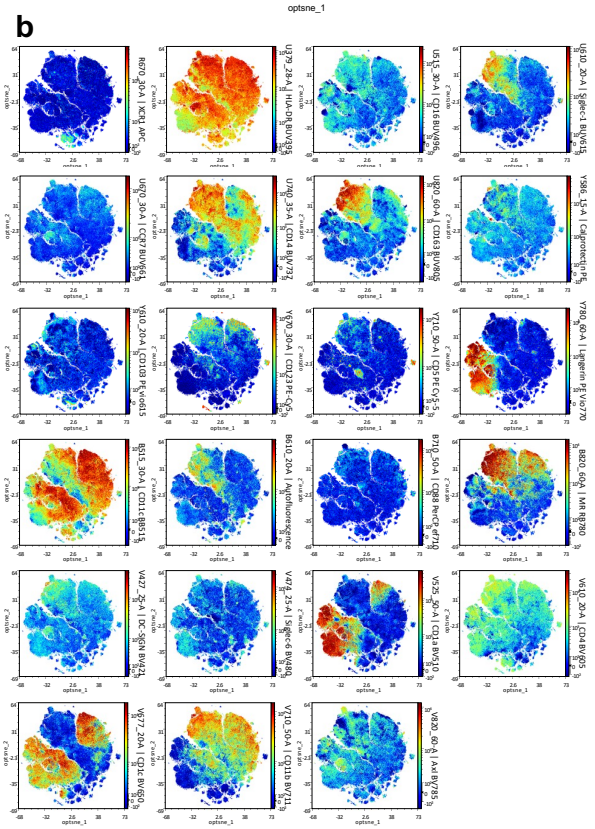
b

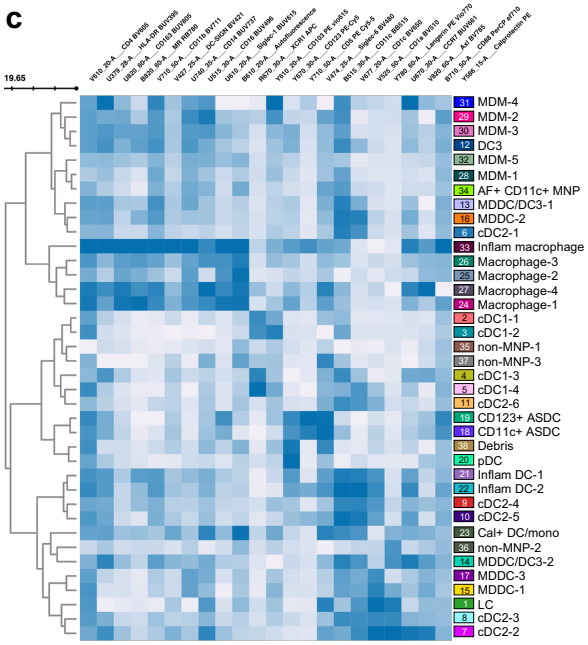
c
19.65
31 MDM-4
29 MDM-2
30 MDM-3
12 DC3
32 MDM-5
28 MDM-1
34 AF+ CD11c+ MNP
13 MDDC/DC3-1
16 MDDC-2
6 cDC2-1
33 Inflam macrophage
26 Macrophage-3
25 Macrophage-2
27 Macrophage-4
24 Macrophage-1
2 cDC1-1
3 cDC1-2
35 non-MNP-1
37 non-MNP-3
4 cDC1-3
5 cDC1-4
11 cDC2-6
19 CD123+ ASDC
18 CD11c+ ASDC
38 Debris
20 pDC
21 Inflam DC-1
22 Inflam DC-2
9 cDC2-4
10 cDC2-5
23 Cal+ DC/mono
36 non-MNP-2
14 MDDC/DC3-2
17 MDDC-3
15 MDDC-1
1 LC
8 cDC2-3
7 cDC2-2

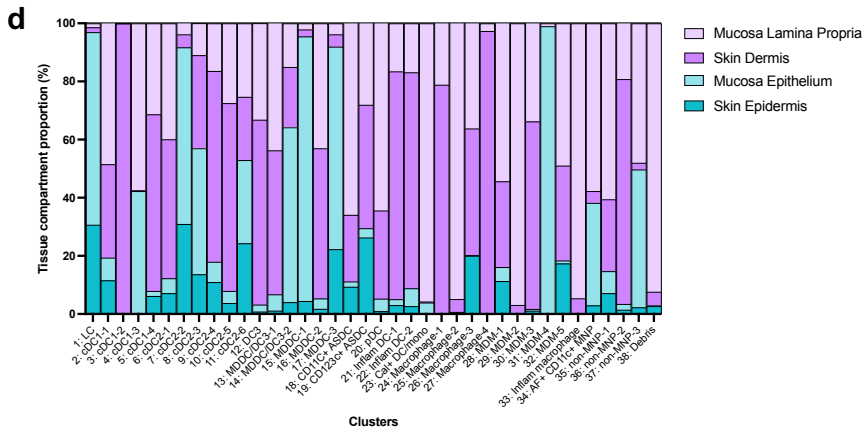
d
Tissue compartment proportion (%)
Clusters
Mucosa Lamina Propria
Skin Dermis
Mucosa Epithelium
Skin Epidermis

Figure 4.4: Identification of genital mononuclear phagocyte subsets using cluster analysis

a) opt-SNE plot of the final 38 cell clusters with their annotations. Population annotations were determined using **b)** opt-SNE heatmap distribution plots of marker expressions, **c)** average marker expression heatmap of all 38 annotated clusters, and **d)** tissue compartment proportions contributing to each cluster (skin epidermis, skin dermis, mucosa epithelium and mucosa LP).

4.3.2.4 Cluster Annotations: Identification of 34 Mononuclear Phagocyte Clusters

The cluster annotations shown in **Figure 4.4a** were defined according to the most current MNP definitions in the literature and determined from the opt-SNE heatmap expression distributions (**Figure 4.4b**), clustered heatmap expression profiles (**Figure 4.4c**) and the epithelial-dermal/LP tissue compartment proportions of each cluster (**Figure 4.4d**). Of the 38 clusters, we determined that 34 were MNP subsets. A summary of all cluster annotations, including the defining and differential markers is detailed in **Table 4.6**. Populations were defined as follows:

LC (cluster 1): $CD1c^+$ $CD1a^+$ $Langerin^+$ $CD11c^{lo}$ (Bertram et al., 2019) and predominantly within the stratified squamous epithelium (epidermis/epithelium).

DC1 (clusters 2-5): $XCR1^+$ $CD4^+$ $CD11c^+$ (Mair and Liechti, 2021). Cluster 3 was donor specific (only comprised of one donor) (**Figure 4.3**), and characterised by differential expression of CD103, while cluster 4 represented an activated cDC1, expressing CCR7 (Ohl et al., 2004). Cluster 5 expressed CD1c and low levels of CD1a – both classical cDC2 associated markers but defined as a cDC1 due to very high expression of XCR1, which is exclusive to cDC1s. It is of note that $CD1a^+$ cDC1s have been previously described in skin by Alcántara-Hernández and colleagues (2017).

DC2 (clusters 6-11): $CD11c^+$ $CD1c^+$ $XCR1^-$ $CD14^-$ $CD163^-$ AF^- (Rhodes et al., 2021). Cluster 6 was the only cDC2 population lacking CD1a, a marker increasingly thought to be associated with skin-derived DCs and inducible by epithelial factors (Alcántara-Hernández et al., 2017, van de Ven et al., 2011, Bigley et al., 2015, Lang et al., 2023, Angel et al., 2006), suggesting these may represent a population of cDC2s newly migrated from blood. Clusters 7, 8 and 11 were all epidermal/epithelial predominant populations, with 7 and 8 expressing langerin, and 7 expressing CCR7 indicative of an activated cell population. Cluster 9 was defined by expression of MR, and 10 by CD5, the latter fitting the profile of a $CD5^+$ cDC2 previously described in blood by

Bourdely et al. (2020) and Dutertre et al. (2019). Interestingly, this $CD5^+$ cDC2 population appeared less abundant in the mucosal tissues, consistent with previous observations from our lab showing a higher frequency of $CD5^+$ cDC2s in dermal skin compared to mucosal LP (**Supplementary figure 4.3**) (Freja Warner van Dijk Honours Thesis, 2021).

DC3 (cluster 12): $CD1c^+$ $CD11c^+$ $CD163^+$ $CD14^+$ $Autofluorescent^-$ (AF) (Villani et al., 2017, Dutertre et al., 2019, Bourdely et al., 2020, Cytlak et al., 2020). A clear distinguishing marker is yet to be identified for DC3s. Like cDC2s and MDDCs, DC3s express CD1c and CD11c, and like macrophages, they express CD14 and CD163. Therefore, DC3s are also likely present within other clusters. Hence, clusters 13 and 14 were deemed to be combined population of *MDDC/DC3s* ($CD1c^+$ $CD11c^+$ $CD163^{int}$ $CD14^+$ AF^-) with cluster 14 comprised of activated epithelial cells as they expressed high CCR7.

MDDC (clusters 15-17): $CD1c^+$, $CD11c^+$ and $CD14^+$ $CD163^-$ (Rhodes et al., 2021, McGovern et al., 2014). Clusters 15 and 17 were CD1a expressing epithelial MDDCs, with cluster 15 being $langerin^+$. Cluster 16 was an activated epithelial MDDC subset ($CCR7^+$).

ASDC (cluster 18 and 19): $CD5^+$ $CD123^+$ $Siglec\text{-}6^+$ with the $CD11c^+$ ASDC expressing higher levels of CD11c and $CD123^+$ ASDC expressing higher levels of Siglec-1 (Villani et al., 2017, See et al., 2017, Alcántara-Hernández et al., 2017, Warner van Dijk et al., 2024).

pDC (Cluster 20): $CD123^+$ $CD5^-$ $Siglec\text{-}6^-$.

Inflammatory DC (clusters of 21 and 22): Based on the definition of an inflammatory $CD1a^+$ $CD123^{int}$ $BDCA2^+$ activated DC population by Chen et al. (2020) in acute sterile inflammation and Tang-Huau et al. (2018) in tonsil we defined $CD123^+$ $CD1a^+$ $CD1c^+$ $CD11c^+$ $CCR7^+$ $CD14^+$ MR^+ cells as inflammatory DCs. This population could be differentiated by CD5 expression – cluster 21 $CD5^-$ and cluster 22 $CD5^+$ – correlating to a highly inflammatory skin $CD5^+$ DC population (Korenfeld et al., 2017).

DC/Monocytes (Cluster 23): $Calprotectin^+$ AF^+ $CD11c^+$ $CD1c^+$ $langerin^+$ based on the findings of (Bujko et al., 2018, Villani et al., 2017, Dutertre et al., 2019). It has been

reported that monocytes can emit low levels of AF (Knab et al., 2025), however, this is significantly lower than AF emitted by macrophages. Notably, cluster 23 was predominantly observed in a single donor and therefore requires further investigation.

Macrophages (clusters 24-27): AF^+ $CD163^+$ MR^+ Siglec-1^+ $CD14^+$ – all classical features of a tissue resident macrophage (Bujko et al., 2018). Clusters 24, 26 and 27 expressed CD11c, a marker more indicative of a monocytic-cell which is gradually downregulated as residence establishes (Bujko et al., 2018, Richter et al., 2018). However, this level sat below both cDC2s and MDMs and hence was assigned the label 'Macrophage'. Cluster 27 additionally expressed CCR7 and Axl, indicating an activated Macrophage. Axl upregulation has been previously linked to inflammatory macrophage states (DeBerge et al., 2021, Liu et al., 2025).

MDM (clusters 28-32): $CD11c^+$ $CD14^+$ $CD163^+$ AF^- and distinguished from DC3s by their lack of CD1c (Bujko et al., 2018, Rhodes et al., 2021). Clusters 28, 29 and 31 did not express MR and Siglec-1 indicative of recent differentiation from monocytes, unlike clusters 30 and 32 which were MR^+ and Siglec-1^+ indicative of a more established tissue macrophage (Bujko et al., 2018). Cluster 32 likely represented a population further along this trajectory to tissue residence, with a further loss of CD11c expression and acquired AF signal (Njoroge et al., 2001). Clusters 29 and 31 both uniquely expressed CD103, though cluster 29 only contained one donor, as did cluster 31. $CD103^+$ macrophages have been described as a subset of monocytic macrophages (Mf2) in intestinal tissue by Bujko et al. However, that population also expressed CD1c and MR, which was not mirrored by clusters 29 and 31. Cluster 31 additionally expressed CCR7 and was predominantly epidermal, suggesting an activated epidermal MDM.

Inflammatory macrophage (Cluster 33): defined by its mixed expression profile of tissue residency, monocytic origin, activation and inflammatory markers. Its positive expression of AF, CD163, MR, Siglec-1 and CD14 were strong indicators of tissue residence, however CD11c, Calprotectin and CD88 were more suggestive of recent monocytic differentiation (Bujko et al., 2018, Domanska et al., 2022, Bourdely et al., 2020, Dutertre et al., 2019). CCR7, Axl and CD5 further supports an activated and inflammatory phenotype (DeBerge et al., 2021, Liu et al., 2025, Korenfeld et al., 2017, Ohl et al., 2004). This cluster only contained one donor and likely reflects a unique

signature of inflammation.

Novel MNP population (cluster 34): AF^{int} $CD11c^{+}$ $CD14^{+}$ $CD163^{lo}$ $CD1c^{-}$ MR^{-} Siglec-1^{-} cells were identified that did not clearly align with any known MNP subset and termed here *AF⁺ CD11c⁺ MNPs.* Of particular interest these cells were AF^{+} and expressed CD11c which has never been described. It should be noted that the distribution of this cluster on the opt-SNE map appeared patchy, which may reflect true biological heterogeneity, however projection artifacts cannot be discounted.

Non-MNP/debris (Clusters 35-38): low HLA-DR expression, no MNP marker expression and random distribution on the opt-SNE. Deemed non-MNPs or debris.

Table 4.6: Final cluster annotations

Cluster number	Defining subset markers	Primary tissue location (>50%)	Final cluster name	Descriptive cluster name
1	$CD1c^{+}$ $CD1a^{+}$ $Langerin^{+}$ $CD11c^{lo}$	Epithelium	LC	LC
2	$XCR1^{+}$ $CD4^{+}$ $CD11c^{+}$	Dermis/LP	cDC1-1	cDC1
3	$XCR1^{+}$ $CD4^{+}$ $CD11c^{+}$ **$CD103^{+}$**	Dermis/LP	cDC1-2	$CD103^{+}$ cDC1
4	$XCR1^{+}$ $CD4^{int}$ CD11c+ **$CD1c^{+}$ $CCR7^{+}$**	Dermis/LP	cDC1-3	Activated $CD1c^{+}$ cDC1
5	$XCR1^{+}$ $CD4^{+}$ **$CD11c^{int}$ $CD1c^{+}$ $CD1a^{lo}$**	Dermis/LP	cDC1-4	$CD1c^{+}$ $CD1a^{lo}$ cDC1
6	$CD11c^{+}$ $CD1c^{+}$	Dermis/LP	cDC2-1	cDC2
7	$CD11c^{+}$ $CD1c^{+}$ **$CD1a^{+}$ $Langerin^{+}$ $CCR7^{+}$ Axl^{+}**	Epithelium	cDC2-2	Activated epidermal $Langerin^{+}$ cDC2
8	$CD11c^{+}$ $CD1c^{+}$ **$CD1a^{+}$ $Langerin^{+}$**	Epithelium (57%)	cDC2-3	$Langerin^{+}$ cDC2
9	$CD11c^{+}$ $CD1c^{+}$ **$CD1a^{+}$ MR^{+}**	Dermis/LP	cDC2-4	$CD1a^{+}$ MR^{+} cDC2
10	$CD11c^{+}$ $CD1c^{+}$ **$CD1a^{+}$ $CD5^{+}$**	Dermis/LP	cDC2-5	$CD1a^{+}$ $CD5^{+}$ cDC2
11	$CD11c^{+}$ $CD1c^{+}$ **$CD1a^{+}$**	Epithelium (53%)	cDC2-6	$CD1a^{+}$ cDC2
12	$CD1c^{+}$ $CD11c^{+}$ $CD163^{+}$ $CD14^{+}$ AF^{-}	Dermis/LP	DC3	DC3
13	$CD1c^{+}$ $CD11c^{+}$ $CD163^{int}$ $CD14^{+}$ AF^{-}	Dermis/LP	MDDC/DC3-1	MDDC/DC3
14	$CD1c^{+}$ $CD11c^{+}$ $CD163^{int}$ $CD14^{int}$ AF^{-} **$Langerin^{+}$ $CCR7^{+}$**	Epithelium	MDDC/DC3-2	Activated epidermal $Langerin^{+}$ MDDC/DC3
15	$CD11c^{+}$ $CD1c^{+}$ $CD14^{+}$ **$CD1a^{+}$ $Langerin^{+}$**	Epithelium	MDDC-1	Epidermal $Langerin^{+}$ MDDC
16	$CD11c^{+}$ $CD1c^{+}$ $CD14^{int}$ **MR^{+} $CCR7^{int}$**	Dermis/LP	MDDC-2	Activated MR^{+} MDDC
17	$CD11c^{+}$ $CD1c^{+}$ $CD14^{+}$ **$CD1a^{+}$**	Epithelium	MDDC-3	Epidermal MDDC

18	CD5$^+$ CD123$^+$ Siglec-6$^+$ **CD11c^{int} Siglec-1^{int}**	Dermis/LP	CD11c$^+$ ASDC	CD11c$^+$ ASDC
19	CD5$^+$ CD123$^+$ Siglec-6$^+$ **CD11c$^-$ Siglec-1$^+$**	Dermis/LP	CD123$^+$ ASDC	CD123$^+$ ASDC
20	CD123$^+$ CD5$^-$ Siglec-6$^-$	Dermis/LP	pDC	pDC
21	CD123$^+$ CD1a$^+$ CD11c$^+$ CD1c$^+$ CCR7$^+$ CD14^{int} MR$^+$	Dermis/LP	Inflam DC-1	Inflam DC
22	CD123$^+$ CD1a$^+$ CD11c$^+$ CD1c$^+$ CCR7$^+$ CD14^{int} MR^{int} **CD5$^+$**	Dermis/LP	Inflam DC-2	CD5$^+$ inflam DC
23	Calprotectin$^+$ AF$^+$ CD11c$^+$ CD1c$^+$ Langerin$^+$	Dermis/LP	Cal+ DC/mono	Cal+ DC/mono
24	AF$^+$ CD163$^+$ **MR^{++} Siglec-1^{++}** CD14$^+$ CD11c^{int}	Dermis/LP	Macrophage-1	Macrophage
25	AF$^+$ CD163$^+$ MR$^+$ Siglec-1$^+$ CD14$^+$ **CD11c$^-$**	Dermis/LP	Macrophage-2	CD11c$^-$ macrophage
26	AF$^+$ CD163$^+$ MR$^+$ Siglec-1$^+$ CD14$^+$ CD11c^{int}	Dermis/LP	Macrophage-3	Macrophage
27	AF$^+$ CD163$^+$ MR$^+$ Siglec-1$^+$ CD14$^+$ CD11c^{int} **CCR7$^+$ Axl$^+$**	Dermis/LP	Macrophage-4	Activated Axl$^+$ macrophage
28	CD11c$^+$ CD14$^+$ **CD163^{lo}** AF$^-$ MR$^-$ Siglec-1$^-$	Dermis/LP	MDM-1	MDM
29	CD11c$^+$ CD14$^+$ CD163$^+$ AF$^-$ MR$^-$ **Siglec-1^{lo} CD103$^+$**	Dermis/LP	MDM-2	CD103$^+$ Siglec-1^{lo} MDM
30	CD11c$^+$ CD14$^+$ CD163$^+$ AF$^-$ **MR$^+$ Siglec-1^{int}**	Dermis/LP	MDM-3	MR$^+$ Siglec-1$^+$ MDM
31	CD11c$^+$ CD14$^+$ CD163$^+$ AF$^-$ MR$^-$ Siglec-1$^-$ **CD103$^+$ CCR7$^+$**	Epithelium	MDM-4	Activated epidermal CD103$^+$ MDM
32	**CD11c$^-$** CD14$^+$ CD163$^+$ **MR$^+$ AF^{lo} Siglec-1^{int}**	Dermis/LP	MDM-5	CD11c$^-$ AF^{lo} MDM
33	AF$^+$ CD163^{++} MR^{++} Siglec-1^{++} CD14$^+$ CD11c^{int} CD5$^+$ CCR7$^+$ Axl$^+$ CD88$^+$ Calprotectin$^+$	Dermis/LP	Inflam macrophage	Inflam macrophage
34	AF^{int} CD11c$^+$ CD14$^+$ CD163^{lo} CD1c$^-$ MR$^-$ Siglec-1$^-$	Dermis/LP	AF$^+$ CD11c$^+$ MNP	AF$^+$ CD11c$^+$ MNP
35	AF$^+$ HLA-DR^{lo} CD4$^-$	Dermis/LP	Non-MNP-1	Non-MNP-1
36	HLA-DR^{lo} CD4$^-$ Langerin$^+$	Dermis/LP	Non-MNP-2	Non-MNP-2
37	AF$^+$ HLA-DR^{lo}	Dermis/LP	Non-MNP-3	Non-MNP-3
38	CD123$^+$ Siglec-6$^+$ (no significant pattern, cell spray on opt-SNE map)	Dermis/LP	Debris	Debris

Bold markers represent features that distinguish clusters belonging to the same cell subset (i.e. cDC1-1, cDC1-2).

4.3.3 Characterising the Mononuclear Phagocyte Landscape in Human Genital Skin and Mucosa

4.3.3.1 Redesigning a Flow Cytometry Gating Strategy to Integrate New and Redefined Mononuclear Phagocyte Populations from Clustering Analysis

The high dimensionality clustering analysis prompted a redesign of the gating strategy described in **Chapter 3** (**Figure 3.1**), as it revealed several previously unidentified populations and provided a more comprehensive insight to the marker expression profiles of MNPs in genital tissue, requiring an updated approach to identify them (**Figure 4.5**). The initial gating of single, live, non-lymphocytes ($CD3^-$ $CD19^-$), pDCs ($CD123^+$ $CD4^+$ $CD5^-$ Siglec-6^- $CD11b^-$) and ASDCs ($CD5^+$ Siglec-6^+ $CD4^+$ $CD123^{int}$ $CD11b^-$) remained consistent with **Figure 3.1**, with the exception of adding a neutrophil gate, defined as SSC-A^+ $CD11b^+$ HLA-DR^-.

The clustering analysis revealed three distinct populations of interest: Calprotectin$^+$ DC/monocytes; AF^+ $CD11c^+$ MNPs; $CD123^+$ $CD1a^+$ Inflammatory DCs. The first two populations are both AF^+, prompting a restructure of macrophage gating. In the original strategy, Macrophages were identified in a terminal gate as AF^+ $CD14^+$ $CD1c^-$ to distinguish them from MDMs, MDDCs and cDC2s. However, with the identification of two additional AF^+ populations, it became apparent that the cDC1 and cDC2 gates were likely contaminated with AF^+ cells (**Supplementary figure 4.4**). Consequently, Macrophages, calprotectin$^+$ DC/monocytes and AF^+ $CD11c^+$ MNPs were moved higher in the gating hierarchy in the modified gating strategy. In the revised strategy, all AF^+ cells are captured in a CD11c vs AF^+ gate upstream of DC and MDM gates. Within this gate, **calprotectin$^+$ DC/monocytes** are defined as AF^+ calprotectin$^+$ $CD163^-$, **Macrophages** as AF^+ Siglec-1^+ $CD163^+$ and **AF^+ $CD11c^+$ MNPs** as AF^+ Siglec-1^- $CD163^-$ $CD11c^+$. The dual expression of Siglec-1 and CD163 was selected to define Macrophages, as these markers displayed the two strongest signatures across all macrophage clusters. The inflammatory DCs were included in the gating strategy after the MR vs $XCR1^-$ gate, upstream of the DC and MDM gates, and identified as $CD123^+$ $CD1a^+$.

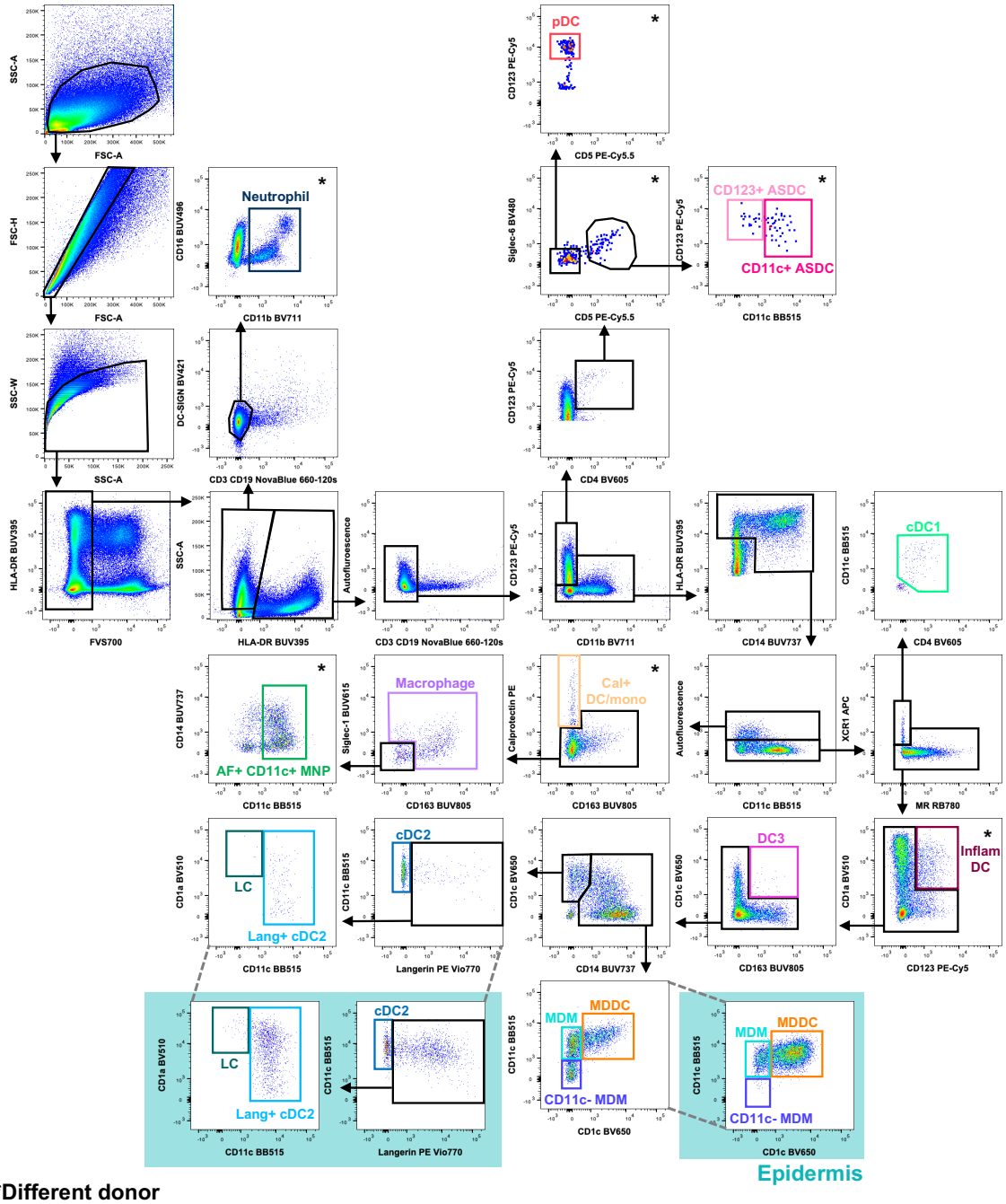

***Different donor**

Figure 4.5: Revised gating strategy to identify all known mononuclear phagocyte populations in human genital skin

Cells were isolated from vaginal tissue using techniques described in **section 4.2.2.2**, stained with the flow cytometry panel outlined in **Supplementary table 3.2** and acquired on the BD FACSymphony. Representative gating strategy shows the redefined MNP populations as revealed by cluster analysis. Cells were first gated as single (FSC-H vs FSC-A and SSC- W vs SSC-A), live cells (FVS700$^-$). **Neutrophils** were identified as HLA-DR$^-$ SSC-A$^+$ DC-SIGN$^-$ CD3$^-$ CD19$^-$ CD11b$^+$ cells. All other MNPs were gated as HLA-DR$^+$. T and B cells were excluded using a CD3/CD19 dump gate. **pDCs** were defined as Siglec-6$^-$ CD5$^-$ CD123^{hi}, whilst **ASDCs** were CD123$^{int\text{-}hi}$ Siglec-6$^+$ CD5$^+$ and further divided by expression of CD11c. Proceeding the identification of pDCs and ASDCs, HLA-DR^{lo} CD14$^-$ cells were excluded. This resultant population was then divided by autofluorescence (AF). The AF$^+$ gate yielded three MNP populations: **calprotectin$^+$ DC/monocytes** as calprotectin$^+$ CD163$^-$, **Macrophages** as Siglec-1$^+$ CD163$^+$ and **AF$^+$ CD11c$^+$ MNPs** as Siglec-1$^-$ CD163$^-$ CD11c$^+$. All other MNPs followed on from the AF$^-$ gate. **cDC1s** were gated as a population of XCR1$^+$ MR$^-$ cells and defined as CD4$^+$ CD11c$^{+/lo}$ (the CD4$^-$ CD11c$^-$ population was excluded). The XCR1$^-$ vs MR gate identified the CD123$^+$ CD1a$^+$ **Inflammatory (Inflam) DCs**.

Continued over page

The non-Inflammatory DCs lead to the identification of DC3s as CD163$^+$ CD1c$^+$, and the non-DC3s to a CD14 vs CD1c plot. The CD14$^-$ CD1c$^+$ population identified **cDC2s** as langerin$^-$ CD11c$^+$. The langerin$^+$ gate led to the identification **langerin$^+$ (Lang) cDC2s** as CD11c$^+$ vs CD1a and **LCs** as CD11c^{lo} CD1a^{hi}. The CD14$^+$ vs CD1c cells contained the monocyte-derived populations: **MDDCs** were CD1c$^+$ CD11c$^+$, **MDMs** were CD1c$^-$ CD11c$^+$ and **CD11c$^-$ MDMs** were CD1c$^-$ CD11c$^-$. The same gating strategy was used for both the LP/dermis and epithelium. This representative strategy is demonstrated with vaginal LP, apart from the three plots highlighted in blue which show the equivalent epithelial populations. All gating was performed using a single donor, except for plots marked with an asterisk (*), which employed a different donor to illustrate a specific population.

Clustering analysis also provided a more extensive overview of marker expression, showing the presence of markers on populations not previously well defined in genital tissues. For instance, cDC1s were initially identified as CD4$^+$ CD14$^-$, however, clustering revealed that many cDC1s in genital tissue also express CD11c, instigating their redefinition as dual CD4$^+$ CD11c$^+$ - although this gate encompasses a spectrum of expression merely excluding the double negative population. Similarly, langerin$^+$ cDC2s were previously identified early in the gating, before DC3s and MDDCs, based on the assumption langerin expression was exclusive to cDC2s. However, cluster analysis demonstrated that both DC3s and MDDCs can also express langerin, and subsequently the gating of langerin$^+$ cDC2s was moved downstream of these populations. Another clear finding from the cluster analysis was the identification of a transitional macrophage population in between MDMs and tissue resident macrophages, characterised by lower CD11c expression. This was incorporated into the revised gating strategy from the CD14$^+$ vs CD1c compartment identifying **MDMs** as CD14$^+$ CD11c$^+$ CD1c$^-$, **CD11c$^-$ MDMs** as CD14$^+$ CD11c- CD1c- and **MDDCs** as CD14$^+$ CD11c$^+$ CD1c$^+$. The gating of DC3s, cDC2s and LCs remains largely unchanged.

The activated CCR7$^+$ subsets identified through clustering were not explicitly gated as CCR7 expression reflects a cellular state of activation rather than a distinct subset and can be quantified at the population level.

One of the most consequential findings from the cluster analysis was that every MNP population identified in the dermis or LP was also identified in the epithelium (**Figure 4.4d**). Previously, these compartments were treated as two very distinct entities, with completely separate gating strategies. However, the clustering results support the use of a single gating strategy across both tissue compartments.

4.3.3.2 Mononuclear Phagocyte Populations are Highly Heterogenous across Skin and Mucosal Genital Tissues

To investigate the MNP populations across skin and mucosal genital tissues utilising the revised gating strategy in **Figure 4.5**, 4 foreskins, 3 labia, 18 vaginas and 3 cervixes (Table 4.5) were processed and stained with a 25-parameter FACSymphony panel (**Supplementary table 3.2**), excluding KI67 biotin Streptavidin DyLight800. Some of these samples were the same as those used for the clustering analysis.

The relative proportions of each MNP subset in the dermis/LP and epithelium were calculated as a percentage of HLA-DR$^+$ CD3$^-$ CD19$^-$ cells. For the dermis/LP, comparisons were made across all the tissues and tissue types comprising the male and female genital tracts, including skin (outer foreskin and labia), type II mucosa (inner foreskin, vagina and ectocervix) and type I mucosa (endocervix) (**Figure 4.6a**). Each individual tissue exhibited a distinct and unique MNP environment. Of significance, Macrophages were the dominant population in the outer foreskin, labia and inner foreskin. Comparatively, the vagina was dominated by MDMs, whilst in ectocervix and endocervix, CD11c$^-$ MDMs were most abundant. However, due to limited donor numbers across all tissues and donor variability, minimal statistical significance was achieved. When comparing the average proportions of MNP subsets relative to total MNPs (**Figure 4.6b**), Macrophages proportions in skin trended higher than those in mucosal tissues, whereas MDM proportions were higher in mucosa. DC3s and Inflammatory DCs appeared to be more skin-specific populations, predominantly found in foreskin and labia, although still present in vagina. Conversely, AF$^+$ CD11c$^+$ MNPs were a distinctly vaginal population. cDC1s, cDC2s and MDDCs displayed no distinct pattern, and differed in their proportions across tissues.

The epithelium comprises skin (outer foreskin) and type II mucosa (inner foreskin, vagina and ectocervix) (**Figure 4.6c**). LCs were the predominant population in both outer and inner foreskin. Comparatively, the vagina contained a relatively even distribution of langerin$^+$ cDC2s and MDDCs, while MDMs dominated the ectocervix. As a proportion of total MNPs (**Figure 4.6d**), cDC2s in the inner foreskin were more abundant than in outer foreskin, but not as abundant as the vagina. MDDCs and MDMs formed a large proportion of MNPs in the vagina and ectocervix, though were minimal in inner and outer foreskin.

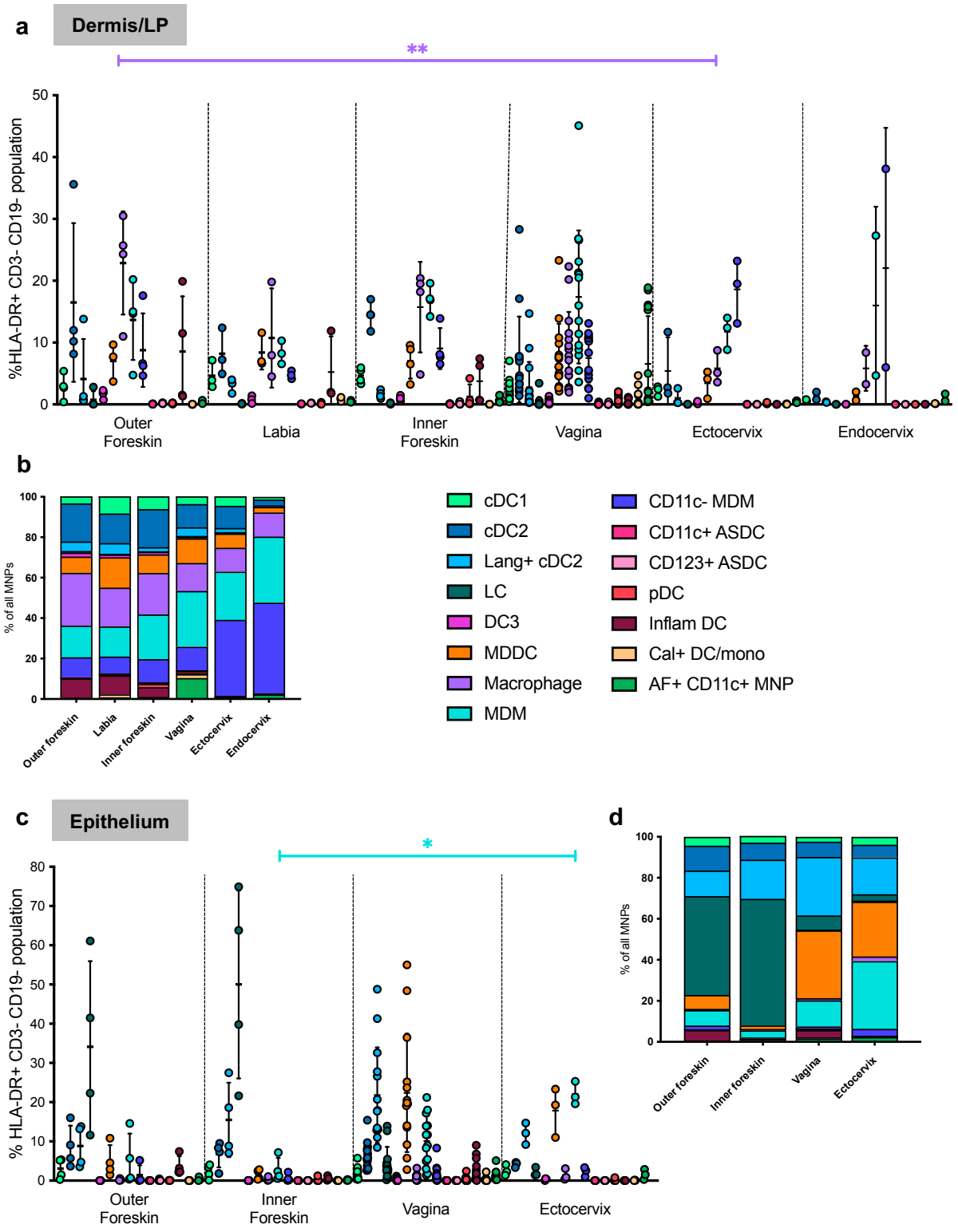

Figure 4.6: Proportional comparison of mononuclear phagocyte populations across human genital skin and mucosa

Isolated vaginal immune cells were stained with the flow cytometry panel outlined in **Supplementary table 3.2**. **a)** Relative proportions of each MNP subset were determined as a percentage of the HLA-DR^{+} CD3^{-} CD19^{-} gate across the human dermal/LP genital tracts including outer foreskin (n=4), labia (n=3), inner foreskin (n=4), vagina (n=15), ectocervix (n=3) and endocervix (n=2). The mean +/- standard deviation plotted and statistical analysis was performed using the mixed-effects analysis with Tukey's multiple comparisons (*p<0.05, **p<0.01). **b)** Proportions of total MNPs were from data presented in **a**. **c-d)** The same proportions were calculated for the epithelium of outer foreskin (n=4), inner foreskin (n=4), vagina (n=15) and ectocervix (n=3).

Inflammatory DCs appeared more abundant in vaginal epithelium compared to the LP, while Macrophages and CD11c^{-} MDMs were sparse in the epithelium of all tissues. Interestingly, the inner foreskin contained more similar proportions of cells to the outer foreskin than to its type II mucosal counterparts, suggesting an intermediate profile, potentially due to its anatomical proximity to skin.

Next, we explored phenotypical differences in MNP populations across skin and mucosa. CD163, a marker expressed by all macrophages and DC3s, showed a consistent decrease in expression from skin to mucosa across all four populations in the dermis/LP (**Figure 4.7a**). CD163 expression was notably lower in the vagina and cervix compared to outer foreskin, inner foreskin and labia. Furthermore, inner foreskin Macrophages expressed significantly less CD163 than outer foreskin Macrophages. Another marker of interest, CD14, was expressed more highly in tissues of the FGT by all Macrophages, DC3s, MDDCs, Inflammatory DCs, calprotectin^{+} DC/monocyte and AF^{+} CD11c^{+} MNP (**Figure 4.7b**). This increased expression was observed in both the LP and epithelium and was particularly elevated in the labia and vagina, suggestive of a possible sex-based biological difference in CD14 expression.

One of the most unexpected observations was the presence of CD14 expressing MNPs in the vaginal epithelium – an observation not well documented in the literature. To define where these cells were residing *in situ*, we used IMC which revealed several distinct epithelial macrophage populations (**Figure 4.7c**). Unfortunately, due to signal and detection errors (an unknown fault in panel optimisation) we were unable to resolve CD14 signal in the epithelium. However, using the known macrophage marker FXIIIa, we defined macrophage populations, which are known CD14 expressing cells. We identified a more mature tissue resident macrophage defined as HLA-DR^{+} CD11c^{+} FXIIIa^{hi} langerin^{-} (**Figure 4.7c right side**) (Zaba et al., 2007) and an MDMs as HLA-DR^{+} CD11c^{+} FXIIIa^{lo} langerin^{+} (**Figure 4.7c left side**) (Dull et al., 2021). DCs had no detectable FXIIIa expression (**Figure 4.7c right side**). We therefore confirmed the presence of MDMs and Macrophages within the epithelium, which were randomly distributed through the epithelium but close to the basement membrane.

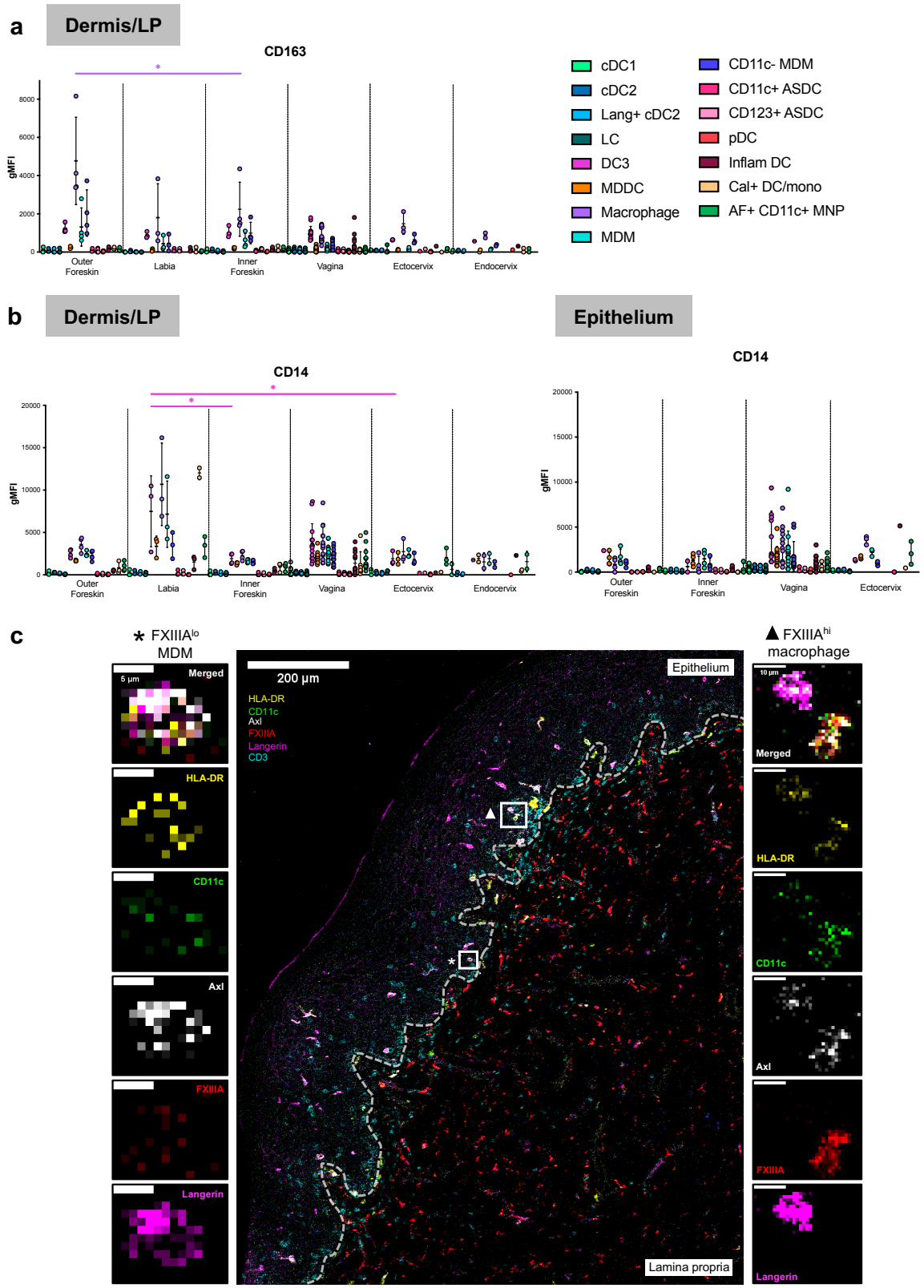

Figure 4.7: Expression of CD163 and CD14 by mononuclear phagocyte populations across human genital skin and mucosa

a-b) Cells liberated from genital tissues were stained with the flow cytometry panel outlined in **Supplementary table 3.2**. The geometric mean of fluorescence intensity (gMFI) values for each MNP population across all genital tissue donors were obtained using FlowJo V10.10.0 for **a)** CD163 expression in the dermis/LP and **b)** CD14 expression in the dermis/LP and epithelium. Statistical analysis was performed using the mixed-effects analysis with Tukey's multiple comparisons (*p<0.05, **p<0.01).

Continued over page

c) Fixed vaginal tissue sections were prepared, imaged, and analysed for IMC as described in **section 4.2.4**. Tissue sections were stained with the panel outlined in **Table 4.2**. HLA-DR = yellow, CD11c = green, Axl = white, FXIIIA = red and Langerin = pink. Scale bar of large image = 200 µm, scale bar of individual cell images = 5 µm. Asterisk symbol indicates an MDM (HLA-DR^{+} CD11c^{int} Axl^{+} FXIIIA^{lo} Langerin^{+}) (left) and triangle symbol indicates a Macrophage (HLA-DR^{+} CD11c^{+} Axl^{+} FXIIIA^{hi} Langerin^{-}) (right). Grey dotted line distinguishes the border between the epithelium and LP.

4.3.4 Phenotyping Mononuclear Phagocytes in Vaginal Tissue

In sub-Sarhan Africa, majority of new infections occur in young women across the FGT. Vaginal samples were also the most plentiful tissue available from surgeons throughout the final stages of experimental work for this thesis, and as such, all the following data focuses on characterising the MNPs of vaginal tissue.

4.3.4.1 Defining Dendritic Cell Populations of Vaginal Mucosa

Following the gating of MNPs in tissue using the FACSymphony panel, the expressional profiles of the DC subsets (cDC1, cDC2, langerin^{+} cDC2, DC3 and MDDC) were examined and compared to further characterise DCs in vaginal mucosa.

The key defining markers of cDC1s varied considerably depending on whether they reside in the blood, skin or mucosa. Blood cDC1s are typically identified by expression of CLEC9A, CADM1, CD141 or XCR1 (Botting et al., 2017, Mair and Liechti, 2021). When cDC1s were first described in skin, they were defined as being CD141^{+} CD11c^{+} due to the limited availability of a XCR1 antibody (Chu et al., 2012). After the introduction of multiple XCR1-conjugated fluorophores, cDC1s in skin were re-defined as XCR1^{+} CD141^{+} CLEC9A^{+} CD11c^{lo} (Botting et al., 2017, Rhodes et al., 2021), and in intestinal tissue (type I mucosa), identified as XCR1^{+} CD103^{+} CD11c^{+} SIRPα^{-} (Doyle et al., 2021). We therefore defined cDC1s in vaginal type II mucosa utilising these established cDC1 markers (**Figure 4.8a**). XCR1 expression delineated a distinct population of cDC1s in vaginal tissues. Overlay with other markers revealed that while some XCR1^{+} cells co-expressed CD141, no XCR1^{+} cells co-expressed CLEC9A, CADM1, CD103 or SIRPα. Further comparison between XCR1^{+} and CD141^{+} expressing cells showed that XCR1 can reliably isolate a discrete cDC1 population, whereas the CD141^{+} population also included cDC2s expressing CD1c and CD5 (**Figure 4.8b**). We also observed that vaginal XCR1^{+} cDC1s express a spectrum of CD11c (**Figure 4.8c**). These findings indicate that vaginal cDC1s possess a unique profile compared to their counterparts in blood, skin and type I mucosa.

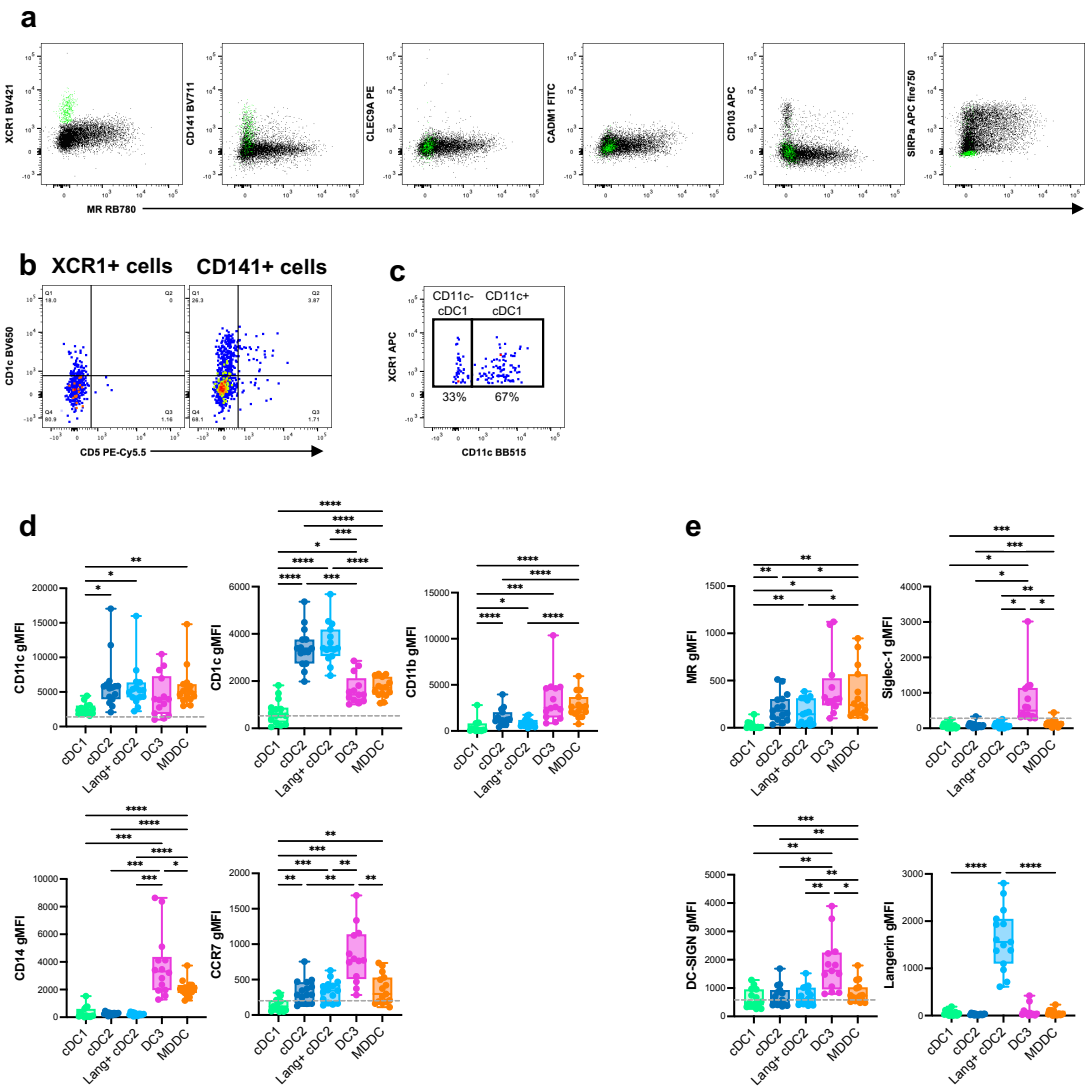

Figure 4.8: Phenotypic profile of dendritic cell populations isolated from vaginal tissue

a-c) Isolated virginal cells were stained with the cDC1 phenotyping flow cytometry panel outlined in **Table 4.3**. **a)** Comparison of defining cDC1 markers XCR1, CD141, CLEC9A, CADM1, CD103 and SIRPα. XCR1$^+$ MR$^-$ cells were gated (green) and overlayed with other markers. **b)** XCR1$^+$ MR$^-$ and CD141$^+$ MR$^-$ were gated and visualised as a CD5 vs CD1c plot with quadrant gates. **c)** XCR1$^+$ MR$^-$ cells were gated to visualise expression of CD11c, displayed a % of CD11c$^-$ and CD11c$^+$ cells. **d-e)** Cells were stained with the flow cytometry panel outlined **Supplementary table 3.2**. Geometric mean of fluorescence intensity (gMFI) values for **d)** DC defining and activation markers (CD11c, CD1c, CD11b, CD14, CCR7) and **e)** HIV binding lectin receptors (MR, Siglec-1, DC-SIGN, langerin) were obtained from Flow Jo V10.10.0 for the DC populations: cDC1, cDC2, Lang$^+$ cDC2, DC3 and MDDC and graphed as box and whisker plots. Statistical analysis was performed using the mixed-effects analysis with Tukey's multiple comparisons (*p<0.05, **p<0.01). Where applicable, grey dotted line indicates minimum detection level for markers (the zero line).

We next quantified the expression of key defining markers across all DC subsets in the vaginal LP using the geometric means of fluorescence intensity (gMFI) (**Figure 4.8d**). gMFI plots with a grey dotted line indicates the minimum detection level, or 'true zero'. Of most interest were the expression profiles of DC3s and MDDCs as there is minimal literature on these cells in human tissues. Like cDC2s, both DC3s and MDDCs

were CD11c$^+$ and CD1c$^+$, however, CD1c expression was approximately half the intensity of cDC2s. DC3s and MDDCs both expressed high levels of CD11b and CD14 compared to other DCs. Notably, more so than any other DC subset, CCR7 was differentially expressed across DC3s, indicating their presence in both activated and inactivated states.

Lastly, we assessed the expression of key lectin receptors known to bind HIV including MR, Siglec-1, DC-SIGN and langerin (**Figure 4.8e**). MR was expressed by all DCs except cDC1s, and most highly by DC3s and MDDCs. DC3s were the only DCs to express Siglec-1 and DC-SIGN. Langerin was most highly expressed by langerin$^+$ cDC2s, although low levels were also detected on cDC1s, DC3s and MDDCs.

4.3.4.2 Defining Macrophage Populations of Vaginal Mucosa

The revised gating strategy identified four macrophage-like populations: an AF$^+$ Macrophage, MDM, CD11c$^-$ MDM and AF$^+$ CD11c$^+$ MNP. Of particular interest were the CD11c$^-$ MDM and AF$^+$ CD11c$^+$ MNP populations which we hypothesised to be a form of intermediary monocyte-macrophage based on the unbiased clustering analysis and findings of Bujko et al. (2018) and Domanska et al. (2022). We quantified the gMFI expression of key macrophage defining markers (**Figure 4.9a**) and HIV lectin receptors MR, Siglec-1, DC-SIGN and langerin (**Figure 4.9b**).

Macrophages and CD11c$^-$ MDMs were the only populations to express tissue resident macrophage associated markers CD163, MR and Siglec-1, with Macrophages consistently expressing the highest levels. Markers linked with monocytic lineage, CD11c and CD11b, were more highly expressed by MDMs and AF$^+$ CD11c$^+$ MNPs. HLA-DR expression was significantly lower on CD11c$^-$ MDMs, and CD1c was exclusively expressed by AF$^+$ CD11c$^+$ MNPs, although expression levels were low. CD14 expression was greatest on Macrophages followed by MDMs, CD11c$^-$ MDM then AF$^+$ CD11c$^+$ MNPs. DC-SIGN and langerin were expressed most highly by Macrophages and AF$^+$ CD11c$^+$ MNPs at comparable levels, with low expression detectable on both MDM subsets.

Overall, the data suggests that CD11c$^-$ MDMs could indeed represent a definite intermediate or transitionary macrophage state, consistently exhibiting expression levels between MDMs and Macrophages. In contrast, the profile of AF$^+$ CD11c$^+$ MNPs

presents more complex. These MNPs express CD11c and CD11b and lack CD163 and Siglec-1, mimicking MDMs, yet simultaneously displaying characteristics of macrophages as, AF^+, $HLA\text{-}DR^{hi}$ and $DC\text{-}SIGN^+$. It is plausible that AF^+ $CD11c^+$ MNPs represent a unique vaginal transitional macrophage subset, although their functionality and ability to capture HIV remains to be determined.

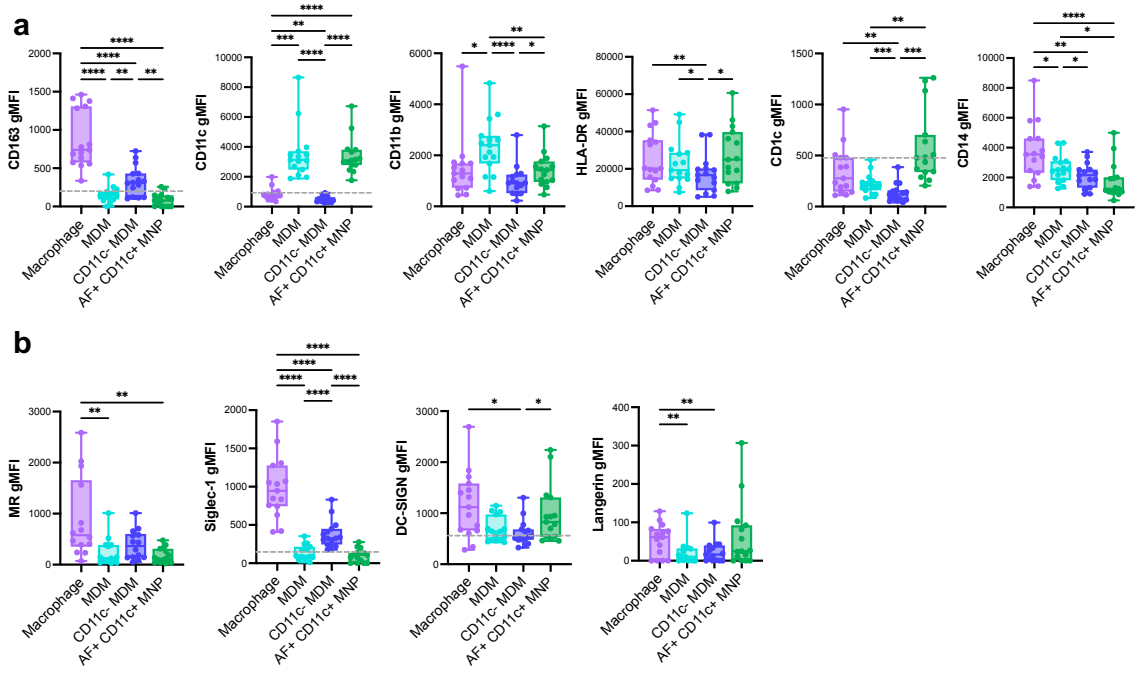

Figure 4.9: Phenotypic profile of macrophage populations isolated from vaginal tissue

Isolated vaginal immune cells were stained with the flow cytometry panel outlined in **Supplementary table 3.2**. gMFI values for **a)** macrophage defining markers (CD163, CD11c, CD11b, HLA-DR, CD1c, CD14) and **b)** HIV binding lectin receptors (MR, Siglec-1, DC-SIGN, langerin) were obtained for the populations: Macrophage, MDM, $CD11c^-$ MDM and AF^+ $CD11c^+$ MNP and graphed as box and whisker plots. Statistical analysis was performed using the mixed-effects analysis with Tukey's multiple comparisons (*p<0.05, **p<0.01). Grey dotted line indicates minimum detection level for markers (the zero line).

4.3.4.3 Comparative Expression Profiles of Lamina Propria and Epithelial Mononuclear Phagocytes

As all marker profiling of MNPs had been performed using cells from the vaginal LP, we sought to further assess potential differences in marker expression between the LP and epithelium. For visual clarity, the gMFI values for each marker were averaged across all donors for both compartments and displayed in **Figure 4.10**. However, statistical analysis was performed using matched LP-epithelial data from individual donors, shown in **Supplementary figure 4.5**.

Of interest, CD11c and MR were expressed more highly by populations in the LP (**Figure 4.10a**, **Supplementary figure 4.5a**). CD11c was higher on all LP cell populations compared to epithelium except Macrophages, pDCs and CD123^{+} ASDCs – populations which all lack CD11c expression. MR expression was elevated on all DC populations in the LP, except cDC1, as well as all three macrophage populations, Inflammatory DCs and AF^{+} CD11c^{+} MNPs.

Contrastingly, CD1a, langerin and CD1c were more highly expressed by cells in the epithelium (**Figure 4.10b, Supplementary figure 4.5b**). Both CD1a and langerin displayed a universal trend for higher expression in the epithelium across all donors, consistent with findings that epithelial factors upregulate CD1a and langerin (Bigley et al., 2015, Lang et al., 2023).

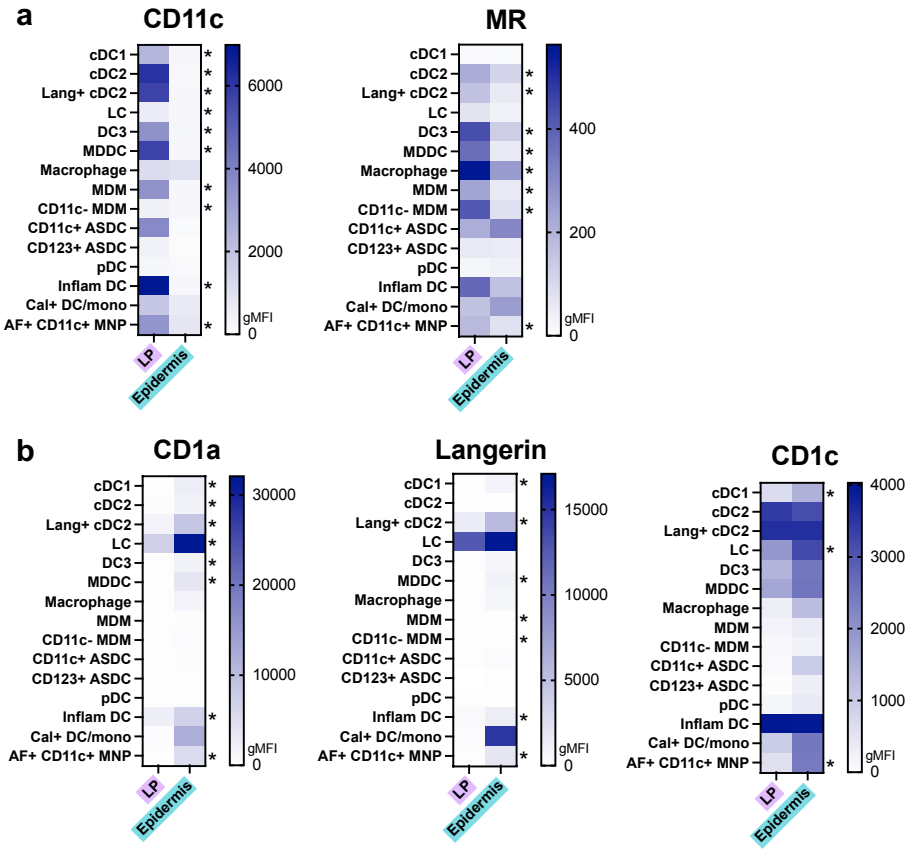

Figure 4.10: Differential average marker expression between mononuclear phagocyte populations of the vaginal LP and epithelium

Cells were isolated from vaginal tissue and stained with the flow cytometry panel outlined in **Supplementary table 3.2**. Heatmaps show average gMFI values for marker expression in MNP populations from the LP (Left column, purple) compared to the epithelium (right column, teal). **a)** CD11c and MR is higher in the LP and **b)** CD1a, Langerin and CD1c is higher in the epithelium. Statistical analysis was performed using the multiple Mann-Whitney test for pairwise comparison (*p<0.05).

4.3.5 Characterising Inflammatory Vaginal Mononuclear Phagocytes

A central point of this study was gaining further insights into the MNP populations residing in an inflammatory milieu, particularly in tissue from the FGT. Thus far, all vaginal samples have been analysed and assessed in bulk with no inflammatory division. Therefore, we next assessed differences in the MNP landscape between uninflamed and inflamed tissue.

First, an inflammation grading system was developed to classify each vaginal sample. After collection from surgeons and tissue thinning, a small piece (~ 5 mm x 5 mm) was set aside for half the vaginal samples (n=7). This portion was preserved for histological analysis; stained with H&E and imaged to assess the immune cell infiltrate and inform the degree of inflammation. An increased immune cell infiltrate is indicative of a higher level of acute inflammation.

The number of immune cells within a 60 µm region extending from the epithelial basement membrane into the underlying LP (**Supplementary figure 4.6**) was counted and the cell density then determined as the number of cells per μm^2. The samples were subsequently ranked from highest to lowest cell density, and the values were normalised and scaled to a range of 0-1 using the formula:

$$Normalised\ value = \frac{\chi\ -\ minimum\ value}{maximum\ value\ -\ minumum\ value}$$

Representative H&E images demonstrating a low and high cell density is shown in **Figure 4.11a**.

As not all vaginal samples were stained with H&E, we established a correlation between the density of cells and the degree of inflammation and matched this with the flow cytometry data. For each H&E stained sample, the corresponding flow cytometry data was analysed for the proportion of CD4 T cells (defined as a % of $CD3^+$ $CD19^+$ cells) (**Figure 4.11b**) and pDCs (% of HLA-DR^+ $CD3^-$ $CD19^-$ cells), both of which are immune populations known to migrate into inflamed tissues (Saadeh et al., 2016, Collins et al., 2016). A summary of the cell density, scaling values and matched flow cytometry proportions of CD4 T cells and pDCs is provided in **Table 4.7**. To explore these relationships, correlation gradients were generated between the cell density values and proportions of CD4 T cells and pDCs. A strong positive correlation was

observed with CD4 T cells (r=0.691, p=0.021) (**Figure 4.11d**) whilst interestingly, no correlation was noted with pDCs (r=0.0131, p=0.807) (**Figure 4.11d**).

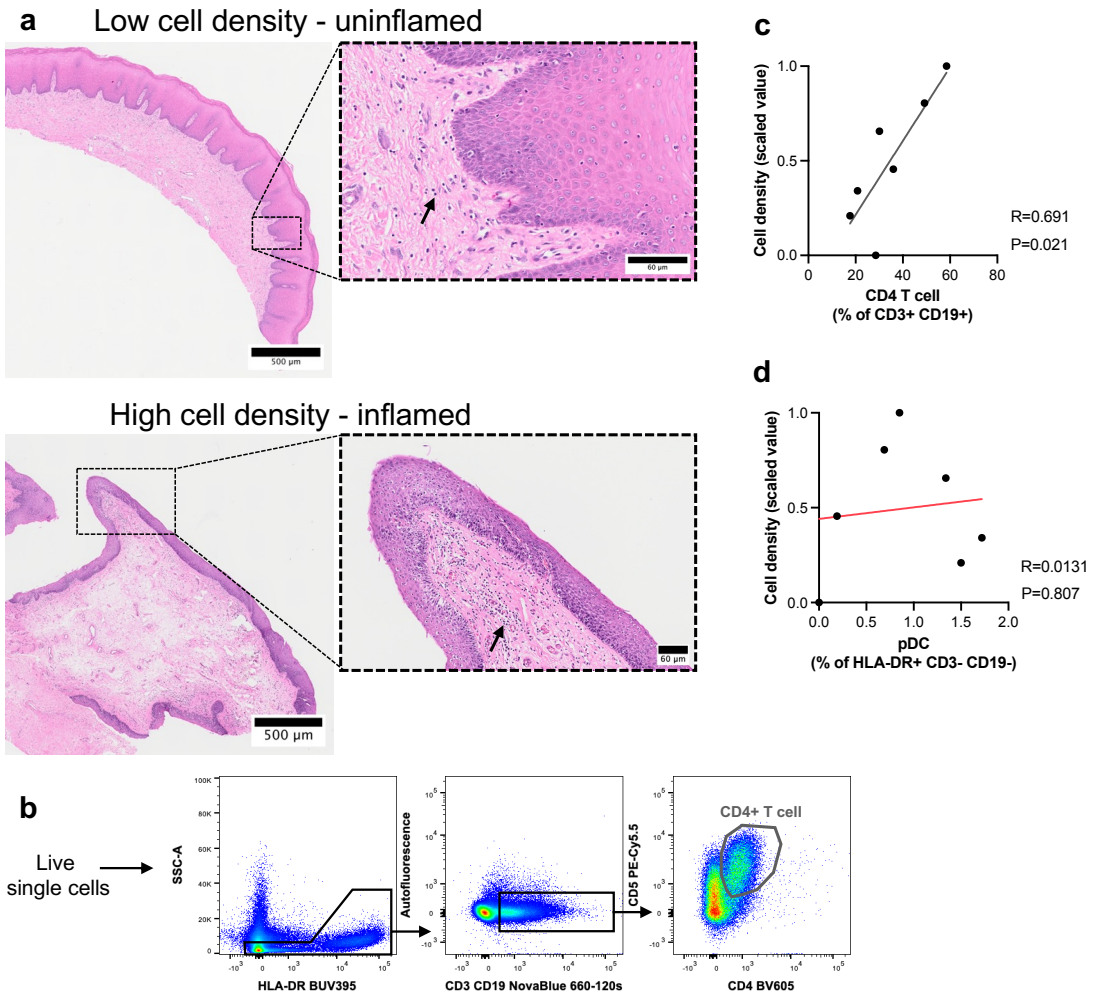

Figure 4.11: Inflammation grading of vaginal samples

5 mm x 5 mm sections of vaginal tissue (n=7) were fixed in 4% PFA, paraffin embedded, sectioned and stained with H&E as described in **section 4.2.5**. The remaining tissue was processed for flow cytometry. Images were acquired at 40x magnification on the Olympus VS200 Slide scanner and processed on ImageJ to create a 60 µm region of interest (ROI). QuPath's automated cell detection counted the immune cells within the ROI and determined cell density by calculating the number of cells/ μm^2 and normalised each sample to a scale of 0-1. **a)** An uninflamed sample had a low cell density (closer to scaled range of 0) whilst **b)** an inflamed sample had a high cell density (closer to scaled range of 1). The black arrows indicate an immune cell. **c)** The samples processed for flow cytometry were stained with panel outlined in **Supplementary table 3.2**. CD4 T cells were identified and gated in each sample as live, single, SSC-A$^-$ CD3$^+$ CD19$^+$ CD5$^+$ CD4$^+$ and pDCs were defined as per the gating strategy in **Figure 4.5**. Scatter plots with linear regression lines were created to illustrate the relationship between a samples' **d)** scaled cell density value and proportion of CD4 T cells (% of CD3$^+$ CD19$^+$ cells), where R = 0.691 and p = 0.021 and **f)** scaled cell density value and proportion of pDCs (% of HLA-DR$^+$ CD3$^-$ CD19$^-$ cells), where r = 0.0131 and p = 0.807. The r-value indicates the correlation coefficient and p-value the significance (*p<0.05).

Table 4.7: Inflammation correlation between H&E measured cell infiltrate and flow cytometry cell proportions in vaginal samples

Sample	Cell density (no. cells/μm^2)	Scaled cell density	CD4 T cells (% CD3$^+$ CD19$^+$ cells)	pDC (% HLA-DR$^+$ CD3$^-$ CD19$^-$ cells)
Vagina 1	0.0049	1	58.5	0.85
Vagina 2	0.0046	0.80	49.2	0.69
Vagina 3	0.0043	0.66	30.1	1.34
Vagina 4	0.0040	0.46	36	0.19
Vagina 5	0.0038	0.34	21.8	1.72
Vagina 6	0.0036	0.21	17.6	1.5
Vagina 7	0.0033	0	28.5	0

Based on the strong correlation between cell density and CD4 T cells, the proportion of CD4 T cells was calculated for the remaining vaginal samples with no matched H&E data. A sample was deemed inflamed if the proportion of CD4 T cells exceeded 30%, and either ASDCs were present, or the proportion of neutrophils was greater than 3%. The 30% CD4 T cell threshold was derived from Vagina 3, exhibiting a scaled density of 0.66 and CD4 T cell count of 30.1%. We have previously demonstrated ASDCs to be exclusively present in inflamed tissues (Warner van Dijk et al., 2024). Additionally, neutrophil infiltration is a classic indicator of tissue inflammation. The division of vaginal samples between uninflamed (n=7) and inflamed (n=7) is summarised in **Table 4.8**.

4.3.5.1 An Inflammatory Environment Induces Proportional and Phenotypic Changes in Mononuclear Phagocyte Populations

Proportional comparisons of MNP subsets in vaginal LP and epithelium were conducted identical to those in **Section 4.3.3.2**, with samples being divided into uninflamed or inflamed. In the LP, the proportion of MDMs in inflamed tissue was significantly higher than those in uninflamed tissue. Similar trends were observed for cDC1s, langerin$^+$ cDC2s, DC3s and MDDCs (**Figure 4.12a**). In the epithelium, inflammation was associated with a substantial enrichment of langerin$^+$ cDC2s, while CD11c$^-$ MDMs exhibited a decreasing trend in inflamed tissue (**Figure 4.12b**). These proportional shifts highlight distinct differences in MNP composition not only between inflammation states, but also between the LP and epithelium compartments.

Table 4.8: Inflammation grading of vaginal samples

Sample	CD4 T cells (% $CD3^+$ $CD19^+$ cells)	ASDC presence?	Neutrophil presence? (yes if >3% of HLA-DR^- SSC-A^+ cells)	Inflammatory status (>30% CD4 T cells and ASDC presence or neutrophil presence)
Vagina 1	58.5	Yes	Yes (3.64%)	Inflamed
Vagina 2	49.2	No	Yes (65.4%)	Inflamed
Vagina 3	30.1	No	Yes (13.7%)	Inflamed
Vagina 4	36	Yes	Yes (19%)	Inflamed
Vagina 5	21.8	No	No	Uninflamed
Vagina 6	17.6	No	Yes (4.93%)	Uninflamed
Vagina 7	28.5	Yes	Yes (8.36%)	Inflamed
Vagina 8	9	No	No	Uninflamed
Vagina 9	26.8	No	No	Uninflamed
Vagina 10	24.2	No	No	Uninflamed
Vagina 11	45.6	Yes	Yes (55.3%)	Inflamed
Vagina 12	41.7	Yes	No	Inflamed
Vagina 13	1.43	No	No	Uninflamed
Vagina 14	12.7	No	No	Uninflamed

We next examined changes in marker expression across all MNP populations between uninflamed and inflamed tissue. As in **section 4.3.4.3**, the mean gMFI values were calculated across all donors (**Figure 4.13**) and statistical analysis performed on each individual donor (**Supplementary figure 4.7**). In the LP (**Figure 4.13a, Supplementary figure 4.7a**), CD11c was elevated on cDC1s in inflamed tissue, however no other significant trends were observed in this cell population. CD163, langerin, CCR7 and HLA-DR were all consistently higher on most MNP populations derived from inflamed tissue; higher CCR7 and HLA-DR was indicative of an activated state. Interestingly, MR was reduced in inflamed tissue. In the epithelium (**Figure 4.13b, Supplementary figure 4.7b**), similar tends were observed for CCR7, HLA-DR and MR. Notably, Axl expression was consistently elevated across all inflamed MNP populations, with significant increases on cDC2s, MDDCs and MDMs.

Altogether, these findings highlight differences in cell composition and marker expression between uninflamed and inflamed tissue environments, suggesting that inflammation drives the influx of new cells, particularly those of a monocytic origin, and modulates marker expression, subsequently altering the phenotype of most populations.

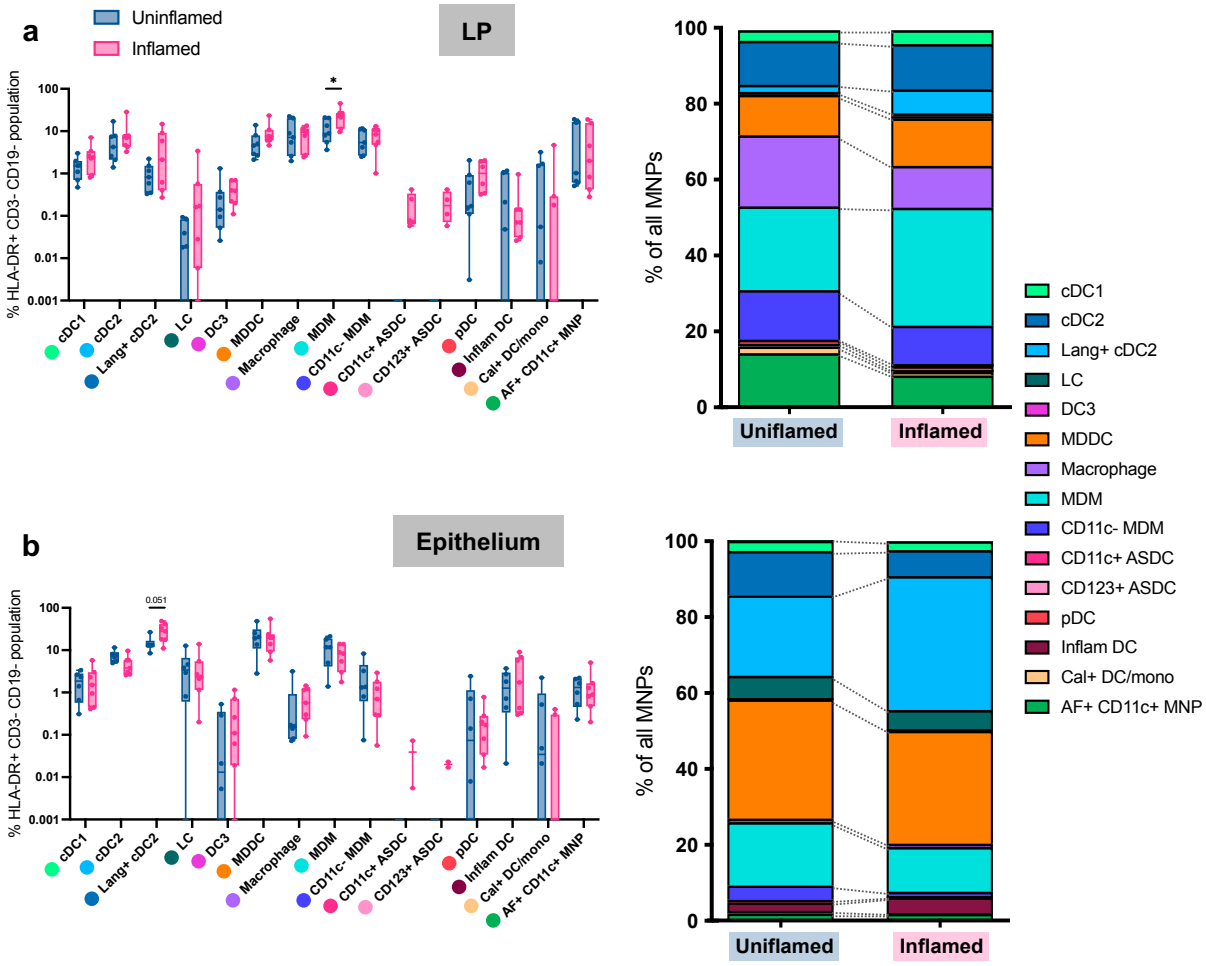

Figure 4.12: Proportional comparison of uninflamed and inflamed mononuclear phagocyte populations from vaginal mucosa

Vaginal immune cells were stained with the flow cytometry panel shown in **Supplementary table 3.2** and divided by their assigned inflammatory status outlined in **Table 4.8**. Relative proportions of each uninflamed (blue, n=7) and inflamed (pink, n=7) MNP subset were determined as a percentage of the HLA-DR$^+$ CD3$^-$ CD19$^-$ gate (left side graphs) for the **a)** LP and **b)** epithelium and displayed as box and whiskers plots. Proportions of total MNPs (right side graphs) were from data presented in the left graphs. Dotted lines connect populations. Statistical analysis was performed using the multiple Mann-Whitney test for pairwise comparison (*p<0.05).

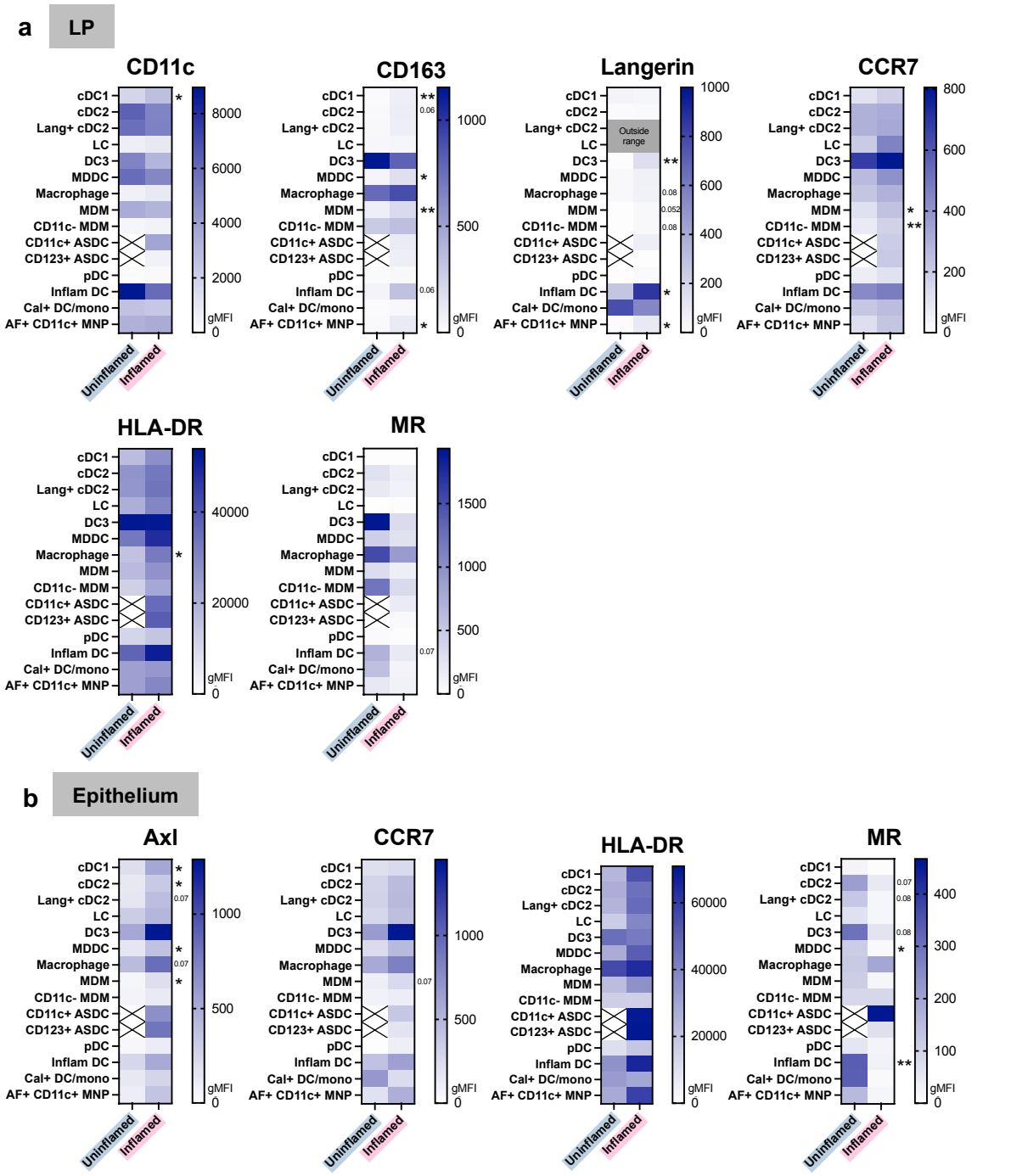

Figure 4.13: Differential average marker expression between uninflamed and inflamed mononuclear phagocyte populations of the vagina

Isolated vaginal cells were stained with the flow cytometry panel in **Supplementary table 3.2** and divided by inflammatory status in **Table 4.8**. Heatmaps show average gMFI values for marker expression in MNP populations from uninflamed samples (left column, blue) and inflamed samples (right column, pink). **a)** In the LP, markers CD11c, CD163, Langerin, CCR7, HLA-DR and MR display differences in expression between the uninflamed and inflamed samples. **b)** In the epithelium, Axl, CCR7, HLA-DR and MR show differences in expression between uninflamed and inflamed. Statistical analysis was performed using the multiple Mann-Whitney test for pairwise comparison (*p<0.05).

4.3.5.2 Defining the Inflammatory Dendritic Cell Populations of Vaginal Mucosa

The clustering analysis in **section 4.3.2.4** identified four cell populations previously reported in the literature as inflammatory (Warner van Dijk et al., 2024, Chen et al., 2020): CD11c^{+} ASDCs, CD123^{+} ASDCs, pDCs and Inflammatory DCs. While neither the inflammatory DCs or pDCs displayed significant proportional differences between uninflamed and inflamed vaginal tissue (**Figure 4.12**), their established association with inflammation in the literature justified further phenotypic investigation.

The gMFI of key defining markers (**Figure 4.14a**) and HIV lectin receptors MR, Siglec-1, DC-SIGN and langerin (**Figure 4.14b**), were quantified for the inflammatory samples in the vaginal LP. ASDCs were characterised as HLA-DR^{hi}, CD5^{+}, Siglec-6^{+} and CD123$^{lo/+}$, and pDCs HLA-DR^{lo}, CD5^{-}, Siglec-6$^{lo/-}$ and CD123^{hi}. These findings are consistent with previous definitions in human blood (Warner van Dijk et al., 2024), however this represents their first characterisation in human genital mucosal tissue. Interestingly, ASDCs, particularly the CD11c^{+} subset, also uniquely expressed CD88, a marker traditionally expressed by monocytes (Mair and Liechti, 2021, Dutertre et al., 2019), suggesting CD88 to be a potential marker for tissue ASDC identification. Although ASDCs were first described as Axl^{+} Siglec-6^{+} cells (Villani et al., 2017), our data suggests that in tissue environments, CD5 and Siglec-6 may be more reliable markers. The fluorophore assigned to Axl in our flow cytometry panel strongly interacted with the AF signal emitted by the tissue resident macrophages, which are also known to highly express Axl (Fujimori et al., 2015). Therefore, the detected Axl signal across most populations was sub-optimal and potentially accounts for its lack of expression on ASDCs. This interaction was not as prominent in the epithelium as there was less AF signal. CD5 is a more distinct marker, expressed exclusively by a subset of cDC2s and ASDCs and hence a more suitable tissue marker.

The inflammatory DCs displayed an unusual heterogeneous phenotypical profile, expressing a broad variety of markers including CD5, CD11c, CD1c, CD14, CD163, CCR7, CD1a, MR, Siglec-1, DC-Sign and langerin, all with a large range in expression. Collectively, these markers represent a complex combination of DC and macrophage characteristics. To better understand this heterogeneity, we further investigated the CD1a^{+} CD123^{+} compartment deemed ‘Inflammatory DC’.

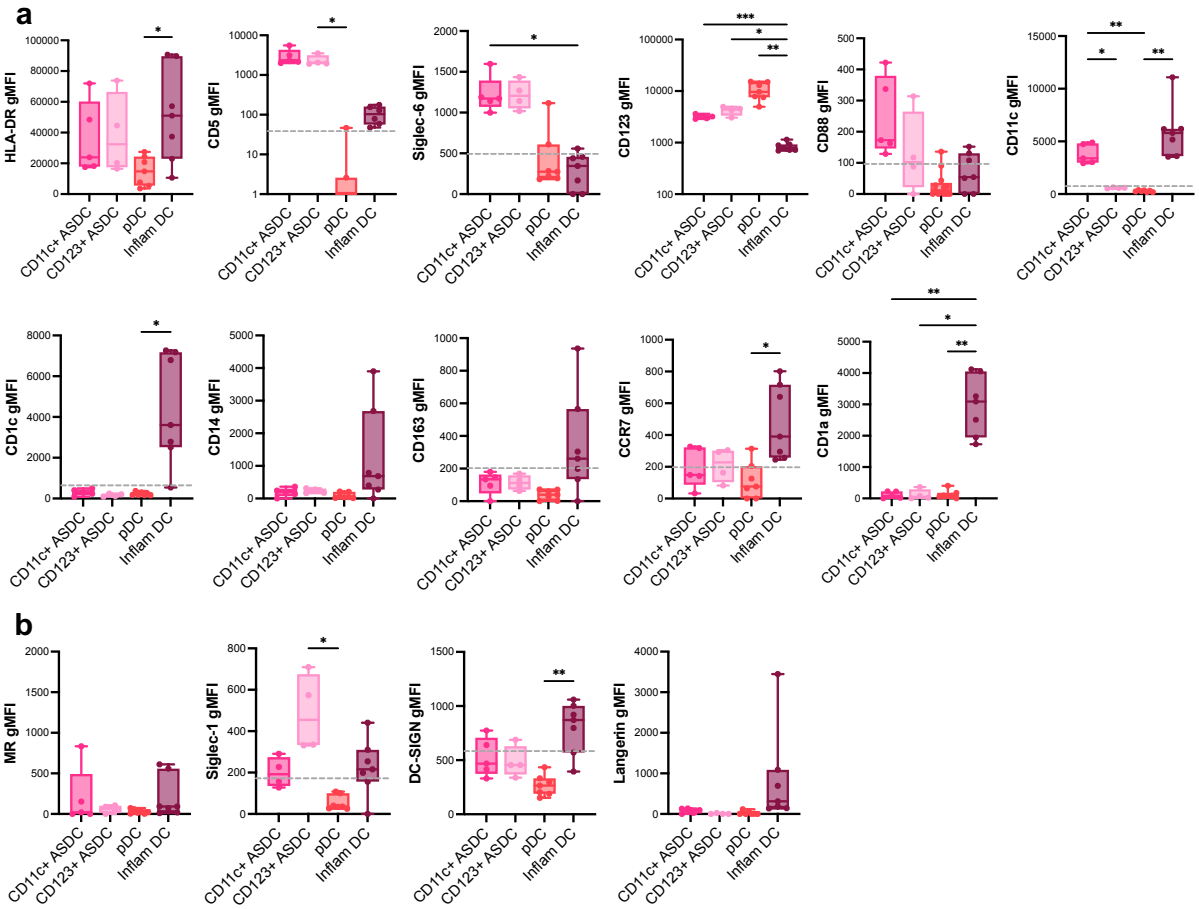
a
HLA-DR gMFI
CD5 gMFI
Siglec-6 gMFI
CD123 gMFI
CD88 gMFI
CD11c gMFI
CD1c gMFI
CD14 gMFI
CD163 gMFI
CCR7 gMFI
CD1a gMFI
CD11c+ ASDC
CD123+ ASDC
pDC
Inflam DC
b
MR gMFI
Siglec-1 gMFI
DC-SIGN gMFI
Langerin gMFI

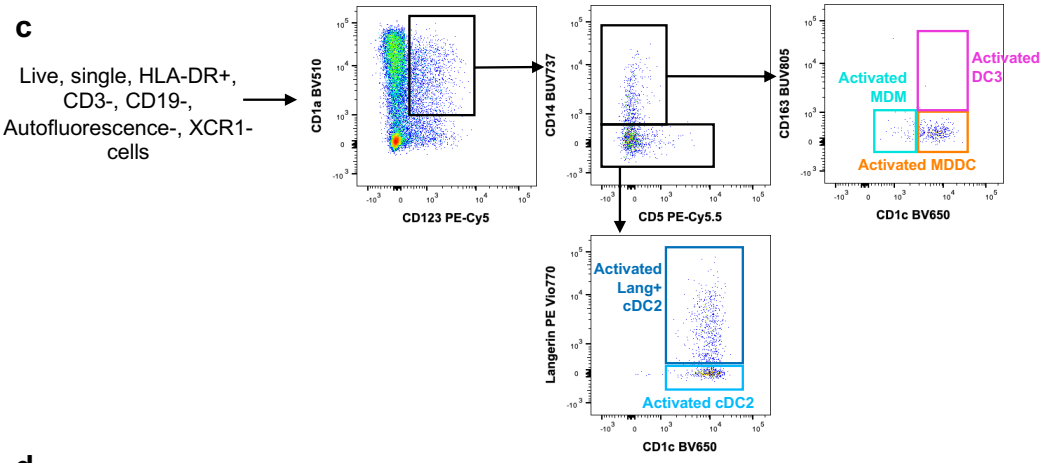
c
Live, single, HLA-DR+, CD3-, CD19-, Autofluorescence-, XCR1- cells
CD1a BV510
CD123 PE-Cy5
CD14 BUV737
CD5 PE-Cy5.5
CD163 BUV805
CD1c BV650
Activated MDM
Activated DC3
Activated MDDC
Langerin PE Vio770
Activated Lang+ cDC2
Activated cDC2

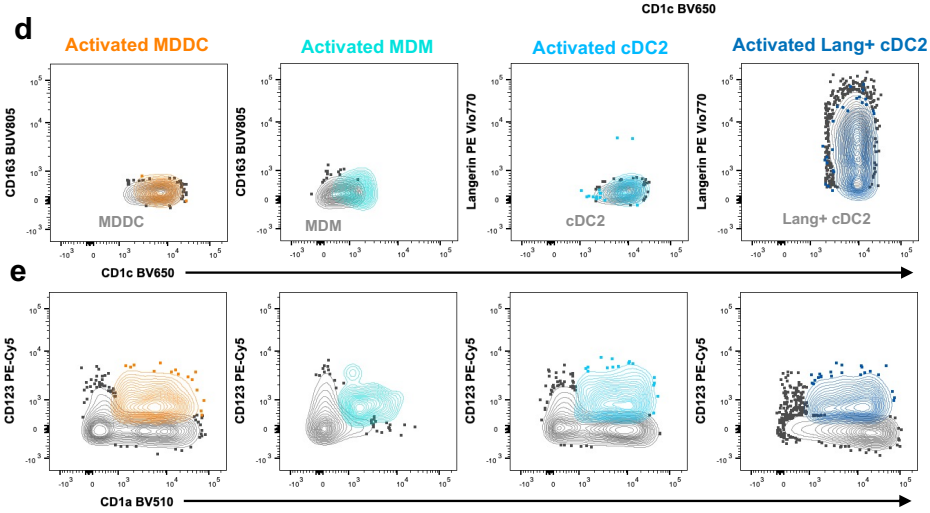
d
Activated MDDC
Activated MDM
Activated cDC2
Activated Lang+ cDC2
CD163 BUV805
Langerin PE Vio770
MDDC
MDM
cDC2
Lang+ cDC2
CD1c BV650
e
CD123 PE-Cy5
CD1a BV510

Figure 4.14: Phenotypic profile of inflammatory dendritic cell populations isolated from vaginal tissue

Vaginal cells were isolated and stained using the panel shown in **Supplementary table 3.2**. gMFI values for **a)** interesting defining markers (HLA-DR, CD5, Siglec-6, CD123, CD88, CD11c, CD1c, CD14, CD163, CCR7, CD1a) and **b)** HIV binding lectin receptors (MR, Siglec-1, DC-SIGN, Langerin) were obtained for the populations: $CD11c^+$ ASDC, $CD123^+$ ASDC, pDC and Inflam DC and graphed as box and whisker plots. Statistical analysis was performed using the mixed-effects analysis with Tukey's multiple comparisons (*p<0.05, **p<0.01, ***p<0.001). Grey dotted line indicates minimum detection level for markers (the zero line). A zero line higher than the graphs defined zero indicates spread into the detection channel. **c)** The CD123+ CD1a+ Inflammatory DCs were further gated to define five distinct, activated MNP subsets: $CD14^+$ $CD163^+$ $CD1c^+$ **DC3**, $CD14^+$ $CD163^-$ $CD1c^+$ **MDDC**, $CD14^+$ $CD163^-$ $CD1c^-$ **MDM,** $CD14^-$ $langerin^+$ $CD1c^+$ **$langerin^+$ cDC2** and $CD14^-$ $langerin^-$ $CD1c^+$ **cDC2**. Each activated subset was overlaid with its non-activated counterpart as **d)** defined in the gating described in c, and **e)** as a plot of CD1a vs CD123.

We found that within this population, the cells could be divided into distinct populations based on canonical markers: MDDCs ($CD14^+$ $CD1c^+$ $CD163^-$), MDMs ($CD14^+$ $CD1c^-$ $CD163^-$), DC3s ($CD14^+$ $CD1c^+$ $CD163^+$), cDC2s (CD14- $CD1c^+$ $langerin^-$) and $langerin^+$ cDC2s ($CD14^-$ $CD1c^+$ $langerin^+$) (**Figure 4.14c**). We hypothesised that this inflammatory DC population represented a pool of activated MNP subsets, upregulating CD123 in response to environmental stimuli rather than a distinct population. We confirmed the similarity between the core populations and their activated states by overlaying the two, as shown in **Figure 4.14d**, and found the only differential feature was the increased expression of CD123 (**Figure 4.14e**).

4.3.6 Defining HIV Interactions with Mononuclear Phagocytes in Vaginal Mucosa

Following the definition and phenotypic profiling of MNPs in vaginal tissue, we next assessed the capacity of each of the 15 identified vaginal MNP subsets to bind HIV by examining their HIV-binding receptor profiles and performing HIV uptake assays.

Due to the time restraints associated with this thesis, only three vaginal donors were processed for HIV uptake assays. However, all vaginal donors were included in the analysis of HIV binding receptor expression.

4.3.6.1 Vaginal Mononuclear Phagocytes Express a Unique Array of HIV Binding Receptors

CD4 is the main HIV entry receptor, while the lectin receptors MR, Siglec-1, DC-SIGN and langerin are all known to bind and mediate endocytic uptake of HIV. To assess the potential for HIV binding and uptake, the percentage expression of these five HIV-binding receptors was quantified across all previously defined MNP subsets (**Figure**

4.15a). Percentage expression was used over gMFI in this instance to determine the frequency of cells expressing a certain marker in each population rather than the intensity of expression per cell.

CD4 expression was high across all MNPs in the LP, exceeding 80% in all populations except for CD11c$^-$ MDMs, Calprotectin$^+$ DC/monocytes and AF$^+$ CD11c$^+$ MNPs, though they still showed expression above 60%. This indicates that all 15 MNP subsets possess a reasonably high ability to bind HIV via CD4.

The expression patterns of HIV binding lectin receptors showed that cDC1s and pDCs lacked expression of MR, Siglec-1 and DC-SIGN. Of all lectin receptors, MR had the most widespread expression across subsets, with the highest expression on Macrophages (mean 67%), followed by comparable levels on DC3s, MDDCs, CD11c- MDMs and inflammatory DCs (mean ~50%), then cDC2s, langerin$^+$ cDC2s, MDMs, Calprotectin$^+$ DC/monocytes and AF$^+$ CD11c$^+$ MNPs (mean ~30%).

Siglec-1 expression was again significantly highest on Macrophages, more than twice that of any other population (mean 88%). Moderate expression was detected on DC3s, CD11c$^-$ MDMs and CD123$^+$ ASDCs (mean ~30%), while MDDCs, MDMs, CD11c$^+$ ASDCs, inflammatory DCs, Calprotectin$^+$ DC/monocytes and AF$^+$ CD11c$^+$ MNPs were low expressors (mean ~10-20%).

DC-SIGN followed a similar pattern, with Macrophages expressing the highest levels (mean 58%), followed by DC3s and CD11c$^-$ MDMs, as well as Calprotectin$^+$ DC/monocytes and AF$^+$ CD11c$^+$ MNPs (mean ~20-30%). Low expression was observed on MDDCs, MDMs, and inflammatory DCs (mean ~10%).

Langerin expression was, as expected, dominated by langerin$^+$ cDC2s and LCs. Moderate levels were observed on inflammatory DCs (mean 22%) and Calprotectin$^+$ DC/monocytes (mean 45%) and low expression detected across all other subsets (mean ~5%).

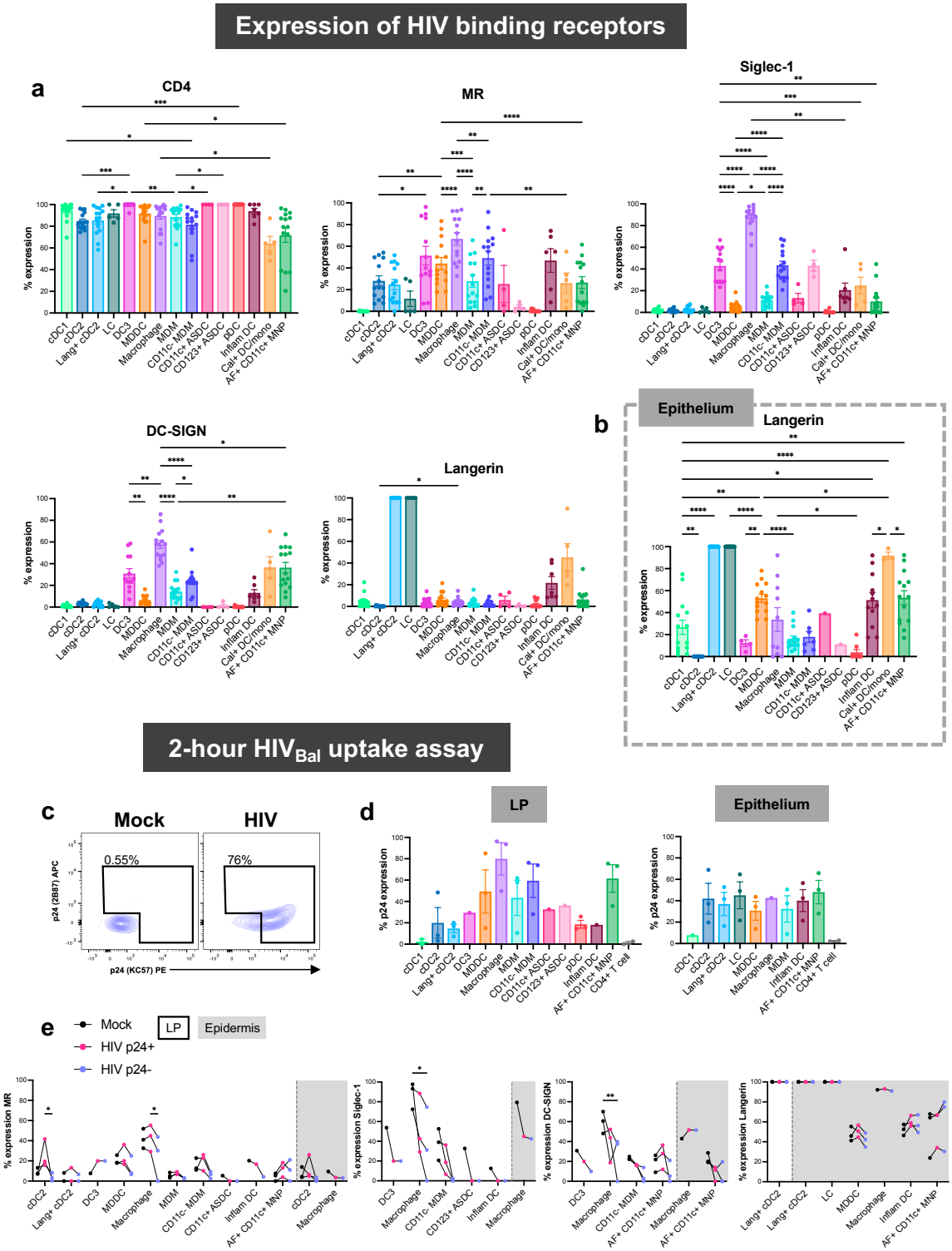

Figure 4.15: HIV uptake capacity of vagina mononuclear phagocyte populations

a-b) Isolated vaginal immune cells were stained with the panel in **Supplementary table 3.2**. Percentage expression of HIV binding receptors CD4, MR, Siglec-1, DC-SIGN and langerin was gated on each MNP population in the **a)** LP and **b)** epithelium (langerin only shown). Statistical analysis was performed using the mixed-effects analysis with Tukey's multiple comparisons (*p<0.05, **p<0.01, ***p<0.001, ****p<0.0001). Not all significances are displayed. **c-f)** Cells were liberated from vaginal mucosa and exposed to HIV_{BaL} (MOI=5) for 2 hours before staining with the uptake panel in **Table 4.4**. **c)** Representative gating demonstrating dual p24 expression, with the mock treated sample used to determine $p24^+$ gate.

Continued over page

d) Percentage of dual p24 expression across all MNP subsets and CD4 T cells. There were insufficient donor numbers (n=3) to perform statistical analysis across all populations. **e)** Percentage expression of MR, Siglec-1, DC-SIGN and Langerin on select MNP subsets (>20% marker expression and >10% uptake) for mock cells, HIV $p24^+$ cells and HIV p24- cells. Statistical analysis was performed using the two-way ANOVA (*p = <0.05).

The pattern of epithelial expression of all receptors was similar to those in the LP (**Supplementary figure 4.8a**), with the exception of langerin, which showed a differential expression profile as previously described in **section 4.3.4.3**. In the epithelium, langerin expression increased across all subsets (**Figure 4.15b**). The most distinctive increases were noted in MDDCs and AF^+ $CD11c^+$ MNPs, which expressed langerin at 5 times the level it was in the LP (both means from 6% to 53%), indicating an increased likelihood of HIV binding via langerin in the epithelium.

Collectively, Macrophages expressed the highest levels of MR, Siglec-1 and DC-SIGN, the latter two being extensively linked to HIV binding and uptake in the literature (Geijtenbeek et al., 2000, Perez-Zsolt et al., 2019, Ruffin et al., 2019). Additionally, DC3s, CD11c- MDMs, $Calprotectin^+$ DC/monocytes and AF^+ $CD11c^+$ MNPs all displayed moderate expression of MR, Siglec-1 and DC-SIGN, indicating that they can potentially mediate endocytic uptake of HIV.

The list of all significances for each receptor across all 15 MNP subsets can be found in **Supplementary table 4.3** and **Supplementary table 4.4**.

4.3.6.2 Vaginal Mononuclear Phagocytes Can Bind HIV within 2 Hours of Exposure

After establishing the HIV binding receptor profiles of vaginal MNPs, we next investigated their capacity to bind and take up HIV. Isolated vaginal cells were incubated with a lab adapted strain of HIV_{BaL} (MOI 5) for two hours, then surface stained with the flow cytometry panel outlined in **Chapter 3**. Cells were then stained intracellularly with two anti-p24 antibodies, an HIV capsid protein which allows for the quantification of HIV uptake. Dual p24 signal was detected using a mock condition for gating (**Figure 4.15c**). CD103 PE Vio615 and calprotectin PE were removed from this panel to accommodate dual p24 staining, therefore no uptake data was collected for $Calprotectin^+$ DC/monocytes. As a further comparison, CD4 T cells were gated and included in the uptake data.

In both the LP and epithelium, CD4 T cells and cDC1s showed no or low p24 signal compared to all other MNP subsets, indicating limited HIV binding (**Figure 4.15d**). In the LP, Macrophages exhibited the highest HIV uptake with a mean p24 expression of 80% (± 15) correlating with their highest expression of HIV-binding lectin receptors. This was followed by MDDCs (mean 49% ± 20), MDMs (mean 43% ± 16), CD11c- MDMs (mean 59% ± 16) and AF^+ $CD11c^+$ MNPs (mean 61% ± 1). The least amount of uptake was observed by cDC2s (mean 20% ± 14), $langerin^+$ cDC2s (mean 15% ± 4) and pDCs (mean 19% ± 4), but nonetheless still present. DC3s, both ASDC subsets and inflammatory DCs demonstrated 20-30% p24 expression, however each population was derived from a single donor (n=1). As such these findings should be interpreted with caution, although, they represent the first evidence of these populations binding HIV in vaginal tissue. Further experimental repeats across all populations would need to be performed to confirm any statistically significant findings.

In the epithelium, HIV uptake across all subsets ranged between 30-50%. Of note, no apparent distinction in binding efficiency was observed between cDC2, $langerin^+$ cDC2 and LCs – a contrast to that observed in skin, where $langerin^+$ cDC2s demonstrated higher HIV binding after 2 hours than LCs (Bertram et al., 2019).

We additionally investigated our previously observed phenomenon in colorectal macrophages, where Siglec-1 expression decreased following HIV exposure (**Supplementary figure 4.8b**) (unpublished, Erica Vine PhD Thesis, 2025). To explore whether this phenomenon also occurred in vaginal MNPs, we compared the percentage expression of all four lectin receptors across mock cells, HIV $p24^+$ cells and HIV $p24^-$ cells (**Figure 4.15e**). The populations chosen for this analysis expressed the marker of interest at >20% and >10% p24 expression. Interestingly, a distinct pattern was observed for both MR and Siglec-1. The expression of MR on the HIV $p24^+$ cells was elevated compared to mock and HIV $p24^-$ cells, indicating cells with higher MR expression preferentially bound HIV within 2 hours. Conversely, consistent with our observations in colorectal tissue, Siglec-1 expression was lower on the HIV $p24^+$ cells compared to mock, and lower or equivalent on the HIV $p24^-$ cells relative to HIV $p24^+$. Although Siglec-1 blocking could not be performed to confirm this internalisation in vaginal MNPs, Siglec-1 blocking in colorectal macrophages resulted in a 60% reduction in p24 expression, supporting Siglec-1 to be a key HIV binding receptor with capabilities to quickly internalise the virus (**Supplementary figure 4.8c**)

(unpublished, Erica Vine PhD Thesis, 2025). No apparent trend was observed for DC-SIGN or langerin.

Taken together, it is evident that vaginal MNPs possess the capacity to bind HIV through diverse expression of HIV binding receptors. Macrophages are the most efficient at HIV binding and uptake as they exhibit the highest lectin receptor expression and p24% expression. However, additional donors should be included in the future to confirm these findings and further explore other MNPs HIV binding potential. Future work should also investigate HIV blocking assays to confirm the above and explore productive HIV infection and transfer to CD4 T cells in vaginal tissue.

4.4 Discussion

Defining the MNP landscape in human genital tissues is critical to providing a biologically relevant insight into the early events of pathogen capture and the following immune cascade. A global research limitation in this field is restricted access to human anogenital tissue. However, in this study, our privileged access to a range of human genital tissues, including foreskin, labia, vagina and cervix, has allowed for an extensive definition of the specific MNPs that reside in genital tissues. Utilising high parameter flow cytometry and unbiased clustering tools we defined 15 MNP populations present within inflamed and uninflamed tissues and investigated their capacity to bind and take up HIV. The different genital tissues contained highly heterogeneous MNP compositions, each tissue having a unique constitution regardless of their classification as a skin or mucosa. In vaginal tissue, the phenotypic profiles of cDC1s, DC3s and transitional state macrophages were further characterised, as these were unique populations in vagina. In particular, we showed for the first time that CD14 expressing MNPs, particularly MDDCs and MDMs, were abundant in the epithelium. We also revealed that CD123-expressing populations (including pDCs, ASDCs and CD123$^+$ CD1a$^+$ Inflammatory DCs) were present in inflamed tissues and that MDMs and langerin$^+$ cDC2s infiltrated the LP and epithelium respectively. Each MNP had a unique HIV lectin receptor profile, mostly displaying potential to bind HIV. Macrophages were most efficient at binding and taking up HIV after 2 hours of topical exposure, likely owing to their high expression of DC-SIGN and Siglec-1. DCs and other macrophage subsets were also able to bind HIV, although to a lesser extent than macrophages.

4.4.1 Mononuclear Phagocytes are Highly Heterogenous across Different Genital Tissues

Genital tissues are comprised of skin (outer foreskin and labia), type II mucosa (inner foreskin, vagina and ectocervix) or type I mucosa (endocervix). Skin has a thick outermost layer of keratinised cells (stratum corneum) whereas in type II mucosa this layer is thinner. Tissues classified as skin or mucosa have traditionally been considered histologically similar across different anatomical regions, for example, the skin of the labia and outer foreskin, or the type II mucosa of the inner foreskin and vagina (Iwasaki, 2010). Furthermore, we previously showed that there were only minor

differences in the composition of immune cell populations that inhabit different genital tissue types (Rhodes et al., 2021). However, here we observed the proportions of MNPs in the outer and inner foreskin to be more akin to each other than to their tissue category. This was particularly seen in the epithelium where more than 50% of both the inner and outer foreskin MNP composition was LCs, a classical skin epidermal feature (Rhodes et al., 2021) (**Figure 4.6d**). In fact, several studies have demonstrated there to be no difference in stratum corneum thickness between inner and outer foreskin (Dinh et al., 2010, Dinh et al., 2012, Qin et al., 2009), emphasising the two tissues to be histologically very similar. Additionally, the inner and outer foreskin are in close proximity anatomically, compared to the labia (skin) and vagina (type II mucosa). This can be linked to their embryological development, as the inner and outer foreskin both arise from the external genitalia portion of the embryonic gonad whilst the labia differentiates from the external gonad and vagina from internal gonad (Pinson et al., 2023). These structural and developmental similarities support our observations that the inner foreskin more resembles skin in its immune composition than type II mucosa.

We also observed a distinct sex-based difference in the expression of CD14, which was expressed more highly in tissues of the female genital tract (FGT), particularly labia and vagina, in both the LP and epithelium (**Figure 4.7b**). CD14 functions as a pattern recognition receptor for molecules such as bacterial lipopolysaccharides (LPS) (Pugin et al., 1994), facilitating innate immune responses including phagocytosis in macrophages (Devitt et al., 2003) and driving inflammation in disease states, such as Crohn's Disease (Kamada et al., 2008). There are limited reports examining the sex-based differences in CD14 expression – one study reported increased CD14 expression on placental macrophages from female infants (Paparini et al., 2024) whilst another saw higher CD14 expression on male blood monocytes (Jiang et al., 2014). However, a mouse study found that exogenous *in vivo* estrogen administration elevated CD14 expression on peritoneal macrophages (Rettew et al., 2009), suggesting that female sex hormones may influence CD14 expression. Although this study did not examine if endogenous estrogen influenced CD14 expression, it is well established that tissues of the FGT are highly estrogen-sensitive, having significantly higher levels of estrogen and estrogen receptors compared to plasma (Wiegerinck et al., 1983, Forsberg, 1995). Thus, the differing hormone levels that occur through the

menstrual cycle may account for the elevated CD14 expression seen across the FGT. Furthermore, in post-menopausal patients, hormone replacement therapy likely influences CD14 expression. Although menopausal statuses for tissues we obtained in this study were not reported, the use of topical vaginal estrogen to treat vaginal prolapse perioperatively is a standard medical practice (Sicilia et al., 2025) – potentially explaining the ubiquitous elevation in CD14 expression in patients of an older age.

4.4.2 Vaginal Mononuclear Phagocytes are Phenotypically Unique Compared to Skin and Other Mucosal Tissues

A central focus of this study was to conduct an extensive characterisation of all MNPs residing in the vaginal mucosa based on the most recent MNP classifications, which in the cases of DC3s, are mostly based on studies in human **blood** (Bourdely et al., 2020, Villani et al., 2017, Dutertre et al., 2019, Mair and Liechti, 2021). Other MNP subset definitions were based on studies in **trunk skin** (Alcántara-Hernández et al., 2017, Bertram et al., 2019, Rhodes et al., 2021) and **mucosa** (often intestinal) (Doyle et al., 2021, Parthasarathy et al., 2024). This study is the first to comprehensively define these populations in the genital tissues where HIV transmission occurs.

4.4.2.1 cDC1

Vaginal cDC1s displayed a phenotype different to blood, skin and intestinal cDC1s presenting as XCR1^{+} CD11c$^{+/lo}$ CD141$^{+/-}$ CADM1^{-} CLEC9A^{-} CD103^{-} SIRPα^{-} (**Figure 4.8a-c**). Mair and Liechti (2021) recommended the use of CD141 and CADM1 over XCR1 to identify cDC1s in blood owing to the lack of complete co-expression between XCR1 and CD141. However, we found XCR1 to be a more suitable defining marker in vagina. While we saw some variance in XCR1 and CD141 co-expression, XCR1 isolated a cleaner, more distinct population of cDC1s, as the CD141^{+} cells contained a population of cDC2s. CD141 is well reported to be an unreliable cDC1 marker in tissue, expressed also by monocytes, cDC2s and MDMs especially during inflammation (Haniffa et al., 2012, Botting et al., 2017). Our unbiased clustering also revealed that vaginal cDC1s expressed CD11c, an interesting finding as trunk skin cDC1s are CD11c^{-} (Botting et al., 2017, Rhodes et al., 2021) whereas intestinal cDC1s are CD11c^{+}, albeit expressed at lower levels than on cDC2s and MDDCs (Doyle et al., 2021). In this study we saw that there was a wide spectrum of CD11c expression by

cDC1s residing within different tissues (**Figure 4.4**), suggesting that CD11c expression levels are at least partially mediated by the tissue micro-environment. Moreover, CD11c was upregulated by cDC1s derived from inflamed tissues (**Figure 4.13a**), as previously seen in splenic monocytes (Drutman et al., 2012).

4.4.2.2 DC3

DC3s are currently a subject of much interest in the DC literature since their recent discovery. The literature best defines them as $CD45^+$ HLA-DR^+ $CD1c^+$ $CD163^+$ $CD14^{+/-}$, though this is largely based on cells derived from blood. Their definition as a distinct DC subset is based on studies that have shown distinct developmental lineages from cDC1s and cDC2s (Villani et al., 2017, Dutertre et al., 2019, Bourdely et al., 2020, Cytlak et al., 2020). A critical challenge remains their accurate definition in tissue, with a lack of distinct identifying surface markers (Parthasarathy et al., 2024). CD1c and CD14 are defining markers of MDDCs, while CD163 and CD14 are features of macrophages. We further confirmed this phenotypical similarity in vaginal tissue, demonstrating DC3s and MDDCs to have indistinguishable expression of CD11c, CD11b and MR. DC3s were only distinguishable by their higher expression of CD14 and CCR7 (**Figure 4.8d&e**). Interestingly, Rhodes et al. (2021) found MDDCs to express the highest levels of CCR7, indicative of their capacity for spontaneous migration out of tissue, however their MDDCs would have contained DC3s. Expressional similarity was also observed with macrophages, as we detected Siglec-1 and DC-SIGN expression on DC3s – markers thought to be macrophage exclusive (Rhodes et al., 2021). Furthermore, when comparing the expression of CD163 across all genital tissues, CD163 was expressed more highly in skin compared to mucosa, particularly by Macrophages (**Figure 4.7a**), suggesting CD163 to be a distinct marker in skin and blood, but not in mucosa. Whilst DC3s, MDDCs and macrophages have varying patterns of the forementioned markers, the need for up to 10 markers to ensure accurate definition is far from ideal. There is a demand to identify DC3-exclusive markers, especially in mucosa. As a future direction, employing the use of high depth single cell RNA sequencing technologies on enriched MNPs ($CD45^+$ HLA-DR^+) derived from a range of anogenital tissues would allow for an extensive exploration of markers unique to mucosal DC3s.

It should also be noted that DC3s were proportionally small in the vagina and cervix compared to the foreskin and labia, signifying they are perhaps a more skin-specific population (**Figure 4.6a&b**). For future investigation, more donors should be collected across all genital tissues to compare DC3s proportions and phenotype, with the addition of blood and trunk skin as comparison controls.

4.4.2.3 Transitional Macrophages

A notable finding of the unbiased clustering analysis was the identification of multiple macrophage populations beyond the traditional distinction of tissue resident macrophages (AF^+ $CD11c^-$) and MDMs (AF^- $CD11c^+$). Bujko et al. (2018) identified four distinct macrophage subsets in intestinal tissue, termed Mf1-4, where Mf1s represented the most monocytic macrophages and Mf4s as tissue resident macrophages. The Mf1s phenotypically aligned with our MDMs as $CD11c^+$ $CD14^+$ $CD11b^{++}$ $CD163^{lo}$ MR^- AF^-, and Mf4s with our Macrophages as $CD11c^+$ $CD14^{++}$ $CD11b^{+/lo}$ $CD163^+$ MR^+ AF^+. We additionally saw a distinction in the lectin receptors Siglec-1 and DC-SIGN, being highly expressed by macrophages and minimally by MDMs (**Figure 4.9**). Bujko and colleagues concluded Mf2/3 to be intermediary differentiation stages between early monocytes and tissue residence, based on expression profiles and functionality – MDMs being more pro-inflammatory and macrophages more homeostatic. Whilst our $CD11c^-$ MDMs and AF^+ $CD11c^+$ MNPs were not identical to Mf2/3s, we hypothesised these populations to also be intermediary macrophages, each displaying different, in-between features of either being monocytic or tissue resident. Importantly, the AF^+ $CD11c^+$ MNPs were a uniquely transitional macrophage in the vagina. This transitional state was further supported by the relatively low abundance of $CD11c^-$ MDMs and AF^+ $CD11c^+$ MNPs in the epithelium compared to MDMs (**Figure 4.6c&d**). Monocyte-derived cells are highly migratory (Ginhoux et al., 2006) whereas tissue resident macrophages have a limited migratory capacity and therefore unlikely to reside in the epithelium (Tamoutounour et al., 2013).

$Calprotectin^+$ monocytes/DCs were also identified as AF^+. Monocytes can emit low levels of AF signal (Knab et al., 2025), with some studies suggesting that AF signatures can increase in pathological conditions including atherosclerosis and breast cancer (Fink et al., 1996, Heaster et al., 2020). However, this population was

not further phenotypically explored in this study due to limited sample numbers and their many-or-none presence. Additionally, no uptake data was recorded as calprotectin was removed from the panel to accommodate p24. Future investigations should look to modify the flow cytometry panel to ensure calprotectin's inclusion.

4.4.3 Redefining the Epithelial Landscape of Vaginal Tissue: Epithelial CD14$^+$ Mononuclear Phagocytes

The stratified squamous epithelium that comprises the epidermis of skin and epithelium of type II mucosa has been traditionally thought to contain LCs only and therefore has been largely ignored in terms of defining other MNPs. An important feature of this investigation was the use of a single gating strategy to define MNPs in the LP and epidermis/epithelium. This revealed that CD14$^+$ MNPs, primarily MDDCs and MDMs, constitute almost 50% of all vaginal epithelial MNP populations (**Figure 4.6d**). Previous *in vivo* studies in mice have demonstrated that circulating monocytes can migrate into the epidermis and differentiate into LCs, a process enhanced during inflammation (Ginhoux et al., 2006, Seré et al., 2012). An *in vitro* model of reconstructed human skin found that dermal CD14$^+$ cells could also migrate into the epidermis and differentiate, morphologically and phenotypically, into LCs, downregulating CD14 and upregulating langerin and CD1a (Larregina et al., 2001). Birbeck granules, a unique structural LC feature, were observed in ~60% of cells. This differentiation was driven by a range of environmental stimuli including epithelial factor MIP-3α and inflammatory factor GM-CSF. In response to UV radiation in human skin, CD14$^+$ monocytes and macrophages have been seen to infiltrate the epidermis (Achachi et al., 2015). Our data confirms previous reports of the presence of epithelial CD14$^+$ MNPs and importantly adds quantification.

Whether vaginal epithelium is dominated by LCs (van Teijlingen et al., 2023, Liu et al., 2021) or by DCs (Bertram et al., 2019, Bertram et al., 2023) remains debated. In this study, we confirmed the latter. This raises the question of whether the CD14$^+$ MNPs migrating into vaginal epithelium are indeed differentiating into LCs, given their minimal presence. Both Larregina et al. (2001) and Achachi et al. (2015) reported a decrease in CD14 expression on their respective epithelial CD14$^+$ MNPs 6-10 days post stimulation with cytokines or UV radiation, and an upregulation of langerin and CD1a. We similarly observed a heightened expression of langerin and CD1a across

almost all epithelial populations (**Figure 4.10b**), both of which are known to be induced by the epithelial factor TGF-β1 (Lang et al., 2023, Capucha et al., 2018). Interestingly, Achachi and colleagues additionally observed upregulation of markers CD1c, MR and CD163 on day 4 post stimulation, suggesting the emergence of monocyte-derived DC and macrophage populations. Furthermore Birbeck granules are considered a defining feature of LCs but their biogenesis has been shown to be dependent on very high langerin expression, making them a default feature of langerin expression rather than an exclusive feature of LCs (Mc Dermott et al., 2002). Together, this information could suggest that $CD14^+$ monocytes and MNPs migrate into epithelium and, differentiate into MDMs and MDDCs, and acquire the expression of langerin, CD1a and Birbeck granules by nature of the epithelial environment. Additionally, epithelial $CD14^+$ MNPs may represent cells in a transitional state, to becoming cDC2s or LCs, that have not yet downregulated CD14. Future investigations should determine the functionality of these epithelial $CD14^+$ MNPs relative to LCs and cDC2s, tracking changes in phenotype and function as the enter the epithelial space.

4.4.4 Defining Mononuclear Phagocytes in Inflamed Tissues

After phenotyping the vaginal MNPs, we next investigated changes in MNP landscape between homeostatic and inflammatory samples. Across the LP and epithelial compartments, most populations displayed an upregulation of CCR7, a lymph node homing marker, and HLA-DR, a classical immune cell marker associated with immune activation (**Figure 4.13**). Both markers have been previously implicated with inflammatory environments and disease states and considered biomarkers of inflammation, induced by inflammatory factors prostaglandin E2, IFN-γ and TNFα (Hauser et al., 2016, Scandella et al., 2002, Epstein et al., 2013, Ouyang et al., 1988, Cross et al., 2021). Interestingly, MR was expressed at a lower level by cells in inflamed tissues. In the context of macrophages, high MR expression is characteristic of M2-like mature, homeostatic macrophages, supporting their increased prevalence in uninflamed tissue (Wright et al., 2021). Although this does not directly account for the decreased expression on DC subsets, a similar principle of tissue residency and maturity could apply. Interestingly however, CD163, which is generally co-expressed with MR on mature macrophages, was increased in its expression.

In the epithelium, there was a ubiquitous upregulation of Axl across most MNP populations during inflammation, consistent with the Axl$^+$ CD1c$^+$ epithelial DC described by Lang et al. (2023), who demonstrated that Axl expression is driven by the epithelial and inflammatory factors TGF-β1 and BMP7. The same study also reported an upregulation of langerin on human cord blood CD34$^+$ progenitor cells in the presence of GM-CSF and TGF-β1, cytokines associated with inflammation or tissue repair (Hamilton et al., 1980, Deng et al., 2024). Correspondingly, we also observed an increase in langerin expression in inflammation, although this was restricted to the LP (**Figure 4.13a**). Similarly, Arrighi et al. (2003) showed that pro-inflammatory factors TNF-α, LPS and IL-1β drove a striking increase in langerin and CCR7 expression, driving CD34$^+$ precursors towards an 'LC-like' phenotype capable of migrating to lymph nodes. In contrast, van Teijlingen et al. (2023) reported that immature vaginal LCs downregulated langerin expression following LPS stimulation. Whether langerin is upregulated in inflammation remains contested, however, given that langerin is an HIV binding receptor, clarifying its role in inflammation is of high importance.

4.4.4.1 Monocyte-derived Macrophages are Enriched in Inflamed Tissues

In vaginal LP, MDMs were significantly enriched in inflammation (**Figure 4.12a**). MDDCs were also proportionally increased, although significance was not achieved. In the event of inflammation, blood monocytes are recruited to tissue sites in response to local inflammatory signals where they differentiate into macrophages or DCs (Italiani and Boraschi, 2014). Many studies have described the tissue presence of inflammatory CD1c$^+$ CD14$^+$ MDDCs with strong T cell priming abilities, as described in Crohn's disease intestine (Martin et al., 2019), psoriatic skin (Singh et al., 2016) and inflamed spleen (Segura et al., 2013) and cervix (Perez-Zsolt et al., 2019). However, Richter et al. (2018) reported a population of monocytic macrophages, similar to our MDMs, in intestinal tissue resembling DCs and concluded these cells had likely been previously misidentified as DCs. Two further studies, looking at rheumatoid arthritis (Marzaioli et al., 2022) and Crohn's disease (Kamada et al., 2008), reported an enrichment of CD14$^+$ MNPs in inflammation, though neither actually distinguished between MDDCs and MDMs. In vaginal tissue, Duluc et al. (2013) did not separate MDMs and tissue resident macrophages. Without the DC marker CD1c and tissue resident markers such as AF, MDMs cannot be accurately discriminated. Given that

as MDMs represented our most prominent inflammatory population, their targeted inclusion in future inflammatory investigations will be essential.

4.4.4.2 Epithelial Langerin$^+$ cDC2s are Enriched in Inflamed Tissues

The proportion of langerin$^+$ cDC2s was significantly increased in inflamed epithelium (**Figure 4.12b**). This DC is almost certainly what makes up the majority of epidermal CD11c$^+$ DCs (epi-DC) identified by Bertram et al. (2019) – a MNP population distinct from LCs which can be discerned by their expression of MR and higher expression of CD1c, CD11b and CD11c. Epithelial DC populations have been previously described by several groups under different aliases: Inflammatory Dendritic Epithelial Cell (IDEC) (Wollenberg et al., 1996), Vaginal Dendritic Epithelial Cell (VDEC) (Pena-Cruz et al., 2018) and LC2 (Liu et al., 2021). Bertram et al. (2023) demonstrated that IDECs, VDECs, epidermal CD11c$^+$ DCs and LC2s were all likely independent identifications of the same cell population. Importantly, IDECs and LC2s were both found to be enriched in inflammation, implicated in inflammatory skin conditions such as psoriasis of body skin and foreskin, affirming our own observations of the enriched inflammatory langerin$^+$ cDC2s. An investigation performed using an *in vivo* mouse model found a population of acute inflammatory LCs derived from blood monocytes to infiltrate the epithelium immediately following an inflammatory response (Seré et al., 2012). However, epi-DCs were shown to be highly transcriptionally related dermal DC2 (Bertram et al., 2019).

4.4.4.3 DC3s and Inflammation

Many recent studies have reported DC3s to be enriched in a range of tissues and inflammatory disease settings including blood in lupus erythematosus (Dutertre et al., 2019) and COVID-19 (Winheim et al., 2021), kidney in lupus nephritis (Chen et al., 2024), synovium in osteoarthritis (Qiu et al., 2022), inflamed bronchoalveolar lavage (Jardine et al., 2019), body skin in psoriasis (Nakamizo et al., 2021) and malignant tumours (Santegoets et al., 2020, Subtil et al., 2024). However, we saw only a slight trend of increased DC3 proportions in inflamed tissues that was not statistically significant (**Figure 4.12**). Previous investigations have concluded that CD14$^+$ DC3s are specifically pro-inflammatory (Dutertre et al., 2019), however we did not observe any changes in CD14 expression on DC3s derived from inflamed and uninflamed

tissue. More donors are required to determine any distinct differences, however, the small proportion of DC3s in vaginal mucosa compared to skin may account for these limited proportional differences.

4.4.5 CD123 as a Marker of Inflammatory Mononuclear Phagocytes

Based off our previous ASDC definitions in blood, as outlined in **Chapter 2** (Warner van Dijk et al., 2024), we characterised ASDCs for the first time in vaginal tissue, finding CD5 and Siglec-6 to be the best discriminatory markers (**Figure 4.14a**). Interestingly, both ASDC subsets, particularly the CD11c^{+} ASDCs, distinctly expressed CD88, a monocytic marker (Dutertre et al., 2019) exclusively expressed by monocyte lineages including MDDCs (Nakano et al., 2015) and MDMs (Huang et al., 2021). We did not observe CD88 expression on our monocyte-derived populations (not shown). CD88 is the receptor for complement component C5A, a key mediator of innate pathogen clearance and a potent inflammatory driver that recruits immune cells (Guo and Ward, 2005). This expression of CD88 on ASDCs alludes to their potential pro-inflammatory functions.

We identified a CD123^{+} CD1a^{+} cell population, that matches the description of a BDCA-2^{+} CD123^{int} CD1a^{+} DC reported by Chen et al. (2020) in human inflamed skin. Chen and colleagues found these cells capable of antigen presentation and lymph node migration, different to pDCs and ASDCs. They alluded to historical misidentification of this population, concluding many previous definitions of tissue pDCs were likely contaminated by this novel, hyper activated inflammatory DC subset. Whilst this is the first study to formally recognise an inflammatory CD123-expressing DC subset distinct from pDCs, several previous investigations have alluded to their presence. A number of studies have independently identified a ‘mature DC’ expressing immunoregulatory molecules required for orchestrating inflammatory responses including CCR7, LAMP3 and BIRC3, enriched in inflamed human skin, tonsil and tumour tissues (Tang-Huau et al., 2018, Nakamizo et al., 2021, He et al., 2020, Mair et al., 2022, Li et al., 2023). Whilst none of these studies included CD123 and CD1a in their investigations, the fundamental immunoregulatory signatures were parallelled. Indeed, the early description of IDECs by Wollenberg et al. (2002) may in fact have included this population of CD123^{+} DCs, as their analysis reported a CD11c^{hi} CD123^{+} population in atopic dermatitis skin that were distinct from pDCs. Upon closer

examination, it also appears this population was present in the IDEC gate of psoriasis vulgaris and lupus erythematosus. In our identification of the CD123$^+$ CD1a$^+$ Inflammatory DCs, we further confirmed the presence of MDDC, MDM, DC3, cDC2 and langerin$^+$ cDC2 populations within this gate (**Figure 4.14c-e**). We hypothesise these inflammatory DCs are individual populations upregulating expression of CD123 and CD1a in response to inflammatory stimuli rather than a distinct population of its own, although any differences in functionality remains unknown. Of note, these CD123$^+$ CD1a$^+$ inflammatory DCs were more abundant in foreskin and labia than vagina (**Figure 4.6a&b**), implying that this state of activation may be more specific to skin environments rather than mucosal. Additionally, whilst this population was defined as being inflammatory, we did not observe any differences in their abundance between inflamed and uninflamed samples. This is likely because mucosal tissues with a rich microbiome, such as the vagina, are never truly 'uninflamed'. As a result, cell populations unique to inflamed tissues are still present, but in lower abundance, than in tissues with a higher degree of inflammation.

A commonality between all four inflammatory populations was their expression of CD123 – a marker, up until recently, thought to be exclusive to pDCs. CD123 is the receptor for interlukin-3 (IL-3), a key cytokine responsible for orchestrating inflammation in a number of inflammatory diseases and infections (Podolska et al., 2024). Previous studies have shown that pDCs exposed to IL-3 become 'DC-like' and are capable of T cell activation and polarisation (Alculumbre et al., 2018, Bénard et al., 2023), though these reports excluded ASDCs, leaving the influence of IL-3 influence on *bona fide* DCs unknown. Interestingly, IL-3 has been shown to induce the expression of HIV binding lectin receptors MR and DC-SIGN on MDMs derived *in vitro* from blood monocytes, although this effect may be hindered by other inflammatory cytokines (Cardone et al., 2013). We did not observe increased expression of MR and DC-SIGN on our CD123$^+$ populations in inflammation. CD123 is a marker also expressed by inflammatory neutrophils, eosinophils and basophils (Xie et al., 2022). Collectively, these findings indicate that CD123 is a critical receptor in the inflammatory process and a broad indicator for inflammatory or activated cell states. Importantly, pDCs are not the only MNP population to express CD123.

4.4.6 Vaginal Mononuclear Phagocytes and HIV

4.4.6.1 Macrophage Populations Preferentially Bind HIV in Vaginal Mucosa

Macrophages bound the most HIV within 2 hours of exposure in the vaginal LP, closely followed by CD11c$^-$ MDMs and AF$^+$ CD11c$^+$ MNPs, then MDDCs and MDMs. This hierarchy of uptake across macrophage subsets of tissue residence, transitional and monocytic has been previously observed by our lab in colorectal tissue (unpublished) (Vine, 2025) and closely parallels their expression patterns of Siglec-1 and DC-SIGN, with the highest levels on tissue resident Macrophages (**Figure 4.15a**). Siglec-1 and DC-SIGN are well known for their ability to efficiently mediate HIV uptake into non-degenerative intracellular vesicles and facilitate first phase transfer (Pino et al., 2015, Izquierdo-Useros et al., 2012, Yu et al., 2008, Geijtenbeek et al., 2000). Siglec-1 appeared to mediate a particularly rapid internalisation of the virus as evidenced by the drop in Siglec-1 expression between mock and HIV conditions (**Figure 4.15e**), although Siglec-1 blocking assays are needed in the future to confirm true binding and internalisation. DC-SIGN proved to be a particularly efficient HIV binder on AF$^+$ CD11c$^+$ MNPs (Siglec-1^{lo} DC-SIGN$^+$), a population with an identical p24 percentage to CD11c$^-$ MDMs and with lower DC-SIGN expression. Interestingly, Rhodes et al. (2021) found MDDCs derived from abdominal skin to take up significantly more HIV with 2 hours compared to Macrophages and MDMs, whereas Vine (unpublished, Erica Vine PhD Thesis, 2025) found colorectal macrophages to be more efficient at HIV uptake than DCs. Macrophage populations are far more abundant in vaginal and colorectal tissue compared to abdomen and hence may account for this observed difference in uptake (Rhodes et al., 2021). This however emphasises the cellular and functional differences between tissue types and importance of utilising anogenital tissues for the study of HIV.

4.4.6.2 Dendritic Cells can Take Up HIV in Vaginal Mucosa

cDC2s in the LP were capable of binding HIV, although binding levels were lower than those observed in macrophages, consistent with their lack of Siglec-1 and DC-SIGN expression. Their moderate expression of MR may account for their HIV uptake, supported by the peak expression of MR on HIV$^+$ cells, indicating that viral binding occurred most prominently on MR-expressing cells (**Figure 4.15e**). However, MR has been shown to target HIV for rapid destruction by lysosomes rather into vesicular

caves for transfer to T cells (Turville et al., 2004, Lai et al., 2009). It is therefore likely that there is a yet to be identified CLR that mediates HIV uptake and onwards transfer to CD4 T cells.

Of particular interest to this study were the interactions between DC3s and HIV, an aspect not yet investigated in the literature. We found that vaginal DC3s highly expressed the HIV lectin receptors MR, DC-SIGN and Siglec-1 (**Figure 4.15a**), consistent with findings of Dutertre et al. (2019) and Villani et al. (2017) who reported Siglec-1 expression on blood DC3s. In a single donor, we further demonstrated that DC3s were capable of binding HIV, an observation that requires repeating on cells derived from additional donors (**Figure 4.15d**).

In the vaginal epithelium, expression of MR, Siglec-1 and DC-SIGN mirrored expressional patterns in the LP, however langerin expression was significantly higher across most MNP populations. Langerin has been previously shown to mediate HIV uptake and transfer to CD4 T cells by LCs (Nasr et al., 2014). Interestingly, in our study no difference was observed in uptake between cDC2s, langerin$^+$ cDC2s and LCs (**Figure 4.15b**), contrasting the findings of Bertram et al. (2019), who reported epidermal cDC2s to be more efficient at HIV uptake than LCs. Indeed, no epithelial MNP population emerged as a distinctly preferential for HIV uptake. Although, epithelial cDC2s demonstrated superior uptake compared to their LP counterparts.

However, the lectin receptor profile of epithelial cDC2s did not differ to their LP counterparts and therefore does not explain the greater uptake observed. The same was true for MDDCs and pDCs, whose minimal expression of MR, Siglec-1 DC-SIGN and langerin does not account for the levels of uptake detected in these populations. This poses the question of whether additional, unidentified lectin receptors are mediating HIV binding on MNP populations. CLEC4A is a known HIV binding lectin receptor and highly expressed across tissue MNPs, particularly skin cDC2s (Rhodes et al., 2021) and vaginal and cervical CD14$^+$ MNPs (Duluc et al., 2013, Parthasarathy et al., 2024). Previous studies have demonstrated that cultured MDDCs are capable of HIV uptake and transfer via CLEC4A (Lambert et al., 2008, Lambert et al., 2013), however its binding capacity in tissue remains undetermined. CLEC4A expression on blood pDCs has also been hypothesised to explain the HIV uptake and first phase transfer observed in pDCs described in **Chapter 2** (Warner van Dijk et al., 2024),

though whether this is also applicable in genital tissue is not yet known. Additionally, Rhodes et al., (2021) identified another lectin receptor, CLEC5A, to be exclusively and highly expressed by skin-derived cDC2s and MDDCs. While CLEC5A has not yet been examined in the context of HIV, it has been implicated in the binding of other viral pathogens including Dengue Virus and Japanese Encephalitis Virus (Chen et al., 2008, Sung and Hsieh, 2019, Tosiek et al., 2022). Future investigations should therefore assess the expression of CLEC4A and CLEC5A across all MNP subsets in human genital tissues through their inclusion in the flow cytometry panel.

Due to limited sample numbers, the HIV uptake donors weren't divided by inflammation status, however, it could be hypothesised that MDMs and langerin^{+} cDC2s may represent significant HIV binding cells in vaginal inflammation given their proportional increases and reasonable capacity to bind HIV. Both ASDC subsets and Inflammatory DCs demonstrated HIV binding ability in vaginal mucosa, although this data only represents n=1. Langerin was the only HIV lectin receptor that we observed to be upregulated in inflammation. This combined with its increased expression in the epithelium warrants further investigation of the potency and efficiency of langerin as an HIV uptake mediator in human genital tissues.

Notably, this investigation only offers preliminary insights into the HIV binding capacity of MNPs, based on a limited sample size (n=3). It does not contextualise the ability of these cells to mediate first phase viral transfer to CD4 T cells, nor does it examine their capacity for productive infection and de novo HIV synthesis. These limitations point to critical investigative directions in future work.

4.4.7 Concluding Remarks

The results of this study provide a comprehensive characterisation of the most current MNP populations residing in genital tissues, in both homeostasis and inflammation, and demonstrate their HIV biding capacity via four prominent lectin receptors: MR, Siglec-1, DC-SIGN and langerin. We emphasised the vitality of conducting investigations on human genital tissue-derived cells to accurately reflect the MNP landscape that would encounter HIV *in vivo*, as the composition, phenotypic profile and HIV uptake ability of genital MNPs differs substantially from those in abdominal/trunk skin and blood. Indeed, even within the genital tract itself, including foreskin, labia, vagina and cervix, the MNP landscape is highly heterogeneous.

However, this study lacks a functional immunological perspective. Further functional characterisation of these MNP populations, such as their cytokine and chemokine secretion profiles and their capacity to activate and polarise T cells, would provide essential context for understanding the immunological roles of each population, and whether their functions are associated with homeostasis or inflammation. Additional samples across all genital tissues are required to validate and extend the preliminary investigations of MNP profiling and HIV uptake presented in this chapter.

Young women of Sub-Saharan Africa display a disproportionate burden of new HIV infection rates, with the risk further heightened by an inflammatory genital mucosa. The refined definitions of vaginal MNP populations presented in this study, particularly inflammatory populations, and their potential interactions with HIV could ultimately strengthen the knowledge base required for targeted prevention strategies, and eventually, the development of a vaccine effective in the female mucosa.

4.5 Supplementary Material

4.5.1 Figures

Jake Rhodes, PhD thesis, 2020

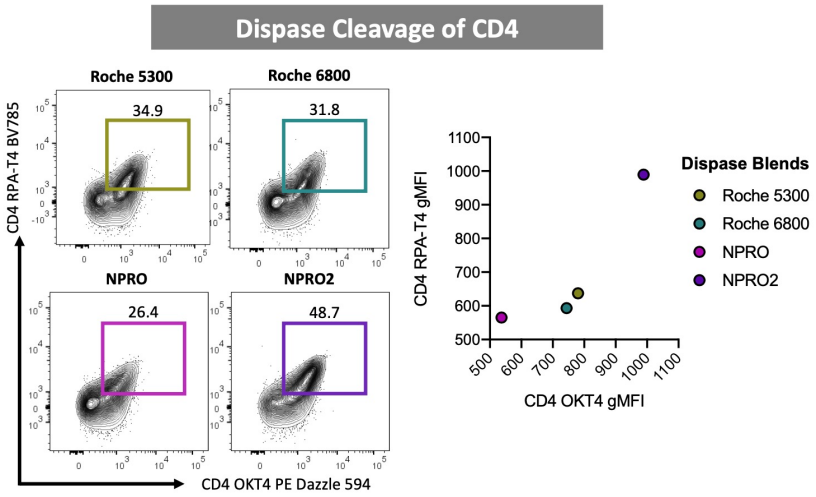

Supplementary figure 4.1: ***"Enzymatic cleavage of key HIV receptors"***

"Abdominal skin explants were treated with four different dispase blends (Roche 5300, Roche 6800, NPRO and NPRO2) overnight at 4°C was processed as per protocol and stained for flow cytometry analysis. Two clones for the HIV entry receptor CD4 were included (OKT4 and RPA-T4) to assess cleavage. Left: contour plot showing percentage of dual CD4$^+$ cells, gate defined used FMO control (not shown). Right: gMFI for both clones were plotted to assess cleavage."

This figure and figure legend was extracted from the PhD thesis of past student Jake Rhodes (2020).

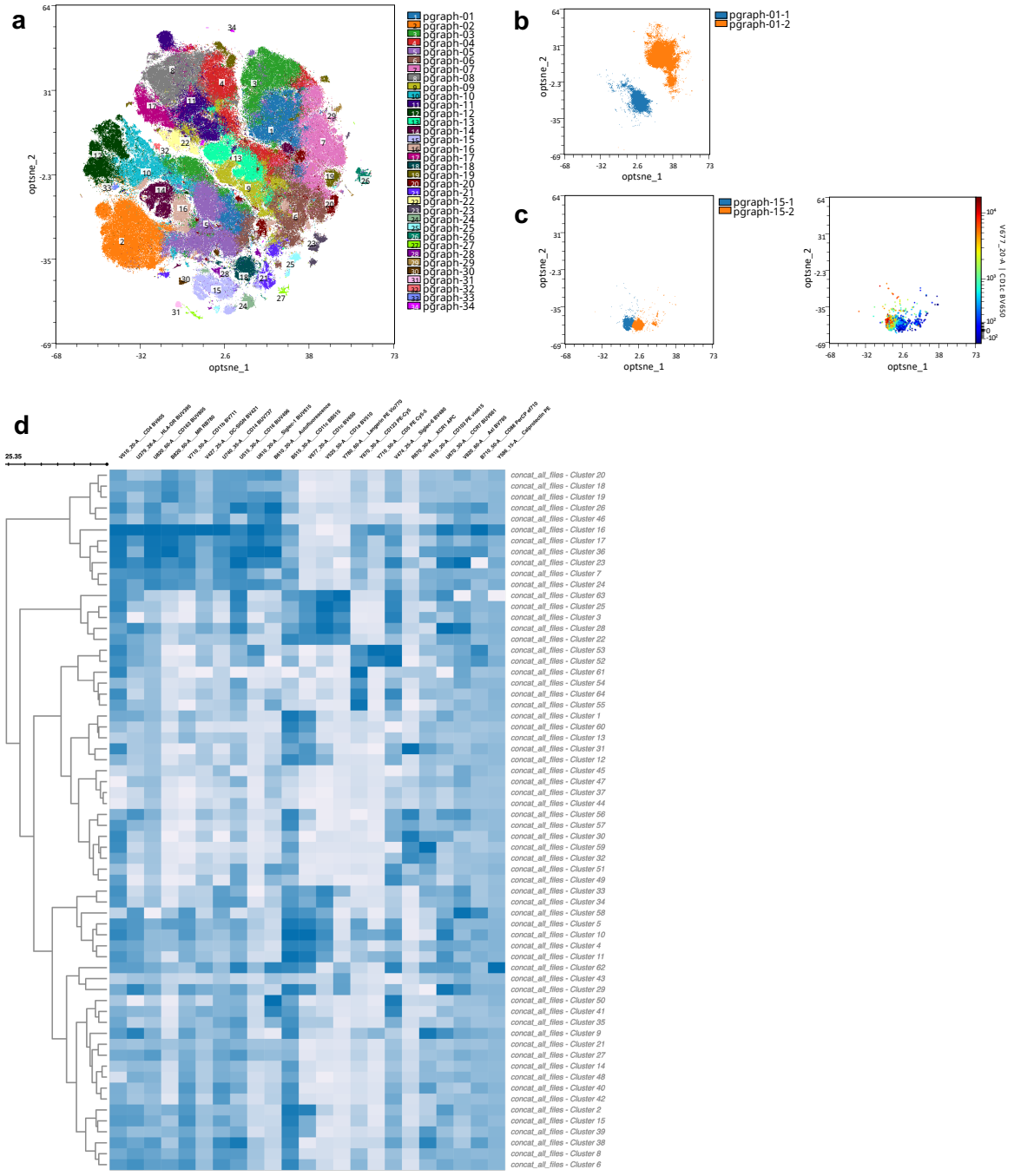

Supplementary figure 4.2: Unsupervised clustering of human genital tissues

a) The clustering algorithm PhenoGraph identified 34 distinct cell clusters. 21 of those clusters were further subclustered by either **b)** a visual separation of cell groups within the cluster or **c)** a distinct divide in marker expression. **e)** A heatmap of the average expression of each marker was generated across all 64 resultant clusters (**Figure 4.3d**).

Freja Warner van Dijk, Honours thesis, 2021

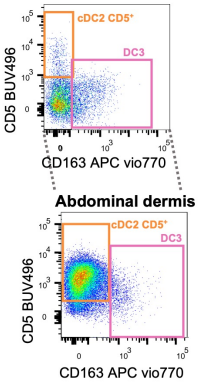

Supplementary figure 4.3: Identification of CD5$^+$ cDC2s in mucosal tissue and skin

Immune cells were liberated from inner foreskin using techniques described in **section 4.2.2.2**. The displayed cells were gated as live, single, CD45$^+$, HLA-DR$^+$, CD1c$^+$, Autofluorescent$^-$, langerin$^-$, CD88$^-$. The CD5$^+$ cDC2s were gated as CD5$^+$ CD163$^-$ and DC3s as CD5$^-$ CD163$^+$.

This figure was extracted and the figure legend adapted from the Honours thesis of Freja Warner van Dijk (2021).

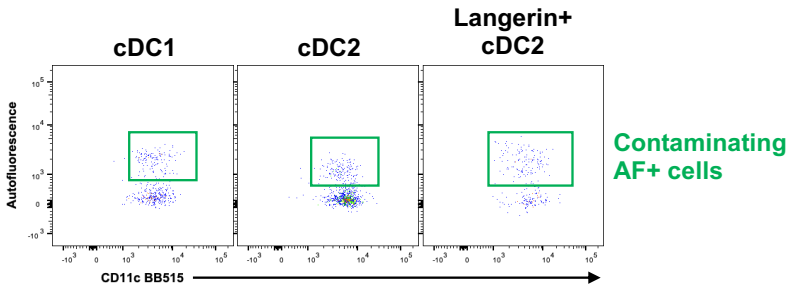

Supplementary figure 4.4: Identification of contaminating AF$^+$ cells in vaginal tissue

Cells were isolated from vaginal tissue using techniques described in **section 4.2.2.2** and stained with the flow cytometry panel outlined in **Supplementary table 3.2**. cDC1s, cDC2s and Langerin$^+$ cDC2s were identified using the gating strategy described in **Chapter 3**, **Figure 3.1**. Each of these subsets contained a contaminating population of AF$^+$ cells (green box).

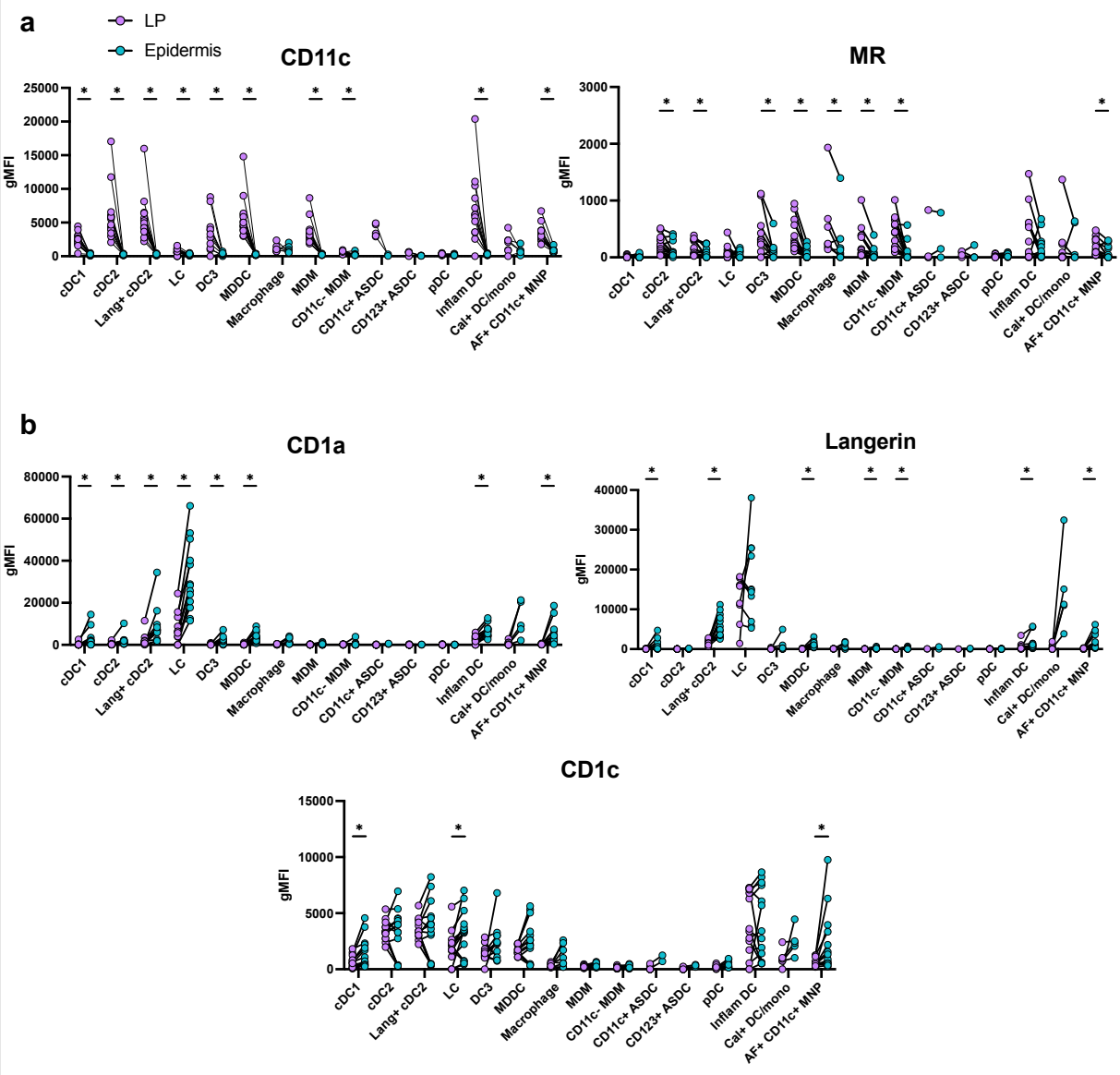

Supplementary figure 4.5: Differential marker expression between mononuclear phagocyte populations of the vaginal LP and epithelium

Cells were isolated from vaginal tissue and stained with the flow cytometry panel outlined in **Supplementary table 3.2**. Graphs show gMFI values for marker expression in MNP populations from the LP (Left, purple) compared to the epithelium (right, teal). Each dot represents an individual donor, with lines connecting matched LP and epithelial populations. **a)** CD11c and MR is higher in the LP and **b)** CD1a, Langerin and CD1c is higher in the epithelium. Statistical analysis was performed using the multiple Mann-Whitney test for pairwise comparison (*p<0.05).

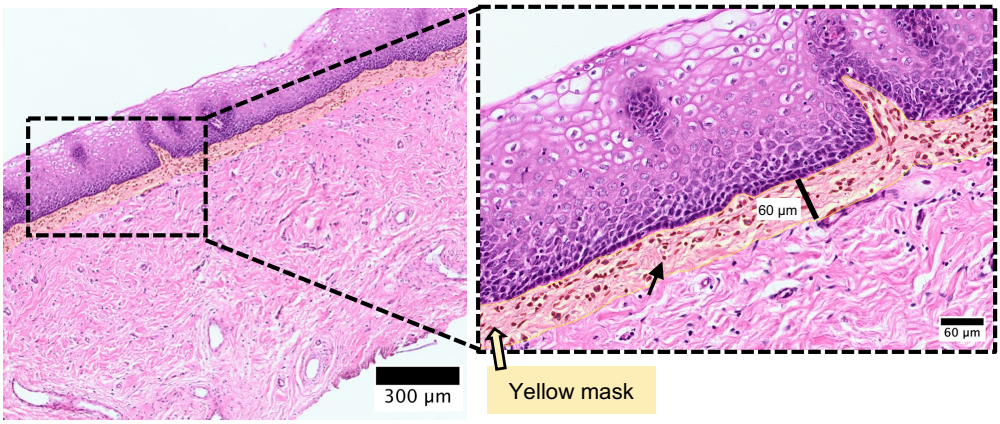

Supplementary figure 4.6: H&E image preparation

Small ~ 5 mm x 5 mm sections of vaginal tissue were fixed in 4% PFA, paraffin embedded, sectioned and stained with H&E as described in **section 4.2.5**. Images were acquired at 40x magnification on the Olympus VS200 Slide scanner and processed on ImageJ to create a 60 µm region of interest (ROI) extending from the basement membraned of the epithelium into the LP (yellow mask region). The black arrow indicates an immune cell.

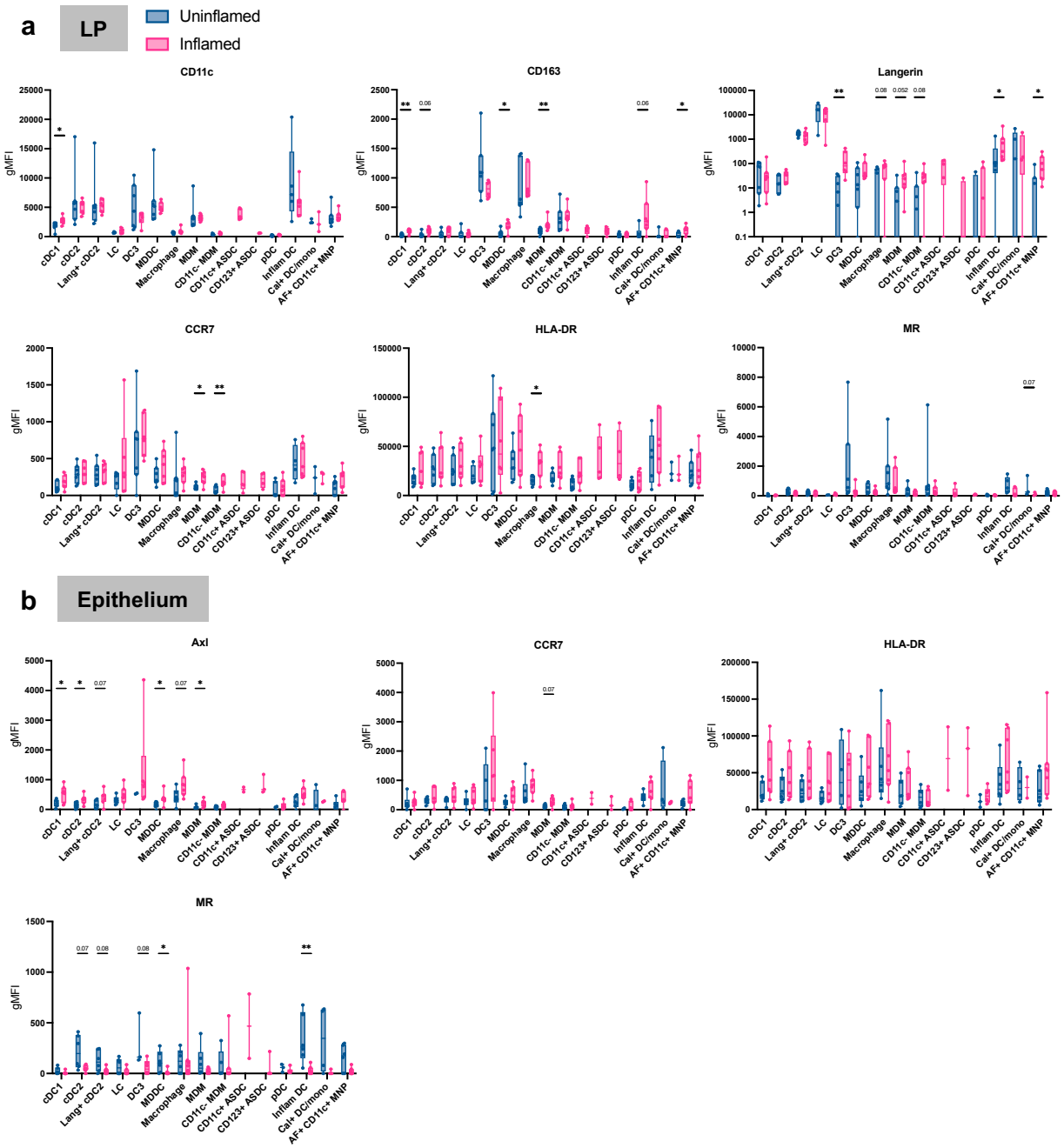

Supplementary figure 4.7: Differential marker expression between uninflamed and inflamed mononuclear phagocyte populations of the vagina

Isolated vaginal cells were stained with the flow cytometry panel in **Supplementary table 3.2** and divided by inflammatory status in **Table 4.8**. Box and whisker plots show gMFI values for marker expression in MNP populations from uninflamed samples (left, blue) and inflamed samples (right, pink). Each dot represents an individual donor. **a)** In the LP, markers CD11c, CD163, Langerin, CCR7, HLA-DR and MR display differences in expression between the uninflamed and inflamed samples. **b)** In the epithelium, Axl, CCR7, HLA-DR and MR show differences in expression between uninflamed and inflamed. Statistical analysis was performed using the multiple Mann-Whitney test for pairwise comparison (*p<0.05).

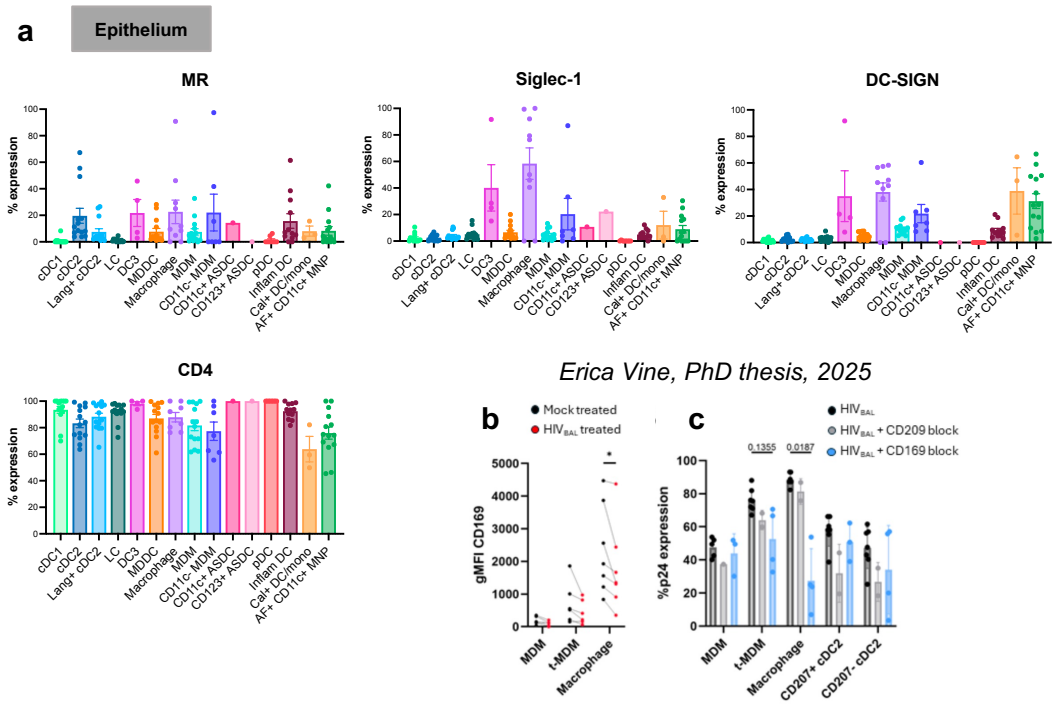

Supplementary figure 4.8: HIV uptake capacity of vaginal and colorectal mononuclear phagocyte populations

a) Isolated epithelial vaginal immune cells were stained with the panel in **Table 4.4**. Percentage expression of HIV binding receptors CD4, MR, Siglec-1 and DC-SIGN was gated on each MNP population. Statistical significances are summarised in **Supplementary table 4.4**. **b-c)** ***Adapted from PhD thesis of Erica Vine (2025):*** Isolated colorectal cells were enriched through $CD45^+$ selection and exposed to HIV_{BaL} (MOI=5) for 2 hours. **b)** gMFI of Siglec-1 (CD169) expression on macrophage subsets for mock and HIV treated samples. **c)** $CD45^+$ cells were incubated with monoclonal anti-Siglec-1 or dual anti-DC-SIGN (CD209) for 30 mins prior to HIV. Percentage of dual p24 expression across MNP subsets. Statistical analysis was performed using the Wilcoxon matched pairs signed rank test and one-way ANOVA (*p = <0.05).

b and **c** of this figure was extracted and the figure legend adapted from the PhD thesis of past student Erica Vine (2025).

4.5.2 Tables

Supplementary table 4.1: PhenoGraph cluster splitting

Initial cluster number	Number of clusters resulting	Reason for split	New cluster number (Figure 1D)
Pgraph-01	2	Distance	1, 2
Pgraph-03	2	Distance	4, 5
Pgraph-04	3	Distance	6, 7, 8
Pgraph-05	4	Distance & Expression	9, 10, 11, 12
Pgraph-06	2	Distance	13, 14
Pgraph-08	2	Expression	16, 17
Pgraph-09	4	Distance & Expression	18, 19, 20, 21
Pgraph-11	2	Distance	23, 24
Pgraph-13	2	Distance	26, 27
Pgraph-14	2	Distance	28, 29
Pgraph-15	3	Distance & Expression	30, 31, 32
Pgraph-16	3	Distance	33, 34, 35
Pgraph-19	3	Distance	38, 39, 40
Pgraph-20	2	Distance	41, 42
Pgraph-21	3	Distance	43, 44, 45
Pgraph-23	2	Distance	47, 48
Pgraph-25	2	Expression	50, 51
Pgraph-26	2	Expression	52, 53
Pgraph-27	2	Distance	54, 55
Pgraph-28	2	Distance	56, 57
Pgraph-30	2	Distance	59, 60

Supplementary table 4.2: PhenoGraph cluster merging

Cluster numbers merged (Figure 1D)	New cluster number (Figure 2A)
3, 25	1
30, 32, 57	2
1, 13, 60	6
28, 63	7
2, 39	16
34, 58	17
9, 52	18
54, 55, 61	20
17, 36	24
18, 19, 20, 24, 26	26

14, 40, 42, 48	28
7, 8	30
21, 27	31
35, 41	34
37, 44, 45, 47	35
49, 50, 51	37

Supplementary table 4.3: Summary of statistical significances of the percentage expression of HIV binding receptors in the lamina propria (Figure 4.15A) using mixed-effects analysis with Tukey's multiple comparisons test

Marker	Subset comparison	p-value	Significance
CD4	cDC1 vs. CD11c- MDM	0.0113	*
	cDC2 vs. DC3	0.0003	***
	cDC2 vs. pDC	0.0003	***
	Lang+ cDC2 vs. DC3	0.0412	*
	DC3 vs. MDM	0.0087	**
	DC3 vs. CD11c- MDM	0.0047	**
	DC3 vs. AF+ CD11c+ MNP	0.0273	*
	MDDC vs. AF+ CD11c+ MNP	0.0294	*
	Macrophage vs. Cal+ DC/mono	0.0349	*
	MDM vs. CD11c+ ASDC	0.0321	*
	MDM vs. CD123+ ASDC	0.0321	*
	MDM vs. pDC	0.0491	*
	CD11c- MDM vs. pDC	0.0132	*
DC-SIGN	cDC1 vs. cDC2	0.0437	*
	cDC1 vs. DC3	0.0018	**
	cDC1 vs. MDDC	0.0193	*
	cDC1 vs. Macrophage	<0.0001	****
	cDC1 vs. MDM	0.0006	***
	cDC1 vs. CD11c- MDM	<0.0001	****
	cDC1 vs. AF+ CD11c+ MNP	0.0002	***
	cDC2 vs. DC3	0.0024	**
	cDC2 vs. Macrophage	<0.0001	****
	cDC2 vs. MDM	0.0026	**
	cDC2 vs. CD11c- MDM	<0.0001	****
	cDC2 vs. CD11c+ ASDC	0.0307	*
	cDC2 vs. pDC	0.0002	***
	cDC2 vs. AF+ CD11c+ MNP	0.0005	***
	Lang+ cDC2 vs. DC3	0.003	**

	Lang+ cDC2 vs. Macrophage	<0.0001	****
	Lang+ cDC2 vs. MDM	0.0006	***
	Lang+ cDC2 vs. CD11c- MDM	<0.0001	****
	Lang+ cDC2 vs. AF+ CD11c+ MNP	0.0002	***
	LC vs. Macrophage	0.0025	**
	LC vs. MDM	0.049	*
	LC vs. AF+ CD11c+ MNP	0.0201	*
	DC3 vs. MDDC	0.0027	**
	DC3 vs. Macrophage	0.0071	**
	DC3 vs. CD11c+ ASDC	0.007	**
	DC3 vs. CD123+ ASDC	0.0291	*
	DC3 vs. pDC	0.0015	**
	MDDC vs. Macrophage	<0.0001	****
	MDDC vs. MDM	0.037	*
	MDDC vs. CD11c- MDM	0.0023	**
	MDDC vs. pDC	0.0045	**
	MDDC vs. AF+ CD11c+ MNP	0.0022	**
	Macrophage vs. MDM	<0.0001	****
	Macrophage vs. CD11c- MDM	<0.0001	****
	Macrophage vs. CD11c+ ASDC	0.0367	*
	Macrophage vs. pDC	<0.0001	****
	Macrophage vs. Inflam DC	0.0161	*
	Macrophage vs. AF+ CD11c+ MNP	0.0104	*
	MDM vs. CD11c- MDM	0.0241	*
	MDM vs. pDC	0.0002	***
	MDM vs. AF+ CD11c+ MNP	0.0044	**
	CD11c- MDM vs. CD11c+ ASDC	0.0022	**
	CD11c- MDM vs. CD123+ ASDC	0.0108	*
	CD11c- MDM vs. pDC	<0.0001	****
	pDC vs. AF+ CD11c+ MNP	0.0003	***
Langerin	cDC1 vs. Lang+ cDC2	<0.0001	****
	cDC1 vs. LC	0.0003	***
	cDC2 vs. Lang+ cDC2	<0.0001	****
	cDC2 vs. LC	<0.0001	****
	cDC2 vs. Macrophage	0.0455	*
	Lang+ cDC2 vs. DC3	<0.0001	****
	Lang+ cDC2 vs. MDDC	<0.0001	****
	Lang+ cDC2 vs. Macrophage	<0.0001	****
	Lang+ cDC2 vs. MDM	<0.0001	****
	Lang+ cDC2 vs. CD11c- MDM	<0.0001	****

	Lang+ cDC2 vs. CD11c+ ASDC	0.0016	**
	Lang+ cDC2 vs. CD123+ ASDC	<0.0001	****
	Lang+ cDC2 vs. pDC	<0.0001	****
	Lang+ cDC2 vs. Inflam DC	0.0003	***
	Lang+ cDC2 vs. AF+ CD11c+ MNP	<0.0001	****
	LC vs. DC3	<0.0001	****
	LC vs. MDDC	0.0002	***
	LC vs. Macrophage	<0.0001	****
	LC vs. MDM	<0.0001	****
	LC vs. CD11c- MDM	<0.0001	****
	LC vs. CD11c+ ASDC	0.0211	*
	LC vs. CD123+ ASDC	0.0211	*
	LC vs. pDC	<0.0001	****
	LC vs. AF+ CD11c+ MNP	0.0013	**
MR	cDC1 vs. cDC2	0.0024	**
	cDC1 vs. Lang+ cDC2	0.0079	**
	cDC1 vs. DC3	0.0029	**
	cDC1 vs. MDDC	0.0002	***
	cDC1 vs. Macrophage	<0.0001	****
	cDC1 vs. MDM	0.0117	*
	cDC1 vs. CD11c- MDM	0.0002	***
	cDC1 vs. AF+ CD11c+ MNP	0.0156	*
	cDC2 vs. DC3	0.0234	*
	cDC2 vs. MDDC	0.0041	**
	cDC2 vs. Macrophage	<0.0001	****
	cDC2 vs. CD11c- MDM	0.019	*
	cDC2 vs. pDC	0.0042	**
	Lang+ cDC2 vs. MDDC	0.0376	*
	Lang+ cDC2 vs. Macrophage	0.0002	***
	Lang+ cDC2 vs. CD11c- MDM	0.0447	*
	Lang+ cDC2 vs. pDC	0.0196	*
	LC vs. CD123+ ASDC	0.0406	*
	DC3 vs. pDC	0.0055	**
	MDDC vs. Macrophage	<0.0001	****
	MDDC vs. MDM	0.0008	***
	MDDC vs. pDC	0.0005	***
	MDDC vs. AF+ CD11c+ MNP	<0.0001	****
	Macrophage vs. MDM	<0.0001	****
	Macrophage vs. CD11c- MDM	0.0029	**
	Macrophage vs. pDC	<0.0001	****

	Macrophage vs. Cal+ DC/mono	0.019	*
	Macrophage vs. AF+ CD11c+ MNP	<0.0001	****
	MDM vs. CD11c- MDM	0.0054	**
	MDM vs. pDC	0.0265	*
	CD11c- MDM vs. pDC	0.0004	***
	CD11c- MDM vs. Cal+ DC/mono	0.0024	**
	CD11c- MDM vs. AF+ CD11c+ MNP	0.0112	*
	pDC vs. AF+ CD11c+ MNP	0.038	*
Siglec-1	cDC1 vs. DC3	<0.0001	****
	cDC1 vs. Macrophage	<0.0001	****
	cDC1 vs. MDM	0.0022	**
	cDC1 vs. CD11c- MDM	<0.0001	****
	cDC1 vs. CD123+ ASDC	0.0478	*
	cDC2 vs. DC3	<0.0001	****
	cDC2 vs. Macrophage	<0.0001	****
	cDC2 vs. MDM	0.0008	***
	cDC2 vs. CD11c- MDM	<0.0001	****
	cDC2 vs. CD123+ ASDC	0.0413	*
	Lang+ cDC2 vs. LC	0.0326	*
	Lang+ cDC2 vs. DC3	<0.0001	****
	Lang+ cDC2 vs. Macrophage	<0.0001	****
	Lang+ cDC2 vs. MDM	0.0014	**
	Lang+ cDC2 vs. CD11c- MDM	<0.0001	****
	Lang+ cDC2 vs. CD123+ ASDC	0.0391	*
	LC vs. DC3	0.0012	**
	LC vs. Macrophage	<0.0001	****
	LC vs. MDM	0.0451	*
	LC vs. CD11c- MDM	0.0255	*
	DC3 vs. MDDC	<0.0001	****
	DC3 vs. Macrophage	<0.0001	****
	DC3 vs. MDM	<0.0001	****
	DC3 vs. pDC	<0.0001	****
	DC3 vs. Cal+ DC/mono	0.0005	***
	DC3 vs. AF+ CD11c+ MNP	0.002	**
	MDDC vs. Macrophage	<0.0001	****
	MDDC vs. MDM	0.0425	*
	MDDC vs. CD11c- MDM	<0.0001	****
	Macrophage vs. MDM	<0.0001	****
	Macrophage vs. CD11c- MDM	<0.0001	****
	Macrophage vs. CD11c+ ASDC	0.0056	**

	Macrophage vs. pDC	<0.0001	****
	Macrophage vs. Inflam DC	0.0031	**
	Macrophage vs. Cal+ DC/mono	0.0252	*
	Macrophage vs. AF+ CD11c+ MNP	<0.0001	****
	MDM vs. CD11c- MDM	<0.0001	****
	MDM vs. pDC	0.0002	***
	CD11c- MDM vs. pDC	<0.0001	****
	CD11c- MDM vs. AF+ CD11c+ MNP	0.0014	**
	CD123+ ASDC vs. pDC	0.0337	*

Supplementary table 4.4: Summary of statistical significances of the percentage expression of HIV binding receptors in epithelium (Figure 4.15b and Supplementary figure 4.8a) using a mixed-effects analysis with Tukey's multiple comparisons test

Marker	Subset comparison	p-value	Significance
CD4	cDC1 vs. Cal+ DC/mono	0.0084	**
	cDC1 vs. AF+ CD11c+ MNP	0.0091	**
	LC vs. Cal+ DC/mono	0.0179	*
	LC vs. AF+ CD11c+ MNP	0.031	*
	DC3 vs. Cal+ DC/mono	0.0139	*
	MDM vs. pDC	0.0373	*
	CD11c- MDM vs. pDC	0.0188	*
	pDC vs. Cal+ DC/mono	0.0009	***
	pDC vs. AF+ CD11c+ MNP	0.0007	***
	Inflam DC vs. Cal+ DC/mono	0.0162	*
	Inflam DC vs. AF+ CD11c+ MNP	0.0312	*
DC-SIGN	cDC1 vs. DC3	0.0003	***
	cDC1 vs. Macrophage	<0.0001	****
	cDC1 vs. CD11c- MDM	0.0304	*
	cDC1 vs. Cal+ DC/mono	0.0003	***
	cDC1 vs. AF+ CD11c+ MNP	<0.0001	****
	cDC2 vs. DC3	0.0006	***
	cDC2 vs. Macrophage	<0.0001	****
	cDC2 vs. Cal+ DC/mono	0.0006	***
	cDC2 vs. AF+ CD11c+ MNP	<0.0001	****
	Lang+ cDC2 vs. DC3	0.0005	***
	Lang+ cDC2 vs. Macrophage	<0.0001	****
	Lang+ cDC2 vs. CD11c- MDM	0.0435	*
	Lang+ cDC2 vs. Cal+ DC/mono	0.0005	***
	Lang+ cDC2 vs. AF+ CD11c+ MNP	<0.0001	****

	LC vs. DC3	0.0007	***
	LC vs. Macrophage	<0.0001	****
	LC vs. Cal+ DC/mono	0.0007	***
	LC vs. AF+ CD11c+ MNP	<0.0001	****
	DC3 vs. MDDC	0.0025	**
	DC3 vs. MDM	0.0324	*
	DC3 vs. pDC	0.0006	***
	DC3 vs. Inflam DC	0.0233	*
	MDDC vs. Macrophage	<0.0001	****
	MDDC vs. Cal+ DC/mono	0.0021	**
	MDDC vs. AF+ CD11c+ MNP	<0.0001	****
	Macrophage vs. MDM	<0.0001	****
	Macrophage vs. pDC	<0.0001	****
	Macrophage vs. Inflam DC	<0.0001	****
	MDM vs. Cal+ DC/mono	0.0219	*
	MDM vs. AF+ CD11c+ MNP	0.001	***
	CD11c- MDM vs. pDC	0.0454	*
	pDC vs. Cal+ DC/mono	0.0005	***
	pDC vs. AF+ CD11c+ MNP	<0.0001	****
	Inflam DC vs. Cal+ DC/mono	0.0159	*
	Inflam DC vs. AF+ CD11c+ MNP	0.0007	***
	cDC1 vs. cDC2	0.0406	*
	cDC1 vs. Lang+ cDC2	<0.0001	****
Langerin	cDC1 vs. LC	<0.0001	****
	cDC1 vs. MDDC	0.0082	**
	cDC1 vs. Inflam DC	0.03	*
	cDC1 vs. Cal+ DC/mono	<0.0001	****
	cDC1 vs. AF+ CD11c+ MNP	0.0063	**
	cDC2 vs. Lang+ cDC2	<0.0001	****
	cDC2 vs. LC	<0.0001	****
	cDC2 vs. MDDC	<0.0001	****
	cDC2 vs. Macrophage	0.0043	**
	cDC2 vs. Inflam DC	<0.0001	****
	cDC2 vs. Cal+ DC/mono	<0.0001	****
	cDC2 vs. AF+ CD11c+ MNP	<0.0001	****
	Lang+ cDC2 vs. DC3	<0.0001	****
	Lang+ cDC2 vs. MDDC	<0.0001	****
	Lang+ cDC2 vs. Macrophage	<0.0001	****
	Lang+ cDC2 vs. MDM	<0.0001	****
	Lang+ cDC2 vs. CD11c- MDM	<0.0001	****

	Lang+ cDC2 vs. CD123+ ASDC	0.0002	***
	Lang+ cDC2 vs. pDC	<0.0001	****
	Lang+ cDC2 vs. Inflam DC	<0.0001	****
	Lang+ cDC2 vs. AF+ CD11c+ MNP	<0.0001	****
	LC vs. DC3	<0.0001	****
	LC vs. MDDC	<0.0001	****
	LC vs. Macrophage	<0.0001	****
	LC vs. MDM	<0.0001	****
	LC vs. CD11c- MDM	<0.0001	****
	LC vs. CD123+ ASDC	0.0002	***
	LC vs. pDC	<0.0001	****
	LC vs. Inflam DC	<0.0001	****
	LC vs. AF+ CD11c+ MNP	<0.0001	****
	DC3 vs. MDDC	0.0051	**
	DC3 vs. Inflam DC	0.0117	*
	DC3 vs. Cal+ DC/mono	<0.0001	****
	DC3 vs. AF+ CD11c+ MNP	0.0043	**
	MDDC vs. MDM	<0.0001	****
	MDDC vs. CD11c- MDM	0.0023	**
	MDDC vs. pDC	<0.0001	****
	MDDC vs. Cal+ DC/mono	0.0411	*
	Macrophage vs. pDC	0.0303	*
	Macrophage vs. Cal+ DC/mono	0.0001	***
	MDM vs. Inflam DC	<0.0001	****
	MDM vs. Cal+ DC/mono	<0.0001	****
	MDM vs. AF+ CD11c+ MNP	<0.0001	****
	CD11c- MDM vs. Inflam DC	0.0071	**
	CD11c- MDM vs. Cal+ DC/mono	<0.0001	****
	CD11c- MDM vs. AF+ CD11c+ MNP	0.0018	**
	CD123+ ASDC vs. Cal+ DC/mono	0.0078	**
	pDC vs. Inflam DC	<0.0001	****
	pDC vs. Cal+ DC/mono	<0.0001	****
	pDC vs. AF+ CD11c+ MNP	<0.0001	****
	Inflam DC vs. Cal+ DC/mono	0.0311	*
	Cal+ DC/mono vs. AF+ CD11c+ MNP	0.047	*
MR	No significances		
Siglec-1	cDC1 vs. DC3	0.0006	***
	cDC1 vs. Macrophage	<0.0001	****
	cDC2 vs. DC3	0.0006	***
	cDC2 vs. Macrophage	<0.0001	****

	Lang+ cDC2 vs. DC3	0.0013	**
	Lang+ cDC2 vs. Macrophage	<0.0001	****
	LC vs. DC3	0.0022	**
	LC vs. Macrophage	<0.0001	****
	DC3 vs. MDDC	0.0044	**
	DC3 vs. MDM	0.0019	**
	DC3 vs. pDC	0.0008	***
	DC3 vs. Inflam DC	0.0027	**
	DC3 vs. AF+ CD11c+ MNP	0.0124	*
	MDDC vs. Macrophage	<0.0001	****
	Macrophage vs. MDM	<0.0001	****
	Macrophage vs. CD11c- MDM	<0.0001	****
	Macrophage vs. pDC	<0.0001	****
	Macrophage vs. Inflam DC	<0.0001	****
	Macrophage vs. Cal+ DC/mono	0.0002	***
	Macrophage vs. AF+ CD11c+ MNP	<0.0001	****

Chapter 5. Final Discussion, Future Directions and Concluding Remarks

5.1 Overview

Defining the mononuclear phagocyte (MNP) landscape of human genital tissues is fundamental to understanding the initial interactions between HIV, the immune system and the dynamics of transmission. Critically, this knowledge could facilitate development of prophylactic treatments, immunotherapies and mucosal vaccines. MNPs include dendritic cells (DC), Langerhans cells (LC), macrophages and monocytes. As professional antigen presenting cells (APC), MNPs are an integral first line of immune defence, capturing pathogens at skin and mucosal surfaces and then interacting with T cells to trigger an adaptive immune response. HIV hijacks this APC function of MNPs by either infecting the MNP via CD4/CCR5 or being taken up into neutral pH compartments after binding lectin receptors. In both cases, HIV infects MNPs via independent mechanisms that allow its transport to CD4 T cells. It has been long recognised that elucidating which specific MNP subsets mediate this process is key to understanding HIV pathogenesis and blocking transmission (Gartner et al., 1986, Tschachler et al., 1987, Hu et al., 2000). However, this field is highly dynamic, and with the advances of high parameter single cell technologies, especially single cell RNA sequencing (scRNA-seq), new MNP populations are being rapidly discovered, and old populations redefined (Vine et al., 2022). Furthermore, it's crucial these MNP populations are characterised in human genital tissues – the biologically relevant site of HIV exposure. Many recent and eminent publications employed scRNA-seq to define new MNP populations, such as Villani et al. (2017) and Dutertre et al. (2019), utilised unbiased, machine learning approaches to unravel the array of MNP populations within human blood. Whilst these investigations represent the pioneering front of human MNP research, blood and tissue differ extensively in the MNP populations they contain and the key defining markers they express (Botting et al., 2017, Alcántara-Hernández et al., 2017, Rhodes et al., 2021, Warner van Dijk et al., 2024). In fact, this heterogeneity is observed even within tissue. Rhodes and colleagues (2021) demonstrated key differences in MNP composition between abdominal skin and genital mucosa. The use of blood or abdominal skin offers advantages in terms of availability and higher cells yields, allowing for functional assays. However, if the MNP subsets and the markers they express differ to that of genital tissue then this is of limited relevance to understanding the dynamics of pathogen transmission. In accordance, **Chapter 4** of this thesis demonstrated that

MNP populations differ between specific genital tissues and tissue compartments. This justifies the need for higher parameter single cell investigations of all human genital tissues. Importantly, a pronounced theme of this thesis has been the accurate definition of all MNPs contained with human genital tissues defined according to the most recent literature as well as the definition of new subsets using unbiased analysis (**Chapters 2-4**).

Genital inflammation has been identified as a significant risk factor for HIV acquisition in both men and women (Masson et al., 2015, Esra et al., 2016, Passmore et al., 2016). Importantly however, some forms of pre-exposure prophylaxis (PrEP), which is the primary HIV preventative treatment, is rendered ineffective in an inflammatory genital environment (McKinnon et al., 2018, Klatt et al., 2017). The MNP subsets present in inflamed tissues differ greatly to those in homeostatic conditions, yet the precise populations present and mechanisms driving enhanced HIV uptake and infection remain poorly understood. Given the greater susceptibility to HIV acquisition and undermined efficacy of PrEP, delineating inflammatory MNPs within human genital tissue represents a critical avenue of investigation. Inflammation is a broad and complex term to describe changes in an environment driven by pro-inflammatory signals. These inflammatory changes thought to promote HIV acquisition include a weaker and easily disrupted epithelial barrier that expose underlying MNPs (Arnold et al., 2016, Borgdorff et al., 2016), an influx of additional inflammatory MNPs (Li et al., 2009, Shang et al., 2017) and phenotypical changes to resident MNPs that change their functionality and HIV affinity (Qin et al., 2012, Turville et al., 2004, Rhodes et al., 2021). This thesis has provided additional evidence to support the latter two factors (**Chapter 2 and 4**).

Microbial dysbiosis is a prominent cause of genital inflammation. In the female genital tract (FGT), this disruption is termed bacterial vaginosis (BV), a condition that is highly prevalent in sub-Saharan Africa and often asymptomatic (Koumans et al., 2007, Klebanoff et al., 2004). Consequently, many individuals have an inflammatory genital environment, however, remain unaware and therefore untreated. Inflammation driven by BV is dominated by *Gardnerella vaginalis* and *Prevotella* bacterial species (Masson et al., 2014, Anahtar et al., 2015, Lennard et al., 2018), whereas those with a 'homeostatic' microbiota maintain a *Lactobacillus* species dominance with reduced levels of inflammation and risk of HIV acquisition (Gosmann et al., 2017, Hearps et al.,

2017, Aldunate et al., 2013, Tyssen et al., 2018). Penile microbial dysbiosis presents with an abundance of pro-inflammatory anaerobic species including *Prevotella*, *Dialister* and *Peptostreptococcus,* and is highly prevalent in uncircumcised males (Liu et al., 2017, Prodger et al., 2021). However, the risk of heterosexual transmission for men is much lower than women. Young women in particular have a disproportionately higher risk of HIV acquisition via the FGT (UNAIDS, 2025) – a combination of their complex microbiome, genital anatomy (Chersich and Rees, 2008) and vulnerability to sexual violence (Kuchukhidze et al., 2023). In this thesis, characterising inflammatory MNPs in both blood and genital tissue was a core feature of investigation (**Chapters 2 - 4**). **Chapter 4** particularly emphasised the exploration of the FGT by characterising the MNPs present within vaginal tissue.

This thesis ultimately seeks to further elucidate the complex interplay between genital MNPs, inflammation and HIV acquisition – a triad which remains lacking in the literature despite its profound repercussions in the HIV transmission epicentre of sub-Saharan Africa.

We first explored the link between 'inflammation' and 'HIV' by conducting an in-depth investigation of the inflammatory plasmacytoid DCs (pDC) and more recently identified Axl^+ $Siglec\text{-}6^+$ DCs (ASDC) – re-defining their genomic and phenotypic profiles, immune functionalities and their capacity for HIV uptake, infectivity and onwards transfer to CD4 T cells (**Chapter 2**). ASDCs are still understudied and have predominantly only been observed and investigated in blood. Although we detected ASDCs here in tissue, they are present in tiny numbers, meaning we had to carry out much of this work using blood derived cells. As human blood is widely and readily available, and offers high cell yields, characterising blood ASDCs presented the logical first step. Critically, we divided ASDCs into two distinct subsets, $CD123^+$ ASDCs and $CD11c^+$ ASDCs. This investigation marked the first definition of ASDCs in human genital tissues and the first investigation of ASDCs as two distinct subsets in HIV transmission.

Leveraging our partnerships with gynaecological, urological and plastic surgeons across Western Sydney, we proceeded to map all the known homeostatic and inflammatory MNP populations residing in human genital tissues of the foreskin, labia, vagina and cervix. This work hinged on the development and optimisation of a 26-

parameter flow cytometry panel that was able to accurately delineate all MNPs across skin, type II and type I mucosa (**Chapter 3**). The establishment of the panel sought to connect 'genital MNPs' and 'inflammation' as it included all markers known to be expressed by inflammatory MNPs.

Finally, utilising this high parameter flow cytometry panel, access to human genital tissue and knowledge of inflammatory MNPs, we examined the whole landscape of MNPs in genital tissue, comparing states of homeostasis and inflammation and the capacity for HIV uptake (**Chapter 4**). This study was largely exploratory, using unbiased clustering tools to delineate 15 MNP populations and performing subsequent analysis of select populations of interest. Only vaginal tissue was used for the investigation of inflammation and HIV uptake as this was most abundant when these experiments were performed and a critically relevant tissue given the current disproportionately high transmission trends seen in young women in sub-Saharan Africa.

5.2 Findings, Limitations and Future Directions

It is currently well established that most previous phenotypic and functional definitions of pDCs, are in fact a heterologous mixture of pDCs and ASDCs. In **Chapter 2** we delineated pDCs from the newly identified $CD123^+$ and $CD11c^+$ ASDCs and revealed that all three cells were present in inflamed and not homoeostatic human genital tissue. Previously, ASDCs had only been investigated in blood, tonsil (Villani et al., 2017), spleen (See et al., 2017), inflamed cerebrospinal fluid (Kang et al., 2023), inflamed broncho-alveolar lavage (Jardine et al., 2019) and inflamed skin (Chen et al., 2020). We extended this definition utilising publicly available scRNA-seq datasets, flow cytometry and imaging mass cytometry (IMC) and confirmed ASDCs to be present within lymph nodes, colorectal mucosa, foreskin and labia in several different disease states including psoriasis, cancer and ulcerative colitis. This established them as inflammatory tissue resident MNPs. ASDCs, particularly the $CD11c^+$ subset, were phenotypically more mature than both $CD123^+$ ASDCs and pDCs and had a strong naïve T cell proliferation, activation and polarisation capacity – affirming studies of Villani et al. (2017) and See et al. (2017), although the latter did not differentiate the two ASDC subsets. We found *bona fide* pDCs to be poor T cell stimulators and the only producers of type I interferon (IFN-I) and pro-inflammatory cytokines TNF-α, IL-6

and CCL3-5. Interestingly, several studies have described three subpopulations of pDCs (P1, P2 and P3) after excluding ASDCs of which P3 was capable of inducing T cell stimulation, displayed dendritic morphology and was unable to produce IFN-I (Alculumbre et al., 2018, Onodi et al., 2021, Sosa Cuevas et al., 2022). Any relationship or comparison between this pDC plasticity and ASDCs remains unexplored. Lastly, we showed that both ASDC populations were capable of HIV binding and onwards transfer to CD4 T cells. $CD11c^+$ ASDCs were more efficient at first phase transfer, likely explained by their higher expression of the lectin receptors MR (CD206), langerin (CD207), DC-SIGN (CD209) and CLEC4A (CD367) and the HIV restriction factor SAMHD1, together with showing a more mature phenotype (Harman et al., 2006). $CD123^+$ ASDCs were able to support higher levels of HIV productive infection likely owing to their lower expression of SAMHD1 and high Siglec-1 (CD169) expression which can facilitate HIV entry (Ruffin et al., 2019). INF-I production inhibits viral replication in pDCs (Beignon et al., 2005, Tong et al., 2021), however HIV transfer in first phase was observed and potentially explained by expression of the HIV binding lectin receptor CLEC4A (Lambert et al., 2008). Interestingly, HIV uptake by pDCs was also seen in vaginal tissue in **Chapter 4**. Taken together, we hypothesise that both pDCs and ASDCs are recruited to mucosal tissues in response to inflammation and encounter HIV. Upon arrival, pDCs release pro-inflammatory signals (CCL3-5) that attract CD4 T cells (Shang et al., 2017, Li et al., 2009) which ASDCs stimulate and transfer HIV to. Despite being a small population, ASDCs are a significant inflammatory MNP, present in human genital tissues and capable of HIV binding and onwards transfer to CD4 T cells.

Whilst extensive, our investigation of inflammatory pDCs and ASDCs lacked comparison to other known MNPs populations. At the inception of this PhD candidature, there were minimal published studies comparing all the known tissue MNPs defined according to recent literature, including DC3s, ASDCs (Villani et al., 2017) and epithelial DCs (Bertram et al., 2019). We wanted to investigate the MNP landscape of all the anogenital tissues that HIV could encounter in both homeostasis and inflammation and to define these populations based on the most current definitions using a single flow cytometry panel. This would allow a direct correlation and quantification of specific MNP subset proportions and their activation states across the many anogenital tissues comprised of skin, type II and type I mucosal

tissue. After four years of design and optimisation (interrupted by COVID), and the work of two PhD students, we successfully developed a 26-parameter flow cytometry panel capable of defining all known steady state and inflammatory MNPs across all anogenital tissues (foreskin, penile urethra, labia, vagina, cervix, anus, rectum and colon). This panel was prepared as an Optimised Multicolour Immunofluorescence Panel (OMIP) and submitted to Cytometry A (**Chapter 3**). In addition to MNP phenotyping the panel was designed to assess cell proliferation and migration using KI67, maturation and lymph node homing using CCR7 and HIV binding potential using CD4, MR, DC-SIGN, Siglec-1 and langerin. We also planned the future inclusion of the HIV capsid protein p24 to assess HIV uptake by each MNP subset. We optimised the resolution of the highest and lowest expression of each marker across each tissue to create a single set of cytometer settings that could be applied to each acquisition and ensure continuity across all future generated data. The downstream investigation of anus, rectum and colon was performed by another PhD student, Erica Vine.

Utilising this optimised high parameter flow cytometry panel, we determined the MNP populations resident within foreskin, labia, vagina and cervix (**Chapter 4**). The gating strategy devised in **Chapter 3** was designed using the most up to date definitions of MNP subsets, however very few of these studies included genital MNPs. Therefore, we conducted an unbiased analysis of all MNPs (HLA-DR^{+} CD3^{-} CD19^{-} cells) derived from genital tissue allowing us to identify novel populations. This prompted us to design a new gating strategy to accurately define: **i)** the surface expression of markers by genital cDC1s; **ii)** which MNPs subsets can express langerin (previously thought to be LCs and a subset of cDC2 only); **iii)** which MNPs subsets are autofluorescent (AF) (previously thought tissue resident Macrophages only); **iv)** the definition of four novel MNP populations: **1)** AF^{+} CD11c^{+} MNPs; **2)** Calprotectin^{+} monocytes/DCs; **3)** CD123^{+} CD1a^{+} Inflammatory DCs; **4)** CD11c$^{+/-}$ MDMs. This resulted in the identification of 15 discreet MNP populations which were highly heterogenous across the different genital tissues both in proportions and phenotypic surface marker expression, including CD14 and CD163. Our findings highlight the importance of considering each tissue as unique and not always showing the same patterns of MNP composition as other ‘skin’ or ‘mucosal’ tissues. For example, inner foreskin (type II mucosa) was more similar to outer foreskin (skin) than vagina (type II mucosa) (Dinh et al., 2012, Pinson et al., 2023).

Our next focus was the characterisation of previously established MNP subsets within a genital niche. cDC1s were defined as XCR1^{+} CD11c$^{+/lo}$, an interesting finding as skin cDC1s are CD11c^{-} (Rhodes et al., 2021) whilst intestinal cDC1s are CD11c^{+} (Doyle et al., 2021). Vaginal cDC1s did not express CADM1 or CLEC9A, which were previously considered universal cDC1 markers across tissue and blood, nor CD103 expressed by intestinal cDC1 (Mair and Liechti, 2021, Doyle et al., 2021, Mulder et al., 2021). We also identified two likely transient macrophage populations, CD11c^{-} MDMs and AF^{+} CD11c^{+} MNPs, with intermediary expression of markers associated with monocyte derived and tissue resident macrophages – a population first described by Bujko et al. (2018) in intestinal tissue. Where along this transitional trajectory these two populations lie is a point of future investigation. DC3s were of particular interest, but like many other studies, we concluded there remains a lack of distinct identifying markers to distinguish them from MDDCs and macrophages in tissue (Parthasarathy et al., 2024). We confirmed a high expression of CCR7, CD14, Siglec-1 and DC-SIGN, implicating their potential involvement in inflammation and HIV binding. However, no distinct DC3 proportional differences were observed between inflamed and homeostatic tissue. We hypothesise that DC3s may be a more skin dominant population as vaginal tissue contained very few DC3s. In the vaginal epithelium, CD14^{+} cells comprised a large proportion of the MNP compartment. CD14-expressing epithelial cells have been described before but in a monocytic, pre-LC capacity, and never been quantified, profiled or compared to other MNPs (Larregina et al., 2001, Achachi et al., 2015). We show here for the first time that epithelial CD14^{+} MNPs are as abundant as cDC2s and LCs. Studies mapping their migration, function and HIV transfer capacity are critical directions for future work.

We broadly defined inflammation of vaginal tissue by the presence of ASDCs, neutrophil infiltrate and a high proportion of CD4 T cells. All MNPs in an inflammatory environment were more activated/mature, evidenced by higher expression of CCR7 and HLA-DR (Hauser et al., 2016, Cross et al., 2021). In the context of HIV transmission, this implies MNPs may be more capable of transporting the virus to nearby lymphoid tissue where they can transmit the virus to CD4 T cells. We also observed an influx of MDMs and epithelial langerin^{+} cDC2s in inflamed tissue and the *de novo* appearance of CD123-expressing MNPs. pDCs were once thought the only MNPs to express CD123, however the discovery of CD123^{+} ASDCs and CD123^{+}

CD1a$^+$ inflammatory DCs suggests that CD123 may be a broader marker of inflammation (Podolska et al., 2024). The CD123$^+$ CD1a$^+$ inflammatory DCs we observed here are similar to the activated skin DC described by Chen et al. (2020) and the Inflammatory Dendritic Epidermal Cells (IDEC) identified by Wollenberg et al. (2002). We hypothesise that rather than a distinct population, this inflammatory DC subset is a heterologous mixture of multiple MNP populations that have upregulated CD123 in response to inflammation. However, we did not observe any proportional differences between inflamed and uninflamed samples – likely owing to the complex microbiome and associated background inflammatory nature of vaginal mucosa.

Finally, we demonstrated that in vaginal tissue, macrophages were the most efficient MNP population in binding HIV after 2 hours, correlating with their high expression of Siglec-1 and DC-SIGN (Pino et al., 2015, Izquierdo-Useros et al., 2012, Geijtenbeek et al., 2000). Notably, this differs to our previous findings (Rhodes et al., 2021), demonstrating that abdominal skin MDDCs are more efficient at HIV uptake than macrophages. However, we have shown that colorectal tissue macrophages bind the most HIV (unpublished, Erica Vine PhD Thesis, 2025). This highlights functional differences between macrophages in skin and mucosa and the importance of investigating MNPs in physiologically relevant tissue. MR and langerin likely account for some HIV uptake by DCs (Turville et al., 2004, Nasr et al., 2014), however the possibility remains that there is a yet to be defined HIV binding receptor expressed by key HIV transmitting MNPs. CLEC5A is once such possible candidate, known to be highly expressed by all key HIV transmitting skin MNPs (cDC2s, MDDCs and LCs) (Rhodes et al., 2021) and previously shown to bind Dengue Virus and Japanese Encephalitis Virus (Chen et al., 2008, Sung and Hsieh, 2019, Tosiek et al., 2022). Another candidate is CLEC4A which has been shown to bind HIV *in vitro* derived MDDCs (Lambert et al., 2008) and known to be expressed by skin cDC2s (Rhodes et al., 2021), vaginal and cervical CD14$^+$ MNPs (Duluc et al., 2013, Parthasarathy et al., 2024) and blood pDCs (Warner van Dijk et al., 2024).

This final chapter provides a preliminary yet comprehensive exploration of genital tissue MNPs, beginning to link inflammatory changes in the mucosal environment with enhanced HIV acquisition, though many more samples and accompanying functional investigations are required in the future.

A significant strength of this thesis has been our access to fresh human genital tissue and optimised tissue digestion protocols. One of the fundamental reasons there remain gaps in the literature surrounding the early events of sexual transmission of HIV is difficulty of access to human genital tissue. Our ability to conduct experiments using *ex vivo* MNPs from every genital is globally unique and a result of two decades of establishing partnerships with surgeons, innovative ethics applications and extensive optimisation of tissue digestion protocols to isolate functionally intact MNPs (Botting et al., 2017, Doyle et al., 2021). Key to the isolation of cells in their tissue-resident immature state is the long overnight dispase digestion, which breaks down the basement membrane separating the epithelium from the underlying dermis/lamina propria (LP) followed by a rapid collagenase digestion, which cleaves collagen fibres, liberating immune cells. We have previously shown that trypsin, historically used to digest the stratified squamous epithelium (skin epidermis / type II mucosal epithelium), cleaves key markers required to identify DCs including CD1c, CD11c, CD14 and CD141, as well as the HIV entry receptor CD4. Cleavage of CD11c by trypsin has resulted in epi-DCs being mis-identified as LCs (Bertram et al., 2019), and conflicting reports as to whether LCs can be infected with HIV (Nasr et al., 2014, Lynch et al., 2003, Botting et al., 2017). Furthermore, it is vital the collagenase digestion does not exceed 120 minutes as this results in MNP activation including downregulation of pathogen binding lectin receptors (Botting et al., 2017).

However, the use of MNPs liberated from tissues also has considerable challenges. Tissue access can be unpredictable and varies considerably in size (and associated cell yield) between donors. Tissues such as cervix and rectum, usually derived from cancer removal operations, are often infrequent due to pathology requirements. A significant limitation of **Chapter 4** is its lack of functional data, both from an immunological and HIV perspective. This is largely because almost all anogenital tissue explants are too small to yield enough cells for functional studies, especially low abundance cell populations such as cDC1, DC3, ASDC, pDCs and $CD123^{+}$ $CD1a^{+}$ Inflammatory DCs. Nonetheless, exploration of T cell activation and polarising capacity, cytokine secretion profiles, and HIV infection and transfer assays are all planned investigations for future work.

Finally, due to the time constraints of a PhD in Australia (3.5 years maximum), HIV uptake assays were only performed in 3 donors and will be repeated in at least 4 more

donors. Our experiments utilised the lab adapted strain of HIV-1, HIV_{BaL}, as we can generate high titre virus stocks. Whilst transmitted/founder strains of HIV-1 are more clinically relevant as they represent isolated single viral strains from infected individuals (Keele et al., 2008), they were not assessed in this thesis due to time limitations. However, we have previously demonstrated that there are no differences in the ability of human tissue MNPs to take up, become infected and transfer HIV to CD4 T cells between lab adapted and transmitted founder strains (Baharlou et al., 2022, Rhodes et al., 2021, Bertram et al., 2019). Nevertheless, repeating key findings from this thesis using transmitted/founder HIV strains remains a future direction.

A central feature of this thesis was defining the MNP populations in tissue inflammation. **Chapter 2** delved into some more specific inflammatory conditions, including ulcerative colitis and psoriasis, whilst **Chapter 4** broadly characterised inflammation by the degree of cell infiltrate. Inflammation was classified as being acute and non-specific. However, different inflammatory conditions can lead to different immune cell landscapes. A study by Behr et al. (2025) compared the immunological profiles of the inflammatory skin diseases atopic dermatitis and psoriasis, revealing that the two seeming related conditions had different MNP profiles. They reported psoriasis to be characterised by highly activated pro-inflammatory macrophages, and atopic dermatitis defined by high proportions of MR and CD123-expressing DCs with a tolerogenic profile and tissue resident macrophages ($CD163^+$ MR^+). Although it should be noted that macrophages identified in psoriasis affected skin are likely a combination of $CD14^+$ $CD11b^+$ $CD11c^+$ MDMs and MDDCs. Nonetheless, psoriasis appeared to represent an environment of acute T helper (Th)1/Th17-mediated inflammation (Waite and Skokos, 2012) whilst atopic dermatitis was one of chronic Th2/Th17/Th22-mediated inflammation (Jovanovic et al., 2014). This highlights the complications of broadly classifying inflammation, as we did here, and emphasises the need for future work to further investigate the nature of inflammation. Genital inflammation is additionally influenced by microbiome composition (Masson et al., 2014). Indeed, a recent study demonstrated that a specific bacteria present in BV, *Prevotella timonensis,* enhanced HIV uptake and transmission by DCs (van Smoorenburg et al., 2025). A critical planned future aspect of investigation is matched patient cervicovaginal swabs for each sample processed for flow cytometry or scRNA-seq. The cytokine and microbiome profiles of each swab will be mapped to further

elucidate the immunological landscape of each tissue and inform inflammatory status.

This thesis did not stratify or divide any samples by patient age. For example, foreskin donors ranged from paediatric to aged patients, labia and cervix were from women under 50, whilst vaginal samples trended to be from women over 60 – representing quite a stratification in ages across all genital tissues. The microbiome of infant and adult foreskins has been shown differ significantly, likely influencing the composition and function of the local innate immune cell environment (Murphy et al., 2023). Additionally, children have been reported to exhibit higher blood circulating pDC numbers, whereas adults display more mature and activated DC populations in the colon (Vora et al., 2016). This highlights potential discrepancies in data when grouping paediatric and adult samples. Our foreskin samples were the only tissue derived from paediatric samples, however, observed differences between the foreskin and FGT tissues were likely tissue or sex-specific rather than age-related distinctions. Rodriguez-Garcia et al. (2014) found distinct differences in the proportions and functions of cervical CD4 T cells and Th17 cells between pre- and postmenopausal women which influence susceptibility to HIV infections – a tissue highly sensitive to the influence of sex hormones (Hickey et al., 2011). Whilst hormonal induced changes in MNP populations of the FGT have not been directly investigated, they are likely to occur, highlighting a critical variable across all samples from the FGT. Due to patient deidentification, the menopausal status of our current cohort was not reported and hence stratification was not possible. Additionally, many vaginal prolapse patients are often routinely treated with estrogen perioperatively; however, whilst this may be assumed for all samples, the data was also not disclosed. Given the phenotypical, proportional and functional influences of sex hormones on the innate immune landscape, menopausal status and knowledge of hormone replacement therapy are important data points to discuss with surgeons for future cohorts.

Lastly, the 15 genital MNP populations in **Chapter 4** were identified using unbiased clustering tools which allowed the exploration of a large, concatenated flow cytometry dataset to reveal novel populations and tissue-specific features. However, this investigation was limited to the 26-parameters of the flow cytometry panel. Future employment of scRNA-seq technologies will allow for a more powerful and comprehensive unbiased exploration of human genital tissues, such as those conducted by Parthasarathy et al. (2024) in cervix, Li et al. (2021) in vagina and Liu et

al. (2021) in foreskin. We are in the process of generating our own anogenital scRNA-seq datasets with an emphasis on enriched MNPs and HIV treatment. Use of a dual-fluorescent HIV detection method will allow measurement of near-infrared fluorescent protein (iRFP), expressed in the presence of HIV DNA, and green fluorescent protein (GFP), only expressed by host cells after HIV DNA integration. This will allow the distinction between MNPs capturing HIV via lectin receptors and those that are productively infected, whilst investigating transcriptional changes before and after HIV exposure. Transcriptomic profiling will be conducted alongside antibody sequencing (AbSeq, BD) to facilitate the identification of populations and correlate any transcriptional shifts to protein expression. This intended future work will allow for a more thorough understanding of the MNP landscape in vaginal tissue and the events of early HIV infection. It will further expand on the investigations undertaken in this thesis, confirming populations present, expressional profiles, including identifying unique markers for subsets like DC3s, and identifying preferential HIV target cells.

5.3 Overall Significance and Concluding Remarks

After more than 40 years research, the HIV pandemic remains a significant global issue, despite revolutionary preventive strategies and treatments since its first isolation in 1983 (Barré-Sinoussi et al., 1983). 40.8 million people are currently living with HIV and in 2024 there were 1.3 million new infections, with a disproportionate burden of infection in sub-Sharan Africa, particularly in young girls and women (UNAIDS, 2025). Antiretroviral therapy (ART) has proved a remarkable treatment for HIV infected individuals, able to supress the virus to undetectable levels, restore health and reduce the risk of viral spread. However, ART is a daily oral treatment with a required high patient adherence, is costly and stigmatising. A long-acting injectable ART is on the horizon, yet costs, side effects, and establishing concentrations that won't result in drug resistance, remain significant barriers (Gulick and Flexner, 2019). ART can also be given to high-risk individuals as a preventative treatment, known as PrEP. However, several studies have reported it to be ineffective in inflamed genital mucosa (McKinnon et al., 2018, Klatt et al., 2017), which is particularly problematic in places like sub-Saharan Africa where inflammation is widespread and often untreated (Dabee et al., 2019). Critically, an inflamed genital mucosa increases the risk of HIV acquisition (Masson et al., 2015, Passmore et al., 2016, Esra et al., 2016). There is hence an

urgent need for improved prophylactic treatments that are effective in inflammation, and ultimately, a demand for a vaccine and cure.

To develop targeted treatments and vaccines, we must first understand the initial events of HIV transmission in human genital tissues in conditions of homeostasis and inflammation. Surprisingly, little is known about this interplay between HIV, inflammation and genital tissue MNPs, primarily owing to the difficulties in accessing and working with human genital tissues. This thesis has defined the MNP landscape of human genital tissues in an unprecedented level of detail and their role in HIV acquisition. To the scientific literature, we have contributed a refined functional characterisation of the inflammatory pDCs, $CD11c^+$ ASDCs and $CD123^+$ ASDCs – for the first time demonstrating ASDC presence in human genital tissue. Our extensive characterisation of vaginal MNPs revealed unique population proportions and expression profiles that differed to blood and skin, with distinct changes in inflammation that may influence the capture of HIV. Importantly, these findings identified MNPs, particularly inflammatory MNPs, that bound HIV and may represent important therapeutic target cells to block or aid in vaccine delivery.

Ultimately, this thesis is a small but meaningful advance in understanding the precise immunological mechanisms of early HIV transmission, expanding our knowledge of the MNP composition in genital tissues, a true biological site of HIV transmission, whilst highlighting further research directions that may one day inform strategies to overcome the HIV pandemic.

Chapter 6. References

ACHACHI, A., VOCANSON, M., BASTIEN, P., PÉGUET-NAVARRO, J., GRANDE, S., GOUJON, C., BRETON, L., CASTIEL-HIGOUNENC, I., NICOLAS, J.-F. & GUENICHE, A. 2015. UV Radiation Induces the Epidermal Recruitment of Dendritic Cells that Compensate for the Depletion of Langerhans Cells in Human Skin. *Journal of Investigative Dermatology,* 135**,** 2058-2067.

AGGARWAL, A., IEMMA, T. L., SHIH, I., NEWSOME, T. P., MCALLERY, S., CUNNINGHAM, A. L. & TURVILLE, S. G. 2012. Mobilization of HIV spread by diaphanous 2 dependent filopodia in infected dendritic cells. *PLoS Pathog,* 8**,** e1002762.

ALCÁNTARA-HERNÁNDEZ, M., LEYLEK, R., WAGAR, L. E., ENGLEMAN, E. G., KELER, T., MARINKOVICH, M. P., DAVIS, M. M., NOLAN, G. P. & IDOYAGA, J. 2017. High-Dimensional Phenotypic Mapping of Human Dendritic Cells Reveals Interindividual Variation and Tissue Specialization. *Immunity,* 47**,** 1037-1050.e6.

ALCULUMBRE, S. G., SAINT-ANDRÉ, V., DI DOMIZIO, J., VARGAS, P., SIRVEN, P., BOST, P., MAURIN, M., MAIURI, P., WERY, M., ROMAN, M. S., SAVEY, L., TOUZOT, M., TERRIER, B., SAADOUN, D., CONRAD, C., GILLIET, M., MORILLON, A. & SOUMELIS, V. 2018. Diversification of human plasmacytoid predendritic cells in response to a single stimulus. *Nat Immunol,* 19**,** 63-75.

ALDUNATE, M., TYSSEN, D., JOHNSON, A., ZAKIR, T., SONZA, S., MOENCH, T., CONE, R. & TACHEDJIAN, G. 2013. Vaginal concentrations of lactic acid potently inactivate HIV. *J Antimicrob Chemother,* 68**,** 2015-25.

ALMEIDA, M., CORDERO, M., ALMEIDA, J. & ORFAO, A. 2005. Different subsets of peripheral blood dendritic cells show distinct phenotypic and functional abnormalities in HIV-1 infection. *AIDS,* 19**,** 261-71.

ANAHTAR, M. N., BYRNE, E. H., DOHERTY, K. E., BOWMAN, B. A., YAMAMOTO, H. S., SOUMILLON, M., PADAVATTAN, N., ISMAIL, N., MOODLEY, A., SABATINI, M. E., GHEBREMICHAEL, M. S., NUSBAUM, C., HUTTENHOWER, C., VIRGIN, H. W., NDUNG'U, T., DONG, K. L., WALKER, B. D., FICHOROVA, R. N. & KWON, D. S. 2015. Cervicovaginal bacteria are a major modulator of host inflammatory responses in the female genital tract. *Immunity,* 42**,** 965-76.

ANGEL, C. E., GEORGE, E., BROOKS, A. E., OSTROVSKY, L. L., BROWN, T. L. & DUNBAR, P. R. 2006. Cutting edge: CD1a+ antigen-presenting cells in human dermis respond rapidly to CCR7 ligands. *J Immunol,* 176**,** 5730-4.

ARNOLD, K. B., BURGENER, A., BIRSE, K., ROMAS, L., DUNPHY, L. J., SHAHABI, K., ABOU, M., WESTMACOTT, G. R., MCCORRISTER, S., KWATAMPORA, J., NYANGA, B., KIMANI, J., MASSON, L., LIEBENBERG, L. J., ABDOOL KARIM, S. S., PASSMORE, J.-A. S., LAUFFENBURGER, D. A., KAUL, R. & MCKINNON, L. R. 2016. Increased levels of inflammatory cytokines in the female reproductive tract are associated with altered expression of proteases, mucosal barrier proteins, and an influx of HIV-susceptible target cells. *Mucosal Immunol,* 9**,** 194-205.

ARRIGHI, J.-F., SOULAS, C., HAUSER, C., SAELAND, S., CHAPUIS, B., ZUBLER, R. H. & KINDLER, V. 2003. TNF-α induces the generation of Langerin/(CD207)+ immature Langerhans-type dendritic cells from both CD14–

CD1a– and CD14+CD1a– precursors derived from CD34+ cord blood cells. *European Journal of Immunology,* 33**,** 2053-2063.

ATASHILI, J., POOLE, C., NDUMBE, P. M., ADIMORA, A. A. & SMITH, J. S. 2008. Bacterial vaginosis and HIV acquisition: a meta-analysis of published studies. *Aids,* 22**,** 1493-501.

BAGGALEY, R. F., OWEN, B. N., SILHOL, R., ELMES, J., ANTON, P., MCGOWAN, I., STRATEN, A., SHACKLETT, B., DANG, Q., SWANN, E. M., BOLTON, D. L. & BOILY, M. C. 2018. Does per-act HIV-1 transmission risk through anal sex vary by gender? An updated systematic review and meta-analysis. *Am J Reprod Immunol,* 80**,** e13039-n/a.

BAHARLOU, H., CANETE, N., VINE, E. E., HU, K., YUAN, D., SANDGREN, K. J., BERTRAM, K. M., NASR, N., RHODES, J. W., GOSSELINK, M. P., DI RE, A., REZA, F., CTERCTEKO, G., PATHMA-NATHAN, N., COLLINS, G., TOH, J., PATRICK, E., HANIFFA, M. A., ESTES, J. D., BYRNE, S. N., CUNNINGHAM, A. L. & HARMAN, A. N. 2022. An in situ analysis pipeline for initial host-pathogen interactions reveals signatures of human colorectal HIV transmission. *Cell Reports,* 40.

BAHARLOU, H., CANETE, N. P., BERTRAM, K. M., SANDGREN, K. J., CUNNINGHAM, A. L., HARMAN, A. N. & PATRICK, E. 2021. AFid: a tool for automated identification and exclusion of autofluorescent objects from microscopy images. *Bioinformatics,* 37**,** 559-567.

BAKDASH, G., BUSCHOW, S. I., GORRIS, M. A., HALILOVIC, A., HATO, S. V., SKÖLD, A. E., SCHREIBELT, G., SITTIG, S. P., TORENSMA, R., DUIVEMAN-DE BOER, T., SCHRÖDER, C., SMITS, E. L., FIGDOR, C. G. & DE VRIES, I. J. 2016. Expansion of a BDCA1+CD14+ Myeloid Cell Population in Melanoma Patients May Attenuate the Efficacy of Dendritic Cell Vaccines. *Cancer Res,* 76**,** 4332-46.

BARRÉ-SINOUSSI, F., CHERMANN, J. C., REY, F., NUGEYRE, M. T., CHAMARET, S., GRUEST, J., DAUGUET, C., AXLER-BLIN, C., VÉZINET-BRUN, F., ROUZIOUX, C., ROZENBAUM, W. & MONTAGNIER, L. 1983. Isolation of a T-lymphotropic retrovirus from a patient at risk for acquired immune deficiency syndrome (AIDS). *Science,* 220**,** 868-71.

BECKER, A. M. D., DECKER, A. H., FLÓREZ-GRAU, G., BAKDASH, G., RÖRING, R. J., STELLOO, S., VERMEULEN, M., PIET, B., AARNTZEN, E., VERDOES, M. & DE VRIES, I. J. M. 2024. Inhibition of CSF-1R and IL-6R prevents conversion of cDC2s into immune incompetent tumor-induced DC3s boosting DC-driven therapy potential. *Cell Rep Med,* 5**,** 101386.

BEHR, N. J., PIERRE, S., ICKELSHEIMER, T., ZIEGLER, N., LUCKHARDT, S., KANNT, A., PINTER, A., GEISSLINGER, G., SCHÄFER, S. M. G., KÖNIG, A. & SCHOLICH, K. 2025. High content imaging shows distinct macrophage and dendritic cell phenotypes for psoriasis and atopic dermatitis. *Sci Rep,* 15**,** 18904.

BEIGNON, A. S., MCKENNA, K., SKOBERNE, M., MANCHES, O., DASILVA, I., KAVANAGH, D. G., LARSSON, M., GORELICK, R. J., LIFSON, J. D. & BHARDWAJ, N. 2005. Endocytosis of HIV-1 activates plasmacytoid dendritic cells via Toll-like receptor-viral RNA interactions. *J Clin Invest,* 115**,** 3265-75.

BELKINA, A. C., CICCOLELLA, C. O., ANNO, R., HALPERT, R., SPIDLEN, J. & SNYDER-CAPPIONE, J. E. 2019. Automated optimized parameters for T-distributed stochastic neighbor embedding improve visualization and analysis of large datasets. *Nature Communications,* 10**,** 5415.

BÉNARD, A., HANSEN, F. J., UHLE, F., KLÖSCH, B., CZUBAYKO, F., MITTELSTÄDT, A., JACOBSEN, A., DAVID, P., PODOLSKA, M. J., ANTHUBER, A., SWIERZY, I., SCHAACK, D., MÜHL-ZÜRBES, P., STEINKASSERER, A., WEYAND, M., WEIGAND, M. A., BRENNER, T., KRAUTZ, C., GRÜTZMANN, R. & WEBER, G. F. 2023. Interleukin-3 protects against viral pneumonia in sepsis by enhancing plasmacytoid dendritic cell recruitment into the lungs and T cell priming. *Front Immunol,* 14**,** 1140630.

BERNHARD, O. K., LAI, J., WILKINSON, J., SHEIL, M. M. & CUNNINGHAM, A. L. 2004. Proteomic analysis of DC-SIGN on dendritic cells detects tetramers required for ligand binding but no association with CD4. *J Biol Chem,* 279**,** 51828-35.

BERTRAM, K. M., BOTTING, R. A., BAHARLOU, H., RHODES, J. W., RANA, H., GRAHAM, J. D., PATRICK, E., FLETCHER, J., PLASTO, T. M., TRUONG, N. R., ROYLE, C., DOYLE, C. M., TONG, O., NASR, N., BARNOUTI, L., KOHOUT, M. P., BROOKS, A. J., WINES, M. P., HAERTSCH, P., LIM, J., GOSSELINK, M. P., CTERCTEKO, G., ESTES, J. D., CHURCHILL, M. J., CAMERON, P. U., HUNTER, E., HANIFFA, M. A., CUNNINGHAM, A. L. & HARMAN, A. N. 2019. Identification of HIV transmitting CD11c+ human epidermal dendritic cells. *Nat Commun,* 10**,** 2759.

BERTRAM, K. M., O'NEIL, T. R., VINE, E. E., BAHARLOU, H., CUNNINGHAM, A. L. & HARMAN, A. N. 2023. Defining the landscape of human epidermal mononuclear phagocytes. *Immunity,* 56**,** 459-460.

BIGLEY, V., MCGOVERN, N., MILNE, P., DICKINSON, R., PAGAN, S., COOKSON, S., HANIFFA, M. & COLLIN, M. 2015. Langerin-expressing dendritic cells in human tissues are related to CD1c+ dendritic cells and distinct from Langerhans cells and CD141high XCR1+ dendritic cells. *J Leukoc Biol,* 97**,** 627-634.

BLOCH, N., O'BRIEN, M., NORTON, T. D., POLSKY, S. B., BHARDWAJ, N. & LANDAU, N. R. 2014. HIV type 1 infection of plasmacytoid and myeloid dendritic cells is restricted by high levels of SAMHD1 and cannot be counteracted by Vpx. *AIDS Res Hum Retroviruses,* 30**,** 195-203.

BORGDORFF, H., GAUTAM, R., ARMSTRONG, S. D., XIA, D., NDAYISABA, G. F., VAN TEIJLINGEN, N. H., GEIJTENBEEK, T. B., WASTLING, J. M. & VAN DE WIJGERT, J. H. 2016. Cervicovaginal microbiome dysbiosis is associated with proteome changes related to alterations of the cervicovaginal mucosal barrier. *Mucosal Immunol,* 9**,** 621-33.

BOTTING, R. A., BERTRAM, K. M., BAHARLOU, H., SANDGREN, K. J., FLETCHER, J., RHODES, J. W., RANA, H., PLASTO, T. M., WANG, X. M., LIM, J. J. K., BARNOUTI, L., KOHOUT, M. P., PAPADOPOULOS, T., MERTEN, S., OLBOURNE, N., CUNNINGHAM, A. L., HANIFFA, M. & HARMAN, A. N. 2017. Phenotypic and functional consequences of different isolation protocols on skin mononuclear phagocytes. *J Leukoc Biol,* 101**,** 1393-1403.

BOURDELY, P., ANSELMI, G., VAIVODE, K., RAMOS, R. N., MISSOLO-KOUSSOU, Y., HIDALGO, S., TOSSELO, J., NUÑEZ, N., RICHER, W., VINCENT-SALOMON, A., SAXENA, A., WOOD, K., LLADSER, A., PIAGGIO, E., HELFT, J. & GUERMONPREZ, P. 2020. Transcriptional and Functional Analysis of CD1c(+) Human Dendritic Cells Identifies a CD163(+) Subset Priming CD8(+)CD103(+) T Cells. *Immunity,* 53**,** 335-352.e8.

BROUILLER, F., NADALIN, F., BONTÉ, P. E., AIT-MOHAMED, O., DELAUGERRE, C., LELIÈVRE, J. D., GINHOUX, F., RUFFIN, N. & BENAROCH, P. 2023. Single-cell RNA-seq analysis reveals dual sensing of HIV-1 in blood Axl(+) dendritic cells. *iScience,* 26**,** 106019.

BUJKO, A., ATLASY, N., LANDSVERK, O. J. B., RICHTER, L., YAQUB, S., HORNELAND, R., ØYEN, O., AANDAHL, E. M., AABAKKEN, L., STUNNENBERG, H. G., BÆKKEVOLD, E. S. & JAHNSEN, F. L. 2018. Transcriptional and functional profiling defines human small intestinal macrophage subsets. *J Exp Med,* 215**,** 441-458.

BUKUSI, E. A., COHEN, C. R., MEIER, A. S., WAIYAKI, P. G., NGUTI, R., NJERI, J. N. & HOLMES, K. K. 2006. Bacterial vaginosis: risk factors among Kenyan women and their male partners. *Sex Transm Dis,* 33**,** 361-7.

CAMERON, P. U., SALEH, S., SALLMANN, G., SOLOMON, A., WIGHTMAN, F., EVANS, V. A., BOUCHER, G., HADDAD, E. K., SEKALY, R. P., HARMAN, A. N., ANDERSON, J. L., JONES, K. L., MAK, J., CUNNINGHAM, A. L., JAWOROWSKI, A. & LEWIN, S. R. 2010. Establishment of HIV-1 latency in resting CD4+ T cells depends on chemokine-induced changes in the actin cytoskeleton. *Proc Natl Acad Sci U S A,* 107**,** 16934-9.

CAPUCHA, T., KOREN, N., NASSAR, M., HEYMAN, O., NIR, T., LEVY, M., ZILBERMAN-SCHAPIRA, G., ZELENTOVA, K., ELI-BERCHOER, L., ZENKE, M., HIERONYMUS, T., WILENSKY, A., BERCOVIER, H., ELINAV, E., CLAUSEN, B. E. & HOVAV, A.-H. 2018. Sequential BMP7/TGF-β1 signaling and microbiota instruct mucosal Langerhans cell differentiation. *Journal of Experimental Medicine,* 215**,** 481-500.

CAPUTO, V., LIBERA, M., SISTI, S., GIULIANI, B., DIOTTI, R. A. & CRISCUOLO, E. 2023. The initial interplay between HIV and mucosal innate immunity. *Front Immunol,* 14**,** 1104423.

CARDONE, M., IKEDA, K. N., VARANO, B., BELARDELLI, F., MILLEFIORINI, E., GESSANI, S. & CONTI, L. 2013. Opposite regulatory effects of IFN-β and IL-3 on C-type lectin receptors, antigen uptake, and phagocytosis in human macrophages. *Journal of Leukocyte Biology,* 95**,** 161-168.

CELLA, M., JARROSSAY, D., FACCHETTI, F., ALEBARDI, O., NAKAJIMA, H., LANZAVECCHIA, A. & COLONNA, M. 1999. Plasmacytoid monocytes migrate to inflamed lymph nodes and produce large amounts of type I interferon. *Nat Med,* 5**,** 919-23.

CHEN, S. T., LIN, Y. L., HUANG, M. T., WU, M. F., CHENG, S. C., LEI, H. Y., LEE, C. K., CHIOU, T. W., WONG, C. H. & HSIEH, S. L. 2008. CLEC5A is critical for dengue-virus-induced lethal disease. *Nature,* 453**,** 672-6.

CHEN, W., JIN, B., CHENG, C., PENG, H., ZHANG, X., TAN, W., TANG, R., LIAN, X., DIAO, H., LUO, N., LI, X., FAN, J., SHI, J., YIN, C., WANG, J., PENG, S.,

YU, L., LI, J., WU, R. Q., KUANG, D. M., SHI, G. P., ZHOU, Y., WANG, F. & JIANG, X. 2024. Single-cell profiling reveals kidney CD163(+) dendritic cell participation in human lupus nephritis. *Ann Rheum Dis,* 83**,** 608-623.

CHEN, Y., LIN, H., COLE, M., MORRIS, A., MARTINSON, J., MCKAY, H., MIMIAGA, M., MARGOLICK, J., FITCH, A., METHE, B., SRINIVAS, V. R., PEDDADA, S. & RINALDO, C. R. 2021. Signature changes in gut microbiome are associated with increased susceptibility to HIV-1 infection in MSM. *Microbiome,* 9**,** 237.

CHEN, Y. L., GOMES, T., HARDMAN, C. S., VIEIRA BRAGA, F. A., GUTOWSKA-OWSIAK, D., SALIMI, M., GRAY, N., DUNCAN, D. A., REYNOLDS, G., JOHNSON, D., SALIO, M., CERUNDOLO, V., BARLOW, J. L., MCKENZIE, A. N. J., TEICHMANN, S. A., HANIFFA, M. & OGG, G. 2020. Re-evaluation of human BDCA-2+ DC during acute sterile skin inflammation. *J Exp Med,* 217.

CHERSICH, M. F. & REES, H. V. 2008. Vulnerability of women in southern Africa to infection with HIV: biological determinants and priority health sector interventions. *Aids,* 22 Suppl 4**,** S27-40.

CHU, C. C., ALI, N., KARAGIANNIS, P., DI MEGLIO, P., SKOWERA, A., NAPOLITANO, L., BARINAGA, G., GRYS, K., SHARIF-PAGHALEH, E., KARAGIANNIS, S. N., PEAKMAN, M., LOMBARDI, G. & NESTLE, F. O. 2012. Resident CD141 (BDCA3)+ dendritic cells in human skin produce IL-10 and induce regulatory T cells that suppress skin inflammation. *J Exp Med,* 209**,** 935-45.

CISSE, B., CATON, M. L., LEHNER, M., MAEDA, T., SCHEU, S., LOCKSLEY, R., HOLMBERG, D., ZWEIER, C., DEN HOLLANDER, N. S., KANT, S. G., HOLTER, W., RAUCH, A., ZHUANG, Y. & REIZIS, B. 2008. Transcription factor E2-2 is an essential and specific regulator of plasmacytoid dendritic cell development. *Cell,* 135**,** 37-48.

COHEN, E., MARIOTTON, J., ROZENBERG, F., SAMS, A., VAN KUPPEVELT, T. H., BARRY DELONGCHAMPS, N., ZERBIB, M., BOMSEL, M. & GANOR, Y. 2022. CGRP inhibits human Langerhans cells infection with HSV by differentially modulating specific HSV-1 and HSV-2 entry mechanisms. *Mucosal Immunol,* 15**,** 762-771.

COLLINS, N., JIANG, X., ZAID, A., MACLEOD, B. L., LI, J., PARK, C. O., HAQUE, A., BEDOUI, S., HEATH, W. R., MUELLER, S. N., KUPPER, T. S., GEBHARDT, T. & CARBONE, F. R. 2016. Skin CD4+ memory T cells exhibit combined cluster-mediated retention and equilibration with the circulation. *Nature Communications,* 7**,** 11514.

CROSS, A. R., LION, J., POUSSIN, K., GLOTZ, D. & MOONEY, N. 2021. Inflammation Determines the Capacity of Allogenic Endothelial Cells to Regulate Human Treg Expansion. *Frontiers in Immunology,* Volume 12 - 2021.

CUADROS, D. F., CROWLEY, P. H., AUGUSTINE, B., STEWART, S. L. & GARCÍA-RAMOS, G. 2011. Effect of variable transmission rate on the dynamics of HIV in sub-Saharan Africa. *BMC Infect Dis,* 11**,** 216-216.

CUNNINGHAM, A., HARMAN, A., KIM, M., NASR, N. & LAI, J. 2013a. Immunobiology of dendritic cells and the influence of HIV infection. *Adv Exp Med Biol,* 762**,** 1-44.

CUNNINGHAM, A. L., HARMAN, A. & NASR, N. 2013b. Initial HIV mucosal infection

and dendritic cells. *EMBO Molecular Medicine,* 5**,** 658-660.

CYTLAK, U., RESTEU, A., PAGAN, S., GREEN, K., MILNE, P., MAISURIA, S., MCDONALD, D., HULME, G., FILBY, A., CARPENTER, B., QUEEN, R., HAMBLETON, S., HAGUE, R., LANGO ALLEN, H., THAVENTHIRAN, J. E. D., DOODY, G., COLLIN, M. & BIGLEY, V. 2020. Differential IRF8 Transcription Factor Requirement Defines Two Pathways of Dendritic Cell Development in Humans. *Immunity,* 53**,** 353-370.e8.

DABEE, S., BARNABAS, S. L., LENNARD, K. S., JAUMDALLY, S. Z., GAMIELDIEN, H., BALLE, C., HAPPEL, A. U., MURUGAN, B. D., WILLIAMSON, A. L., MKHIZE, N., DIETRICH, J., LEWIS, D. A., CHIODI, F., HOPE, T. J., SHATTOCK, R., GRAY, G., BEKKER, L. G., JASPAN, H. B. & PASSMORE, J. S. 2019. Defining characteristics of genital health in South African adolescent girls and young women at high risk for HIV infection. *PLoS One,* 14**,** e0213975.

DE LA CRUZ, N. C., MÖCKEL, M., WIRTZ, L., SUNAOGLU, K., MALTER, W., ZINSER, M. & KNEBEL-MÖRSDORF, D. 2021. Ex Vivo Infection of Human Skin with Herpes Simplex Virus 1 Reveals Mechanical Wounds as Insufficient Entry Portals via the Skin Surface. *J Virol,* 95**,** e0133821.

DE NEVE, J.-W., FINK, G., SUBRAMANIAN, S. V., MOYO, S. & BOR, J. 2015. Length of secondary schooling and risk of HIV infection in Botswana: evidence from a natural experiment. *The Lancet Global Health,* 3**,** e470-e477.

DE WITTE, L., NABATOV, A., PION, M., FLUITSMA, D., DE JONG, M. A., DE GRUIJL, T., PIGUET, V., VAN KOOYK, Y. & GEIJTENBEEK, T. B. 2007. Langerin is a natural barrier to HIV-1 transmission by Langerhans cells. *Nat Med,* 13**,** 367-71.

DEBERGE, M., GLINTON, K., SUBRAMANIAN, M., WILSBACHER, L. D., ROTHLIN, C. V., TABAS, I. & THORP, E. B. 2021. Macrophage AXL receptor tyrosine kinase inflames the heart after reperfused myocardial infarction. *J Clin Invest,* 131.

DELIA, D., CATTORETTI, G., POLLI, N., FONTANELLA, E., AIELLO, A., GIARDINI, R., RILKE, F. & DELLA PORTA, G. 1988. CD1c but neither CD1a nor CD1b molecules are expressed on normal, activated, and malignant human B cells: identification of a new B-cell subset. *Blood,* 72**,** 241-7.

DENG, Z., FAN, T., XIAO, C., TIAN, H., ZHENG, Y., LI, C. & HE, J. 2024. TGF-β signaling in health, disease and therapeutics. *Signal Transduction and Targeted Therapy,* 9**,** 61.

DEVITT, A., PIERCE, S., OLDREIVE, C., SHINGLER, W. & GREGORY, C. 2003. CD14-dependent clearance of apoptotic cells by human macrophages: the role of phosphatidylserine. *Cell Death & Differentiation,* 10**,** 371-382.

DINH, M. H., HIRBOD, T., KIGOZI, G., OKOCHA, E. A., CIANCI, G. C., KONG, X., PRODGER, J. L., BROLIDEN, K., KAUL, R., SERWADDA, D., WAWER, M. J., GRAY, R. H. & HOPE, T. J. 2012. No Difference in Keratin Thickness between Inner and Outer Foreskins from Elective Male Circumcisions in Rakai, Uganda. *PLOS ONE,* 7**,** e41271.

DINH, M. H., MCRAVEN, M. D., KELLEY, Z., PENUGONDA, S. & HOPE, T. J. 2010. Keratinization of the adult male foreskin and implications for male circumcision. *Aids,* 24**,** 899-906.

DOEBEL, T., VOISIN, B. & NAGAO, K. 2017. Langerhans Cells – The Macrophage in Dendritic Cell Clothing. *Trends Immunol,* 38**,** 817-828.

DOMANSKA, D., MAJID, U., KARLSEN, V. T., MEROK, M. A., BEITNES, A. R., YAQUB, S., BÆKKEVOLD, E. S. & JAHNSEN, F. L. 2022. Single-cell transcriptomic analysis of human colonic macrophages reveals niche-specific subsets. *J Exp Med,* 219.

DOYLE, C. M., FEWINGS, N. L., CTERCTEKO, G., BYRNE, S. N., HARMAN, A. N. & BERTRAM, K. M. 2022. OMIP 082: A 25-color phenotyping to define human innate lymphoid cells, natural killer cells, mucosal-associated invariant T cells, and γδ T cells from freshly isolated human intestinal tissue. *Cytometry Part A,* 101**,** 196-202.

DOYLE, C. M., VINE, E. E., BERTRAM, K. M., BAHARLOU, H., RHODES, J. W., DERVISH, S., GOSSELINK, M. P., DI RE, A., COLLINS, G. P., REZA, F., TOH, J. W. T., PATHMA-NATHAN, N., AHLENSTIEL, G., CTERCTEKO, G., CUNNINGHAM, A. L., HARMAN, A. N. & BYRNE, S. N. 2021. Optimal Isolation Protocols for Examining and Interrogating Mononuclear Phagocytes From Human Intestinal Tissue. *Front Immunol,* 12**,** 727952-727952.

DRUTMAN, S. B., KENDALL, J. C. & TROMBETTA, E. S. 2012. Inflammatory spleen monocytes can upregulate CD11c expression without converting into dendritic cells. *J Immunol,* 188**,** 3603-10.

DULL, K., FAZEKAS, F. & TÖRŐCSIK, D. 2021. Factor XIII-A in Diseases: Role Beyond Blood Coagulation. *Int J Mol Sci,* 22.

DULUC, D., GANNEVAT, J., ANGUIANO, E., ZURAWSKI, S., CARLEY, M., BOREHAM, M., STECHER, J., DULLAERS, M., BANCHEREAU, J. & OH, S. 2013. Functional diversity of human vaginal APC subsets in directing T-cell responses. *Mucosal Immunol,* 6**,** 626-38.

DUTERTRE, C. A., BECHT, E., IRAC, S. E., KHALILNEZHAD, A., NARANG, V., KHALILNEZHAD, S., NG, P. Y., VAN DEN HOOGEN, L. L., LEONG, J. Y., LEE, B., CHEVRIER, M., ZHANG, X. M., YONG, P. J. A., KOH, G., LUM, J., HOWLAND, S. W., MOK, E., CHEN, J., LARBI, A., TAN, H. K. K., LIM, T. K. H., KARAGIANNI, P., TZIOUFAS, A. G., MALLERET, B., BRODY, J., ALBANI, S., VAN ROON, J., RADSTAKE, T., NEWELL, E. W. & GINHOUX, F. 2019. Single-Cell Analysis of Human Mononuclear Phagocytes Reveals Subset-Defining Markers and Identifies Circulating Inflammatory Dendritic Cells. *Immunity,* 51**,** 573-589.e8.

EGUÍLUZ-GRACIA, I., BOSCO, A., DOLLNER, R., MELUM, G. R., LEXBERG, M. H., JONES, A. C., DHEYAULDEEN, S. A., HOLT, P. G., BÆKKEVOLD, E. S. & JAHNSEN, F. L. 2016. Rapid recruitment of CD14+ monocytes in experimentally induced allergic rhinitis in human subjects. *Journal of Allergy and Clinical Immunology,* 137**,** 1872-1881.e12.

EPSTEIN, S. P., GADARIA-RATHOD, N., WEI, Y., MAGUIRE, M. G. & ASBELL, P. A. 2013. HLA-DR expression as a biomarker of inflammation for multicenter clinical trials of ocular surface disease. *Exp Eye Res,* 111**,** 95-104.

ESRA, R. T., OLIVIER, A. J., PASSMORE, J.-A. S., JASPAN, H. B., HARRYPARSAD, R. & GRAY, C. M. 2016. Does HIV Exploit the Inflammatory Milieu of the Male Genital Tract for Successful Infection? *Front Immunol,* 7**,** 245-245.

FAIRHURST, R. M., WANG, C. X., SIELING, P. A., MODLIN, R. L. & BRAUN, J. 1998. CD1-restricted T cells and resistance to polysaccharide-encapsulated bacteria. *Immunol Today,* 19**,** 257-9.

FINK, T., ORAEVSKY, A., TITTEL, F., THOMSEN, S. & JACQUES, S. 1996. *Autofluorescence detection of oxidized LDL in monocytes: a novel risk factor for the assessment of atherosclerosis?*, SPIE.

FONG, L., MENGOZZI, M., ABBEY, N. W., HERNDIER, B. G. & ENGLEMAN, E. G. 2002. Productive infection of plasmacytoid dendritic cells with human immunodeficiency virus type 1 is triggered by CD40 ligation. *J Virol,* 76**,** 11033-41.

FONTENEAU, J. F., LARSSON, M., BEIGNON, A. S., MCKENNA, K., DASILVA, I., AMARA, A., LIU, Y. J., LIFSON, J. D., LITTMAN, D. R. & BHARDWAJ, N. 2004. Human immunodeficiency virus type 1 activates plasmacytoid dendritic cells and concomitantly induces the bystander maturation of myeloid dendritic cells. *J Virol,* 78**,** 5223-32.

FORSBERG, J. G. 1995. A morphologist's approach to the vagina--age-related changes and estrogen sensitivity. *Maturitas,* 22 Suppl**,** S7-s15.

FOSTER, T. L., WILSON, H., IYER, S. S., COSS, K., DOORES, K., SMITH, S., KELLAM, P., FINZI, A., BORROW, P., HAHN, B. H. & NEIL, S. J. D. 2016. Resistance of Transmitted Founder HIV-1 to IFITM-Mediated Restriction. *Cell Host Microbe,* 20**,** 429-442.

FUJIMORI, T., GRABIEC, A. M., KAUR, M., BELL, T. J., FUJINO, N., COOK, P. C., SVEDBERG, F. R., MACDONALD, A. S., MACIEWICZ, R. A., SINGH, D. & HUSSELL, T. 2015. The Axl receptor tyrosine kinase is a discriminator of macrophage function in the inflamed lung. *Mucosal Immunol,* 8**,** 1021-1030.

FULCHER, J. A., LI, F., TOBIN, N. H., ZABIH, S., ELLIOTT, J., CLARK, J. L., D'AQUILA, R., MUSTANSKI, B., KIPKE, M. D., SHOPTAW, S., GORBACH, P. M. & ALDROVANDI, G. M. 2022. Gut dysbiosis and inflammatory blood markers precede HIV with limited changes after early seroconversion. *eBioMedicine,* 84.

GANOR, Y., REAL, F., SENNEPIN, A., DUTERTRE, C.-A., PREVEDEL, L., XU, L., TUDOR, D., CHARMETEAU, B., COUEDEL-COURTEILLE, A., MARION, S., ZENAK, A.-R., JOURDAIN, J.-P., ZHOU, Z., SCHMITT, A., CAPRON, C., EUGENIN, E. A., CHEYNIER, R., REVOL, M., CRISTOFARI, S., HOSMALIN, A. & BOMSEL, M. 2019. HIV-1 reservoirs in urethral macrophages of patients under suppressive antiretroviral therapy. *Nature Microbiology,* 4**,** 633-644.

GARTNER, S., MARKOVITS, P., MARKOVITZ, D. M., KAPLAN, M. H., GALLO, R. C. & POPOVIC, M. 1986. The role of mononuclear phagocytes in HTLV-III/LAV infection. *Science,* 233**,** 215-9.

GEIJTENBEEK, T. B. H., KWON, D. S., TORENSMA, R., VAN VLIET, S. J., VAN DUIJNHOVEN, G. C. F., MIDDEL, J., CORNELISSEN, I. L. M. H. A., NOTTET, H. S. L. M., KEWALRAMANI, V. N., LITTMAN, D. R., FIGDOR, C. G. & VAN KOOYK, Y. 2000. DC-SIGN, a Dendritic Cell–Specific HIV-1-Binding Protein that Enhances trans-Infection of T Cells. *Cell,* 100**,** 587-597.

GILLIET, M., CAO, W. & LIU, Y. J. 2008. Plasmacytoid dendritic cells: sensing nucleic acids in viral infection and autoimmune diseases. *Nat Rev Immunol,* 8**,** 594-

606.

GINHOUX, F., TACKE, F., ANGELI, V., BOGUNOVIC, M., LOUBEAU, M., DAI, X.-M., STANLEY, E. R., RANDOLPH, G. J. & MERAD, M. 2006. Langerhans cells arise from monocytes in vivo. *Nature Immunology,* 7**,** 265-273.

GOLINSKI, M. L., DEMEULES, M., DERAMBURE, C., RIOU, G., MAHO-VAILLANT, M., BOYER, O., JOLY, P. & CALBO, S. 2020. CD11c(+) B Cells Are Mainly Memory Cells, Precursors of Antibody Secreting Cells in Healthy Donors. *Front Immunol,* 11**,** 32.

GOSMANN, C., ANAHTAR, M. N., HANDLEY, S. A., FARCASANU, M., ABU-ALI, G., BOWMAN, B. A., PADAVATTAN, N., DESAI, C., DROIT, L., MOODLEY, A., DONG, M., CHEN, Y., ISMAIL, N., NDUNG'U, T., GHEBREMICHAEL, M. S., WESEMANN, D. R., MITCHELL, C., DONG, K. L., HUTTENHOWER, C., WALKER, B. D., VIRGIN, H. W. & KWON, D. S. 2017. Lactobacillus-Deficient Cervicovaginal Bacterial Communities Are Associated with Increased HIV Acquisition in Young South African Women. *Immunity,* 46**,** 29-37.

GULICK, R. M. & FLEXNER, C. 2019. Long-Acting HIV Drugs for Treatment and Prevention. *Annu Rev Med,* 70**,** 137-150.

GUO, R.-F. & WARD, P. A. 2005. Role Of C5a In Inflammatory Responses. *Annual Review of Immunology,* 23**,** 821-852.

GURNEY, K. B., ELLIOTT, J., NASSANIAN, H., SONG, C., SOILLEUX, E., MCGOWAN, I., ANTON, P. A. & LEE, B. 2005. Binding and transfer of human immunodeficiency virus by DC-SIGN+ cells in human rectal mucosa. *J Virol,* 79**,** 5762-73.

GUTIÉRREZ, J. P. & TROSSERO, A. 2021. Socioeconomic inequalities in HIV knowledge, HIV testing, and condom use among adolescent and young women in Latin America and the Caribbean. *Rev Panam Salud Publica,* 45**,** e47.

HAMILTON, J. A., STANLEY, E. R., BURGESS, A. W. & SHADDUCK, R. K. 1980. Stimulation of macrophage plasminogen activator activity by colony-stimulating factors. *J Cell Physiol,* 103**,** 435-45.

HANIFFA, M., GINHOUX, F., WANG, X. N., BIGLEY, V., ABEL, M., DIMMICK, I., BULLOCK, S., GRISOTTO, M., BOOTH, T., TAUB, P., HILKENS, C., MERAD, M. & COLLIN, M. 2009. Differential rates of replacement of human dermal dendritic cells and macrophages during hematopoietic stem cell transplantation. *J Exp Med,* 206**,** 371-85.

HANIFFA, M., SHIN, A., BIGLEY, V., MCGOVERN, N., TEO, P., SEE, P., WASAN, P. S., WANG, X. N., MALINARICH, F., MALLERET, B., LARBI, A., TAN, P., ZHAO, H., POIDINGER, M., PAGAN, S., COOKSON, S., DICKINSON, R., DIMMICK, I., JARRETT, R. F., RENIA, L., TAM, J., SONG, C., CONNOLLY, J., CHAN, J. K., GEHRING, A., BERTOLETTI, A., COLLIN, M. & GINHOUX, F. 2012. Human tissues contain CD141hi cross-presenting dendritic cells with functional homology to mouse CD103+ nonlymphoid dendritic cells. *Immunity,* 37**,** 60-73.

HARMAN, A. N., BYE, C. R., NASR, N., SANDGREN, K. J., KIM, M., MERCIER, S. K., BOTTING, R. A., LEWIN, S. R., CUNNINGHAM, A. L. & CAMERON, P. U. 2013. Identification of lineage relationships and novel markers of blood and skin human dendritic cells. *J Immunol,* 190**,** 66-79.

HARMAN, A. N., LAI, J., TURVILLE, S., SAMARAJIWA, S., GRAY, L., MARSDEN, V., MERCIER, S., JONES, K., NASR, N., RUSTAGI, A., CUMMING, H., DONAGHY, H., MAK, J., GALE, M., CHURCHILL, M., HERTZOG, P. & CUNNINGHAM, A. L. 2011. HIV infection of dendritic cells subverts the IFN induction pathway via IRF-1 and inhibits type 1 IFN production. *Blood,* 118**,** 298-308.

HARMAN, A. N., WILKINSON, J., BYE, C. R., BOSNJAK, L., STERN, J. L., NICHOLLE, M., LAI, J. & CUNNINGHAM, A. L. 2006. HIV induces maturation of monocyte-derived dendritic cells and Langerhans cells. *J Immunol,* 177**,** 7103-13.

HAUSER, M. A., SCHAEUBLE, K., KINDINGER, I., IMPELLIZZIERI, D., KRUEGER, W. A., HAUCK, C. R., BOYMAN, O. & LEGLER, D. F. 2016. Inflammation-Induced CCR7 Oligomers Form Scaffolds to Integrate Distinct Signaling Pathways for Efficient Cell Migration. *Immunity,* 44**,** 59-72.

HE, H., SURYAWANSHI, H., MOROZOV, P., GAY-MIMBRERA, J., DEL DUCA, E., KIM, H. J., KAMEYAMA, N., ESTRADA, Y., DER, E., KRUEGER, J. G., RUANO, J., TUSCHL, T. & GUTTMAN-YASSKY, E. 2020. Single-cell transcriptome analysis of human skin identifies novel fibroblast subpopulation and enrichment of immune subsets in atopic dermatitis. *J Allergy Clin Immunol,* 145**,** 1615-1628.

HEARPS, A. C., TYSSEN, D., SRBINOVSKI, D., BAYIGGA, L., DIAZ, D. J. D., ALDUNATE, M., CONE, R. A., GUGASYAN, R., ANDERSON, D. J. & TACHEDJIAN, G. 2017. Vaginal lactic acid elicits an anti-inflammatory response from human cervicovaginal epithelial cells and inhibits production of pro-inflammatory mediators associated with HIV acquisition. *Mucosal Immunology,* 10**,** 1480-1490.

HEASTER, T. M., HUMAYUN, M., YU, J., BEEBE, D. J. & SKALA, M. C. 2020. Autofluorescence Imaging of 3D Tumor-Macrophage Microscale Cultures Resolves Spatial and Temporal Dynamics of Macrophage Metabolism. *Cancer Res,* 80**,** 5408-5423.

HERVAS-STUBBS, S., PEREZ-GRACIA, J. L., ROUZAUT, A., SANMAMED, M. F., LE BON, A. & MELERO, I. 2011. Direct effects of type I interferons on cells of the immune system. *Clin Cancer Res,* 17**,** 2619-27.

HICKEY, D. K., PATEL, M. V., FAHEY, J. V. & WIRA, C. R. 2011. Innate and adaptive immunity at mucosal surfaces of the female reproductive tract: stratification and integration of immune protection against the transmission of sexually transmitted infections. *Journal of Reproductive Immunology,* 88**,** 185-194.

HONDA, K. & TANIGUCHI, T. 2006. IRFs: master regulators of signalling by Toll-like receptors and cytosolic pattern-recognition receptors. *Nat Rev Immunol,* 6**,** 644-58.

HU, J., GARDNER, M. B. & MILLER, C. J. 2000. Simian immunodeficiency virus rapidly penetrates the cervicovaginal mucosa after intravaginal inoculation and infects intraepithelial dendritic cells. *J Virol,* 74**,** 6087-95.

HU, K., O'NEIL, T., CANETE, N., BAHARLOU, H. & HARMAN, A. 2024. OMIP-103: A 35-marker imaging mass cytometry panel for the co-detection of HIV and immune cell populations in human formalin fixed paraffin embedded intestinal

tissue. *Cytometry Part A,* 105**,** 488-492.

HUANG, H.-I., JEWELL, M. L., YOUSSEF, N., HUANG, M.-N., HAUSER, E. R., FEE, B. E., RUDEMILLER, N. P., PRIVRATSKY, J. R., ZHANG, J. J., REYES, E. Y., WANG, D., TAYLOR, G. A., GUNN, M. D., KO, D. C., COOK, D. N., CHANDRAMOHAN, V., CROWLEY, S. D. & HAMMER, G. E. 2021. Th17 Immunity in the Colon Is Controlled by Two Novel Subsets of Colon-Specific Mononuclear Phagocytes. *Frontiers in Immunology,* Volume 12 - 2021.

ITALIANI, P. & BORASCHI, D. 2014. From Monocytes to M1/M2 Macrophages: Phenotypical vs. Functional Differentiation. *Front Immunol,* 5**,** 514.

IWASAKI, A. 2010. Antiviral immune responses in the genital tract: clues for vaccines. *Nature Reviews Immunology,* 10**,** 699-711.

IYER, S. S., BIBOLLET-RUCHE, F., SHERRILL-MIX, S., LEARN, G. H., PLENDERLEITH, L., SMITH, A. G., BARBIAN, H. J., RUSSELL, R. M., GONDIM, M. V., BAHARI, C. Y., SHAW, C. M., LI, Y., DECKER, T., HAYNES, B. F., SHAW, G. M., SHARP, P. M., BORROW, P. & HAHN, B. H. 2017. Resistance to type 1 interferons is a major determinant of HIV-1 transmission fitness. *Proc Natl Acad Sci U S A,* 114**,** E590-e599.

IZQUIERDO-USEROS, N., LORIZATE, M., CONTRERAS, F. X., RODRIGUEZ-PLATA, M. T., GLASS, B., ERKIZIA, I., PRADO, J. G., CASAS, J., FABRIÀS, G., KRÄUSSLICH, H. G. & MARTINEZ-PICADO, J. 2012. Sialyllactose in viral membrane gangliosides is a novel molecular recognition pattern for mature dendritic cell capture of HIV-1. *PLoS Biol,* 10**,** e1001315.

IZQUIERDO-USEROS, N., NARANJO-GÓMEZ, M., ARCHER, J., HATCH, S. C., ERKIZIA, I., BLANCO, J., BORRÀS, F. E., PUERTAS, M. C., CONNOR, J. H., FERNÁNDEZ-FIGUERAS, M. T., MOORE, L., CLOTET, B., GUMMULURU, S. & MARTINEZ-PICADO, J. 2009. Capture and transfer of HIV-1 particles by mature dendritic cells converges with the exosome-dissemination pathway. *Blood,* 113**,** 2732-41.

JARDINE, L., BARGE, D., AMES-DRAYCOTT, A., PAGAN, S., COOKSON, S., SPICKETT, G., HANIFFA, M., COLLIN, M. & BIGLEY, V. 2013. Rapid detection of dendritic cell and monocyte disorders using CD4 as a lineage marker of the human peripheral blood antigen-presenting cell compartment. *Front Immunol,* 4**,** 495.

JARDINE, L., WISCOMBE, S., REYNOLDS, G., MCDONALD, D., FULLER, A., GREEN, K., FILBY, A., FORREST, I., RUCHAUD-SPARAGANO, M. H., SCOTT, J., COLLIN, M., HANIFFA, M. & SIMPSON, A. J. 2019. Lipopolysaccharide inhalation recruits monocytes and dendritic cell subsets to the alveolar airspace. *Nat Commun,* 10**,** 1999.

JEWKES, R. K., DUNKLE, K., NDUNA, M. & SHAI, N. 2010. Intimate partner violence, relationship power inequity, and incidence of HIV infection in young women in South Africa: a cohort study. *Lancet,* 376**,** 41-8.

JIANG, W., ZHANG, L., LANG, R., LI, Z. & GILKESON, G. 2014. Sex Differences in Monocyte Activation in Systemic Lupus Erythematosus (SLE). *PLOS ONE,* 9**,** e114589.

JIN, W., LI, C., DU, T., HU, K., HUANG, X. & HU, Q. 2014. DC-SIGN plays a stronger role than DCIR in mediating HIV-1 capture and transfer. *Virology,* 458-459**,** 83-

92.

JOLLY, C., KASHEFI, K., HOLLINSHEAD, M. & SATTENTAU, Q. J. 2004. HIV-1 cell to cell transfer across an Env-induced, actin-dependent synapse. *J Exp Med,* 199**,** 283-93.

JOVANOVIC, K., SIEBECK, M. & GROPP, R. 2014. The route to pathologies in chronic inflammatory diseases characterized by T helper type 2 immune cells. *Clin Exp Immunol,* 178**,** 201-11.

KAMADA, N., HISAMATSU, T., OKAMOTO, S., CHINEN, H., KOBAYASHI, T., SATO, T., SAKURABA, A., KITAZUME, M. T., SUGITA, A., KOGANEI, K., AKAGAWA, K. S. & HIBI, T. 2008. Unique CD14+ intestinal macrophages contribute to the pathogenesis of Crohn disease via IL-23/IFN-γ axis. *The Journal of Clinical Investigation,* 118**,** 2269-2280.

KANG, J., KIM, M., YOON, D. Y., KIM, W. S., CHOI, S. J., KWON, Y. N., KIM, W. S., PARK, S. H., SUNG, J. J., PARK, M., LEE, J. S., PARK, J. E. & KIM, S. M. 2023. AXL(+)SIGLEC6(+) dendritic cells in cerebrospinal fluid and brain tissues of patients with autoimmune inflammatory demyelinating disease of CNS. *Clin Immunol,* 253**,** 109686.

KEELE, B. F., GIORGI, E. E., SALAZAR-GONZALEZ, J. F., DECKER, J. M., PHAM, K. T., SALAZAR, M. G., SUN, C., GRAYSON, T., WANG, S., LI, H., WEI, X., JIANG, C., KIRCHHERR, J. L., GAO, F., ANDERSON, J. A., PING, L.-H., SWANSTROM, R., TOMARAS, G. D., BLATTNER, W. A., GOEPFERT, P. A., KILBY, J. M., SAAG, M. S., DELWART, E. L., BUSCH, M. P., COHEN, M. S., MONTEFIORI, D. C., HAYNES, B. F., GASCHEN, B., ATHREYA, G. S., LEE, H. Y., WOOD, N., SEOIGHE, C., PERELSON, A. S., BHATTACHARYA, T., KORBER, B. T., HAHN, B. H. & SHAW, G. M. 2008. Identification and characterization of transmitted and early founder virus envelopes in primary HIV-1 infection. *Proceedings of the National Academy of Sciences,* 105**,** 7552-7557.

KLATT, N. R., CHEU, R., BIRSE, K., ZEVIN, A. S., PERNER, M., NOËL-ROMAS, L., GROBLER, A., WESTMACOTT, G., XIE, I. Y., BUTLER, J., MANSOOR, L., MCKINNON, L. R., PASSMORE, J.-A. S., ABDOOL KARIM, Q., ABDOOL KARIM, S. S. & BURGENER, A. D. 2017. Vaginal bacteria modify HIV tenofovir microbicide efficacy in African women. *Science,* 356**,** 938.

KLEBANOFF, M. A., SCHWEBKE, J. R., ZHANG, J., NANSEL, T. R., YU, K. F. & ANDREWS, W. W. 2004. Vulvovaginal symptoms in women with bacterial vaginosis. *Obstet Gynecol,* 104**,** 267-72.

KNAB, A., GIARDINA, C., GREY, S. T., GOLDYS, E. M. & CAMPBELL, J. M. 2025. Illuminating Immunity: A Systematic Review of Immune Cell Autofluorescence. *Journal of Biophotonics,* 18**,** e202400576.

KORENFELD, D., GORVEL, L., MUNK, A., MAN, J., SCHAFFER, A., TUNG, T., MANN, C. & KLECHEVSKY, E. 2017. A type of human skin dendritic cell marked by CD5 is associated with the development of inflammatory skin disease. *JCI Insight,* 2.

KOUMANS, E. H., STERNBERG, M., BRUCE, C., MCQUILLAN, G., KENDRICK, J., SUTTON, M. & MARKOWITZ, L. E. 2007. The prevalence of bacterial vaginosis in the United States, 2001-2004; associations with symptoms, sexual

behaviors, and reproductive health. *Sex Transm Dis,* 34**,** 864-9.

KRISTENSEN, M. W., KEJLBERG-JENSEN, S., SØRENSEN, A. S., VORUP-JENSEN, T., W. KRAGSTRUP, T., HOKLAND, M. & ANDERSEN, M. N. 2021. Behold Cytometrists: One Block Is Not Enough! Cyanine-Tandems Bind Non-Specifically to Human Monocytes. *Cytometry Part A,* 99**,** 265-268.

KUCHUKHIDZE, S., PANAGIOTOGLOU, D., BOILY, M. C., DIABATÉ, S., EATON, J. W., MBOFANA, F., SARDINHA, L., SCHRUBBE, L., STÖCKL, H., WANYENZE, R. K. & MAHEU-GIROUX, M. 2023. The effects of intimate partner violence on women's risk of HIV acquisition and engagement in the HIV treatment and care cascade: a pooled analysis of nationally representative surveys in sub-Saharan Africa. *Lancet HIV,* 10**,** e107-e117.

LAGA, M., MANOKA, A., KIVUVU, M., MALELE, B., TULIZA, M., NZILA, N., GOEMAN, J., BEHETS, F., BATTER, V., ALARY, M. & ET AL. 1993. Non-ulcerative sexually transmitted diseases as risk factors for HIV-1 transmission in women: results from a cohort study. *Aids,* 7**,** 95-102.

LAI, J., BERNHARD, O. K., TURVILLE, S. G., HARMAN, A. N., WILKINSON, J. & CUNNINGHAM, A. L. 2009. Oligomerization of the macrophage mannose receptor enhances gp120-mediated binding of HIV-1. *J Biol Chem,* 284**,** 11027-38.

LAMBERT, A. A., AZZI, A., LIN, S. X., ALLAIRE, G., ST-GELAIS, K. P., TREMBLAY, M. J. & GILBERT, C. 2013. Dendritic cell immunoreceptor is a new target for anti-AIDS drug development: identification of DCIR/HIV-1 inhibitors. *PLoS One,* 8**,** e67873.

LAMBERT, A. A., GILBERT, C., RICHARD, M., BEAULIEU, A. D. & TREMBLAY, M. J. 2008. The C-type lectin surface receptor DCIR acts as a new attachment factor for HIV-1 in dendritic cells and contributes to trans- and cis-infection pathways. *Blood,* 112**,** 1299-307.

LANE, B. R., LORE, K., BOCK, P. J., ANDERSSON, J., COFFEY, M. J., STRIETER, R. M. & MARKOVITZ, D. M. 2001. Interleukin-8 stimulates human immunodeficiency virus type 1 replication and is a potential new target for antiretroviral therapy. *J Virol,* 75**,** 8195-202.

LANG, M., KRUMP, C., MESHCHERYAKOVA, A., TAM-AMERSDORFER, C., SCHWARZENBERGER, E., PASSEGGER, C., CONNOLLY, S., MECHTCHERIAKOVA, D. & STROBL, H. 2023. Microenvironmental and cell intrinsic factors governing human cDC2 differentiation and monocyte reprogramming. *Frontiers in Immunology,* Volume 14 - 2023.

LARREGINA, A. T., MORELLI, A. E., SPENCER, L. A., LOGAR, A. J., WATKINS, S. C., THOMSON, A. W. & FALO, L. D. 2001. Dermal-resident CD14+ cells differentiate into Langerhans cells. *Nature Immunology,* 2**,** 1151-1158.

LEDERLE, A., SU, B., HOLL, V., PENICHON, J., SCHMIDT, S., DECOVILLE, T., LAUMOND, G. & MOOG, C. 2014. Neutralizing antibodies inhibit HIV-1 infection of plasmacytoid dendritic cells by an FcγRIIa independent mechanism and do not diminish cytokines production. *Sci Rep,* 4**,** 5845.

LEMOS, M. P., LAMA, J. R., KARUNA, S. T., FONG, Y., MONTANO, S. M., GANOZA, C., GOTTARDO, R., SANCHEZ, J. & MCELRATH, M. J. 2014. The inner foreskin of healthy males at risk of HIV infection harbors epithelial CD4+ CCR5+

cells and has features of an inflamed epidermal barrier. *PLoS One,* 9**,** e108954.

LENNARD, K., DABEE, S., BARNABAS, S. L., HAVYARIMANA, E., BLAKNEY, A., JAUMDALLY, S. Z., BOTHA, G., MKHIZE, N. N., BEKKER, L. G., LEWIS, D. A., GRAY, G., MULDER, N., PASSMORE, J. S. & JASPAN, H. B. 2018. Microbial Composition Predicts Genital Tract Inflammation and Persistent Bacterial Vaginosis in South African Adolescent Females. *Infect Immun,* 86.

LENNERT, K. & REMMELE, W. 1958. [Karyometric research on lymph node cells in man. I. Germinoblasts, lymphoblasts & lymphocytes]. *Acta Haematol,* 19**,** 99-113.

LEVINE, JACOB H., SIMONDS, ERIN F., BENDALL, SEAN C., DAVIS, KARA L., AMIR, E.-AD D., TADMOR, MICHELLE D., LITVIN, O., FIENBERG, HARRIS G., JAGER, A., ZUNDER, ELI R., FINCK, R., GEDMAN, AMANDA L., RADTKE, I., DOWNING, JAMES R., PE'ER, D. & NOLAN, GARRY P. 2015. Data-Driven Phenotypic Dissection of AML Reveals Progenitor-like Cells that Correlate with Prognosis. *Cell,* 162**,** 184-197.

LI, J., ZHOU, J., HUANG, H., JIANG, J., ZHANG, T. & NI, C. 2023. Mature dendritic cells enriched in immunoregulatory molecules (mregDCs): A novel population in the tumour microenvironment and immunotherapy target. *Clin Transl Med,* 13**,** e1199.

LI, Q., ESTES, J. D., SCHLIEVERT, P. M., DUAN, L., BROSNAHAN, A. J., SOUTHERN, P. J., REILLY, C. S., PETERSON, M. L., SCHULTZ-DARKEN, N., BRUNNER, K. G., NEPHEW, K. R., PAMBUCCIAN, S., LIFSON, J. D., CARLIS, J. V. & HAASE, A. T. 2009. Glycerol monolaurate prevents mucosal SIV transmission. *Nature,* 458**,** 1034-8.

LI, Y., ZHANG, Q.-Y., SUN, B.-F., MA, Y., ZHANG, Y., WANG, M., MA, C., SHI, H., SUN, Z., CHEN, J., YANG, Y.-G. & ZHU, L. 2021. Single-cell transcriptome profiling of the vaginal wall in women with severe anterior vaginal prolapse. *Nat Commun,* 12**,** 87.

LIU, C. M., PRODGER, J. L., TOBIAN, A. A. R., ABRAHAM, A. G., KIGOZI, G., HUNGATE, B. A., AZIZ, M., NALUGODA, F., SARIYA, S., SERWADDA, D., KAUL, R., GRAY, R. H. & PRICE, L. B. 2017. Penile Anaerobic Dysbiosis as a Risk Factor for HIV Infection. *mBio,* 8**,** e00996-17.

LIU, X., SONG, W., WONG, B. Y., ZHANG, T., YU, S., LIN, G. N. & DING, X. 2019. A comparison framework and guideline of clustering methods for mass cytometry data. *Genome Biology,* 20**,** 297.

LIU, X., ZHU, R., LUO, Y., WANG, S., ZHAO, Y., QIU, Z., ZHANG, Y., LIU, X., YAO, X., LI, X. & LI, W. 2021. Distinct human Langerhans cell subsets orchestrate reciprocal functions and require different developmental regulation. *Immunity,* 54**,** 2305-2320.e11.

LIU, Y., WANG, R., JIANG, J., CAO, Z., ZHAI, F., SUN, W. & CHENG, X. 2018. A subset of CD1c(+) dendritic cells is increased in patients with tuberculosis and promotes Th17 cell polarization. *Tuberculosis (Edinb),* 113**,** 189-199.

LIU, Y., XU, L., DOU, Y. & HE, Y. 2025. AXL: shapers of tumor progression and immunosuppressive microenvironments. *Molecular Cancer,* 24**,** 11.

LUOMA, A. M., SUO, S., WILLIAMS, H. L., SHAROVA, T., SULLIVAN, K., MANOS,

M., BOWLING, P., HODI, F. S., RAHMA, O., SULLIVAN, R. J., BOLAND, G. M., NOWAK, J. A., DOUGAN, S. K., DOUGAN, M., YUAN, G. C. & WUCHERPFENNIG, K. W. 2020. Molecular Pathways of Colon Inflammation Induced by Cancer Immunotherapy. *Cell,* 182**,** 655-671 e22.

LYNCH, G. W., SLAYTOR, E. K., ELLIOTT, F. D., SAURAJEN, A., TURVILLE, S. G., SLOANE, A. J., CAMERON, P. U., CUNNINGHAM, A. L. & HALLIDAY, G. M. 2003. CD4 is expressed by epidermal Langerhans' cells predominantly as covalent dimers. *Exp Dermatol,* 12**,** 700-11.

MAIR, F., ERICKSON, J. R., FRUTOSO, M., KONECNY, A. J., GREENE, E., VOILLET, V., MAURICE, N. J., RONGVAUX, A., DIXON, D., BARBER, B., GOTTARDO, R. & PRLIC, M. 2022. Extricating human tumour immune alterations from tissue inflammation. *Nature,* 605**,** 728-735.

MAIR, F. & LIECHTI, T. 2021. Comprehensive Phenotyping of Human Dendritic Cells and Monocytes. *Cytometry A,* 99**,** 231-242.

MARTIN, J. C., CHANG, C., BOSCHETTI, G., UNGARO, R., GIRI, M., GROUT, J. A., GETTLER, K., CHUANG, L. S., NAYAR, S., GREENSTEIN, A. J., DUBINSKY, M., WALKER, L., LEADER, A., FINE, J. S., WHITEHURST, C. E., MBOW, M. L., KUGATHASAN, S., DENSON, L. A., HYAMS, J. S., FRIEDMAN, J. R., DESAI, P. T., KO, H. M., LAFACE, I., AKTURK, G., SCHADT, E. E., SALMON, H., GNJATIC, S., RAHMAN, A. H., MERAD, M., CHO, J. H. & KENIGSBERG, E. 2019. Single-Cell Analysis of Crohn's Disease Lesions Identifies a Pathogenic Cellular Module Associated with Resistance to Anti-TNF Therapy. *Cell,* 178**,** 1493-1508.e20.

MARZAIOLI, V., CANAVAN, M., FLOUDAS, A., FLYNN, K., MULLAN, R., VEALE, D. J. & FEARON, U. 2022. CD209/CD14+ Dendritic Cells Characterization in Rheumatoid and Psoriatic Arthritis Patients: Activation, Synovial Infiltration, and Therapeutic Targeting. *Frontiers in Immunology,* Volume 12 - 2021.

MASSON, L., ARNOLD, K. B., LITTLE, F., MLISANA, K., LEWIS, D. A., MKHIZE, N., GAMIELDIEN, H., NGCAPU, S., JOHNSON, L., LAUFFENBURGER, D. A., ABDOOL KARIM, Q., ABDOOL KARIM, S. S. & PASSMORE, J. A. 2016. Inflammatory cytokine biomarkers to identify women with asymptomatic sexually transmitted infections and bacterial vaginosis who are at high risk of HIV infection. *Sex Transm Infect,* 92**,** 186-93.

MASSON, L., MLISANA, K., LITTLE, F., WERNER, L., MKHIZE, N. N., RONACHER, K., GAMIELDIEN, H., WILLIAMSON, C., MCKINNON, L. R., WALZL, G., ABDOOL KARIM, Q., ABDOOL KARIM, S. S. & PASSMORE, J.-A. S. 2014. Defining genital tract cytokine signatures of sexually transmitted infections and bacterial vaginosis in women at high risk of HIV infection: a cross-sectional study. *Sex Transm Infect,* 90**,** 580.

MASSON, L., PASSMORE, J.-A. S., LIEBENBERG, L. J., WERNER, L., BAXTER, C., ARNOLD, K. B., WILLIAMSON, C., LITTLE, F., MANSOOR, L. E., NARANBHAI, V., LAUFFENBURGER, D. A., RONACHER, K., WALZL, G., GARRETT, N. J., WILLIAMS, B. L., COUTO-RODRIGUEZ, M., HORNIG, M., LIPKIN, W. I., GROBLER, A., ABDOOL KARIM, Q. & ABDOOL KARIM, S. S. 2015. Genital inflammation and the risk of HIV acquisition in women. *Infectious Diseases Society of America,* 61**,** 260-269.

MATSUI, M., MORIYA, O., YOSHIMOTO, T. & AKATSUKA, T. 2005. T-bet is required for protection against vaccinia virus infection. *J Virol,* 79**,** 12798-806.

MC DERMOTT, R., ZIYLAN, U., SPEHNER, D., BAUSINGER, H., LIPSKER, D., MOMMAAS, M., CAZENAVE, J. P., RAPOSO, G., GOUD, B., DE LA SALLE, H., SALAMERO, J. & HANAU, D. 2002. Birbeck granules are subdomains of endosomal recycling compartment in human epidermal Langerhans cells, which form where Langerin accumulates. *Mol Biol Cell,* 13**,** 317-35.

MCALEER, J. P. & KOLLS, J. K. 2011. Mechanisms controlling Th17 cytokine expression and host defense. *J Leukoc Biol,* 90**,** 263-70.

MCDONALD, D., WU, L., BOHKS, S. M., KEWALRAMANI, V. N., UNUTMAZ, D. & HOPE, T. J. 2003. Recruitment of HIV and its receptors to dendritic cell-T cell junctions. *Science,* 300**,** 1295-7.

MCGOVERN, N., SCHLITZER, A., GUNAWAN, M., JARDINE, L., SHIN, A., POYNER, E., GREEN, K., DICKINSON, R., WANG, X.-N., LOW, D., BEST, K., COVINS, S., MILNE, P., PAGAN, S., ALJEFRI, K., WINDEBANK, M., MIRANDA-SAAVEDRA, D., LARBI, A., WASAN, P. S., DUAN, K., POIDINGER, M., BIGLEY, V., GINHOUX, F., COLLIN, M. & HANIFFA, M. 2014. Human dermal $CD14^{+}$ cells are a transient population of monocyte-derived macrophages. *Immunity,* 41**,** 465-477.

MCKINNON, L. R., LIEBENBERG, L. J., YENDE-ZUMA, N., ARCHARY, D., NGCAPU, S., SIVRO, A., NAGELKERKE, N., GARCIA LERMA, J. G., KASHUBA, A. D., MASSON, L., MANSOOR, L. E., KARIM, Q. A., KARIM, S. S. A. & PASSMORE, J. S. 2018. Genital inflammation undermines the effectiveness of tenofovir gel in preventing HIV acquisition in women. *Nat Med,* 24**,** 491-496.

MENEZES, S., MELANDRI, D., ANSELMI, G., PERCHET, T., LOSCHKO, J., DUBROT, J., PATEL, R., GAUTIER, E. L., HUGUES, S., LONGHI, M. P., HENRY, J. Y., QUEZADA, S. A., LAUVAU, G., LENNON-DUMÉNIL, A. M., GUTIÉRREZ-MARTÍNEZ, E., BESSIS, A., GOMEZ-PERDIGUERO, E., JACOME-GALARZA, C. E., GARNER, H., GEISSMANN, F., GOLUB, R., NUSSENZWEIG, M. C. & GUERMONPREZ, P. 2016. The Heterogeneity of Ly6C(hi) Monocytes Controls Their Differentiation into iNOS(+) Macrophages or Monocyte-Derived Dendritic Cells. *Immunity,* 45**,** 1205-1218.

MICHALOW, J., HALL, L., ROWLEY, J., ANDERSON, R. L., HAYRE, Q., CHICO, R. M., EDUN, O., KNIGHT, J., KUCHUKHIDZE, S., MAJAYA, E., REED, D. M., STEVENS, O., WALTERS, M. K., PETERS, R. P. H., CORI, A., BOILY, M.-C. & IMAI-EATON, J. W. 2025. Prevalence of chlamydia, gonorrhoea, and trichomoniasis among male and female general populations in sub-Saharan Africa from 2000 to 2024: a systematic review and meta-regression analysis. *eClinicalMedicine,* 83**,** 103210.

MICHEA, P., NOËL, F., ZAKINE, E., CZERWINSKA, U., SIRVEN, P., ABOUZID, O., GOUDOT, C., SCHOLER-DAHIREL, A., VINCENT-SALOMON, A., REYAL, F., AMIGORENA, S., GUILLOT-DELOST, M., SEGURA, E. & SOUMELIS, V. 2018. Adjustment of dendritic cells to the breast-cancer microenvironment is subset specific. *Nat Immunol,* 19**,** 885-897.

MLISANA, K., NAICKER, N., WERNER, L., ROBERTS, L., VAN LOGGERENBERG,

F., BAXTER, C., PASSMORE, J. A., GROBLER, A. C., STURM, A. W., WILLIAMSON, C., RONACHER, K., WALZL, G. & ABDOOL KARIM, S. S. 2012. Symptomatic vaginal discharge is a poor predictor of sexually transmitted infections and genital tract inflammation in high-risk women in South Africa. *J Infect Dis,* 206**,** 6-14.

MULDER, K., PATEL, A. A., KONG, W. T., PIOT, C., HALITZKI, E., DUNSMORE, G., KHALILNEZHAD, S., IRAC, S. E., DUBUISSON, A., CHEVRIER, M., ZHANG, X. M., TAM, J. K. C., LIM, T. K. H., WONG, R. M. M., PAI, R., KHALIL, A. I. S., CHOW, P. K. H., WU, S. Z., AL-ERYANI, G., RODEN, D., SWARBRICK, A., CHAN, J. K. Y., ALBANI, S., DEROSA, L., ZITVOGEL, L., SHARMA, A., CHEN, J., SILVIN, A., BERTOLETTI, A., BLÉRIOT, C., DUTERTRE, C. A. & GINHOUX, F. 2021. Cross-tissue single-cell landscape of human monocytes and macrophages in health and disease. *Immunity,* 54**,** 1883-1900.e5.

MURPHY, B., HOPTROFF, M., ARNOLD, D., CAWLEY, A., SMITH, E., ADAMS, S. E., MITCHELL, A., HORSBURGH, M. J., HUNT, J., DASGUPTA, B., GHATLIA, N., SAMARAS, S., MACGUIRE-FLANAGAN, A. & SHARMA, K. 2023. Compositional Variations between Adult and Infant Skin Microbiome: An Update. *Microorganisms,* 11.

NAIK, S. H., SATHE, P., PARK, H. Y., METCALF, D., PROIETTO, A. I., DAKIC, A., CAROTTA, S., O'KEEFFE, M., BAHLO, M., PAPENFUSS, A., KWAK, J. Y., WU, L. & SHORTMAN, K. 2007. Development of plasmacytoid and conventional dendritic cell subtypes from single precursor cells derived in vitro and in vivo. *Nat Immunol,* 8**,** 1217-26.

NAKAMIZO, S., DUTERTRE, C. A., KHALILNEZHAD, A., ZHANG, X. M., LIM, S., LUM, J., KOH, G., FOONG, C., YONG, P. J. A., TAN, K. J., SATO, R., TOMARI, K., YVAN-CHARVET, L., HE, H., GUTTMAN-YASSKY, E., MALLERET, B., SHIBUYA, R., IWATA, M., JANELA, B., GOTO, T., LUCINDA, T. S., TANG, M. B. Y., THENG, C., JULIA, V., HACINI-RACHINEL, F., KABASHIMA, K. & GINHOUX, F. 2021. Single-cell analysis of human skin identifies CD14+ type 3 dendritic cells co-producing IL1B and IL23A in psoriasis. *J Exp Med,* 218.

NAKANO, H., MORAN, T. P., NAKANO, K., GERRISH, K. E., BORTNER, C. D. & COOK, D. N. 2015. Complement receptor C5aR1/CD88 and dipeptidyl peptidase-4/CD26 define distinct hematopoietic lineages of dendritic cells. *J Immunol,* 194**,** 3808-19.

NASR, N., LAI, J., BOTTING, R. A., MERCIER, S. K., HARMAN, A. N., KIM, M., TURVILLE, S., CENTER, R. J., DOMAGALA, T., GORRY, P. R., OLBOURNE, N. & CUNNINGHAM, A. L. 2014. Inhibition of two temporal phases of HIV-1 transfer from primary Langerhans cells to T cells: the role of langerin. *J Immunol,* 193**,** 2554-64.

NASR, N., MADDOCKS, S., TURVILLE, S. G., HARMAN, A. N., WOOLGER, N., HELBIG, K. J., WILKINSON, J., BYE, C. R., WRIGHT, T. K., RAMBUKWELLE, D., DONAGHY, H., BEARD, M. R. & CUNNINGHAM, A. L. 2012. HIV-1 infection of human macrophages directly induces viperin which inhibits viral production. *Blood,* 120**,** 778-88.

NELSON, S. G. & LIU, C. M. 2024. Penile microbiome: decoding its impact on HIV risk. *Current Opinion in HIV and AIDS,* 19**,** 241-245.

NEURATH, M. F., WEIGMANN, B., FINOTTO, S., GLICKMAN, J., NIEUWENHUIS, E., IIJIMA, H., MIZOGUCHI, A., MIZOGUCHI, E., MUDTER, J., GALLE, P. R., BHAN, A., AUTSCHBACH, F., SULLIVAN, B. M., SZABO, S. J., GLIMCHER, L. H. & BLUMBERG, R. S. 2002. The transcription factor T-bet regulates mucosal T cell activation in experimental colitis and Crohn's disease. *J Exp Med,* 195**,** 1129-43.

NJOROGE, J. M., MITCHELL, L. B., CENTOLA, M., KASTNER, D., RAFFELD, M. & MILLER, J. L. 2001. Characterization of viable autofluorescent macrophages among cultured peripheral blood mononuclear cells. *Cytometry,* 44**,** 38-44.

NOVAK, N., VALENTA, R., BOHLE, B., LAFFER, S., HABERSTOK, J., KRAFT, S. & BIEBER, T. 2004. FcepsilonRI engagement of Langerhans cell-like dendritic cells and inflammatory dendritic epidermal cell-like dendritic cells induces chemotactic signals and different T-cell phenotypes in vitro. *J Allergy Clin Immunol,* 113**,** 949-57.

O'DOHERTY, U., PENG, M., GEZELTER, S., SWIGGARD, W. J., BETJES, M., BHARDWAJ, N. & STEINMAN, R. M. 1994. Human blood contains two subsets of dendritic cells, one immunologically mature and the other immature. *Immunology,* 82**,** 487-93.

O'NEIL, T. R., HARMAN, A. N., CUNNINGHAM, A. L., NASR, N. & BERTRAM, K. M. 2023. OMIP-096: A 24-color flow cytometry panel to identify and characterize CD4+ and CD8+ tissue-resident T cells in human skin, intestinal, and type II mucosal tissue. *Cytometry A,* 103**,** 851-856.

O'NEIL, T. R., HU, K., TRUONG, N. R., ARSHAD, S., SHACKLETT, B. L., CUNNINGHAM, A. L. & NASR, N. 2021. The Role of Tissue Resident Memory CD4 T Cells in Herpes Simplex Viral and HIV Infection. *Viruses,* 13.

ODELL, I. D. 2024. Cross-tissue organization of myeloid cells in scleroderma and related fibrotic diseases. *Curr Opin Rheumatol*.

OHL, L., MOHAUPT, M., CZELOTH, N., HINTZEN, G., KIAFARD, Z., ZWIRNER, J., BLANKENSTEIN, T., HENNING, G. & FÖRSTER, R. 2004. CCR7 Governs Skin Dendritic Cell Migration under Inflammatory and Steady-State Conditions. *Immunity,* 21**,** 279-288.

ONAI, N., KURABAYASHI, K., HOSOI-AMAIKE, M., TOYAMA-SORIMACHI, N., MATSUSHIMA, K., INABA, K. & OHTEKI, T. 2013. A clonogenic progenitor with prominent plasmacytoid dendritic cell developmental potential. *Immunity,* 38**,** 943-57.

ONODI, F., BONNET-MADIN, L., MEERTENS, L., KARPF, L., POIROT, J., ZHANG, S. Y., PICARD, C., PUEL, A., JOUANGUY, E., ZHANG, Q., LE GOFF, J., MOLINA, J. M., DELAUGERRE, C., CASANOVA, J. L., AMARA, A. & SOUMELIS, V. 2021. SARS-CoV-2 induces human plasmacytoid predendritic cell diversification via UNC93B and IRAK4. *J Exp Med,* 218.

OUYANG, Q., EL-YOUSSEF, M., YEN-LIEBERMAN, B., SAPATNEKAR, W., YOUNGMAN, K. R., KUSUGAMI, K. & FIOCCHI, C. 1988. Expression of HLA-DR antigens in inflammatory bowel disease mucosa: Role of intestinal lamina propria mononuclear cell-derived interferon γ. *Digestive Diseases and Sciences,* 33**,** 1528-1536.

PAPARINI, D. E., GRASSO, E., AGUILERA, F., ARSLANIAN, M. A., LELLA, V.,

LARA, B., SCHAFIR, A., GORI, S., MERECH, F., HAUK, V., SCHUSTER, C., MARTÍ, M., MELLER, C., RAMHORST, R., VOTA, D. & LEIRÓS, C. P. 2024. Sex-specific phenotypical, functional and metabolic profiles of human term placenta macrophages. *Biology of Sex Differences,* 15**,** 80.

PARTHASARATHY, S., MORENO DE LARA, L., CARRILLO-SALINAS, F. J., WERNER, A., BORCHERS, A., IYER, V., VOGELL, A., FORTIER, J. M., WIRA, C. R. & RODRIGUEZ-GARCIA, M. 2024. Human genital dendritic cell heterogeneity confers differential rapid response to HIV-1 exposure. *Frontiers in Immunology,* 15.

PASSMORE, J. A., JASPAN, H. B. & MASSON, L. 2016. Genital inflammation, immune activation and risk of sexual HIV acquisition. *Curr Opin HIV AIDS,* 11**,** 156-62.

PEDERSEN, C. B., DAM, S. H., BARNKOB, M. B., LEIPOLD, M. D., PURROY, N., RASSENTI, L. Z., KIPPS, T. J., NGUYEN, J., LEDERER, J. A., GOHIL, S. H., WU, C. J. & OLSEN, L. R. 2022. cyCombine allows for robust integration of single-cell cytometry datasets within and across technologies. *Nature Communications,* 13**,** 1698.

PELKA, K., HOFREE, M., CHEN, J. H., SARKIZOVA, S., PIRL, J. D., JORGJI, V., BEJNOOD, A., DIONNE, D., GE, W. H., XU, K. H., CHAO, S. X., ZOLLINGER, D. R., LIEB, D. J., REEVES, J. W., FUHRMAN, C. A., HOANG, M. L., DELOREY, T., NGUYEN, L. T., WALDMAN, J., KLAPHOLZ, M., WAKIRO, I., COHEN, O., ALBERS, J., SMILLIE, C. S., CUOCO, M. S., WU, J., SU, M. J., YEUNG, J., VIJAYKUMAR, B., MAGNUSON, A. M., ASINOVSKI, N., MOLL, T., GODER-REISER, M. N., APPLEBAUM, A. S., BRAIS, L. K., DELLOSTRITTO, L. K., DENNING, S. L., PHILLIPS, S. T., HILL, E. K., MEEHAN, J. K., FREDERICK, D. T., SHAROVA, T., KANODIA, A., TODRES, E. Z., JANE-VALBUENA, J., BITON, M., IZAR, B., LAMBDEN, C. D., CLANCY, T. E., BLEDAY, R., MELNITCHOUK, N., IRANI, J., KUNITAKE, H., BERGER, D. L., SRIVASTAVA, A., HORNICK, J. L., OGINO, S., ROTEM, A., VIGNEAU, S., JOHNSON, B. E., CORCORAN, R. B., SHARPE, A. H., KUCHROO, V. K., NG, K., GIANNAKIS, M., NIEMAN, L. T., BOLAND, G. M., AGUIRRE, A. J., ANDERSON, A. C., ROZENBLATT-ROSEN, O., REGEV, A. & HACOHEN, N. 2021. Spatially organized multicellular immune hubs in human colorectal cancer. *Cell,* 184**,** 4734-4752 e20.

PENA-CRUZ, V., AGOSTO, L. M., AKIYAMA, H., OLSON, A., MOREAU, Y., LARRIEUX, J. R., HENDERSON, A., GUMMULURU, S. & SAGAR, M. 2018. HIV-1 replicates and persists in vaginal epithelial dendritic cells. *J Clin Invest,* 128**,** 3439-3444.

PEREZ-ZSOLT, D., CANTERO-PÉREZ, J., ERKIZIA, I., BENET, S., PINO, M., SERRA-PEINADO, C., HERNÁNDEZ-GALLEGO, A., CASTELLVÍ, J., TAPIA, G., ARNAU-SAZ, V., GARRIDO, J., TARRATS, A., BUZÓN, M. J., MARTINEZ-PICADO, J., IZQUIERDO-USEROS, N. & GENESCÀ, M. 2019. Dendritic Cells From the Cervical Mucosa Capture and Transfer HIV-1 via Siglec-1. *Front Immunol,* 10**,** 825.

PINO, M., ERKIZIA, I., BENET, S., ERIKSON, E., FERNÁNDEZ-FIGUERAS, M. T., GUERRERO, D., DALMAU, J., OUCHI, D., RAUSELL, A., CIUFFI, A., KEPPLER, O. T., TELENTI, A., KRÄUSSLICH, H. G., MARTINEZ-PICADO, J.

& IZQUIERDO-USEROS, N. 2015. HIV-1 immune activation induces Siglec-1 expression and enhances viral trans-infection in blood and tissue myeloid cells. *Retrovirology,* 12**,** 37.

PINSON, K., MELBER, D. J., NGUYEN, N.-H., MONTANEY, L., BASU, R., MIMS, J., PRETORIUS, D. & LAMALE-SMITH, L. 2023. The Development of Normal Fetal External Genitalia Throughout Gestation. *Journal of Ultrasound in Medicine,* 42**,** 293-307.

PODOLSKA, M. J., GRÜTZMANN, R., PILARSKY, C. & BÉNARD, A. 2024. IL-3: key orchestrator of inflammation. *Frontiers in Immunology,* Volume 15 - 2024.

PRODGER, J. L., ABRAHAM, A. G., TOBIAN, A. A. R., PARK, D. E., AZIZ, M., ROACH, K., GRAY, R. H., BUCHANAN, L., KIGOZI, G., GALIWANGO, R. M., SSEKASANVU, J., NNAMUTETE, J., KAGAAYI, J., KAUL, R. & LIU, C. M. 2021. Penile bacteria associated with HIV seroconversion, inflammation, and immune cells. *JCI Insight,* 6.

PUGIN, J., HEUMANN, D., TOMASZ, A., KRAVCHENKO, V. V., AKAMATSU, Y., NISHIJIMA, M., GLAUSER, M. P., TOBIAS, P. S. & ULEVITCH, R. J. 1994. CD14 is a pattern recognition receptor. *Immunity,* 1**,** 509-516.

PURYEAR, W. B., AKIYAMA, H., GEER, S. D., RAMIREZ, N. P., YU, X., REINHARD, B. M. & GUMMULURU, S. 2013. Interferon-inducible mechanism of dendritic cell-mediated HIV-1 dissemination is dependent on Siglec-1/CD169. *PLoS Pathog,* 9**,** e1003291.

QIN, Q., ZHENG, X. Y., WANG, Y. Y., SHEN, H. F., SUN, F. & DING, W. 2009. Langerhans' cell density and degree of keratinization in foreskins of Chinese preschool boys and adults. *Int Urol Nephrol,* 41**,** 747-53.

QIN, Y., LI, Y. Y., JIANG, A. P., JIANG, J. F. & WANG, J. H. 2012. Stimulation of Cryptococcus neoformans isolated from skin lesion of AIDS patient matures dendritic cells and promotes HIV-1 trans-infection. *Biochem Biophys Res Commun,* 423**,** 709-14.

QIU, G., ZHONG, S., XIE, J., FENG, H., SUN, S., GAO, C., XU, X., KANG, B., XU, H., ZHAO, C., RAN, L., XINYU, A., XU, B., MENG, X., MENG, L., ZHANG, X. & XIAO, L. 2022. Expanded CD1c(+)CD163(+) DC3 Population in Synovial Tissues Is Associated with Disease Progression of Osteoarthritis. *J Immunol Res,* 2022**,** 9634073.

RANA, H., TRUONG, N. R., JOHNSON, B., BAHARLOU, H., HERBERT, J. J., KANDASAMY, S., GODDARD, R., COHEN, R. C., WINES, M., NASR, N., HARMAN, A. N., BERTRAM, K. M., SANDGREN, K. J. & CUNNINGHAM, A. L. 2024. Herpes simplex virus spreads rapidly in human foreskin, partly driven by chemokine-induced redistribution of Nectin-1 on keratinocytes. *PLoS Pathog,* 20**,** e1012267.

REIZIS, B., IDOYAGA, J., DALOD, M., BARRAT, F., NAIK, S., TRINCHIERI, G., TUSSIWAND, R., CELLA, M. & COLONNA, M. 2023. Reclassification of plasmacytoid dendritic cells as innate lymphocytes is premature. *Nat Rev Immunol,* 23**,** 336-337.

RETTEW, J. A., HUET, Y. M. & MARRIOTT, I. 2009. Estrogens Augment Cell Surface TLR4 Expression on Murine Macrophages and Regulate Sepsis Susceptibility in Vivo. *Endocrinology,* 150**,** 3877-3884.

REYNOLDS, G., VEGH, P., FLETCHER, J., POYNER, E. F. M., STEPHENSON, E., GOH, I., BOTTING, R. A., HUANG, N., OLABI, B., DUBOIS, A., DIXON, D., GREEN, K., MAUNDER, D., ENGELBERT, J., EFREMOVA, M., POLAŃSKI, K., JARDINE, L., JONES, C., NESS, T., HORSFALL, D., MCGRATH, J., CAREY, C., POPESCU, D. M., WEBB, S., WANG, X. N., SAYER, B., PARK, J. E., NEGRI, V. A., BELOKHVOSTOVA, D., LYNCH, M. D., MCDONALD, D., FILBY, A., HAGAI, T., MEYER, K. B., HUSAIN, A., COXHEAD, J., VENTO-TORMO, R., BEHJATI, S., LISGO, S., VILLANI, A. C., BACARDIT, J., JONES, P. H., O'TOOLE, E. A., OGG, G. S., RAJAN, N., REYNOLDS, N. J., TEICHMANN, S. A., WATT, F. M. & HANIFFA, M. 2021. Developmental cell programs are co-opted in inflammatory skin disease. *Science,* 371.

RHODES, J. W. 2020. *Investigating Mononuclear Phagocytes in Human Anogenital and Colorectal Tissues: Their Role in the Sexual Transmission of HIV.* Doctor of Philosophy, The University of Sydney.

RHODES, J. W., BOTTING, R. A., BERTRAM, K. M., VINE, E. E., RANA, H., BAHARLOU, H., VEGH, P., O'NEIL, T. R., ASHHURST, A. S., FLETCHER, J., PARNELL, G. P., GRAHAM, J. D., NASR, N., LIM, J. J. K., BARNOUTI, L., HAERTSCH, P., GOSSELINK, M. P., DI RE, A., REZA, F., CTERCTEKO, G., JENKINS, G. J., BROOKS, A. J., PATRICK, E., BYRNE, S. N., HUNTER, E., HANIFFA, M. A., CUNNINGHAM, A. L. & HARMAN, A. N. 2021. Human anogenital monocyte-derived dendritic cells and langerin+cDC2 are major HIV target cells. *Nat Commun,* 12**,** 2147.

RHODES, J. W., TONG, O., HARMAN, A. N. & TURVILLE, S. G. 2019. Human Dendritic Cell Subsets, Ontogeny, and Impact on HIV Infection. *Front Immunol,* 10**,** 1088-1088.

RICHTER, L., LANDSVERK, O. J. B., ATLASY, N., BUJKO, A., YAQUB, S., HORNELAND, R., ØYEN, O., AANDAHL, E. M., LUNDIN, K. E. A., STUNNENBERG, H. G., BÆKKEVOLD, E. S. & JAHNSEN, F. L. 2018. Transcriptional profiling reveals monocyte-related macrophages phenotypically resembling DC in human intestine. *Mucosal Immunology,* 11**,** 1512-1523.

RODRIGUEZ-GARCIA, M., BARR, F. D., CRIST, S. G., FAHEY, J. V. & WIRA, C. R. 2014. Phenotype and susceptibility to HIV infection of CD4+ Th17 cells in the human female reproductive tract. *Mucosal Immunology,* 7**,** 1375-1385.

RUFFIN, N., GEA-MALLORQUÍ, E., BROUILLER, F., JOUVE, M., SILVIN, A., SEE, P., DUTERTRE, C.-A., GINHOUX, F. & BENAROCH, P. 2019. Constitutive Siglec-1 expression confers susceptibility to HIV-1 infection of human dendritic cell precursors. *PNAS,* 116**,** 21685-21693.

SAADEH, D., KURBAN, M. & ABBAS, O. 2016. Update on the role of plasmacytoid dendritic cells in inflammatory/autoimmune skin diseases. *Experimental Dermatology,* 25**,** 415-421.

SAID, A. & WEINDL, G. 2015. Regulation of Dendritic Cell Function in Inflammation. *J Immunol Res,* 2015**,** 743169.

SALLUSTO, F. & LANZAVECCHIA, A. 1994. Efficient presentation of soluble antigen by cultured human dendritic cells is maintained by granulocyte/macrophage colony-stimulating factor plus interleukin 4 and downregulated by tumor necrosis factor alpha. *J Exp Med,* 179**,** 1109-18.

SALVADÉ, V., MANUEL, O., GOLSHAYAN, D. & OBREGON, C. 2024. Monocyte-derived dendritic cells can be detected in urine of kidney transplant recipients with pathogenic asymptomatic bacteriuria. *Front Transplant,* 3**,** 1366104.

SANDLER, N. G., BOSINGER, S. E., ESTES, J. D., ZHU, R. T., THARP, G. K., BORITZ, E., LEVIN, D., WIJEYESINGHE, S., MAKAMDOP, K. N., DEL PRETE, G. Q., HILL, B. J., TIMMER, J. K., REISS, E., YARDEN, G., DARKO, S., CONTIJOCH, E., TODD, J. P., SILVESTRI, G., NASON, M., NORGREN, R. B., JR., KEELE, B. F., RAO, S., LANGER, J. A., LIFSON, J. D., SCHREIBER, G. & DOUEK, D. C. 2014. Type I interferon responses in rhesus macaques prevent SIV infection and slow disease progression. *Nature,* 511**,** 601-5.

SANTEGOETS, S. J., DUURLAND, C. L., JORDANOVA, E. J., VAN HAM, V. J., EHSAN, I., LOOF, N. M., NARANG, V., DUTERTRE, C. A., GINHOUX, F., VAN EGMOND, S. L., M, J. P. W. & VAN DER BURG, S. H. 2020. CD163(+) cytokine-producing cDC2 stimulate intratumoral type 1 T cell responses in HPV16-induced oropharyngeal cancer. *J Immunother Cancer,* 8.

SCANDELLA, E., MEN, Y., GILLESSEN, S., FÖRSTER, R. & GROETTRUP, M. 2002. Prostaglandin E2 is a key factor for CCR7 surface expression and migration of monocyte-derived dendritic cells. *Blood,* 100**,** 1354-1361.

SCARLATTI, G., TRESOLDI, E., BJÖRNDAL, A., FREDRIKSSON, R., COLOGNESI, C., DENG, H. K., MALNATI, M. S., PLEBANI, A., SICCARDI, A. G., LITTMAN, D. R., FENYÖ, E. M. & LUSSO, P. 1997. In vivo evolution of HIV-1 co-receptor usage and sensitivity to chemokine-mediated suppression. *Nat Med,* 3**,** 1259-65.

SEE, P., DUTERTRE, C.-A., CHEN, J., GÜNTHER, P., MCGOVERN, N., IRAC, S. E., GUNAWAN, M., BEYER, M., HÄNDLER, K., DUAN, K., SUMATOH, H. R. B., RUFFIN, N., JOUVE, M., GEA-MALLORQUÍ, E., HENNEKAM, R. C. M., LIM, T., YIP, C. C., WEN, M., MALLERET, B., LOW, I., SHADAN, N. B., FEN, C. F. S., TAY, A., LUM, J., ZOLEZZI, F., LARBI, A., POIDINGER, M., CHAN, J. K. Y., CHEN, Q., RÉNIA, L., HANIFFA, M., BENAROCH, P., SCHLITZER, A., SCHULTZE, J. L., NEWELL, E. W. & GINHOUX, F. 2017. Mapping the human DC lineage through the integration of high-dimensional techniques. *Science,* 356**,** eaag3009.

SEGURA, E. 2022. Human dendritic cell subsets: An updated view of their ontogeny and functional specialization. *Eur J Immunol,* 52**,** 1759-1767.

SEGURA, E., TOUZOT, M., BOHINEUST, A., CAPPUCCIO, A., CHIOCCHIA, G., HOSMALIN, A., DALOD, M., SOUMELIS, V. & AMIGORENA, S. 2013. Human inflammatory dendritic cells induce Th17 cell differentiation. *Immunity,* 38**,** 336-48.

SERÉ, K., BAEK, J.-H., OBER-BLÖBAUM, J., MÜLLER-NEWEN, G., TACKE, F., YOKOTA, Y., ZENKE, M. & HIERONYMUS, T. 2012. Two Distinct Types of Langerhans Cells Populate the Skin during Steady State and Inflammation. *Immunity,* 37**,** 905-916.

SHANG, L., DUAN, L., PERKEY, K. E., WIETGREFE, S., ZUPANCIC, M., SMITH, A. J., SOUTHERN, P. J., JOHNSON, R. P. & HAASE, A. T. 2017. Epithelium-innate immune cell axis in mucosal responses to SIV. *Mucosal Immunol,* 10**,** 508-519.

SHI, H., HE, H., SUN, C., FU, J., GHOSH, D., DENG, C. & SHENG, Y. 2020. Association of toll-like receptor polymorphisms with acquisition of HIV infection and clinical findings: A protocol for systematic review and meta-analysis. *Medicine (Baltimore),* 99**,** e23663.

SHIMIZU, K., LIBBY, P., ROCHA, V. Z., FOLCO, E. J., SHUBIKI, R., GRABIE, N., JANG, S., LICHTMAN, A. H., SHIMIZU, A., HOGG, N., SIMON, D. I., MITCHELL, R. N. & CROCE, K. 2011. Loss of myeloid related protein-8/14 exacerbates cardiac allograft rejection. *Circulation,* 124**,** 2920-32.

SICILIA, G., VITALE, S. G., D'ALTERIO, M. N., SAPONARA, S., SCICCHITANO, F., FULGHESU, A. M., NAPPI, R. E. & ANGIONI, S. 2025. The Role of Vaginal Oestrogen Therapy in Postmenopausal Women With Pelvic Organ Prolapse: Does It Have Any Impact on Perioperative Outcomes? A Systematic Review of Randomised Controlled Trials. *BJOG: An International Journal of Obstetrics & Gynaecology,* n/a.

SIEGAL, F. P., KADOWAKI, N., SHODELL, M., FITZGERALD-BOCARSLY, P. A., SHAH, K., HO, S., ANTONENKO, S. & LIU, Y. J. 1999. The nature of the principal type 1 interferon-producing cells in human blood. *Science,* 284**,** 1835-7.

SILVIN, A., YU, C. I., LAHAYE, X., IMPERATORE, F., BRAULT, J.-B., CARDINAUD, S., BECKER, C., KWAN, W.-H., CONRAD, C., MAURIN, M., GOUDOT, C., MARQUES-LADEIRA, S., WANG, Y., PASCUAL, V., ANGUIANO, E., ALBRECHT, R. A., IANNACONE, M., GARCÍA-SASTRE, A., GOUD, B., DALOD, M., MORIS, A., MERAD, M., PALUCKA, A. K. & MANEL, N. 2017. Constitutive resistance to viral infection in human CD141+ dendritic cells. *Sci Immunol,* 2**,** eaai8071.

SINGH, T. P., ZHANG, H. H., BOREK, I., WOLF, P., HEDRICK, M. N., SINGH, S. P., KELSALL, B. L., CLAUSEN, B. E. & FARBER, J. M. 2016. Monocyte-derived inflammatory Langerhans cells and dermal dendritic cells mediate psoriasis-like inflammation. *Nat Commun,* 7**,** 13581.

SMILLIE, C. S., BITON, M., ORDOVAS-MONTANES, J., SULLIVAN, K. M., BURGIN, G., GRAHAM, D. B., HERBST, R. H., ROGEL, N., SLYPER, M., WALDMAN, J., SUD, M., ANDREWS, E., VELONIAS, G., HABER, A. L., JAGADEESH, K., VICKOVIC, S., YAO, J., STEVENS, C., DIONNE, D., NGUYEN, L. T., VILLANI, A. C., HOFREE, M., CREASEY, E. A., HUANG, H., ROZENBLATT-ROSEN, O., GARBER, J. J., KHALILI, H., DESCH, A. N., DALY, M. J., ANANTHAKRISHNAN, A. N., SHALEK, A. K., XAVIER, R. J. & REGEV, A. 2019. Intra- and Inter-cellular Rewiring of the Human Colon during Ulcerative Colitis. *Cell,* 178**,** 714-730 e22.

SOKOL, C. L. & LUSTER, A. D. 2015. The chemokine system in innate immunity. *Cold Spring Harb Perspect Biol,* 7.

SOSA CUEVAS, E., BENDRISS-VERMARE, N., MOURET, S., DE FRAIPONT, F., CHARLES, J., VALLADEAU-GUILEMOND, J., CHAPEROT, L. & ASPORD, C. 2022. Diversification of circulating and tumor-infiltrating plasmacytoid DCs towards the P3 (CD80(+) PDL1(-))-pDC subset negatively correlated with clinical outcomes in melanoma patients. *Clin Transl Immunology,* 11**,** e1382.

SOURISSEAU, M., SOL-FOULON, N., PORROT, F., BLANCHET, F. & SCHWARTZ,

O. 2007. Inefficient human immunodeficiency virus replication in mobile lymphocytes. *J Virol,* 81**,** 1000-12.

STANNAH, J., SILHOL, R., ELMES, J., OWEN, B., SHACKLETT, B. L., ANTON, P., MCGOWAN, I., VAN DER STRATEN, A., DIMITROV, D., BAGGALEY, R. F. & BOILY, M.-C. 2020. Increases in HIV Incidence Following Receptive Anal Intercourse Among Women: A Systematic Review and Meta-analysis. *AIDS Behav,* 24**,** 667-681.

STEWART, A., NG, J. C., WALLIS, G., TSIOLIGKA, V., FRATERNALI, F. & DUNN-WALTERS, D. K. 2021. Single-Cell Transcriptomic Analyses Define Distinct Peripheral B Cell Subsets and Discrete Development Pathways. *Front Immunol,* 12**,** 602539.

SUBTIL, B., VAN DER HOORN, I. A. E., CUENCA-ESCALONA, J., BECKER, A. M. D., ALVAREZ-BEGUE, M., IYER, K. K., JANSSEN, J., VAN OORSCHOT, T., POEL, D., GORRIS, M. A. J., VAN DEN DRIES, K., CAMBI, A., TAURIELLO, D. V. F. & DE VRIES, I. J. M. 2024. cDC2 plasticity and acquisition of a DC3-like phenotype mediated by IL-6 and PGE2 in a patient-derived colorectal cancer organoids model. *Eur J Immunol,* 54**,** e2350891.

SUNG, P. S. & HSIEH, S. L. 2019. CLEC2 and CLEC5A: Pathogenic Host Factors in Acute Viral Infections. *Front Immunol,* 10**,** 2867.

SUTTER, K., DICKOW, J. & DITTMER, U. 2018. Interferon alpha subtypes in HIV infection. *Cytokine Growth Factor Rev,* 40**,** 13-18.

TAKAGI, H., FUKAYA, T., EIZUMI, K., SATO, Y., SATO, K., SHIBAZAKI, A., OTSUKA, H., HIJIKATA, A., WATANABE, T., OHARA, O., KAISHO, T., MALISSEN, B. & SATO, K. 2011. Plasmacytoid Dendritic Cells Are Crucial for the Initiation of Inflammation and T Cell Immunity In Vivo. *Immunity,* 35**,** 958-971.

TAMOUTOUNOUR, S., GUILLIAMS, M., MONTANANA SANCHIS, F., LIU, H., TERHORST, D., MALOSSE, C., POLLET, E., ARDOUIN, L., LUCHE, H., SANCHEZ, C., DALOD, M., MALISSEN, B. & HENRI, S. 2013. Origins and Functional Specialization of Macrophages and of Conventional and Monocyte-Derived Dendritic Cells in Mouse Skin. *Immunity,* 39**,** 925-938.

TANG-HUAU, T.-L., GUEGUEN, P., GOUDOT, C., DURAND, M., BOHEC, M., BAULANDE, S., PASQUIER, B., AMIGORENA, S. & SEGURA, E. 2018. Human in vivo-generated monocyte-derived dendritic cells and macrophages cross-present antigens through a vacuolar pathway. *Nat Commun,* 9**,** 2570-2570.

TONG, O., DUETTE, G., O'NEIL, T. R., ROYLE, C. M., RANA, H., JOHNSON, B., POPOVIC, N., DERVISH, S., BROUWER, M. A. E., BAHARLOU, H., PATRICK, E., CTERCTEKO, G., PALMER, S., LEE, E., HUNTER, E., HARMAN, A. N., CUNNINGHAM, A. L. & NASR, N. 2021. Plasmacytoid dendritic cells have divergent effects on HIV infection of initial target cells and induce a pro-retention phenotype. *PLoS Pathog,* 17**,** e1009522.

TOSIEK, M. J., GROESSER, K., PEKCEC, A., ZWIREK, M., MURUGESAN, G. & BORGES, E. 2022. Activation of the Innate Immune Checkpoint CLEC5A on Myeloid Cells in the Absence of Danger Signals Modulates Macrophages' Function but Does Not Trigger the Adaptive T Cell Immune Response. *J*

Immunol Res, 2022**,** 9926305.

TSAI, A., IRRINKI, A., KAUR, J., CIHLAR, T., KUKOLJ, G., SLOAN, D. D. & MURRY, J. P. 2017. Toll-Like Receptor 7 Agonist GS-9620 Induces HIV Expression and HIV-Specific Immunity in Cells from HIV-Infected Individuals on Suppressive Antiretroviral Therapy. *J Virol,* 91.

TSCHACHLER, E., GROH, V., POPOVIC, M., MANN, D. L., KONRAD, K., SAFAI, B., ERON, L., DIMARZO VERONESE, F., WOLFF, K. & STINGL, G. 1987. Epidermal Langerhans cells--a target for HTLV-III/LAV infection. *J Invest Dermatol,* 88**,** 233-7.

TURVILLE, S. G., CAMERON, P. U., HANDLEY, A., LIN, G., PÖHLMANN, S., DOMS, R. W. & CUNNINGHAM, A. L. 2002. Diversity of receptors binding HIV on dendritic cell subsets. *Nat Immunol,* 3**,** 975-83.

TURVILLE, S. G., SANTOS, J. J., FRANK, I., CAMERON, P. U., WILKINSON, J., MIRANDA-SAKSENA, M., DABLE, J., STÖSSEL, H., ROMANI, N., PIATAK, M., JR., LIFSON, J. D., POPE, M. & CUNNINGHAM, A. L. 2004. Immunodeficiency virus uptake, turnover, and 2-phase transfer in human dendritic cells. *Blood,* 103**,** 2170-9.

TYSSEN, D., WANG, Y. Y., HAYWARD, J. A., AGIUS, P. A., DELONG, K., ALDUNATE, M., RAVEL, J., MOENCH, T. R., CONE, R. A. & TACHEDJIAN, G. 2018. Anti-HIV-1 Activity of Lactic Acid in Human Cervicovaginal Fluid. *mSphere,* 3.

UNAIDS 2024. FACT SHEET 2024 Global HIV statistics.

UNAIDS 2025. Global HIV & AIDS statistics — Fact sheet

UNICEF 2024. Global Snapshot on HIV and AIDS.

VAN DE VEN, R., VAN DEN HOUT, M. F. C. M., LINDENBERG, J. J., SLUIJTER, B. J. R., VAN LEEUWEN, P. A. M., LOUGHEED, S. M., MEIJER, S., VAN DEN TOL, M. P., SCHEPER, R. J. & DE GRUIJL, T. D. 2011. Characterization of four conventional dendritic cell subsets in human skin-draining lymph nodes in relation to T-cell activation. *Blood,* 118**,** 2502-2510.

VAN DER SLUIS, R. M., EGEDAL, J. H. & JAKOBSEN, M. R. 2020. Plasmacytoid Dendritic Cells as Cell-Based Therapeutics: A Novel Immunotherapy to Treat Human Immunodeficiency Virus Infection? *Frontiers in Cellular and Infection Microbiology,* 10.

VAN GASSEN, S., CALLEBAUT, B., VAN HELDEN, M. J., LAMBRECHT, B. N., DEMEESTER, P., DHAENE, T. & SAEYS, Y. 2015. FlowSOM: Using self-organizing maps for visualization and interpretation of cytometry data. *Cytometry A,* 87**,** 636-45.

VAN SMOORENBURG, M. Y., REMMERSWAAL, E. B. M., SEGUI-PEREZ, C., VAN HAMME, J. L., STRIJBIS, K. & GEIJTENBEEK, T. B. H. 2025. Vaginal Prevotella timonensis Bacteria Enhance HIV-1 Uptake and Differentially Affect Transmission by Distinct Primary Dendritic Cell Subsets. *Eur J Immunol,* 55**,** e202451192.

VAN TEIJLINGEN, N. H., EDER, J., SARRAMI-FOROOSHANI, R., ZIJLSTRA-WILLEMS, E. M., ROOVERS, J. W. R., VAN LEEUWEN, E., RIBEIRO, C. M. S. & GEIJTENBEEK, T. B. H. 2023. Immune activation of vaginal human

Langerhans cells increases susceptibility to HIV-1 infection. *Sci Rep,* 13**,** 3283.

VILLANI, A. C., SATIJA, R., REYNOLDS, G., SARKIZOVA, S., SHEKHAR, K., FLETCHER, J., GRIESBECK, M., BUTLER, A., ZHENG, S., LAZO, S., JARDINE, L., DIXON, D., STEPHENSON, E., NILSSON, E., GRUNDBERG, I., MCDONALD, D., FILBY, A., LI, W., DE JAGER, P. L., ROZENBLATT-ROSEN, O., LANE, A. A., HANIFFA, M., REGEV, A. & HACOHEN, N. 2017. Single-cell RNA-seq reveals new types of human blood dendritic cells, monocytes, and progenitors. *Science,* 356.

VINE, E. 2025. *Characterisation of Human Colorectal Mononuclear Phagocytes and Investigating their Role in Early HIV Infection.* The University of Sydney.

VINE, E. E., AUSTIN, P. J., O'NEIL, T. R., NASR, N., BERTRAM, K. M., CUNNINGHAM, A. L. & HARMAN, A. N. 2024. Epithelial dendritic cells vs. Langerhans cells: Implications for mucosal vaccines. *Cell Reports,* 43**,** 113977.

VINE, E. E., RHODES, J. W., WARNER VAN DIJK, F. A., BYRNE, S. N., BERTRAM, K. M., CUNNINGHAM, A. L. & HARMAN, A. N. 2022. HIV transmitting mononuclear phagocytes; integrating the old and new. *Mucosal Immunology*.

VORA, R., BERNARDO, D., DURANT, L., REDDI, D., HART, A. L., FELL, J. M., AL-HASSI, H. O. & KNIGHT, S. C. 2016. Age-related alterations in blood and colonic dendritic cell properties. *Oncotarget,* 7**,** 11913-22.

WAITE, J. C. & SKOKOS, D. 2012. Th17 response and inflammatory autoimmune diseases. *Int J Inflam,* 2012**,** 819467.

WALL, K. M., KILEMBE, W., VWALIKA, B., HADDAD, L. B., HUNTER, E., LAKHI, S., CHAVUMA, R., HTEE KHU, N., BRILL, I., VWALIKA, C., MWANANYANDA, L., CHOMBA, E., MULENGA, J., TICHACEK, A. & ALLEN, S. 2017. Risk of heterosexual HIV transmission attributable to sexually transmitted infections and non-specific genital inflammation in Zambian discordant couples, 1994-2012. *Int J Epidemiol,* 46**,** 1593-1606.

WANG, B., ZHOU, B., CHEN, J., SUN, X., YANG, W., YANG, T., YU, H., CHEN, P., CHEN, K., HUANG, X., FAN, X., HE, W., HUANG, J. & LIN, T. 2024. Type III interferon inhibits bladder cancer progression by reprogramming macrophage-mediated phagocytosis and orchestrating effective immune responses. *J Immunother Cancer,* 12.

WANG, Z., YIN, X., MA, M., GE, H., LANG, B., SUN, H., HE, S., FU, Y., SUN, Y., YU, X., ZHANG, Z., CUI, H., HAN, X., XU, J., DING, H., CHU, Z., SHANG, H., WU, Y. & JIANG, Y. 2021. IP-10 Promotes Latent HIV Infection in Resting Memory CD4(+) T Cells via LIMK-Cofilin Pathway. *Front Immunol,* 12**,** 656663.

WARNER VAN DIJK, F. A. 2021. *Defining Mononuclear Phagocytes in Inflamed Tissue and their Role in HIV Acquisition.* Bachelor of Advanced Studies (Honours), The University of Sydney.

WARNER VAN DIJK, F. A., BERTRAM, K. M., O'NEIL, T. R., LI, Y., BUFFA, D. J., HARMAN, A. N., CUNNINGHAM, A. L. & NASR, N. 2025. Recent Advances in Our Understanding of Human Inflammatory Dendritic Cells in Human Immunodeficiency Virus Infection. *Viruses,* 17.

WARNER VAN DIJK, F. A., TONG, O., O'NEIL, T. R., BERTRAM, K. M., HU, K., BAHARLOU, H., VINE, E. E., JENNS, K., GOSSELINK, M. P., TOH, J. W.,

PAPADOPOULOS, T., BARNOUTI, L., JENKINS, G. J., SANDERCOE, G., HANIFFA, M., SANDGREN, K. J., HARMAN, A. N., CUNNINGHAM, A. L. & NASR, N. 2024. Characterising plasmacytoid and myeloid AXL+ SIGLEC-6+ dendritic cell functions and their interactions with HIV. *PLoS Pathog,* 20**,** e1012351.

WATCHMAKER, P. B., LAHL, K., LEE, M., BAUMJOHANN, D., MORTON, J., KIM, S. J., ZENG, R., DENT, A., ANSEL, K. M., DIAMOND, B., HADEIBA, H. & BUTCHER, E. C. 2014. Comparative transcriptional and functional profiling defines conserved programs of intestinal DC differentiation in humans and mice. *Nature Immunology,* 15**,** 98-108.

WAWER, M. J., GRAY, R. H., SEWANKAMBO, N. K., SERWADDA, D., LI, X., LAEYENDECKER, O., KIWANUKA, N., KIGOZI, G., KIDDUGAVU, M., LUTALO, T., NALUGODA, F., WABWIRE-MANGEN, F., MEEHAN, M. P. & QUINN, T. C. 2005. Rates of HIV-1 Transmission per Coital Act, by Stage of HIV-1 Infection, in Rakai, Uganda. *J Infect Dis,* 191**,** 1403-1409.

WELLER, S., BRAUN, M. C., TAN, B. K., ROSENWALD, A., CORDIER, C., CONLEY, M. E., PLEBANI, A., KUMARARATNE, D. S., BONNET, D., TOURNILHAC, O., TCHERNIA, G., STEINIGER, B., STAUDT, L. M., CASANOVA, J. L., REYNAUD, C. A. & WEILL, J. C. 2004. Human blood IgM "memory" B cells are circulating splenic marginal zone B cells harboring a prediversified immunoglobulin repertoire. *Blood,* 104**,** 3647-54.

WIEGERINCK, M. A. H. M., POORTMAN, J., TRUUS, D. H. & THIJSSEN, J. H. H. 1983. In VivoUptake and Subcellular Distribution of Tritium- Labeled Estrogens in Human Endometrium, Myometrium, and Vagina. *The Journal of Clinical Endocrinology & Metabolism,* 56**,** 76-86.

WINHEIM, E., RINKE, L., LUTZ, K., REISCHER, A., LEUTBECHER, A., WOLFRAM, L., RAUSCH, L., KRANICH, J., WRATIL, P. R., HUBER, J. E., BAUMJOHANN, D., ROTHENFUSSER, S., SCHUBERT, B., HILGENDORFF, A., HELLMUTH, J. C., SCHERER, C., MUENCHHOFF, M., VON BERGWELT-BAILDON, M., STARK, K., STRAUB, T., BROCKER, T., KEPPLER, O. T., SUBKLEWE, M. & KRUG, A. B. 2021. Impaired function and delayed regeneration of dendritic cells in COVID-19. *PLoS Pathog,* 17**,** e1009742.

WOLLENBERG, A., GÜNTHER, S., MODERER, M., WETZEL, S., WAGNER, M., TOWAROWSKI, A., TUMA, E., ROTHENFUSSER, S., ENDRES, S. & HARTMANN, G. 2002. Plasmacytoid Dendritic Cells: A New Cutaneous Dendritic Cell Subset with Distinct Role in Inflammatory Skin Diseases. *Journal of Investigative Dermatology,* 119**,** 1096-1102.

WOLLENBERG, A., KRAFT, S., HANAU, D. & BIEBER, T. 1996. Immunomorphological and Ultrastructural Characterization of Langerhans Cells and a Novel, Inflammatory Dendritic Epidermal Cell (IDEC) Population in Lesional Skin of Atopic Eczema. *J Invest Dermatol,* 106**,** 446-453.

WRIGHT, P. B., MCDONALD, E., BRAVO-BLAS, A., BAER, H. M., HEAWOOD, A., BAIN, C. C., MOWAT, A. M., CLAY, S. L., ROBERTSON, E. V., MORTON, F., NIJJAR, J. S., IJAZ, U. Z., MILLING, S. W. F. & GAYA, D. R. 2021. The mannose receptor (CD206) identifies a population of colonic macrophages in health and inflammatory bowel disease. *Sci Rep,* 11**,** 19616.

XIE, H., CHEN, L., ZHANG, H., WANG, J., ZANG, Y., ZHAN, M., GU, F., WANG, S. & HE, S. 2022. Increased expressions of CD123, CD63, CD203c, and Fc epsilon receptor I on blood leukocytes of allergic asthma. *Front Mol Biosci,* 9**,** 907092.

YI, T. J., SHANNON, B., PRODGER, J., MCKINNON, L. & KAUL, R. 2013. Genital immunology and HIV susceptibility in young women. *Am J Reprod Immunol,* 69 Suppl 1**,** 74-9.

YIN, X., YU, H., JIN, X., LI, J., GUO, H., SHI, Q., YIN, Z., XU, Y., WANG, X., LIU, R., WANG, S. & ZHANG, L. 2017. Human Blood CD1c+ Dendritic Cells Encompass CD5high and CD5low Subsets That Differ Significantly in Phenotype, Gene Expression, and Functions. *J Immunol,* 198**,** 1553-1564.

YU, H. J., REUTER, M. A. & MCDONALD, D. 2008. HIV traffics through a specialized, surface-accessible intracellular compartment during trans-infection of T cells by mature dendritic cells. *PLoS Pathog,* 4**,** e1000134.

ZABA, L. C., FUENTES-DUCULAN, J., EUNGDAMRONG, N. J., ABELLO, M. V., NOVITSKAYA, I., PIERSON, K. C., GONZALEZ, J., KRUEGER, J. G. & LOWES, M. A. 2009. Psoriasis Is Characterized by Accumulation of Immunostimulatory and Th1/Th17 Cell-Polarizing Myeloid Dendritic Cells. *Journal of Investigative Dermatology,* 129**,** 79-88.

ZABA, L. C., FUENTES-DUCULAN, J., STEINMAN, R. M., KRUEGER, J. G. & LOWES, M. A. 2007. Normal human dermis contains distinct populations of CD11c+BDCA-1+ dendritic cells and CD163+FXIIIA+ macrophages. *The Journal of Clinical Investigation,* 117**,** 2517-2525.

ZALAR, A., FIGUEROA, M. I., RUIBAL-ARES, B., BARÉ, P., CAHN, P., DE BRACCO, M. M. & BELMONTE, L. 2010. Macrophage HIV-1 infection in duodenal tissue of patients on long term HAART. *Antiviral Res,* 87**,** 269-71.

ZEVIN, A. S., XIE, I. Y., BIRSE, K., ARNOLD, K., ROMAS, L., WESTMACOTT, G., NOVAK, R. M., MCCORRISTER, S., MCKINNON, L. R., COHEN, C. R., MACKELPRANG, R., LINGAPPA, J., LAUFFENBURGER, D. A., KLATT, N. R. & BURGENER, A. D. 2016. Microbiome Composition and Function Drives Wound-Healing Impairment in the Female Genital Tract. *PLoS Pathog,* 12**,** e1005889.

ZHENG, Q., HOU, J., ZHOU, Y., YANG, Y., XIE, B. & CAO, X. 2015. Siglec1 suppresses antiviral innate immune response by inducing TBK1 degradation via the ubiquitin ligase TRIM27. *Cell Res,* 25**,** 1121-36.

ZIEGLER-HEITBROCK, L., ANCUTA, P., CROWE, S., DALOD, M., GRAU, V., HART, D. N., LEENEN, P. J., LIU, Y. J., MACPHERSON, G., RANDOLPH, G. J., SCHERBERICH, J., SCHMITZ, J., SHORTMAN, K., SOZZANI, S., STROBL, H., ZEMBALA, M., AUSTYN, J. M. & LUTZ, M. B. 2010. Nomenclature of monocytes and dendritic cells in blood. *Blood,* 116**,** e74-80.

ZIEGLER-HEITBROCK, L., OHTEKI, T., GINHOUX, F., SHORTMAN, K. & SPITS, H. 2023a. Reclassifying plasmacytoid dendritic cells as innate lymphocytes. *Nature Reviews Immunology,* 23**,** 1-2.

ZIEGLER-HEITBROCK, L., OHTEKI, T., GINHOUX, F., SHORTMAN, K. & SPITS, H. 2023b. Reply to 'Reclassification of plasmacytoid dendritic cells as innate lymphocytes is premature'. *Nat Rev Immunol,* 23**,** 338-339.

ZOU, Z., CHASTAIN, A., MOIR, S., FORD, J., TRANDEM, K., MARTINELLI, E., CICALA, C., CROCKER, P., ARTHOS, J. & SUN, P. D. 2011. Siglecs facilitate HIV-1 infection of macrophages through adhesion with viral sialic acids. *PLoS One,* 6**,** e24559.